The Journal of Gemmology

Volume 38 / No. 2 / 2022

Spinel from Tajikistan

Cleopatra's Emerald Mines

Daylight-Fluorescent Hyalite from Namibia

Gahnite from Nigeria

SSEF
SCHWEIZERISCHES GEMMOLOGISCHES INSTITUT
SWISS GEMMOLOGICAL INSTITUTE
INSTITUT SUISSE DE GEMMOLOGIE

Gem-A
THE GEMMOLOGICAL ASSOCIATION OF GREAT BRITAIN

# SSEF

SCHWEIZERISCHES GEMMOLOGISCHES INSTITUT
SWISS GEMMOLOGICAL INSTITUTE
INSTITUT SUISSE DE GEMMOLOGIE

ORIGIN DETERMINATION · TREATMENT DETECTION

DIAMOND GRADING · PEARL TESTING

EDUCATION · RESEARCH

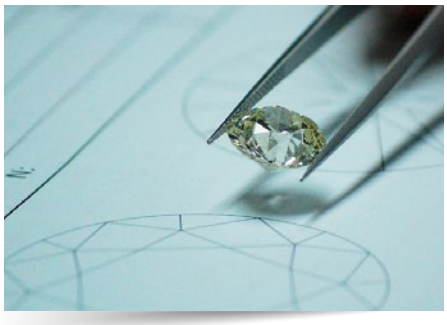

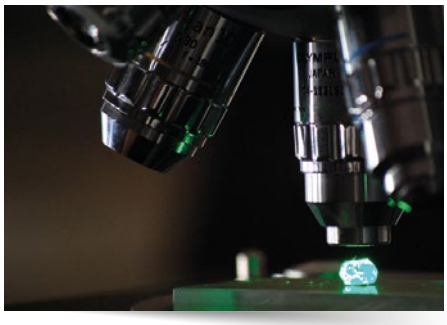

THE SCIENCE OF GEMSTONE TESTING™

Aeschengraben 26, 4051 Basel, Switzerland Tel. +41 61 262 06 40 Fax + 41 61 262 06 41 admin@ssef.ch www.ssef.ch

The Journal of Gemmology

Volume 38 / No. 2 / 2022

**Cover photo:** *Spinel from Kuh-i-Lal, in the Pamir Mountains of Tajikistan, has a long history and has been set into some important jewellery pieces. The gemmological properties of this spinel are described on pp. 138–154 of this issue. The earrings shown here feature polished Tajik spinels (40.71 ct total weight) that are set in 18 ct gold with old-cut cushion diamonds (1.30 ct total weight) and 272 pavé diamonds. Courtesy of IVY New York.*

## COLUMNS




*Photo by Sandeep Kumar Vijay*

## ARTICLES




*Photo courtesy of The Walters Art Museum*


*Photo by R. Hanus*



*The Journal* is published by Gem-A in collaboration with SSEF and with the support of AGL.

Gem-A THE GEMMOLOGICAL ASSOCIATION OF GREAT BRITAIN

SSEF SCHWEIZERISCHES GEMMOLOGISCHES INSTITUT SWISS GEMMOLOGICAL INSTITUTE INSTITUT SUISSE DE GEMMOLOGIE

AGL AMERICAN GEMOLOGICAL LABORATORIES

The Journal of Gemmology




## COVERED BY THE FOLLOWING ABSTRACTING AND INDEXING SERVICES:

Clarivate Analytics' (formerly Thomson Reuters/ISI) Science Citation Index Expanded (in the Web of Science), *Journal Citation Reports (Science Edition)* and *Current Contents (Physical, Chemical and Earth Sciences)*; Elsevier's Scopus; Australian Research Council's Excellence in Research for Australia (ERA) Journal List; China National Knowledge Infrastructure (CNKI Scholar); EBSCO's Academic Search Ultimate; ProQuest (Cambridge Scientific Abstracts); GeoRef; CrossRef; Chemical Abstracts (CA Plus); Mineralogical Abstracts; Index Copernicus ICI Journals Master List; Gale Academic OneFile; British Library Document Supply Service; and Copyright Clearance Center's RightFind application.

Science Citation Index Expanded
Web of Science Clarivate Analytics

## CONTENT SUBMISSION

The Editor-in-Chief is glad to consider original articles, news items, conference reports, announcements and calendar entries on subjects of gemmological interest for publication in *The Journal of Gemmology*. A guide to the various sections and the preparation of manuscripts is given at https://gem-a.com/membership/journal-of-gemmology/submissions, or contact the Editor-in-Chief.

## SUBSCRIPTIONS

Gem-A members receive *The Journal* as part of their membership package, full details of which are given at https://gem-a.com/membership. Laboratories, libraries, museums and similar institutions may become direct subscribers to *The Journal*; download the form from *The Journal*'s home page.

## ADVERTISING

Enquiries about advertising in *The Journal* should be directed to advertising@gem-a.com. For more information, see https://gem-a.com/news-publications/media-pack-2021.





## DESIGN & PRODUCTION

Zest Design, London. www.zest-uk.com

## PRINTER

DG3 Group (Holdings) Ltd, London. https://dg3.com

Mixed Sources
Product group from well-managed forests and other controlled sources
www.fsc.org Cert no. TT-COC-002454
© 1996 Forest Stewardship Council
FSC



ISSN 1355-4565 (Print), ISSN 2632-1718 (Online)


Gem-A
THE GEMMOLOGICAL ASSOCIATION OF GREAT BRITAIN

21 Ely Place
London EC1N 6TD
UK
t: +44 (0)20 7404 3334
f: +44 (0)20 7404 8843
e: information@gem-a.com
w: https://gem-a.com

Registered Charity No. 1109555
A company limited by guarantee and registered in England No. 1945780
Registered office: Palladium House, 1–4 Argyll Street, London W1F 7LD

# What's New

## NEWS AND PUBLICATIONS

### III Conferenza Nazionale Diamante e Gemme di Colore Abstracts

The 3rd National Conference on Diamonds and Coloured Gems was held 22–23 July 2021 in Bari, Italy. The abstracts volume is freely downloadable in PDF format at http://www.gemmologiascientifica.uniba.it/index.php/libro-dei-riassunti.html. One of the 26 abstracts is in English ('The geology and genesis of gem ruby deposits', by Dr Gaston Giuliani), while the others are in Italian. Topics covered include demantoid from Italy, diamond identification and analysis, infrared spectroscopy of emeralds, spinel colouration, topaz, tourmaline and more.


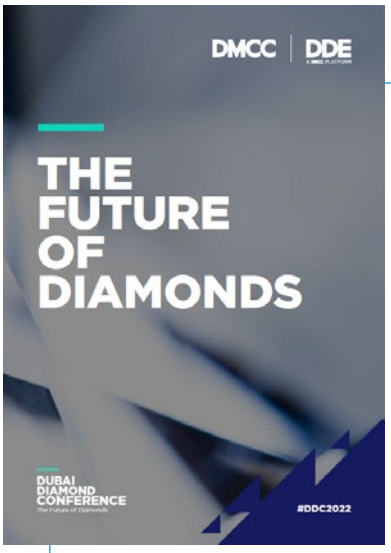


### Dubai Diamond Conference Summary and Highlights

The Dubai Multi Commodities Centre hosted the 2022 Dubai Diamond Conference—The Future of Diamonds—on 21 February in the United Arab Emirates. Speakers included senior executives from major diamond organisations worldwide. Video highlights of the conference, including an overview and all four panel sessions, are now available online at https://diamondconference.ae. The panels cover 'Why did diamonds do so well during COVID?', 'The new consumer and lab grown diamonds', 'Rethinking the diamond supply chain', and 'Implications for the trade – Perspectives from the trade associations'. In addition, a conference summary publication is available as a downloadable PDF.

### Gemmological Society of Japan 2021 Annual Meeting Abstracts

Abstracts of 'special lectures' presented during the online June 2021 Annual Meeting of the Gemmological Society of Japan are available at https://www.jstage.jst.go.jp/browse/gsj/43/0/_contents/-char/en. The 13 abstracts cover a variety of topics, including chameleon diamonds, diamond clarity grading, heat treatment of sapphire, larimar, pearl identification, pink jadeite from Myanmar and more. Also available are abstracts from previous conferences.

Abstract of Papers Presented at Annual Meeting of the Gemmological Society of Japan

## The Gemstones and Jewellery Community Platform Reports

The Gemstones and Jewellery Community Platform offers a set of six 'white papers' about key sustainability topics in the coloured stone industry. Geared toward organisations and businesses dealing with gems and jewellery, the reports cover the following: introduction (14 pages), mining (52 pages), trading (39 pages), processing (35 pages), retailing (27 pages) and governing supply chains (48 pages). To download each individual paper, visit https://gemstones-and-jewellery.com/research. In addition, businesses that join the platform have access to resources and training materials, capacity-building templates and self-assessment tools.



## Lab-Grown Diamond Market Research

In March 2022, USA-based The MVEye released a market research report titled *It Takes a Long Time to Become Young: Lab-grown Diamonds and the Next Gen Consumer in 2022*. The report presents the findings of a February 2022 online survey of 754 consumers in the USA aged 20–35. The survey found that 72% knew about lab-grown diamonds and 15% owned at least one of them—up from 10% in 2020. Also, 44% said they would purchase lab-grown diamonds, 32% would choose mined diamonds and 22% were undecided. Notably, 89% said they would pay a premium for jewellery produced with minimal environmental and social impact, and 86% would do so for jewellery with materials having traceable origins. To purchase the report, visit https://www.themveye.com/download-premium-report.php?report=13.

## Sustainability Rated Diamonds' Full Standard

As previously mentioned in *The Journal* (Vol. 37, No. 8, 2021, p. 760), SRS Standards created its *SCS-007 Jewelry Sustainability Standard Series: Sustainability Rated Diamonds* in June 2021, but only a summary of this standard was available. The full standard can now be freely downloaded at https://sustainabilityrateddiamonds.com/about. The 133-page PDF begins with an introduction that covers intended users (industrial-scale miners and synthetic diamond producers interested in assessing their environmentally and socially responsible production practices and performance), scope (entire supply chain from producer to retailer), terminology and more. Chapters then cover social responsibility, governance criteria, environmental factors, sustainable production, diamond origin traceability and 'public assertions'. Appendices include information about the impact of climate change, life cycle co-benefits, water resources, etc.

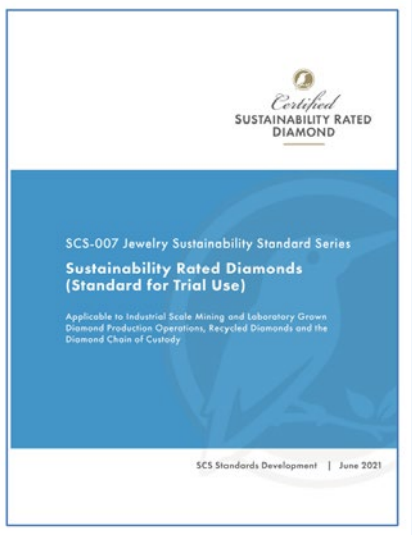

# OTHER RESOURCES

## Webinars and Other Online Gemmological Education

Since the start of the COVID-19 pandemic, a number of gem industry organisations and other groups have provided webinars (and other archived video and audio content) on their websites or YouTube channels that are of interest to gemmologists. See also those listed in previous What's New sections starting with Vol. 37, No. 2, 2020.

### HRD Talks

In December 2021, HRD Antwerp posted on their YouTube channel the first of a planned series of 'HRD Talks' videos that are intended to keep the industry informed about HRD's research on diamonds. This first presentation, by HRD research scientist Ekaterina Kovalenok, focuses on the latest developments in lab-grown diamonds. The topics include CVD synthetics in the D–Z colour range, pink CVD products, yellow HPHT-grown samples and 'hybrid diamonds' (CVD overgrowth on natural diamond substrate). Visit https://www.youtube.com/user/HRDAntwerp.

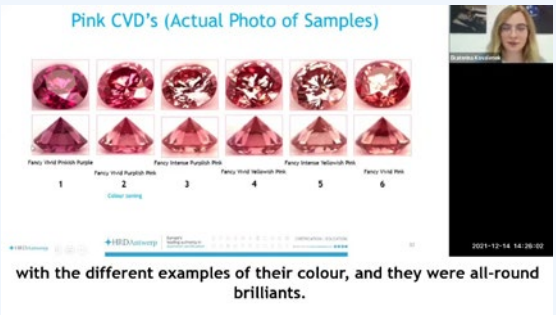


### Jewels of the Trade Podcasts

Jewels of the Trade, a retail jewellers' resource company, offers a series of podcasts that are each about 30–60 minutes long. Of the ten episodes that are currently available, the two most recent ones (posted in April–May) cover demantoid from Madagascar. Other topics are lab-grown diamond, jadeite, ruby, sapphire, turquoise, tsavorite, nephrite and the Hope diamond. Visit https://tinyurl.com/4pebpr9s.


**What's New** provides announcements of new instruments/technology, publications, online resources and more. Inclusion in What's New does not imply recommendation or endorsement by Gem-A. Entries were prepared by Carol M. Stockton unless otherwise noted.

# Gem Notes

## COLOURED STONES

### Apatite from Slovakia

Minerals of the apatite group can form in a wide range of geological environments, and gem-quality material is typically either hydroxylapatite or fluorapatite, with the most common colours being blue, green and yellow (O'Donoghue 2006).

Apatite from Muránska Dlhá Lúka, Slovakia, forms yellow prisms that are usually euhedral and are similar to the well-known apatite crystals from Durango, Mexico (Bačík *et al*. 2020). The Slovak locality lies in the northern part of Stolické Hills, 5 km north-west of the town of Revúca. The area is underlain by biotitic granodiorites to granites, as well as biotitic and two-mica schists, with bodies of amphibolite and serpentinite; these rocks belong to the Kohút zone of the Veporic Superunit crystalline basement (Bačík *et al*. 2020). The apatite crystals are hosted by talc-magnesite veins in the serpentinite body, which formed as a consequence of the fluid regime during regional metamorphic events. The talc and serpentinite (used as a building stone) were worked in a quarry and in two underground galleries between 1920 and 1955.

In 2014, apatite crystals up to 3 cm long were found by author TB in a talc vein (5–30 cm thick) in the central part of the quarry. The smaller crystals were transparent, whereas larger crystals were usually translucent. The authors selected 15 pieces (about 20 g total weight) of gem-quality crystals that were up to 1 cm in diameter, and five of them were faceted into gemstones ranging from 0.36 to 2.25 ct (Figure 1). These were analysed by Raman and visible-near infrared (Vis-NIR) spectroscopy by Bačík *et al*. (2020)—who confirmed they are hydroxylapatite—and their other gemmological properties are reported here.

The yellow colour of the stones showed a moderately strong to strong saturation and a light to medium tone. Their RIs of 1.635–1.640 and hydrostatic SG values of 3.15–3.19 were consistent with those of apatite. The stones were inert to both long- and short-wave UV radiation. Microscopic examination revealed mainly fluid inclusions (sometimes two-phase; Figure 2) and occasional fibres that were too fine to identify with Raman micro-spectroscopy but had the appearance of actinolite. They were commonly slightly curved, although in some cases they formed circles (Figure 3). In addition, some tubular structures were observed.

Hydroxylapatite from Slovakia shows an attractive yellow colour that is similar to heliodor or brazilianite. However, only a small amount of gem-quality material

**Figure 1:** These five faceted apatites (0.36–2.25 ct) are from Muránska Dlhá Lúka, Slovakia, and were examined for this report. Photo by J. Štubňa.

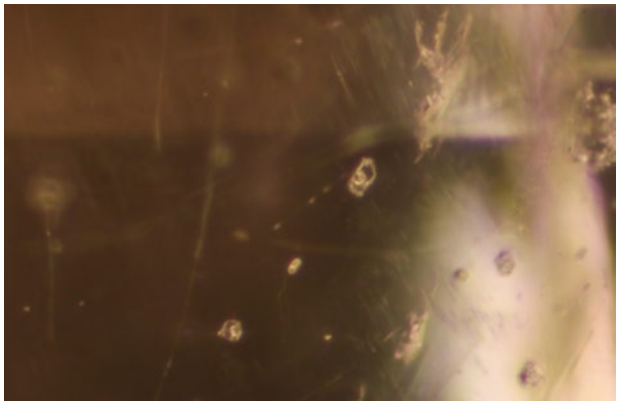

**Figure 2:** Fluid inclusions, which are sometimes two-phase, occur in the Slovak apatite. Photomicrograph by J. Štubňa; magnified 50×.

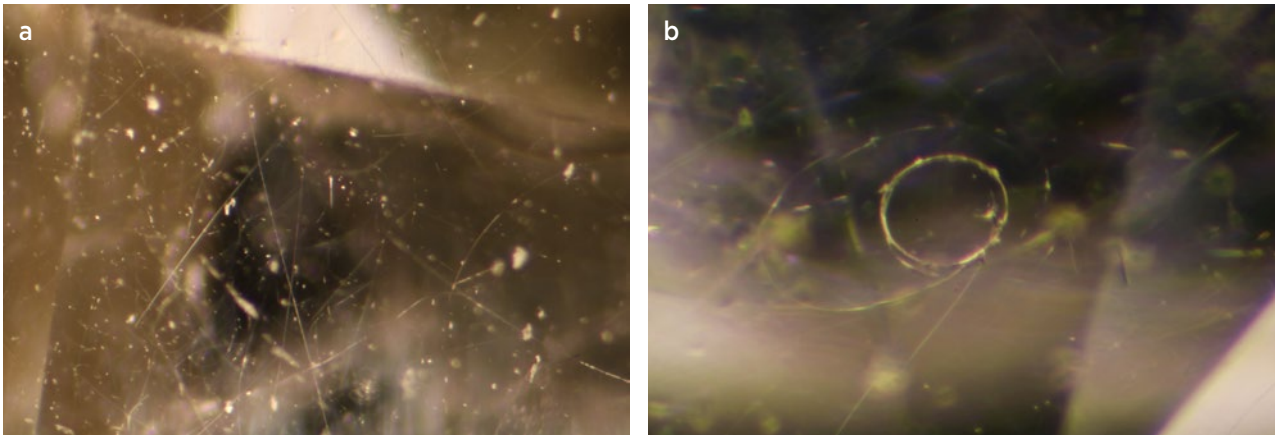


**Figure 3:** (**a**) The apatite from Slovakia occasionally contains fibrous inclusions (probably actinolite) that are (**a**) commonly slightly curved or (**b**) rarely circular. Photomicrographs by J. Štubňa; magnified 20× (a) and 50× (b).

has been found so far, so it is not likely to be encountered on the international gem market.

*Dr Ján Štubňa (janstubna@gmail.com) and Tomáš Bancík*
*Gemmological Laboratory, Constantine the Philosopher University, Nitra, Slovakia*

*Dr Jana Fridrichová, Olena Rybnikova and Dr Peter Bačík*
*Comenius University, Bratislava, Slovakia*

## References

Bačík, P., Fridrichová, J., Štubňa, J., Bancík, T., Illášová, Ľ., Pálková, H., Škoda, R., Mikuš, T. *et al*. 2020. The REE-induced absorption and luminescence in yellow gem-quality Durango-type hydroxylapatite from Muránska Dlhá Lúka, Slovakia. *Minerals*, **10**(11), article 1001 (21 pp.), https://doi.org/10.3390/min10111001.

O'Donoghue, M. 2006. *Gems*. Butterworth-Heinemann, Oxford, xxix + 873 pp.

## Afghan Emerald with *Gota de Aceite* Phenomenon

In October 2021, the American Gemological Laboratories (AGL) received a 2.12 ct faceted emerald for identification and enhancement reporting (Figure 4). It showed a strong *gota de aceite* phenomenon (Figure 5), which is well known in Colombian emeralds (e.g. Ringsrud 2008), and has also been documented in a Zambian emerald (Ahline 2017). Dr Eduard J. Gübelin was the first to describe this optical effect as giving 'an oily appearance to the most beautiful and highly priced Colombian emerald' (Gübelin 1944–1945, p. 179). He attributed it

**Figure 4:** This 2.12 ct emerald was identified as originating from Afghanistan, although it contains a strong *gota de aceite* effect, which is normally associated with Colombian emeralds. Photo by Alex Mercado, AGL.

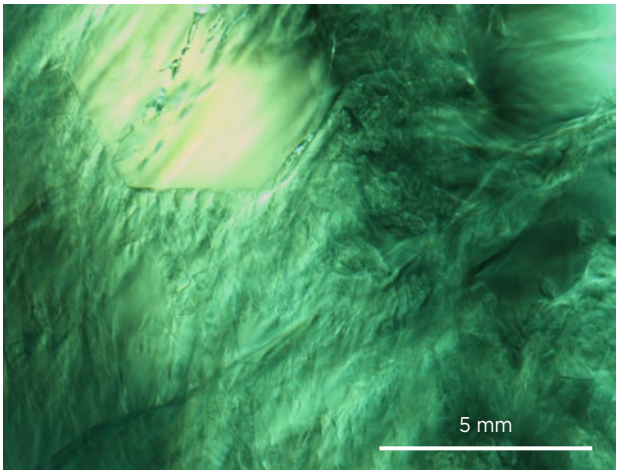


**Figure 5:** Viewed with a microscope, the emerald in Figure 4 displays a roiled *gota de aceite* effect. Photomicrograph by R. Zellagui.

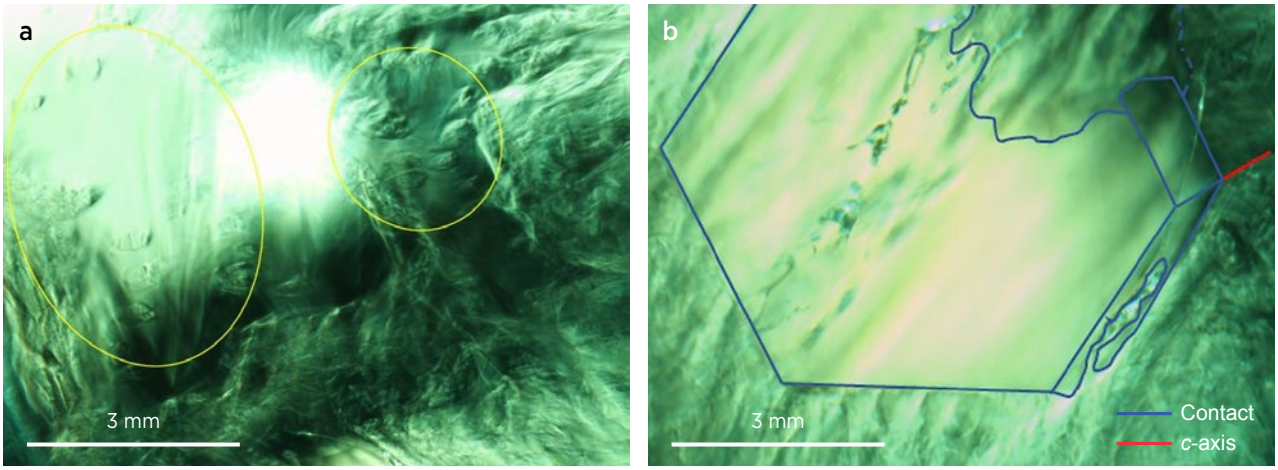


**Figure 6:** (**a**) Geometric growth structures are seen in some areas of the emerald (circled) displaying the *gota de aceite* effect. (**b**) An enlarged view of the hexagonal zone in Figure 5 that lacks the *gota de aceite* effect shows that it is composed of a hexagonal prism. The prism faces are parallel to the *c*-axis, which is inclined in this viewing orientation. Photomicrographs by R. Zellagui.

to calcite inclusions that precipitated during the growth of the emerald. However, according to John Koivula (as reported in Ringsrud 2008, p. 249), the phenomenon is due to irregularities in the internal structure of the emerald, inducing a 'roiled dispersion of light'.

The stone described here also contained other internal features, including geometric growth structures and a hexagonal zone that lacked the *gota de aceite* effect (Figure 6). Such hexagonal zones—but with a much different appearance—were noted recently in a Colombian emerald by Sun and Gao (2022). What made the present emerald particularly interesting, however, is that it showed characteristics that were inconsistent with a Colombian origin. The UV-Vis-NIR spectrum contained minor Fe-related features at about 375 and 830 nm, along with the typical absorption bands due to $Cr^{3+}$ with overlapping $V^{3+}$ (Figure 7). The bands associated with Fe, and especially the one related to $Fe^{3+}$ at

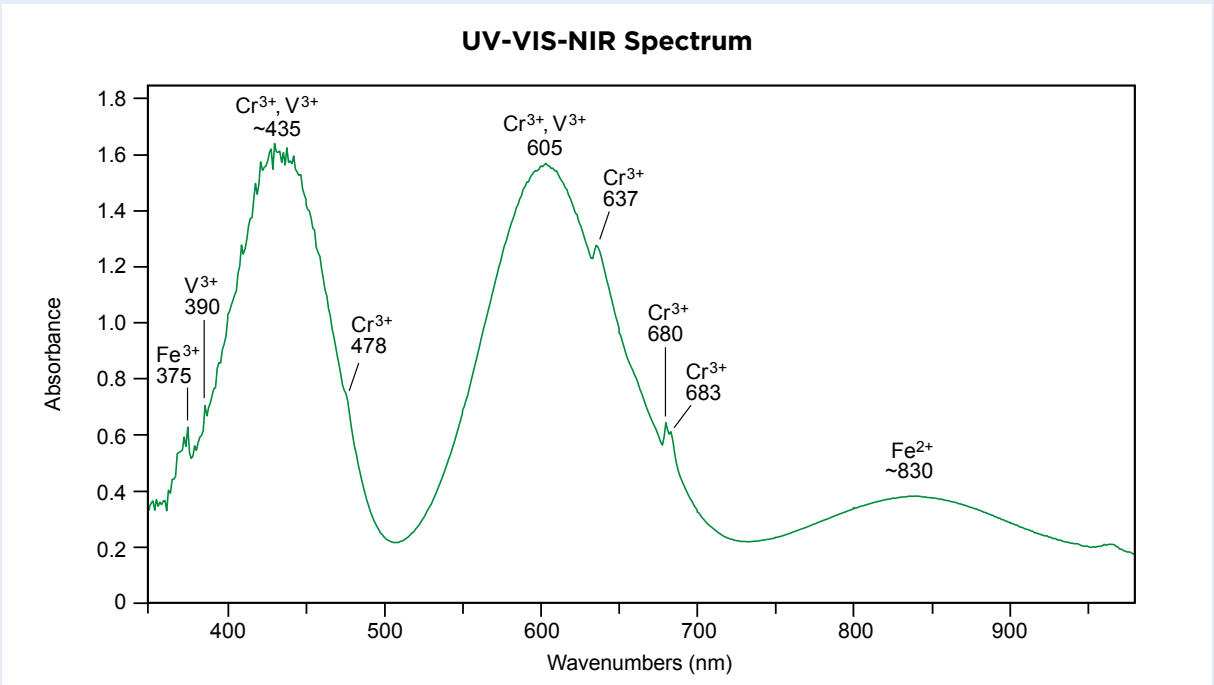


**Figure 7:** The UV-Vis-NIR spectrum of the emerald in Figure 4 reveals main absorption bands in the visible range associated with $Cr^{3+}$ and $V^{3+}$. The $Fe^{3+}$ peak at 375 nm, along with the Fe content determined by EDXRF analysis, provide evidence that this emerald originated from Afghanistan.

375 nm, are usually not present in Colombian emeralds. Energy-dispersive X-ray fluorescence (EDXRF) chemical analysis revealed a trace-element composition of 0.03 wt.% $Cr_2O_3$, 0.04 wt.% $V_2O_3$ and 0.55 wt.% $FeO_{tot}$.

The presence of a 375 nm band in the UV-Vis-NIR spectrum, and the associated relatively high Fe content, point to an origin other than Colombia. Based on combined gemmological, geochemical and UV-Vis-NIR data, AGL determined that this stone is from Afghanistan. This is the first documentation of the *gota de aceite* effect in an emerald of Afghan origin.

*Dr Riadh Zellagui*
*(riadh@aglgemlab.com)*
*American Gemological Laboratories*
*New York, New York, USA*

### References

Ahline, N. 2017. Lab Notes: *Gota de aceite* in a Zambian emerald. *Gems & Gemology*, **53**(4), 460–461.

Gübelin, E.J. 1944–1945. Gemstone inclusions. *Gems & Gemology*, **4**(12), 174–179.

Ringsrud, R. 2008. *Gota de aceite*: Nomenclature for the finest Colombian emeralds. *Gems & Gemology*, **44**(3), 242–245, https://doi.org/10.5741/gems.44.3.242.

Sun, X. & Gao, Y. 2022. Gem Notes: Hexagonal growth structures displaying *gota de aceite* effect in Colombian emerald. *Journal of Gemmology*, **38**(1), 11–12, https://doi.org/10.15506/jog.2022.38.1.11.

## Zircon Inclusions in Emeralds from Lake Manyara, Tanzania

Emeralds were discovered at Lake Manyara, Tanzania, around the end of the 1960s, and the mine was active for about a decade. Since then, gem-quality samples have reached the market only sporadically (Thurm 1972; Schmetzer & Malsy 2011). Various inclusion minerals have been documented in these emeralds, such as phlogopite, talc, albite and possibly quartz (Gübelin & Koivula 1986; Moroz & Eliezri 1999).

During a study of two partially polished rough emeralds from Lake Manyara belonging to the emerald reference collection of the Laboratoire Français de Gemmologie (LFG), several euhedral zircon inclusions were found, occurring as doubly terminated prismatic crystals about 100 µm long (Figures 8 and 9). This is the first time such inclusions have been observed by LFG in emeralds. However, zircon inclusions with pronounced tension halos have been noted in alexandrite from the same mining area (Schmetzer & Malsy 2011).

In the Raman spectrum of zircon, band broadening—that is, an increase in FWHM (full width at half maximum)—of the anti-symmetric stretching vibration ($\nu_3$) of $SiO_4$ near 1000 $cm^{-1}$ can be used to

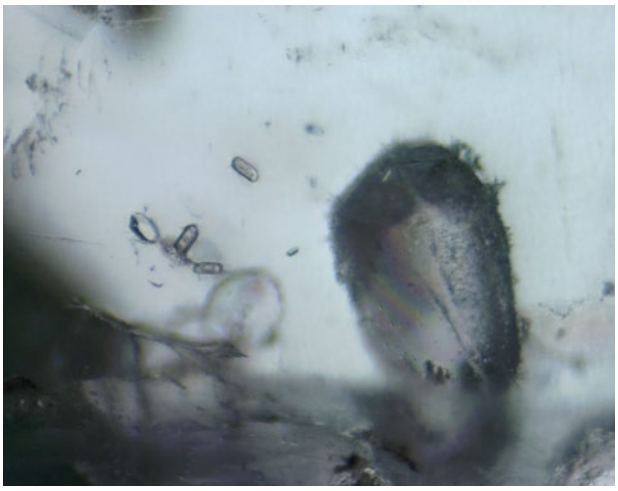

**Figure 8:** Euhedral zircon inclusions (left of centre) in a partially polished emerald from Lake Manyara, Tanzania, are doubly terminated and prismatic in shape. The large, dark-appearing inclusion is apatite. Photomicrograph by U. Hennebois; image width 1.2 mm.

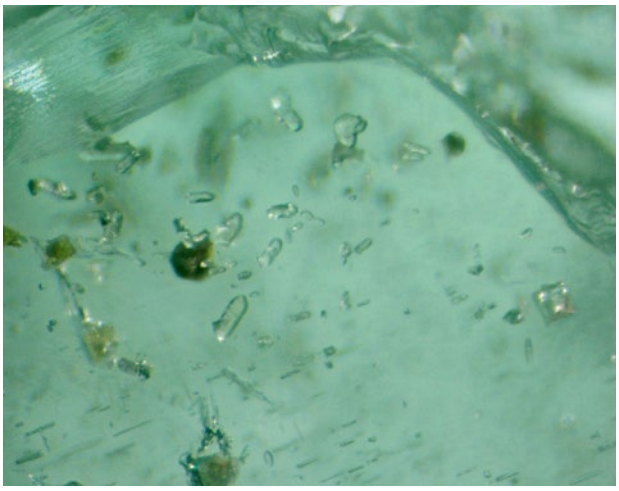

**Figure 9:** A group of euhedral, doubly terminated, prismatic zircon inclusions is accompanied by dark mica plates and rectangular multi-phase inclusions oriented parallel to the *c*-axis in a partially polished emerald from Lake Manyara. Photomicrograph by U. Hennebois; image width 1.4 mm.

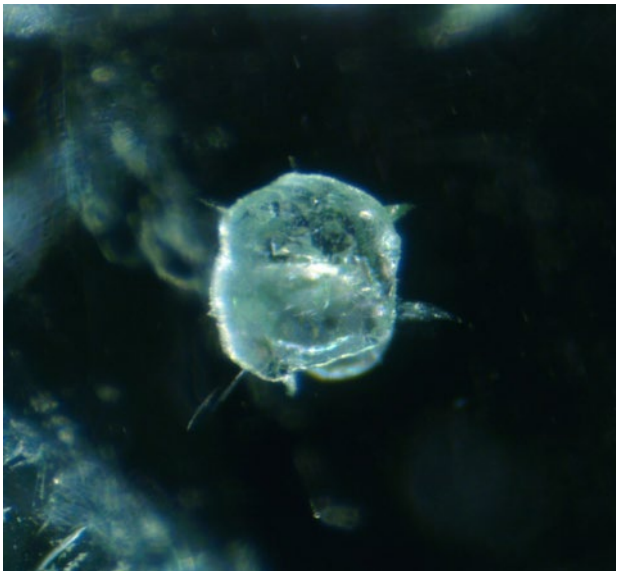

**Figure 10:** A frosty-appearing inclusion, identified as apatite by Raman micro-spectroscopy, is seen in a partially polished emerald from Lake Manyara. Photomicrograph by U. Hennebois; image width 1.0 mm.

estimate the degree of structural (radiation) damage (Nasdala *et al.* 1995). Zircon inclusions in emeralds from different localities might contain different amounts of radiation damage, and if that is the case then this parameter could be used for origin determination. Using a Raman Renishaw inVia spectrometer (514 nm diode-pumped solid-state laser, about 10 mW laser power on the sample, 50× long-working-distance objective lens and about 1.5 $cm^{-1}$ spectral resolution), the FWHM of the main Raman band of the zircon inclusions in these emeralds was found to be about 6.3–13.3 $cm^{-1}$. This suggests moderately crystallised zircon associated with partial radiation damage (cf. Nasdala *et al.* 1995). In addition, the FWHM of this band varied from 6.5 to 13.3 $cm^{-1}$ within the same zircon inclusion. This range of FWHM indicates heterogeneous radiation damage (Zeug *et al.* 2016), but with less variation than was recently observed for zircon inclusions in pink sapphires from Madagascar (Karampelas *et al.* 2022).

Additional inclusions present in these emeralds were dark-coloured mica plates and thin, rectangular, multi-phase inclusions oriented along the *c*-axis (again, see Figure 9). In addition, micro-Raman spectroscopy identified a roundish inclusion with a frosty appearance in one of the samples as apatite (Figure 10). A similar inclusion described in Gübelin and Koivula (1986) was suggested to be quartz.

Zircon inclusions in emeralds have only rarely been mentioned in the literature, in samples from Austria, Brazil, China, Egypt, India, South Africa and Ukraine. A photo of a roundish zircon inclusion with tension cracks in an emerald from India was published by Choudhary (2015), and backscattered-electron images of zircon inclusions in emeralds from Leydsdorp, South Africa, and from Ukraine were shown by Lum *et al.* (2016) and Franz *et al.* (2020), respectively.

*Ugo Hennebois, Aurélien Delaunay and Dr Stefanos Karampelas (s.karampelas@lfg.paris)*
*LFG, Paris, France*

## References

Choudhary, G. 2015. Emeralds from Jharkhand, India: An update. *34th International Gemmological Conference*, Vilnius, Lithuania, 26–30 August, 139–142.

Franz, G., Vyshnevskyi, O., Taran, M., Khomenko, V., Wiedenbeck, M., Schiperski, F. & Nissen, J. 2020. A new emerald occurrence from Kruta Balka, western Peri-Azovian region, Ukraine: Implications for understanding the crystal chemistry of emerald. *American Mineralogist*, **105**(2), 162–181, http://doi.org/10.2138/am-2020-7010.

Gübelin, E.J. & Koivula, J.I. 1986. *Photoatlas of Inclusions in Gemstones*. ABC Edition, Zurich, Switzerland, 532 pp.

Karampelas, S., Pardieu, V., Mevellec, J.-Y. & Fritsch, E. 2022. Gem Notes: Raman spectroscopy of zircon inclusions in unheated pink sapphires from Ilakaka, Madagascar: Opening new perspectives. *Journal of Gemmology*, **38**(1), 16–18, https://doi.org/10.15506/JoG.2022.38.1.16.

Lum, J.E., Viljoen, K.S. & Cairncross, B. 2016. Mineralogical and geochemical characteristics of emeralds from the Leydsdorp area, South Africa. *South African Journal of Geology*, **119**(2), 359–378, https://doi.org/10.2113/gssajg.119.2.359.

Moroz, I.I. & Eliezri, I.Z. 1999. Mineral inclusions in emeralds from different sources. *Journal of Gemmology*, **26**(6), 357–363, https://doi.org/10.15506/JoG.1999.26.6.357.

Nasdala, L., Irmer, G. & Wolf, D. 1995. The degree of metamictization in zircon: A Raman spectroscopic study. *European Journal of Mineralogy*, **7**(3), 471–478, https://doi.org/10.1127/ejm/7/3/0471.

Schmetzer, K. & Malsy, A.-K. 2011. Alexandrite and colour-change chrysoberyl from the Lake Manyara alexandrite-emerald deposit in northern Tanzania. *Journal of Gemmology*, **32**(5), 179–209, https://doi.org/10.15506/JoG.2011.32.5.179.

Thurm, R.E. 1972. The Lake Manyara emeralds of Tanzania. *Journal of Gemmology*, **13**(3), 98–99, https://doi.org/10.15506/JoG.1972.13.3.98.

Zeug, M., Rodríguez Vargas, A.I. & Nasdala, L. 2016. Spectroscopic study of inclusions in gem corundum from Mercaderes, Cauca, Colombia. *Physics and Chemistry of Minerals*, **44**(3), 221–233, https://doi.org/10.1007/s00269-016-0851-4.

## Large Euclase, Reportedly from Zimbabwe

A vivid blue cushion mixed-cut specimen measuring 15.24 × 9.04 × 9.74 mm and weighing 11.77 ct was submitted to the Gemological Science International (GSI) laboratory in Jaipur, India, for identification. When observed from the crown with the unaided eye in transmitted light, a beautiful blue colour was seen (Figure 11a). However, a side view of the stone revealed it was mostly colourless with a narrow blue zone concentrated along the culet (Figure 11b). The placement of this zone at the culet enhanced the visibility of blue colour throughout the stone when viewed from the crown, similar to the effect that is sometimes seen in faceted blue sapphires.

Gemmological properties of the stone were recorded as follows: RIs—1.650–1.670 (birefringence 0.020); hydrostatic SG—3.08; and inert to both long- and short-wave UV radiation. Observation with the gemmological microscope revealed a cleavage trace (Figure 12) and partially healed fractures ('fingerprints') associated with distinct two-phase inclusions (Figure 13), as well as dotted inclusions and tiny transparent crystals. A strong doubling of facet edges was observed, consistent with the specimen's birefringence and relatively large size.

The stone's properties matched those of euclase, a rarely encountered beryllium aluminium hydroxide silicate with the formula $BeAl(SiO_4)(OH)$. This identification was confirmed with Raman spectroscopy. In addition, infrared spectroscopy yielded a spectrum that was also

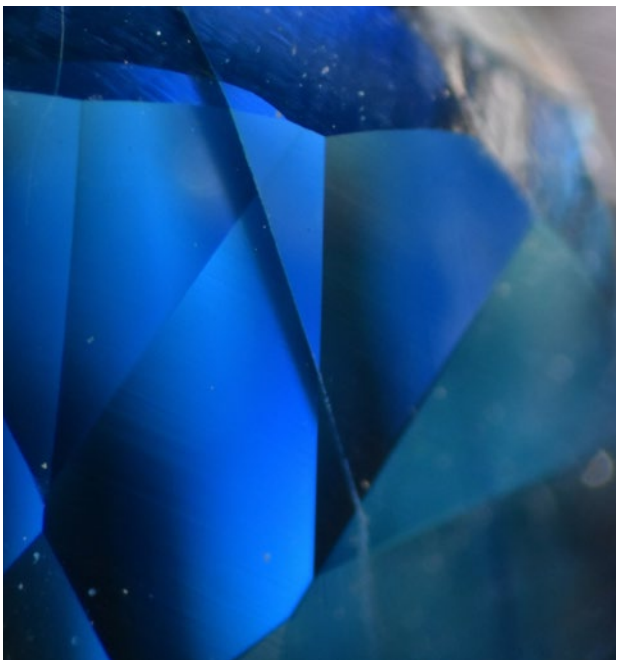

**Figure 12:** A cleavage fracture is seen near the girdle of the euclase. Photomicrograph by Sandeep Kumar Vijay; image width 4.3 mm.

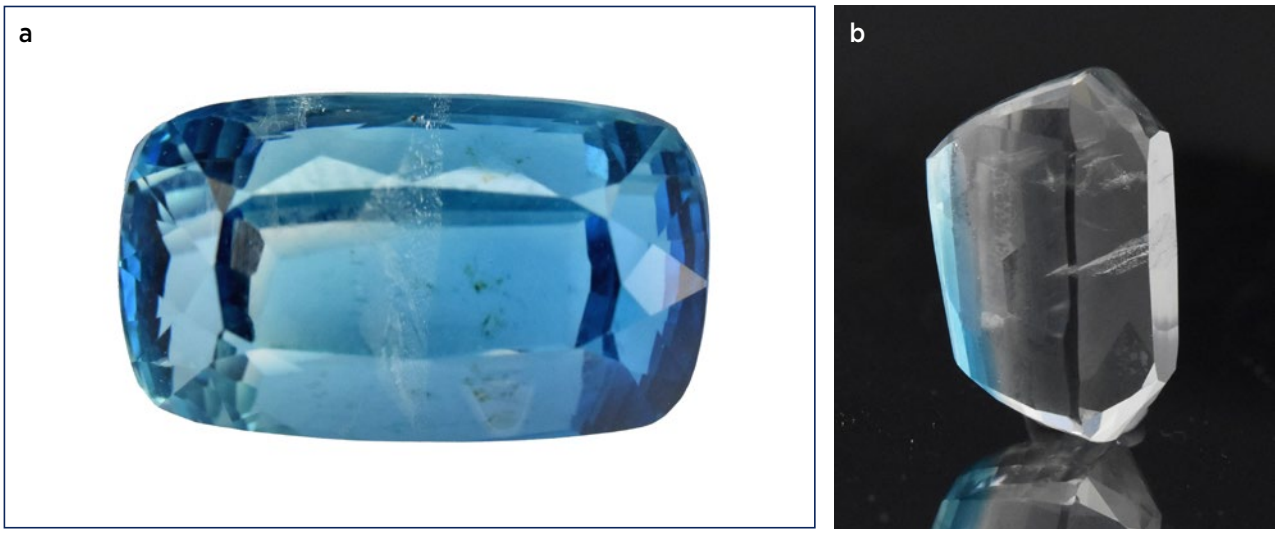


**Figure 11:** This 11.77 ct cushion-mixed cut was identified as euclase. (**a**) It appears blue when viewed face-up, although a side view (**b**) shows the specimen is mostly colourless with a blue zone concentrated along the culet. Photos by Sandeep Kumar Vijay.

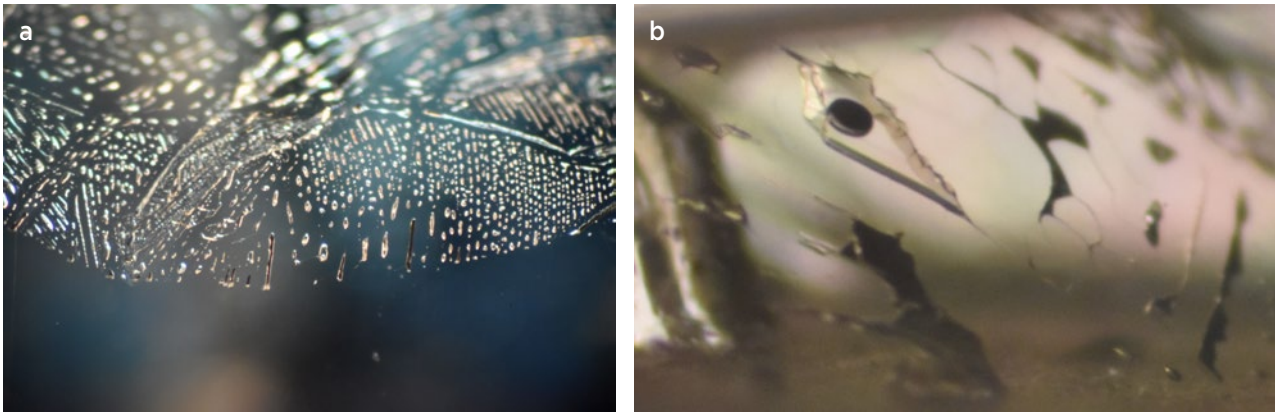


**Figure 13:** The euclase contains (**a**) a partially healed fissure composed of two-phase fluid inclusions arranged in 'fingerprints', and (**b**) larger two-phase inclusions with fluid and gas phases. Photomicrographs by Sandeep Kumar Vijay; image widths 3.2 mm (a) and 4 mm (b).

consistent with the euclase reference in our database. Chemical analysis with EDXRF spectroscopy using a Shimadzu EDX-8000 unit showed traces of Fe, consistent with the blue colouration of euclase (Stocklmayer 1998). The pure blue colour of this specimen, combined with the distinct colourless and blue zoning, is consistent with a Zimbabwe origin (cf. Stocklmayer 1998).

Euclase is rarely faceted as stones weighing more than 2 ct, making this 11.77 ct stone notable. By comparison, the next largest euclase documented in the literature to the authors' knowledge is a greenish blue Colombian stone weighing 9.50 ct (Sauer 2006).

*Meenu Brijesh Vyas FGA (meenuv@gemscience.net)*
*and Gitiksha Khandelwal*
*Gemological Science International*
*Jaipur, India*

### References

Sauer, D.A. 2006. Gem News International: Faceted blue euclase from Colombia. *Gems & Gemology*, **42**(2), 173.

Stocklmayer, S. 1998. Blue euclase from Zimbabwe – A review. *Journal of Gemmology*, **26**(4), 209–218, https://doi.org/10.15506/jog.1998.26.4.209.

## Chromium-bearing Translucent Green Common Opal

Green common opal is best known to gemmologists as 'prase opal', which is coloured by Ni-bearing impurities and has a similar colour appearance to chrysoprase chalcedony. To date, Cr has only rarely been found to be a significant cause of green body colour in opal. Only a few occurrences have been documented: chatoyant stones from Bahia, Brazil (Santiago 2015) and opaque to partially translucent samples from two localities in Turkey (Bank *et al.* 1997; Fritsch *et al.* 2011).

**Figure 14:** These green opals (1.26 ct pear and 1.76 ct oval), reportedly from Peru, were studied for this report and proved to be coloured mainly by $Cr^{3+}$. Photo by K. Feral.

Since 2018, the author has performed a comprehensive search for green opal gems sold online that are potentially coloured by Cr. The stones' reported country of origin was provided by the online retail sellers, but unfortunately no information was available regarding their specific locality, geological setting or production quantity. In early 2022, the author acquired several dark green common opals (e.g. Figure 14), reportedly from Peru, which proved to be the first examples of semi-transparent opal documented to be Cr-bearing and comparable in colour to chrome chalcedony. Multiple translucent opals from other localities obtained since 2018 also proved to contain Cr. These were mostly yellowish green with varying tone and saturation, and

**Figure 15:** Also obtained by the author were translucent yellowish green opals from various stated localities (back row, left to right: 6.31 ct from Turkey, 1.52 ct from Peru and 0.81 ct from Brazil; front row, left to right: 4.45 and 6.17 ct from Ethiopia, and 5.92 ct from Tanzania). Their colour may be due to a combination of Cr, Ni and Fe. Photo by K. Feral.

were represented as being from Peru, Brazil, Turkey, Tanzania and Ethiopia (e.g. Figure 15).

The Peruvian opals ranged from light yellow-green to dark green, with the latter being least common. Gemmological properties obtained for the two Peruvian opals shown in Figure 14 are highlighted in this report. Both gems had an RI of 1.45 and a hydrostatic SG of 2.13, consistent with opal. Under the Chelsea Colour Filter, the pear-shaped gem appeared moderate red and the oval was strong red, suggesting significant Cr content. The stones fluoresced moderate yellow-green to long-wave UV and weak yellow-green to short-wave UV radiation.

No indication of green dye was detected in these gems. Soak tests demonstrated these were not hydrophane opals and thus not easily receptive to dyeing. In addition, careful examination with magnification in immersion (in water) showed no colour concentration along fractures or in scratches or pits, and also no evidence of surface-conformal green colouration. Instead, the green colour was unevenly distributed in cloudy translucent areas of the stones. Soaking them in acetone for 24 hours had no effect on their colour, and no green staining of the acetone was noted either.

UV-Vis-NIR absorption spectroscopy of both opals performed with a GL Gem Spectrometer showed features characteristic of green gem materials coloured by Cr: a transmission window between about 480 and 540 nm in the green region of the spectrum, along with a small, distinct absorption peak in the red at 678 nm specific to $Cr^{3+}$ (Figure 16).

The transition-metal content of the two opals was analysed at Stone Group Labs (Jefferson City, Missouri, USA) using EDXRF spectroscopy. Traces of Cr, Ni and Fe were detected, with Cr as the principal metallic component (Figure 17). No V was detected, nor any radioactive actinides such as U. Both opal samples were diamagnetic, indicating that the combined magnetic susceptibility of Cr, Ni and Fe oxides was below the level of detection by a strong N52 neodymium magnet using the flotation method.

By comparison, the translucent yellowish green opals that the author obtained since 2018 showed varying intensities of pink (rather than red) under the Chelsea Colour Filter, and only a very tiny $Cr^{3+}$ peak at 678 nm in their UV-Vis-NIR spectra. Additionally, EDXRF spectroscopy of selected samples revealed considerably higher Ni and Fe. Consistent with the greater amounts of paramagnetic oxides of these metals, the samples from Ethiopia, Tanzania and Brazil showed weak attraction to the magnet using the flotation method.

The relatively high transparency combined with dark green colouration due mainly to $Cr^{3+}$ in the two characterised stones reportedly from Peru is notable

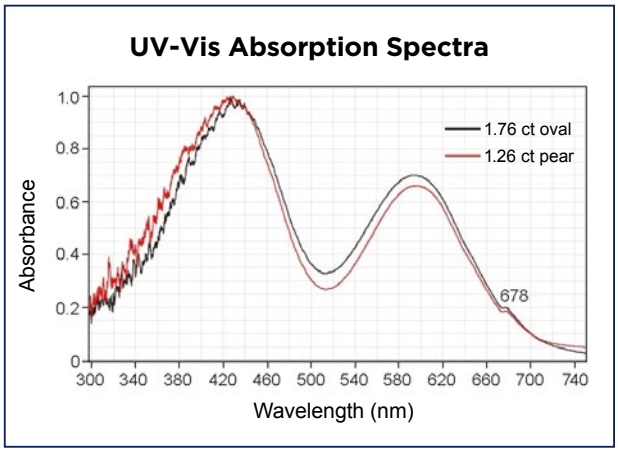


**Figure 16:** UV-Vis absorption spectra of the two green opals from Peru show features indicative of $Cr^{3+}$, including a transmission window in the 480–540 nm region and a small peak at 678 nm. The path length of the beam was approximately 6 mm for the oval cut and 4 mm for the pear-shaped stone.

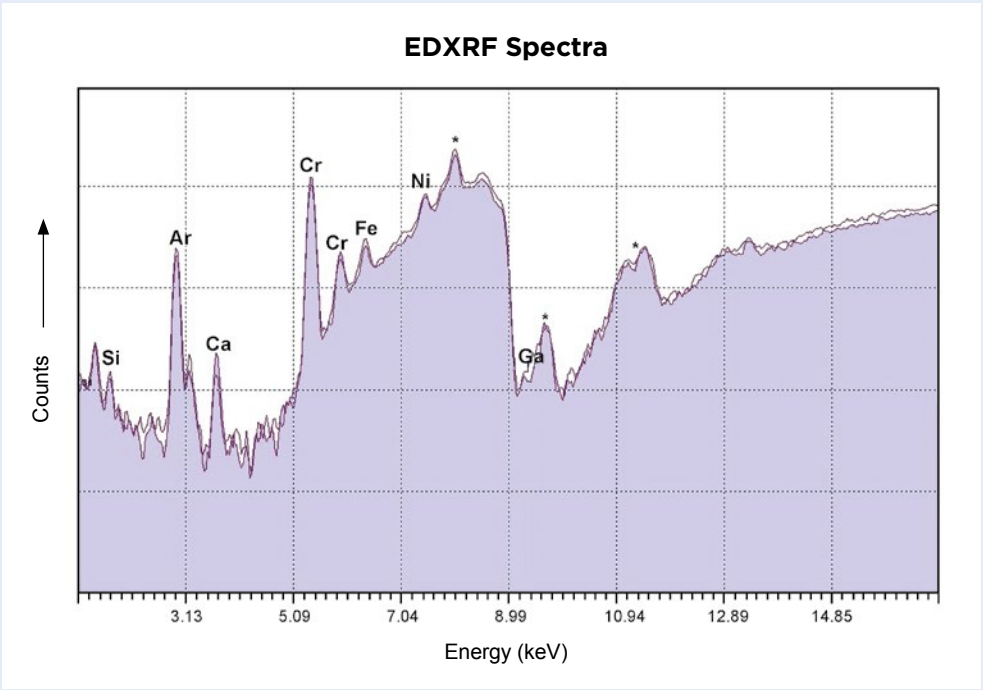


**Figure 17:** EDXRF spectroscopy of the two green opals from Peru shows the presence of Cr as the principal transition metal, with lesser amounts of Ni and Fe. The asterisks are instrumental artefacts and the Ar peak is due to the analysis taking place in air.

for common opal. Because the principal chromophore in these gems was identified as Cr, the author refers to them as 'chrome opal'. However, the yellowish green opals tested for this report were found to be coloured by Cr with additional possible contributions from Ni and Fe, and therefore the author refers to them as 'chromium-bearing green opal' rather than 'chrome opal' or 'prase opal'.

*Acknowledgement*: The author thanks Bear and Cara Williams of Stone Group Labs for providing the EDXRF analyses for this study.

*Kirk Feral (kirk@gemstonemagnetism.com)*
*San Diego, California, USA*

## References

Bank, H., Henn, U. & Milisenda, C.C. 1997. Gemmologie Aktuell: Green opal from Turkey. *Gemmologie: Zeitschrift der Deutschen Gemmologischen Gesellschaft*, **46**(1), 2–3.

Fritsch, E., Rondeau, B. & Kolayli, H. 2011. $Cr^{3+}$-green common opal from Turnali, north-eastern Turkey. *32nd International Gemmological Conference*, Interlaken, Switzerland, 13–17 July, 165–166.

Santiago, C. 2015. *Caracterização Mineralógica e Gemológica das Ocorrências de Opala Verde, Localmente com Efeito Olho-Degato, na Região de Socotó, Bahia*. Bachelor's thesis, Universidade Federal do Rio de Janeiro, Brazil, 79 pp., https://doi.org/10.13140/RG.2.1.4913.5762.

## Blue Sapphires Reportedly from Azad Kashmir

Sapphires from the legendary locality of Kashmir are famous for their attractive velvety appearance and have been pursued by gem connoisseurs for more than a century. The so-called Kashmir sapphires were discovered in 1881 (Atkinson & Kothavala 1983), and initially the locality referred only to the Kashmir valley located in Jammu and Kashmir, a disputed region between India and Pakistan. More recently, some stones from neighbouring areas (e.g. Figure 18) such as the Batakundi-Basil region in the Pakistani-controlled part of Azad Kashmir,

**Figure 18:** These sapphires, reportedly from Azad Kashmir (left 1.77 ct and right 2.22 ct), were examined for this report. Photo by Huixin Zhao.

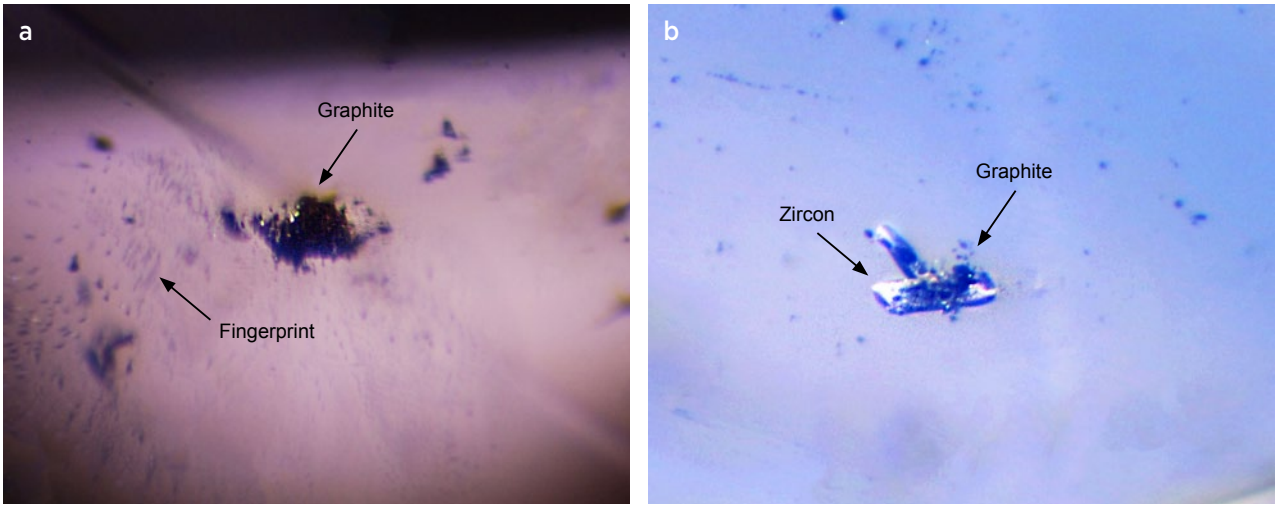


**Figure 19:** Graphite inclusions are present in the sapphires, together with (**a**) 'fingerprints' and (**b**) slightly corroded elongated zircon crystals. Photomicrographs by Huixin Zhao (a, image width 1.9 mm) and Qi Han (b, image width 0.6 mm) in darkfield illumination.

have been referred to as Kashmir sapphires (Pardieu *et al*. 2009; Kiefert 2011 and references therein). This region lies within the border area between Jammu and Kashmir and Pakistan-occupied Gilgit-Baltistan. Because there are significant price differences between the classic Kashmir sapphires and those from elsewhere in this region, it has become necessary to identify their specific origin.

To our knowledge, there are few publications about Azad Kashmir sapphires—which are typically purplish pink to purple—and even fewer on blue sapphires from there. Recently, Guild Gem Laboratories received from trusted dealers two blue sapphires reportedly from Azad Kashmir (Figure 18): a 2.22 ct cushion cut that was bright blue with a slightly violet hue, and a 1.77 ct pear shape of an intense blue colour. Standard gemmological characteristics were consistent with those of sapphire. UV-Vis spectroscopy of the two stones showed features typical of a metamorphic origin.

Microscopic observation revealed numerous black opaque inclusions—confirmed by Raman micro-spectroscopy as graphite (Raman shift at 1580 $cm^{-1}$)—throughout both stones. In addition, we observed two typical inclusion assemblages associated with graphite. One was graphite located at the edge of a 'fingerprint' inclusion (Figure 19a) and another was graphite together with slightly corroded elongated zircon crystals (Figure 19b; main Raman peaks at 1011 and 978 $cm^{-1}$). These inclusion characteristics are consistent with those reported by Pardieu *et al*. (2009) for the purple sapphires of Azad Kashmir. Growth lines (Figure 20a) and alternating blue and purple colour bands (Figure 20b) were present in both samples. Snowflake-like inclusions together with

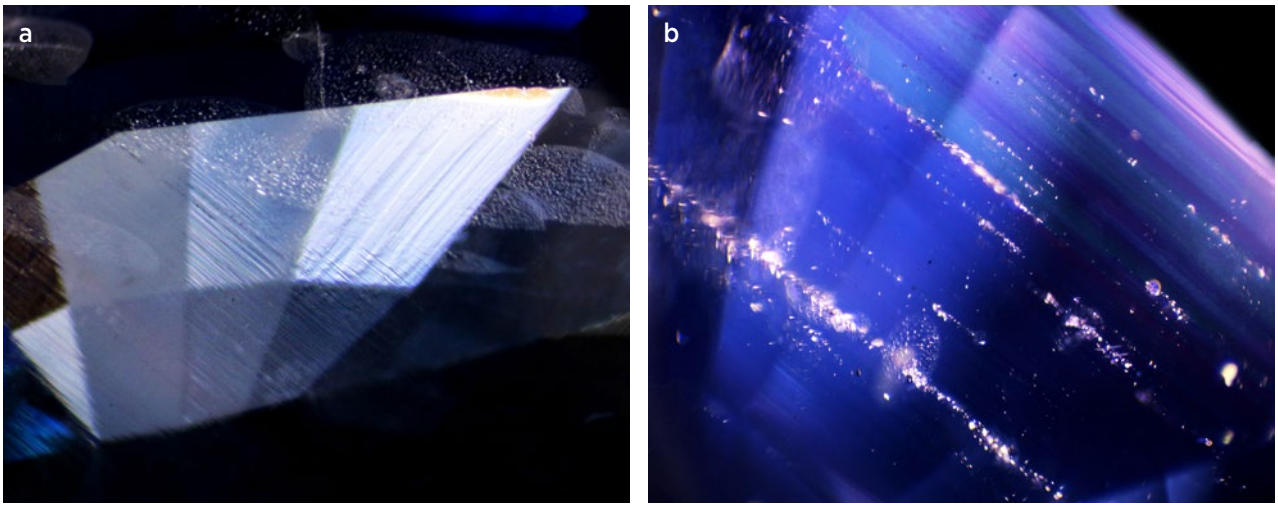


**Figure 20:** Additional internal features in both of the sapphires include (**a**) growth lines and (**b**) snowflake-like inclusions, along with alternating blue and purple colour banding. Photomicrographs by Huixin Zhao; (a) darkfield illumination and image width 1.8 mm, and (b) fibre-optic illumination and image width 5.0 mm.

the white foggy growth bands gave the stones a slightly velvety appearance (again, see Figure 20b).

In classic Kashmir sapphires, isolated zircon crystals without graphite are typical (Schwieger 1990). Many other mineral inclusions have been found in these sapphires, including tourmaline, pargasite, uraninite and plagioclase (Schwieger 1990; Peretti & Peretti 2017; Palke *et al.* 2019), which were absent from the present two samples. Thus, with regard to inclusions, the two stones examined here are similar to the purple sapphires from Azad Kashmir.

It may be possible to differentiate blue sapphires of Azad Kashmir from those of the classic deposits in Jammu and Kashmir on the basis of inclusions. However, additional samples and testing are needed to establish more robust criteria for their separation.

*Tiantian Huang and Yujie Gao*
*(peter.gao@guildgemlab.com)*
*Guild Gem Laboratories*
*Shenzhen, China*

### References

Atkinson, D. & Kothavala, R.Z. 1983. Kashmir sapphire. *Gems & Gemology*, **19**(2), 64–76, https://doi.org/10.5741/gems.19.2.64.

Kiefert, L. 2011. Sapphires from some exotic sources: Azad Kashmir and New Zealand. *32nd International Gemmological Conference*, Interlaken, Switzerland, 13–17 July, 97–99.

Palke, A.C., Saeseaw, S., Renfro, N.D., Sun, Z. & McClure, S.F. 2019. Geographic origin determination of blue sapphire. *Gems & Gemology*, **55**(4), 536–579, https://doi.org/10.5741/gems.55.4.536.

Pardieu, V., Thirangoon, K., Lomthong, P., Saeseaw, S., Thanachakaphad, J. & Du Toit, G. 2009. Sapphires reportedly from Batakundi/Basil area: A preliminary examination and a comparison with rubies and pink sapphires from other deposits in Central Asia. Gemological Institute of America, Bangkok, Thailand, 34 pp., https://www.gia.edu/doc/batakundi_sapphire.pdf, accessed 1 December 2021.

Peretti, A. & Peretti, F. 2017. Identification of sapphires from Madagascar with inclusion features resembling those of sapphires from Kashmir (India). GRS Gemresearch Swisslab AG, Lucerne, Switzerland, 9 pp., https://www.gemresearch.ch/assets/documents/publication-articles/2017_05-kashmir-madagascar-grs-1.pdf, accessed 3 January 2022.

Schwieger, R. 1990. Diagnostic features and heat treatment of Kashmir sapphires. *Gems & Gemology*, **26**(4), 267–280, https://doi.org/10.5741/gems.26.4.267.

## The Serendipity Star Sapphire Aggregate

When referring to Guinness World Records (www.guinnessworldrecords.com), one usually thinks of achievements in sporting events or a personal attribute such as the height of a person, age, etc. *The Guinness Book of World Records* also contains facts on various objects such as outstanding buildings, bridges, etc. Some of the less-featured items include gem materials, minerals or jewellery pieces, such as the world's largest synthetic sapphire or the 'most valuable handbag' by Mouawad that is studded with thousands of diamonds.

In March 2021, an enormous aggregate of sapphire crystals weighing over 500 kg (Figure 21) was discovered in a private mining area of Sri Lanka's Ratnapura District, near Neelagama ('village of blue sapphires'). The specimen was found in secondary deposits that are typical of the area. Named the 'Serendipity Sapphire' (initally 'Queen of Asia'), the specimen was inspected by Sri Lankan gemmologist Gamini Zoysa and featured by several local and international news networks (e.g. https://www.bbc.com/news/world-asia-57981046).

**Figure 21:** The 'Serendipity Sapphire', an aggregate of sapphire crystals discovered in March 2021, weighs 503.2 kg and is recorded in the *Guinness Book of World Records* as the world's largest sapphire cluster. Photo by L. Kiefert.


**Figure 22:** Some of the sapphire crystals in the aggregate attain a length of approximately 10 cm. Photo by Jeanette Fiedler.

In order to achieve the Guinness title of largest sapphire aggregate, the specimen had to be weighed and measured by an independent surveyor (this author) in the presence of two witnesses. It was carefully wrapped for shipping and transported (along with its stand) to Zürich, Switzerland, where the survey took place in the presence of Rimzan Hameed (general manager of Lakmini Gems, Ratnapura), with the remote assistance of the aggregate's owner (Ashan Pavithra Gamage), two witnesses and the staff of a security company.

The wrapped sapphire aggregate was lifted off its stand with a special apparatus and then lowered onto wooden pallets by a forklift, which was also equipped with an internal balance. After recording a weight of 510 kg, the specimen was placed back on its stand, unwrapped and the wrapping material was weighed separately. Subtracting this material's 6.8 kg yielded the aggregate's weight of 503.2 kg (somewhat different from the 510 kg that is commonly reported for it).

To measure the dimensions of the piece, a bubble level and metre sticks were used. Two helpers held staffs vertically at the longest extremities, while the level ensured that the measuring stick was horizontal, and the length was measured. The same process was repeated for the width and depth. The measured values were 101.5 × 78 × 50 cm.

The author then had the opportunity to inspect the piece in more detail. It consisted of white to bluish grey sapphire crystals that were mostly translucent to opaque and up to approximately 10 cm long each (Figure 22). Examination of the crystal boundaries with a UV lamp did not reveal any indications of glue, and the author believes the aggregate is held together naturally and without any obvious human intervention. In order to verify that the sapphires were not simply mounted on the surface, the owners drilled a hole to the centre of the aggregate from its base so an endoscopic exam could be performed (Figure 23). This showed that sapphire crystals extended to the centre of the aggregate.

Some crystals in the aggregate were polished in place to reveal their internal features (consisting of iron staining and acicular inclusions that are probably rutile), and one of these was removed and cut into an attractive star sapphire of approximately 40 ct (Figure 24). In addition, Leelawathanasuk *et al*. (2022) mentioned that a few crystals were polished into cabochons by the owner, and they also showed good asterism. Two samples extracted from the aggregate (one untreated and one heated, which showed an attractive blue colour) were studied by those authors, and microscopic examination revealed inclusions consisting of rutile needles, 'fingerprints', minute particles and dark crystals of uraninite.

As for the genesis of such an aggregate, only speculations can be made at this point. It is possible that the sapphires came from a single formation that was eroded

**Figure 23:** Endoscopic examination of a hole drilled into the aggregate reveals that the sapphire crystals extend all the way to the centre of the specimen. Photo by L. Kiefert.

**Figure 24:** This star sapphire cabochon (approximately 40 ct; 20.69 × 17.12 × 11.55 mm) was fashioned from a crystal removed from the aggregate. Photo by L. Kiefert.

and then deposited at the location where they were found. This could explain the rather uniform appearance of the corundum. Another scenario could be an accretion over centuries of so-called 'geuda' sapphires that used to be discarded long ago during mining, since it was discovered only relatively recently (in the 1970s) that such sapphires could be heat treated. Time and weather might then have cemented the crystals together. Leelawathanasuk *et al*. (2022) reported that 'acid drop testing showed effusive bubbles, indicating the [probable infilling of] carbonate matrix'. Regardless of how this aggregate formed, it is certainly a unique piece and rightfully deserves to be included in the *Guinness Book of World Records*.

*Acknowledgements*: The author thanks Ashan Pavithra Gamage and Rimzan Hameed for the opportunity to inspect the sapphire aggregate, and also Jeanette Fiedler (DDI Foundation German Diamond Institute, Pforzheim, Germany) for help with measuring and collecting data.

*Dr Lore Kiefert FGA (info@gemlabhelp.com)*
*Gemmology Consulting*
*Heidelberg, Germany*

### Reference

Leelawathanasuk, T., Promwongnan, S., Wathanakul, P., Pisutha-Arnond, V., Atichat, W. & Zoysa, G. 2022. New giant gem corundum boulder from Sri Lanka. *Gemmology Today*, March, 50–53.

## Photochromic Scapolite from Baffin Island, Canada

Recently, gem miner and dealer Brad Wilson (Alpine Gems, Kingston, Ontario, Canada) provided for examination two faceted photochromic ('tenebrescent') scapolites from the Kimmirut area of Baffin Island, Nunavut, Canada. The stones were mined between 2004 and 2008 from a locality about 5 km north of the Beluga pit, which is where most of the gem corundum from this area has been found (B. Wilson, pers. comm. 2022).

The two stones consisted of a 0.56 ct round brilliant and a 0.77 ct triangular cut (Figure 25a). The photochromism was seen as a slight but noticeable change from brownish grey to bluish grey after about two minutes of exposure to short-wave UV radiation (Figure 25b). The colour reverted extremely rapidly, within about 3 s

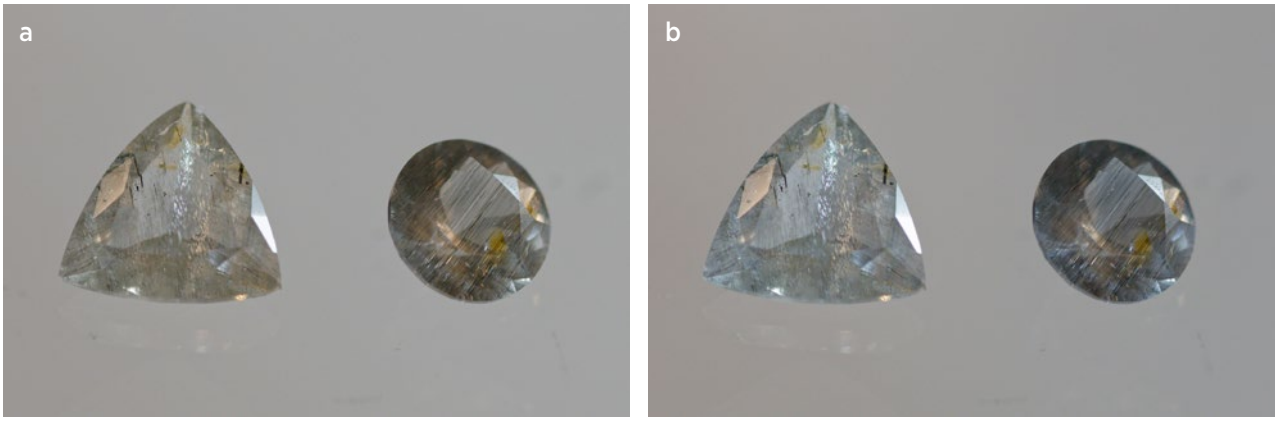


**Figure 25:** These scapolite gemstones (0.77 ct triangular cut and 0.56 ct round brilliant) from Baffin Island, Canada, are (**a**) normally brownish grey and (**b**) turn slightly bluer after about two minutes of exposure to short-wave UV radiation. This photochromism decays so fast (about 3 s) that it is challenging to photograph. Photos by Philippe Deniard.

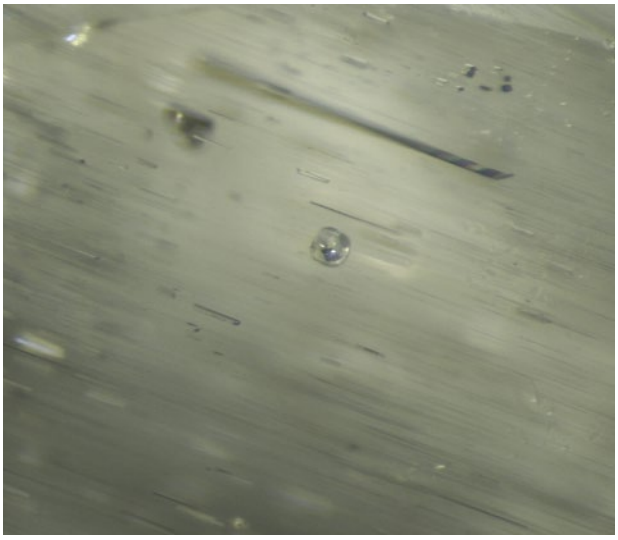

**Figure 26:** Parallel fluid inclusions (each containing a small bubble) are abundant in the photochromic scapolite. The inclusion in the centre is a larger negative crystal with many faces, in which a black daughter crystal is visible in addition to a bubble. Photomicrograph by E. Fritsch; image width 1.7 mm.

after the UV lamp was turned off. Thus, recording the transient colour state with UV-Vis spectroscopy was not possible. The RIs of 1.540–1.560 and SG value of 2.61–2.63 indicate their composition is mostly marialite, with 20–40% meionite (cf. Pradat 2012). This identity was confirmed by Raman spectroscopy using a Jobin Yvon T64000 dispersive spectrometer, equipped with a 514 nm $Ar^+$ green laser and 4 $cm^{-1}$ resolution. A best fit was obtained using the CrystalSleuth software with marialite R070689 in the RRUFF database (https://rruff.info), which is 34% meionite. According to the marialite-dominant composition of the scapolite, the main species in the 'cages' of the atomic structure belong to the $Na_4Cl$ group (see, e.g., Blumentritt & Fritsch 2022).

Both stones exhibited bright yellow-orange fluorescence to long-wave UV radiation, with a weaker reaction to short-wave UV. This well-known luminescence is due to the $S_2^-$ ion (Blumentritt *et al*. 2020 and references therein) and makes scapolite a favourite of fluorescent-mineral collectors.

The two stones contained many parallel growth tubes of various lengths, some of which were flattened (lath-looking; Figure 26). Also present were negative crystals of different sizes and shapes. Most looked like tubes, while other, generally larger ones had many small faces. They contained a small bubble (less than 10% of the volume) and a tiny black daughter crystal (again, see Figure 26). The materials contained in these inclusions were too small to be identified by Raman spectroscopy.

Photochromic scapolite is well known from Afghanistan (McClure *et al*. 2005; Allen *et al*. 2014). It also has a marialite-dominant composition, but exposure to short-wave UV radiation produces a distinct change from colourless to blue, with a much slower decay time of about 120 s (Blumentritt 2021). Nevertheless, there is no reason to believe that the cause of the photochromism is different in samples from the two localities. The change of colour has been attributed to ionisation of a chlorine vacancy, possibly related to the presence of sulphur as an impurity (Blumentritt 2021). Because chlorine is involved, this phenomenon should be observable only when Cl-containing marialite dominates the scapolite solid solution.

*Dr Emmanuel Fritsch FGA*
*(emmanuel.fritsch@cnrs-imn.fr)*
*and Cassandre Moinard*
*IMN-CNRS and*
*University of Nantes, France*

## References

Allen, T., Renfro, N. & Nelson, D. 2014. Gem News International: Tenebrescent irradiated scapolite. *Gems & Gemology*, **50**(1), 91–92.

Blumentritt, F. 2021. *Matériaux à propriétés ciblées par minéralomimétisme : le photochromisme de la sodalite et de la scapolite* [*Materials with properties targeted by mineralomimetism: Photochromism of sodalite and scapolite*]. PhD thesis, University of Nantes, France, 251 pp.

Blumentritt, F. & Fritsch, E. 2022. Photochromism and photochromic gems: A review and some new data (part 2). *Journal of Gemmology*, **38**(1), 80–92, https://doi.org/10.15506/jog.2022.38.1.80.

Blumentritt, F., Latouche, C., Morizet, Y., Caldes, M.-T., Jobic, S. & Fritsch, E. 2020. Unravelling the origin of the yellow-orange luminescence in natural and synthetic scapolites. *Journal of Physical Chemistry Letters*, **11**(12), 4591–4596, https://doi.org/10.1021/acs.jpclett.0c00712.

McClure, S.F., Rossman, G.R., Shigley, J.E. & Laurs, B.M. 2005. Gem News International: Tenebrescent scapolite from Afghanistan. *Gems & Gemology*, **41**(3), 269–271.

Pradat, T. 2012. Scapolite : de la marialite à la méionite [Scapolite: From marialite to meionite]. *Revue de Gemmologie A.F.G.*, No. 181, 11–17.

# SYNTHETICS AND SIMULANTS

## Melee-Sized Colourless HPHT-Grown Synthetic Diamond with Red Fluorescence

Melee-sized colourless high-pressure, high-temperature (HPHT)-grown synthetic diamonds are commonly screened by their bluish green fluorescence and phosphorescence. The phosphorescence is due to boron impurities, and provides an effective means to detect and screen these synthetics. However, during the September 2018 Hong Kong gem shows, it was reported that the phosphorescence of HPHT-grown synthetic diamonds may disappear after irradiation (without altering their body colour). Since then, a few samples showing such characteristics have been encountered in the National Gemstone Testing Center's (NGTC) laboratories in China.

Recently, NGTC's Shenzhen laboratory analysed a large batch of colourless melee containing one sample (0.008 ct) that showed red fluorescence in the GV5000 diamond identification instrument. Fourier-transform infrared (FTIR) spectroscopy showed it was type II. Further examination using a DiamondView instrument revealed a fluorescence pattern indicating an HPHT-grown synthetic diamond. This was visible when the sample was observed from both the crown and pavilion (Figures 27a and 27b, respectively), although the growth patterns were obscured somewhat by the strong red fluorescence. In addition, very weak blue phosphorescence was observed after the excitation energy of the DiamondView was adjusted to maximum (Figure 27c).

Photoluminescence spectroscopy with 325 nm excitation showed peaks at 484 and 488 nm (Figure 28a). The 484 nm emission system is associated with Ni-related optical centres (Collins *et al.* 1990). The use of 532 nm excitation showed radiation-related defects atypical of HPHT-grown synthetic diamond, including the $NV^-$ centre (637.2 nm; responsible for the strong red fluorescence) and the GR1 centre (doublet at 741 and 744 nm); also present were B-related defects at 648.3 and 776 nm (Figure 28b). Additionally, 785 nm excitation produced sharp peaks at 882.3 and 884.0 nm due to $Ni^+$, and numerous emission peaks from unknown optical defects were present in the 800–900 nm range (Figure 28c).

Although colourless synthetic diamonds with red fluorescence are more likely to be grown by chemical vapour deposition, the present sample was identified as an HPHT-grown synthetic, and the photoluminescence features indicated that it had been treated by irradiation and low-temperature annealing. The typical bluish green phosphorescence of HPHT-grown synthetic diamonds is caused by boron (with a phosphorescence

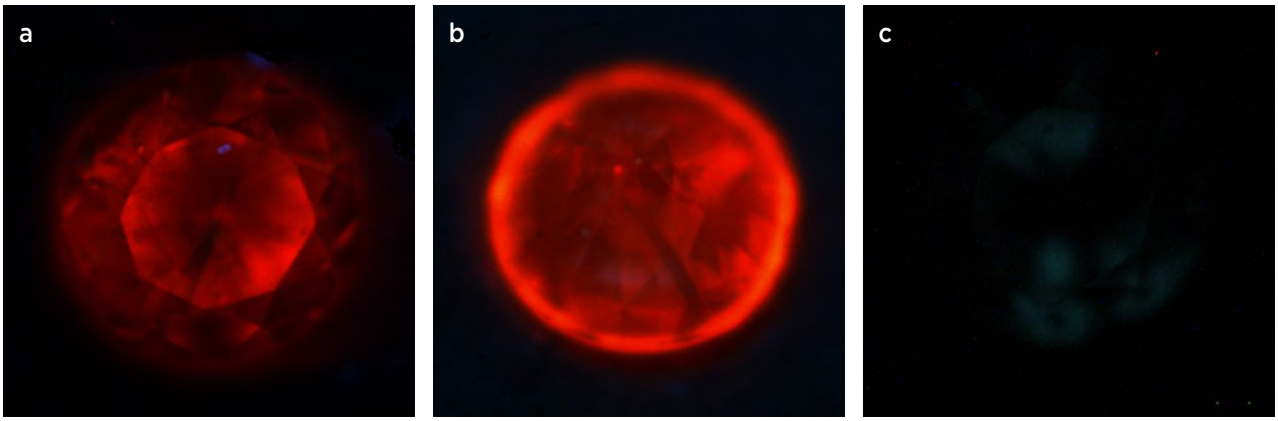


**Figure 27:** This 0.008 ct colourless HPHT-grown synthetic diamond shows strong red fluorescence when observed with the DiamondView instrument due to $NV^-$ centres, and is seen here (**a**) from the crown and (**b**) from the pavilion. (**c**) After the excitation energy was increased to maximum, the sample emitted weak blue phosphorescence. Photos by W. Zhu.

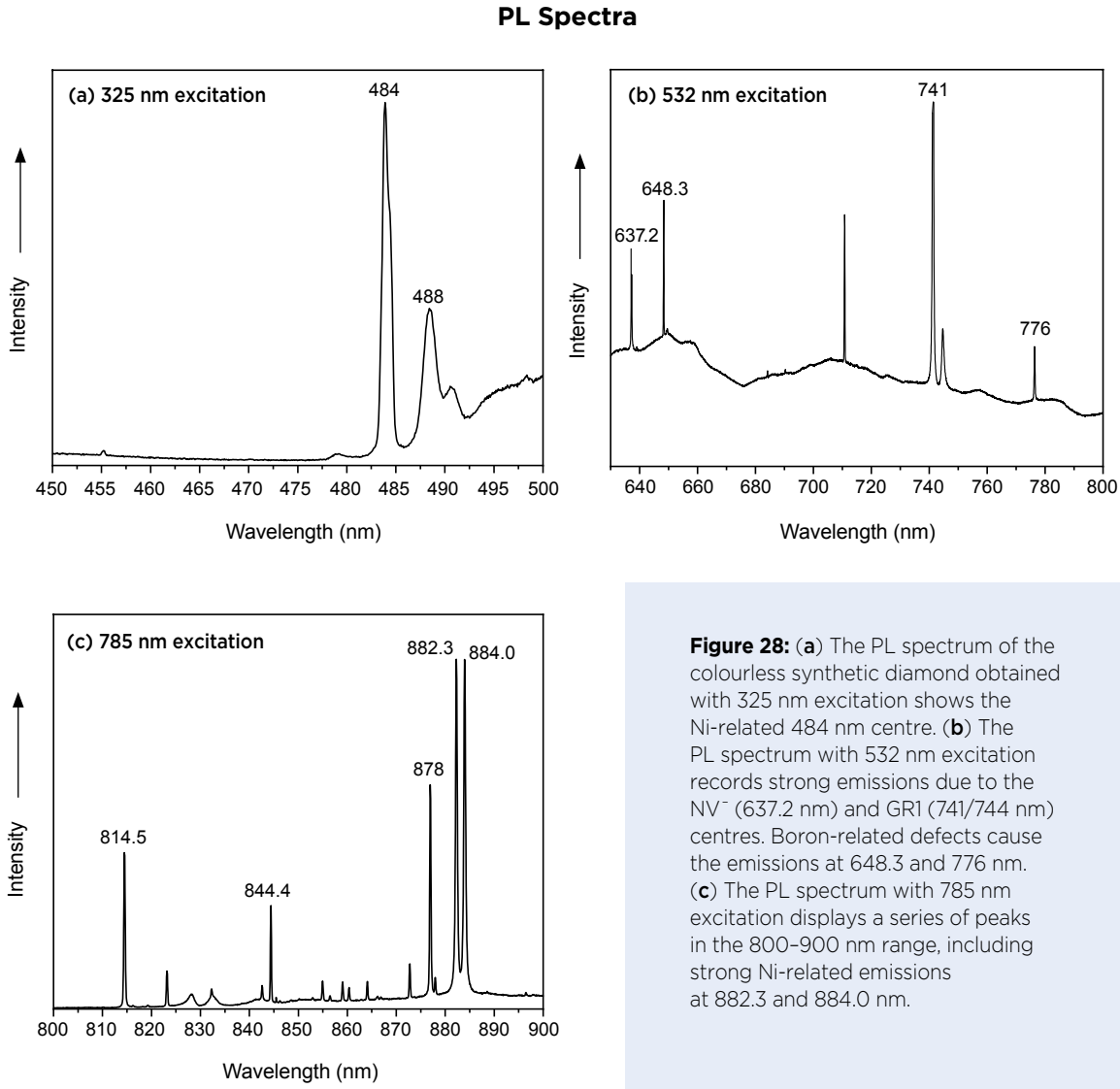


**Figure 28:** (**a**) The PL spectrum of the colourless synthetic diamond obtained with 325 nm excitation shows the Ni-related 484 nm centre. (**b**) The PL spectrum with 532 nm excitation records strong emissions due to the $NV^-$ (637.2 nm) and GR1 (741/744 nm) centres. Boron-related defects cause the emissions at 648.3 and 776 nm. (**c**) The PL spectrum with 785 nm excitation displays a series of peaks in the 800–900 nm range, including strong Ni-related emissions at 882.3 and 884.0 nm.

band centred at 500 nm; Eaton-Magaña & Lu 2011), and no differences in phosphorescence have been observed between irradiated and non-irradiated diamonds (Eaton-Magaña & Ardon 2020). The mechanism of the effect of irradiation on the fluorescence of synthetic diamonds is still unknown.

*Wenfang Zhu*
*(zhuwf@ngtc.com.cn),*
*Xiaoxia Zhu, Zhonghua Song*
*and Huihuang Li*
*NGTC, Shenzhen*
*and Beijing, China*

## References

Collins, A.T., Kanda, H. & Burns, R.C. 1990. The segregation of nickel-related optical centres in the octahedral growth sectors of synthetic diamond. *Philosophical Magazine B*, **61**(5), 797–810, https://doi.org/10.1080/13642819008207562.

Eaton-Magaña, S. & Lu, R. 2011. Phosphorescence in type IIb diamonds. *Diamond and Related Materials*, **20**(7), 983–989, https://doi.org/10.1016/j.diamond.2011.05.007.

Eaton-Magaña, S. & Ardon, T. 2020. Spatial distribution of defects in natural type IIb diamond after irradiation and annealing. *Diamond and Related Materials*, **109**, article 108034 (12 pp.), https://doi.org/10.1016/j.diamond.2020.108034.

## Manufactured Silica Glass Sold as Rock-Crystal Balls

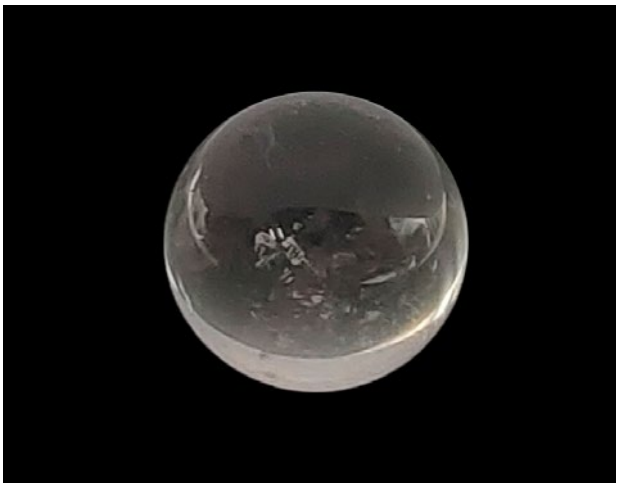

**Figure 29:** This sphere (3 cm in diameter) is typical of material recently offered on the Chinese market as rock-crystal balls. Photo by D. Zhou.

In recent years, a new variety of so-called *rock-crystal ball* has become popular on the Chinese market (Figure 29). Most of these spheres are 3–5 cm in diameter, with a few larger than 10 cm. They appear visually similar to rock-crystal quartz, but their true nature had not been established. Therefore, five samples (3–5 cm diameter) were purchased and gemmologically characterised so they could be properly identified.

The spot RI of each sample was around 1.46, and their hydrostatic SG value was in the range of 2.19–2.20; both of these properties are much lower than those of quartz (RI = 1.54 and SG = 2.66). Viewed with magnification, the floc-like inclusions visible to the unaided eye were found to consist of small gas bubbles (Figure 30a). When examined between crossed polarisers, some birefringent crystallites were also observed (Figure 30b). All of these properties are consistent with those of manufactured silica glass (also called *quartz glass*, *fused quartz* or, more generally, *fused silica*; see Shipley 1948; Hench & Vasconcelos 1990; O'Donoghue 2006; De Jong *et al.* 2011).

Infrared absorption spectra were recorded using a Thermo Nicolet 6700 infrared spectrometer. In the 400–2000 $cm^{-1}$ range, the spectra showed features similar to those found in opal (Figure 31). However, in the 2000–6000 $cm^{-1}$ range were bands at about 3660 and 4520 $cm^{-1}$ that are different from the hydrous features in opal and quartz (Heaney *et al.* 1994; Sodo *et al.* 2016; Jollands *et al.* 2020), but are similar to IR bands previously documented in manufactured silica glass (Brückner 1970).

EDXRF chemical analysis showed that the samples were mainly composed of Si (94–97 wt.% $SiO_2$) along with minor Mg (3–5 wt.% MgO). We infer that Mg was added during the manufacturing process, since it is not a common impurity in the quartz typically used as a starting material for manufacturing silica glass.

Powder X-ray diffraction (XRD) analysis showed diffuse peaks indicating the material is mainly amorphous, but it also revealed one diffraction peak for quartz (Figure 32), which may correspond to the crystallites observed with the microscope (again, see Figure 30b).

Based on our investigation, we infer that the material used to manufacture the 'rock-crystal balls' was produced artificially by the high-temperature melting of natural or synthetic quartz powder. The high-temperature process led to an amorphous state of $SiO_2$, as well as the anomalous hydrous bands recorded in the infrared spectra.

In addition to colourless, such 'crystal balls' are also

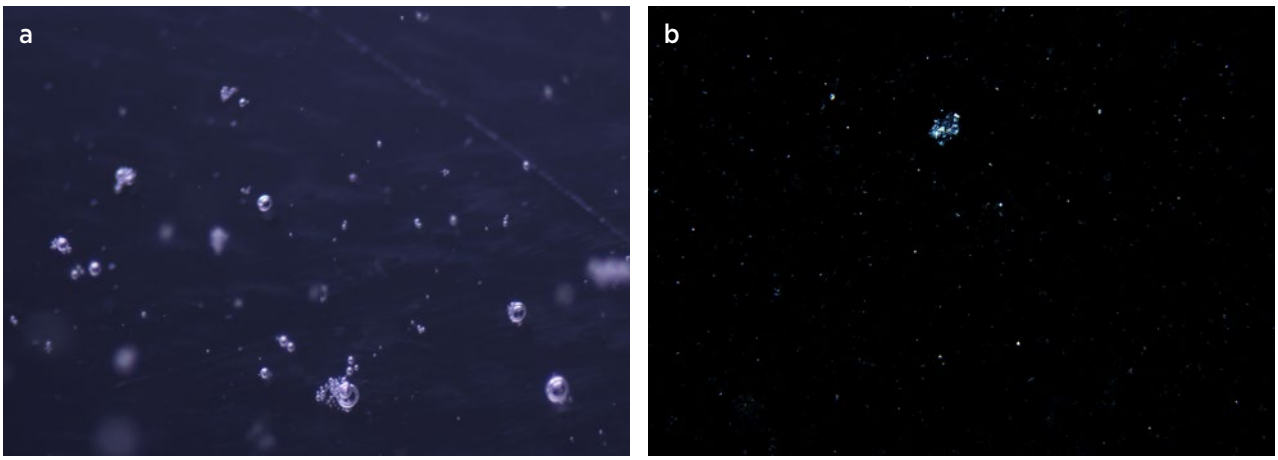


**Figure 30:** (**a**) Eye-visible floc-like inclusions in the spheres consist of small gas bubbles, sometimes in clusters. (**b**) Birefringent crystallites are visible between crossed polarisers. Photomicrographs by D. Zhou; magnified (a) 30× and (b) 200×.

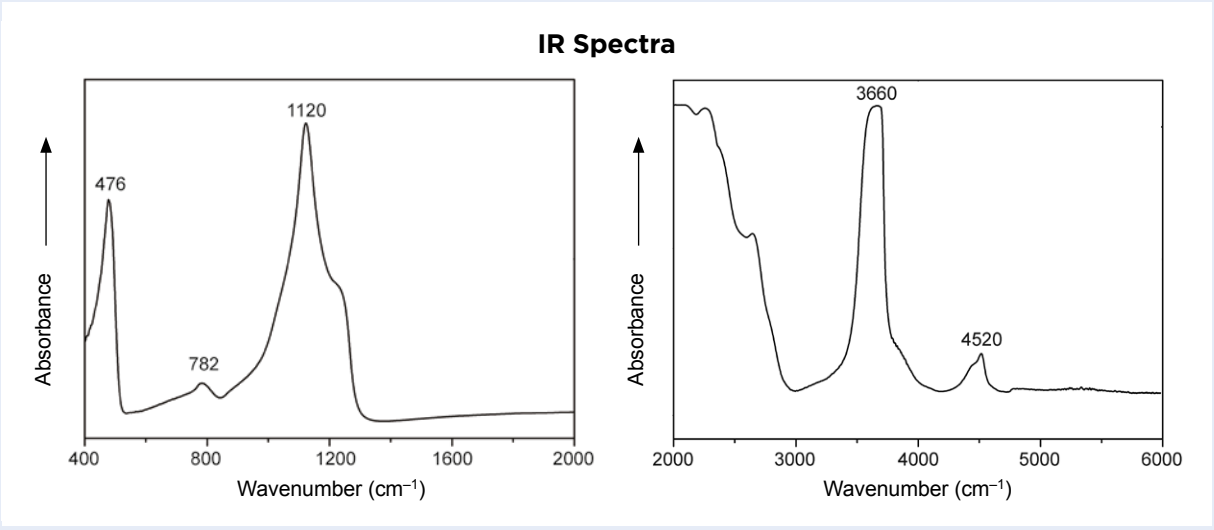


**Figure 31:** (**a**) In the 400–2000 cm$^{-1}$ range, a typical IR absorption spectrum of the sphere material shows bands at 476, 782 and 1120 cm$^{-1}$, similar to the spectrum of opal. (**b**) However, in the 2000–6000 cm$^{-1}$ range, the IR spectrum contains bands at 3660 and 4520 cm$^{-1}$, which are different from features recorded in both quartz and opal in this range.

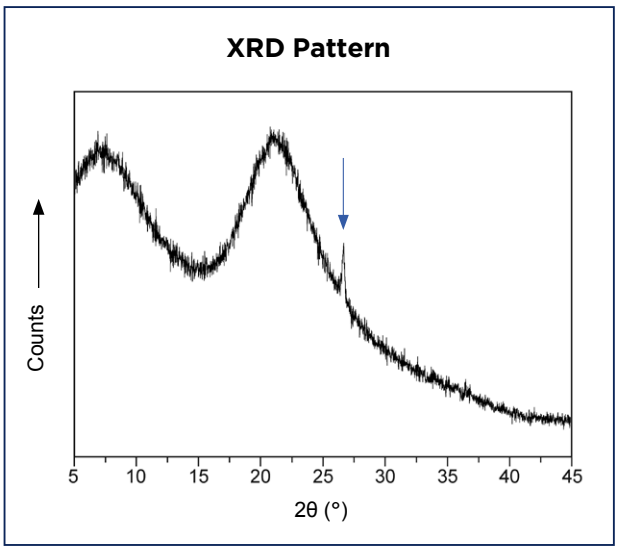


**Figure 32:** The powder XRD pattern of the sphere material shows broad peaks indicating that it is mainly amorphous, along with one diffraction peak associated with quartz (see arrow).

available on the internet in various colours such as red, blue and pale yellow. They are sometimes offered as 'smelting stones', 'smelt quartz', etc., and are available as a wide range of objects in addition to spheres (e.g. obelisks and even specimens shaped to look like natural quartz crystals).

*Danyi Zhou (zhoudy@ngtc.com.cn),*
*Dr Taijin Lu, Jieran Lv and Zhonghua Song*
*National Gemstone Testing Center*
*Beijing, China*

## References

Brückner, R. 1970. Properties and structure of vitreous silica. I. *Journal of Non-Crystalline Solids*, **5**(2), 123–175, https://doi.org/10.1016/0022-3093(70)90190-0.

De Jong, B.H.W.S., Beerkens, R.G.C., van Nijnatten, P.A. & Le Bourhis, E. 2011. Glass, 1. Fundamentals. *In*: *Ullmann's Encyclopedia of Industrial Chemistry*. Wiley—VCH Verlag GmbH & Co. KGaA, Weinheim, Germany, 1–54, https://doi.org/10.1002/14356007.a12_365.pub3.

Heaney, P.J., Prewitt, C.T. & Gibbs, G.V. (eds) 1994. *Silica: Physical Behavior, Geochemistry, and Materials Applications*. Reviews in Mineralogy, Vol. 29, Mineralogical Society of America, Washington DC, USA, xviii + 606 pp., https://doi.org/10.1515/9781501509698.

Hench, L.L. & Vasconcelos, W. 1990. Gel-silica science. *Annual Review of Materials Science*, **20**(1), 269–298, https://doi.org/10.1146/annurev.ms.20.080190.001413.

Jollands, M.C., Blanchard, M. & Balan, E. 2020. Structure and theoretical infrared spectra of OH defects in quartz. *European Journal of Mineralogy*, **32**(3), 311–323, https://doi.org/10.5194/ejm-32-311-2020.

O'Donoghue, M. 2006. *Gems: Their Sources, Descriptions and Identification*. Butterworth-Heinemann, Oxford, xxix + 873 pp.

Shipley, R.M. 1948. *Dictionary of Gems and Gemology*. Gemological Institute of America, Santa Monica, California, USA, xi + 261 pp.

Sodo, A., Casanova Municchia, A., Barucca, S., Bellatreccia, F., Della Ventura, G., Butini, F. & Ricci, M.A. 2016. Raman, FT-IR and XRD investigation of natural opals. *Journal of Raman Spectroscopy*, **47**(12), 1444–1451, https://doi.org/10.1002/jrs.4972.

## An Unusual Pink Synthetic Opal

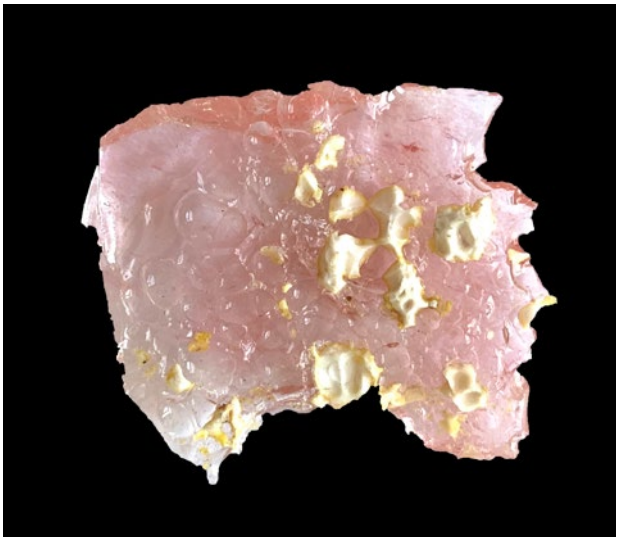

**Figure 33:** This 0.76 g pink sample was identified as synthetic opal. The pale yellow and white surface incrustations were found to be cristobalite. Photo by J. Wu.

The National Gemstone Testing Center (NGTC) laboratory in Shenzhen, China, recently received for identification a rough pink sample weighing 0.76 g (Figure 33). Its RI of approximately 1.42 and hydrostatic SG of approximately 2.18 fell within the range for opal. The sample showed weak-to-moderate and strong yellow fluorescence to long- and short-wave UV radiation, respectively. There was no phosphorescence. Its identity as opal was confirmed by Raman spectroscopy (Figure 34a), and further Raman analyses of some white and yellow incrustations on the specimen's surface consistently showed two main peaks at 427 and 219 $cm^{-1}$ which, according to the RRUFF database, matched well with cristobalite. Its FTIR spectrum (Figure 34b) revealed characteristics shown by some synthetic opals, with bands at 4523, 3674, 2662 and 2266 $cm^{-1}$ (cf. Qi *et al.* 2006; Bhandari & Choudhary 2010). Chemical analysis by EDXRF spectroscopy revealed the expected major amount of Si, along with traces of Na, Mg, K, Ca and Cu.

Microscopic examination revealed fine particles and numerous tiny spherical and ellipsoidal inclusions with various shades of pink-to-red colour and a strong metallic lustre (Figure 35). Several micro-sized particles were observed that ranged up to 140 µm in maximum dimension. The majority of smaller-sized fine particles could not be observed clearly. Fortunately, several of these inclusions were exposed at the surface, and EDXRF chemical analysis revealed that Cu was the major component.

An absorption spectrum of the synthetic pink opal collected in the UV-Vis range showed a broad band centred around 570 nm (Figure 36). This is similar to the absorption feature caused by $Cu_2O$ nano-spheres, which can produce various colours according to their morphology (e.g. cube, microsphere, hollow sphere and core-shell; see Lu *et al.* 2005; Ma *et al.* 2010). Therefore, we suggest that dispersed particles of copper oxides (mainly $Cu_2O$) could be the main cause of the pink colour in this synthetic opal. By contrast, previous studies have

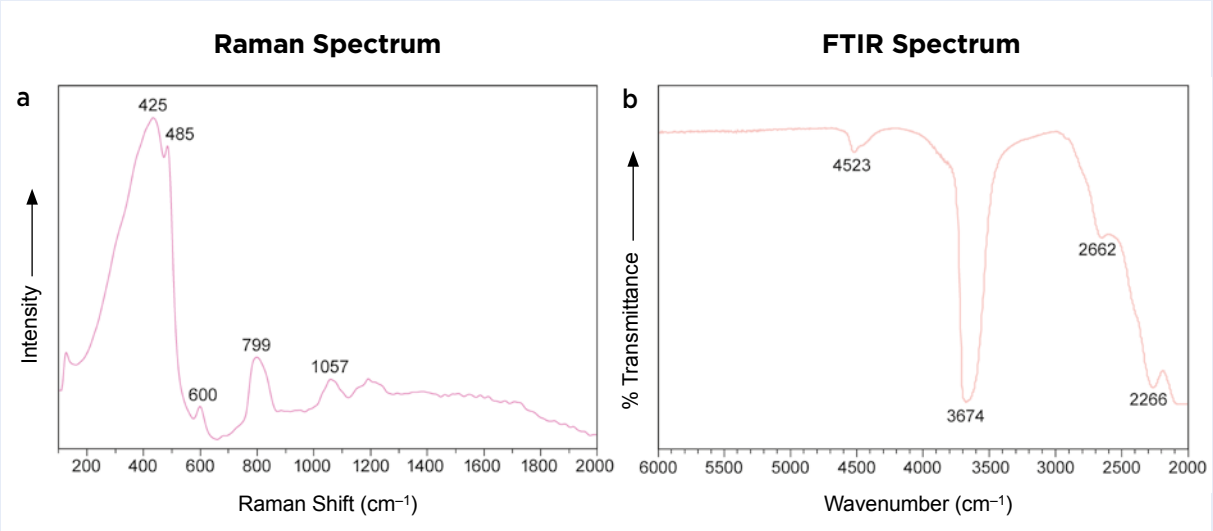


**Figure 34:** (**a**) Raman spectroscopy of the pink sample in Figure 33 confirmed its identity as opal. (**b**) The FTIR transmission spectrum reveals features consistent with synthetic opal.

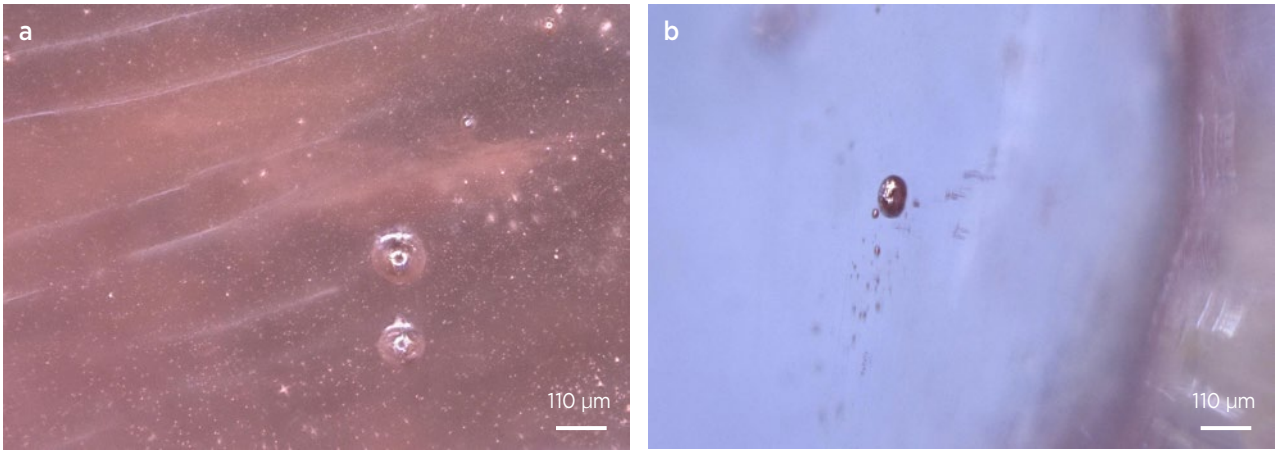


**Figure 35:** Scattered micro-inclusions that are (**a**) spherical and (**b**) ellipsoidal in the synthetic opal show pink colour and a metallic lustre. Fine particles are also present (a). Photomicrographs by J. Wu.

shown that the pink colour of natural opal is caused by organic molecules in palygorskite impurities, rather than $Cu_2O$ (Gaillou *et al*. 2008).

The colour mechanism of this pink synthetic opal may be similar to that of natural fire opal, which is caused by dispersed nano-inclusions (Li *et al*. 2016; Wu *et al*. 2022). This is the first time the authors have encountered pink synthetic opal.

*Jinlin Wu (wujl@ngtc.com.cn),*
*Hong Ma and Huihuang Li*
*NGTC, Shenzhen, China*

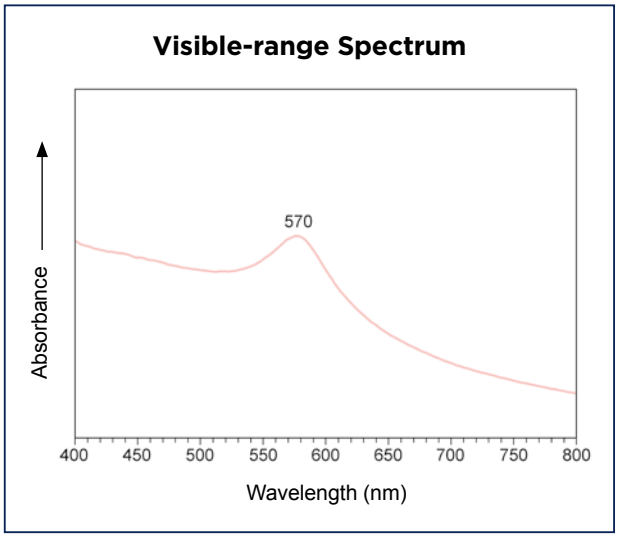


**Figure 36:** The visible-range spectrum of the synthetic opal shows a broad peak centred at 570 nm consistent with the presence of $Cu_2O$, a possible cause of the pink colour.

## References

Bhandari, R. & Choudhary, G. 2010. Update on Mexifire synthetic fire opal. *Gems & Gemology*, **46**(4), 287–290, https://doi.org/10.5741/gems.46.4.287.

Gaillou, E., Delaunay, A., Rondeau, B., Bouhnik-le-Coz, M., Fritsch, E., Cornen, G. & Monnier, C. 2008. The geochemistry of gem opals as evidence of their origin. *Ore Geology Reviews*, **34**(1–2), 113–126, https://doi.org/10.1016/j.oregeorev.2007.07.004.

Li, J., Yin, K., Han, W. & Hong, H. 2016. Mineralogical characteristics and cause of color of a red fire opal. *Journal of Computational and Theoretical Nanoscience*, **13**(3), 2082–2086, https://doi.org/10.1166/jctn.2016.5159.

Lu, C., Qi, L., Yang, J., Wang, X., Zhang, D., Xie, J. & Ma, J. 2005. One-pot synthesis of octahedral $Cu_2O$ nanocages via a catalytic solution route. *Advanced Materials*, **17**(21), 2562–2567, https://doi.org/10.1002/adma.200501128.

Ma, L., Li, J., Sun, H., Qiu, M., Wang, J., Chen, J. & Yu, Y. 2010. Self-assembled $Cu_2O$ flowerlike architecture: Polyol synthesis, photocatalytic activity and stability under simulated solar light. *Materials Research Bulletin*, **45**(8), 961–968, https://doi.org/10.1016/j.materresbull.2010.04.009.

Qi, L., Huang, Y. & Yin, K. 2006. Gemmological characteristics and play of colour effect of artificial opals from Russia. *Journal of Gems & Gemmology*, **8**(3), 10–15 (in Chinese with English abstract).

Wu, J., Ma, H., Ma, Y., Ning, P., Tang, N. & Li, H. 2022. Comparison of natural and dyed fire opal. *Crystals*, **12**(3), 322–336, https://doi.org/10.3390/cryst12030322.

## Quench-Fractured Bicoloured Synthetic Quartz: A Doubly Treated Gem Material

The application of various treatments to enhance the quality and attractiveness of gems has a long history. These days, however, such enhancements are not limited to natural stones. Treatments are increasingly being applied to synthetics, either to create desired properties not produced by synthesis alone or to give the sample a more natural appearance. Some prime examples are synthetic star rubies and sapphires that are produced by a factory in Bangkok, Thailand, through titanium diffusion followed by heating and slow cooling (Wanthanachaisaeng *et al.* 2022).

An interesting new development is 'texture-treated' synthetic quartz. This is commonly made from bicoloured material (e.g. Figure 37) that is hydrothermally grown as monochrome quartz, and then the colour of half the sample is changed by heating that portion in air (for example, simply by putting stones halfway into hot sand). However, treaters are reluctant to disclose details of their enhancement procedures. In our experiments, we found that heating synthetic amethyst to 300°C causes initial colour fading. At 450°C, only 10 minutes of heating is sufficient to completely decolourise initially vivid violet synthetic quartz. The fact that synthetic amethyst does not heat to a citrine hue indicates that its colour cause is different from that of natural amethyst.

FTIR absorption spectra of the hydroxyl stretching range were obtained in transmission mode (and converted into absorbance) using a Bruker Tensor 27 spectrometer for a faceted—and, thus, randomly oriented—bicoloured violet-and-colourless sample. The keel edge was ground down and polished, resulting in a 5-mm-wide 'window' parallel to the table facet. Five unpolarised measurements were made sequentially from the violet to colourless end (Figure 38) using a 3 mm pinhole placed in the IR beam. The resulting spectra were dominated by a broad band peaking at 3437 $cm^{-1}$ and several narrow bands, with the most intense one at 3585 $cm^{-1}$. These spectra deviate from those of most natural quartz samples, which typically have a major band at 3378 $cm^{-1}$ that is assigned to AlOH defects (Kats 1961; Stalder 2021). Moreover, our spectra are similar to those of synthetic quartz reported by Kats (1961) and natural quartz treated in '(OH) fluid' described by Rovetta *et al.* (1989). The assignment of the 3437 $cm^{-1}$ band remains unknown, whereas the 3585 $cm^{-1}$ band is due to intrinsic defects unrelated to trace-metal ions, presumably isolated $(OH)^-$ groups (Jollands *et al.* 2020). The boron-related band at 3595 $cm^{-1}$ (Jollands *et al.* 2020) was absent from our spectra, consistent with its usefulness for distinguishing natural from synthetic amethyst (Karampelas *et al.* 2011). We observed that the temperature gradient during the one-sided heating gradually affects OH incorporation: The intensity of the 3585 $cm^{-1}$ band increased from violet towards colourless at the expense of the 3544 $cm^{-1}$ band (for the latter, cf. Balitsky *et al.* 2004). The total OH absorbance remained

**Figure 37:** These two pairs of bicoloured synthetic quartz (14.8–23.5 ct) demonstrate the appearance of this material before (top row) and after (bottom row) intentional fracturing. Composite photo by M. Wildner.

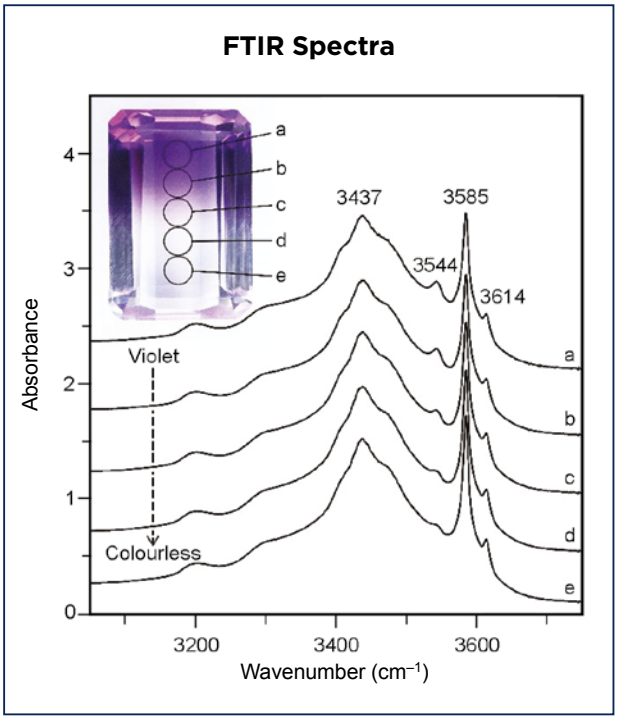


**Figure 38:** Five FTIR absorption spectra were obtained from a transparent, bicoloured synthetic quartz sample (21.8 ct; sample thickness 8.3 mm). The spectra are offset vertically by 0.5 units of absorbance for clarity (absorbance values apply only to spectrum e). Note the heating-induced changes in the OH-band intensities at 3585 and 3544 $cm^{-1}$.

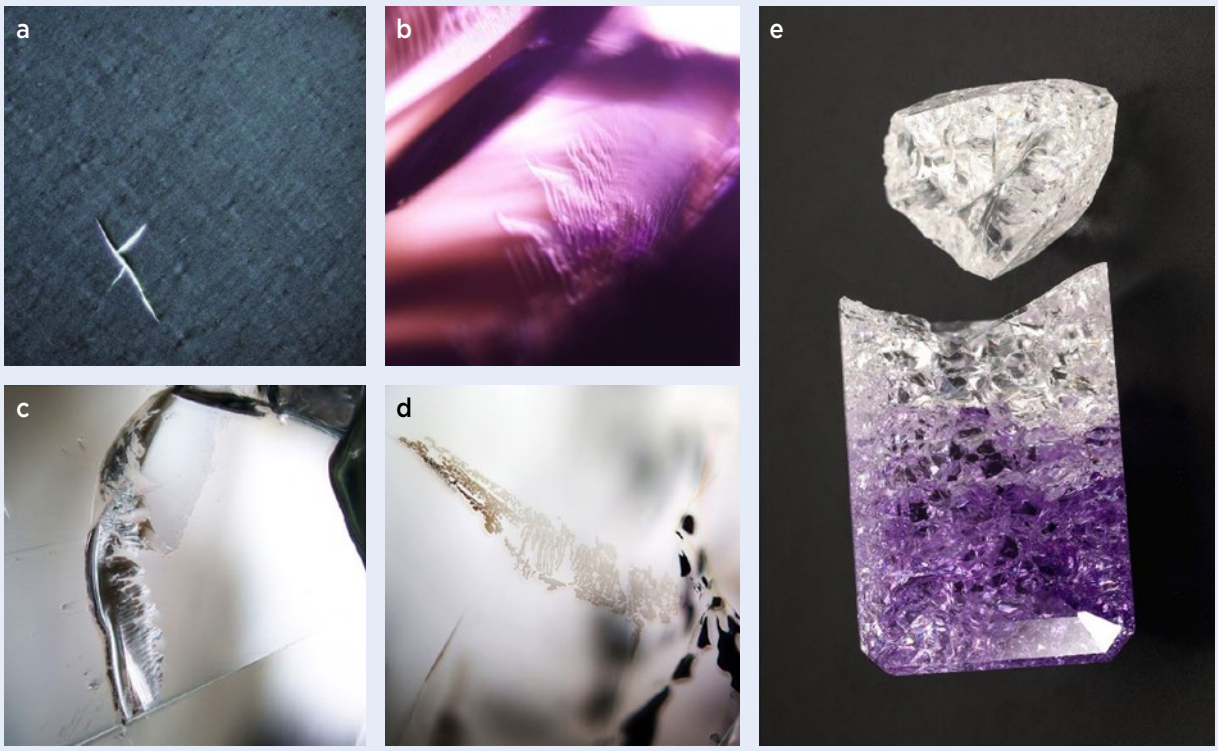


**Figure 39:** (**a**) Cross-polarised transmitted-light image (width 250 µm) of a 25 µm thin section of heat-treated and subsequently quench-fractured synthetic quartz shows wavy extinction due to strain and local strain release by opening of fractures. (**b–d**) Plane-polarised transmitted-light images (width 1.5 mm) show various fractures in faceted heat-treated and subsequently quench-fractured synthetic quartz. Note the partial fracture-filling residues in image (d). (**e**) Too-intense fracturing often results in durability problems, as shown by this 20.7 ct synthetic quartz. Photomicrographs (a–d) by Chutimun Chanmuang N. and photo (e) by M. Wildner.

more-or-less unaffected, indicating that the structural OH sites changed without much escape of OH.

The colour treatment is followed by 'textural treatment', in which the faceted, bicoloured material is heated again—apparently at rather moderate temperatures, as the colouration is not affected. The hot samples are then quenched in liquid to cause internal strain close to the material's elasticity maximum (recognised from wavy extinction in cross-polarised light), eventually causing fracturing (Figure 39a–d). However, successful intentional fracturing takes experience, as it can introduce instability, which may constitute a problem for the durability of this material. A lot of waste seems to be involved in the fracturing process, and it is not uncommon to encounter such specimens that have fallen apart (Figure 39e). In contrast to the long-known 'quench-crackled' quartz, in which the fracture pattern is dyed to impart colouration, the present material is body-coloured. We did not observe any signs of dyeing or other intentional fracture-filling. The minor fillings we observed (Figure 39d) are most likely attributed to contamination during the quenching in liquid.

Quench-fractured synthetic quartz has an admittedly distinctive appearance (Figure 40) that makes it stand out from typical bicoloured transparent quartz, synthetic corundum and imitations (Nasdala *et al.* 2020) on the

**Figure 40:** These four faceted samples (9.6–32.6 ct) of quench-fractured monochrome or bicoloured synthetic quartz illustrate some of the colour variations available. Composite photo by M. Wildner.

market. The future will tell whether or not this material will be welcomed by the gem industry for setting in costume jewellery.

*Acknowledgements*: We thank Andreas Wagner for sample preparation, Prof. Dr Eugen Libowitzky for help with the FTIR analyses, and Prof. Dr Gerald Giester, Prof. Dr Jens Götze and Prof. Dr Roland Stalder for helpful discussions.

*Dr Bhuwadol Wanthanachaisaeng*
*(bhuwadol@g.swu.ac.th)*
*Srinakharinwirot University*
*Bangkok, Thailand*

*Prof. Dr Lutz Nasdala, Dr Chutimun Chanmuang N. and Prof. Dr Manfred Wildner*
*University of Vienna, Austria*

## References

Balitsky, V.S., Balitsky, D.V., Bondarenko, G.V. & Balitskaya, O.V. 2004. The 3543 $cm^{-1}$ infrared absorption band in natural and synthetic amethyst and its value in identification. *Gems & Gemology*, **40**(2), 146–161, https://doi.org/10.5741/gems.40.2.146.

Jollands, M.C., Blanchard, M. & Balan, E. 2020. Structure and theoretical infrared spectra of OH defects in quartz. *European Journal of Mineralogy*, **32**(3), 311–323, https://doi.org/10.5194/ejm-32-311-2020.

Karampelas, S., Fritsch, E., Zorba, T. & Paraskevopoulos, K.M. 2011. Infrared spectroscopy of natural vs. synthetic amethyst: An update. *Gems & Gemology*, **47**(3), 196–201, https://doi.org/10.5741/gems.47.3.196.

Kats, A. 1961. *Hydrogen in alpha-quartz*. PhD thesis, Delft University of Technology, Delft, The Netherlands, 147 pp.

Nasdala, L., Chanmuang N., C., Giester, G. & Wanthanachaisaeng, B. 2020. Gem Notes: Multicoloured synthetic corundum and multicoloured glass doublets in the Thai gem market. *Journal of Gemmology*, **37**(1), 18–20.

Rovetta, M.R., Blacic, J.D., Hervig, R.L. & Holloway, J.R. 1989. An experimental study of hydroxyl in quartz using infrared spectroscopy and ion microprobe techniques. *Journal of Geophysical Research*, **94**(B5), 5840–5850, https://doi.org/10.1029/JB094iB05p05840.

Stalder, R. 2021. OH point defects in quartz – A review. *European Journal of Mineralogy*, **33**(2), 145–163, https://doi.org/10.5194/ejm-33-145-2021.

Wanthanachaisaeng, B., Nasdala, L., Chanmuang N., C. & Wildner, M. 2022. Synthetics and simulants in the Thai gemstone market: An update. *7th International Gem & Jewelry Conference (GIT2021)*, Chanthaburi, Thailand, 2–3 February, 173–176.

# An innovator in gemstone reporting

• Identification of colored gemstones • Country of origin determination • Full quality and color grading analysis

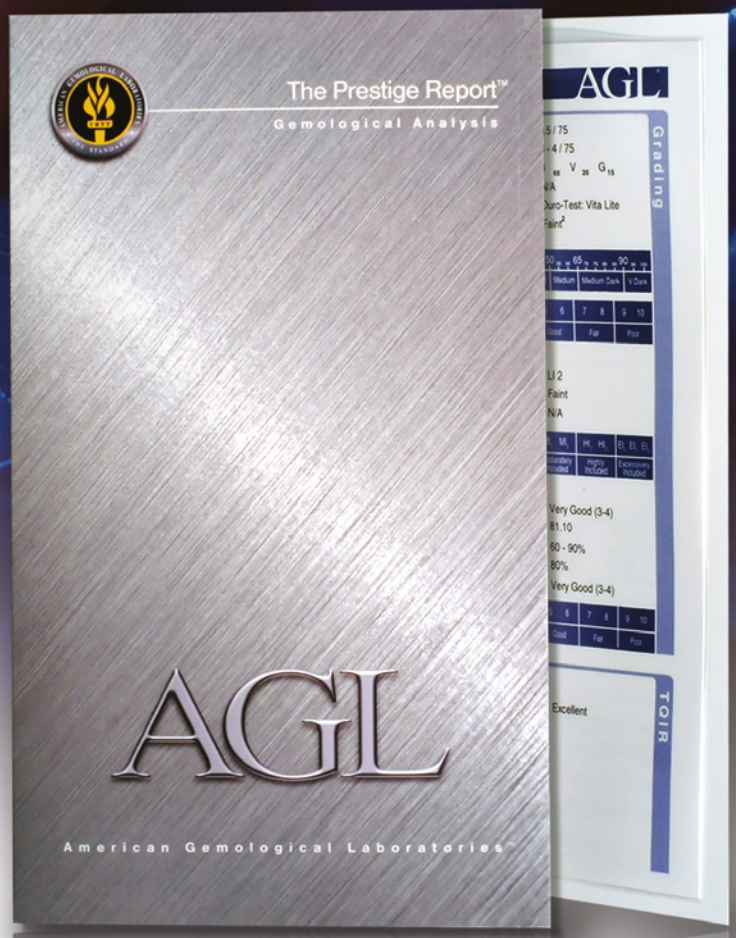


AMERICAN GEMOLOGICAL LABORATORIES AGL

580 5th Ave • Suite 706 • New York, NY 10036, USA
www.aglgemlab.com • +1 (212) 704 - 0727

# Spinel from the Pamir Mountains in Tajikistan

Dietmar Schwarz, Yicen Liu, Zhengyu Zhou, Pantaree Lomthong and Theodore Rozet

**ABSTRACT:** A detailed mineralogical and gemmological documentation was performed on 115 unheated spinels from the Kuh-i-Lal mining area in Tajikistan. These were compared to data for three samples from the Parawara mine in the Sar-e-Sang area of Afghanistan and one stone from an unspecified location 'in the Afghan part of Badakhshan'. The Tajik spinels showed little variation in colour: pink to purplish pink and, in rare cases, orangey pink; in general, they can be described as 'rose coloured'. The optical, physical and chemical properties of Tajik spinels displayed rather limited variability compared to those from other localities, such as Myanmar, Vietnam and Tanzania. They also contained a relatively limited range of inclusion minerals: graphite, two varieties of the spinel group (transparent colourless to greyish and opaque black crystals), carbonates (calcite, dolomite and magnesite), forsterite, apatite, zircon, mica (biotite/phlogopite and muscovite) and pyrite. Most of these minerals belong to assemblages trapped in primary and (pseudo-)secondary cavities. These cavities display a wide variation in size, shape and nature of the filling material. Tajik spinels have the lowest minor- and trace-element contents (Ti, V, Cr, Fe and Zn) recorded in samples from the Himalaya region.

*The Journal of Gemmology*, **38**(2), 2022, pp. 138–154, https://doi.org/10.15506/JoG.2022.38.2.138


It has been frequently stated in the trade that spinel is an underappreciated gem material. This might be true for some parts of the world, but surely not in Asia. At the time of the Mughals (sixteenth to eighteenth centuries), spinel was one of the most desirable gems in India, along with ruby and emerald. Spinel gems mainly came from the old 'Badakhshan' region, with some probably from Sri Lanka. The Mughals were particularly fond of large red spinels, typically of slightly irregular pear shape. Some have inscriptions naming their original royal owners (see, e.g., Figure 1 and Ball 1893)—something that greatly adds to the price they fetch today.

One reason for the modest reputation of spinel in Western cultures in the past is the fact that many beautiful specimens were identified as ruby and were eclipsed for a long time by that better-known gem (Ogden 2020). Since the beginning of the new millennium, however, spinel's popularity has increased greatly due to several factors. With its wide range of colours (pink to red [Figure 2], orange, violet to purple and green to blue) and its high transparency, spinel has gained a greater commercial importance. Another reason for its rising popularity is the increasing scarcity of other coloured stone varieties of fine quality (especially ruby) and their—sometimes dramatic—increase in prices. Due to spinel's attractiveness combined with its availability—owing to a regular supply from traditional sources such as Myanmar, Vietnam, Tajikistan, Sri Lanka, Kenya and Tanzania, and new finds in Madagascar and Mozambique (Figure 3)—it has been an excellent candidate to fill market demand for fine coloured stones. In addition, spinel's image has benefited from the lack of controversial treatment processes applied to it. Considering its increasing commercial presence, additional information about spinel has become relevant to satisfy the need for accurate geographic origin determination.

Kuh-i-Lal, located in the Pyanj River Valley of what is today Tajikistan, is one of the traditional historical sources of spinel. These mines—also known in the gemmological literature as the 'Badakhshan ruby mines'—are among the oldest in the world. They are thought to have been

**Figure 1:** The 133.5 ct Carew spinel, in the collection of the V&A Museum in London, is engraved with the titles of Jahangir (r. 1605–1627), Shah Jahan (dated 1629–1630) and 'Alamgir' (Aurangzeb; dated 1666). The spinel is drilled from both ends across its longest dimension, with a gold pin secured by a diamond at the top and bottom. Accession number IM.243-1922, bequeathed by the Rt Hon. Julia Mary, Lady Carew; photos © Victoria and Albert Museum, London.

**Figure 2:** These faceted spinels from the Kuh-i-Lal mining area in Tajikistan illustrate the fine quality of the material from this locality. From front to back, they weigh 3.20, 7.49, 10.38, 12.88 and 16.33 ct. The red colour of the largest stone is rare for Tajik spinels. Photo courtesy of Pamir Gems Co. Ltd (Bangkok, Thailand).

discovered following a seventh century CE earthquake (Pardieu & Hughes 2008), and were the world's main producers of large spinels for centuries—including the so-called *balas rubies*. Kuh-i-Lal is probably the source of the 'Black Prince's Ruby', the 'Timur Ruby' and other large spinels from Persian, Russian, Mughal and European treasuries (Pardieu & Hughes 2008).

The Kuh-i-Lal deposit is located in the south-western Pamir Mountains on the Tajikistan side of the Badakhshan region (Figure 4), which also comprises a portion of today's north-eastern Afghanistan. Together with occurrences in Afghanistan (Jegdalek), Pakistan (Hunza Valley), Nepal (Paigutan), Myanmar (Mogok and Nanyaseik) and northern Vietnam (Luc Yen), it lies within a 'gem belt' extending from Central Asia to Southeast Asia (Garnier *et al.* 2006). The deposits are located within the Himalayan mountain belt, which formed during the Tertiary continental collision between the Indian and Eurasian plates. Contrary to most other marble-hosted spinel sources, the Kuh-i-Lal mines do not produce rubies. During much of the twentieth century,


**Figure 3:** The global distribution of pink-to-red spinel occurrences is shown on this map (modified from Giuliani *et al.* 2018). These localities include Tajikistan (Kuh-i-Lal), Afghanistan (Jegdalek), Pakistan (Hunza Valley), Nepal (Paigutan), Myanmar (Mogok and Nanyaseik), northern Vietnam (Luc Yen), Sri Lanka, Tanzania (Ipanko, Tunduru and Kiswila), Kenya (Pamreso), Madagascar (Ilakaka) and Mozambique (unspecified localities).

little was known about these mines (e.g. Figure 5) due to restricted access when the area was part of the former Soviet Union, and the deposits have been visited by few modern gemmologists (e.g. Hughes & Pardieu 2006; Pardieu & Farkhodova 2019).

Since early 2017, attractive purple spinels originating from the Afghan part of Badakhshan have appeared in gem markets in Pakistan and Thailand. Many of these spinels reportedly came from the Parawara mine near the Sar-e-Sang lapis deposits at Lajuar Madan in the Kokcha Valley (again, see Figure 4). In the Bangkok market, the


**Figure 4:** In Central Asia, the main ruby deposits are located in Afghanistan (Jegdalek), Pakistan (Hunza Valley) and Tajikistan (Kukurt/Snezhnoe, Snijnie or Snezhny), and spinel localities occur in Tajikistan (Kuh-i-Lal) and Afghanistan (e.g. Parawara, in the Sar-e-Sang region). The Badakhshan region is indicated by the green-coloured areas, and includes portions of both Tajikistan and Afghanistan.


**Figure 5:** The historic Kuh-i-Lal spinel mines, one of which is shown here in two different views, are situated on the Tajik side of the Badakhshan region. Photos courtesy of Pamir Gems Co. Ltd (Bangkok, Thailand).

Parawara spinels became known as 'Iris purple spinels'. Faceted stones in the range of 5–9 ct, and exceptionally up to 15 ct, have been reported (Boehm 2017).

This article provides a detailed mineralogical and gemmological characterisation of spinels from Kuh-i-Lal, and also a brief comparison to those from Afghanistan.

## BACKGROUND

### *Mineralogy and Crystallography of Spinel*

Natural Mg-Al spinel ($MgAl_2O_4$) as a gem material is known in a wide range of colours. The most appreciated is red, but pink-to-purple and blue are also favoured. *Spinel* is a term also used to describe a group of minerals with the same (cubic) crystal structure and the basic formula $A^{2+}B^{3+}_2X^{2-}_4$, with A and B representing various cations and X being oxygen in the case of gem spinels. Gem-quality spinels are commonly almost pure end-member $MgAl_2O_4$, with Zn, Fe, Cr and V present in variable concentrations. A variety of trace elements have also been detected in spinels from various localities: Li, Be, Ti, Mn, Co, Ni, Cu, Ga, Zr and Sn (Malsy & Klemm 2010; Giuliani *et al.* 2017).

In the 'normal' spinel formula $AB_2O_4$, the A ions occupy tetrahedrally coordinated sites and the B ions are in octahedrally coordinated sites. 'Inverse' spinel is also known and can be described as $B(AB)O_4$, where the B cations may occupy both sites and the A cations are in the octahedral site. Any intermediate combination of normal and inverse spinel is usually described as 'disordered'. Most gem spinels are 'ordered' $MgAl_2O_4$, but heating can cause them to be disordered, and this can be used as a criterion to determine if a stone has undergone heat treatment (Saeseaw *et al.* 2009).

### *Geology and Genetic Aspects*

Like ruby, gem-quality spinel is often associated with marble host rocks. According to Garnier *et al.* (2008), the deposits in the Himalayan mountain belt are spatially related to ruby deposits hosted by platform carbonate rocks that are generally metamorphosed to amphibolite facies. The marble units are intercalated generally with biotite-garnet-sillimanite or -kyanite gneisses and granites. Overall, the marbles are composed of calcite, dolomite, spinel, forsterite, apatite, margarite, pargasite and chlorite (sheridanite-clinochlore), with or without graphite, pyrite and pyrrhotite. The marble units consist of discontinuous horizons up to 300 m thick that are

oriented parallel to the main regional foliations, thrusts or shear zones related to the Cenozoic Himalayan orogenesis (Garnier *et al*. 2008).

Spinel in marble is a marker of high-temperature metamorphism (Okrusch *et al.* 1976; Hauzenberger *et al*. 2001; Garnier *et al.* 2008). Under amphibolite-facies conditions, spinel, sapphirine and corundum are the main stable mineral phases. The typical reaction between corundum and spinel during metamorphism is as follows (Garnier *et al*. 2008):

$$\underset{\text{Spinel}}{MgAl_2O_4} + \underset{\text{Calcite}}{CaCO_3} + CO_2 \leftrightarrow \underset{\text{Corundum}}{Al_2O_3} + \underset{\text{Dolomite}}{CaMg(CO_3)_2}$$

This reaction shows the intimate relationship between the formation of ruby and spinel in marble host rocks. Depending on the physicochemical conditions, spinel can form at the expense of ruby, or ruby can crystallise in place of spinel. The principal reaction for ruby formation is the destabilisation of spinel in contact with calcite during the retrograde metamorphic path (e.g. at Jegdalek, Hunza and Luc Yen).

The source of Al in the host marble that is necessary for gem mineralisation (i.e. around 38% Al for spinel and 53% Al for ruby) has long been debated, but is mainly thought to be derived from phengite impurities (Garnier *et al*. 2008; Harlow & Bender 2013; Giuliani *et al*. 2014). The sedimentation of the marble protolith on a marine platform ensured the presence of clay minerals produced by continental weathering (Okrusch *et al.* 1976; Rossovskiy *et al.* 1982; Garnier *et al*. 2008) and a supply of detrital minerals, dolomitic and magnesite carbonates, organic matter, black shales and evaporites.

The sources of V, Cr, Fe and Ti in the sedimentary basin were most likely Cr-V-bearing clays or micro-fragments of mafic rocks coming from the continent (Giuliani *et al*. 2015). Nevertheless, the distribution of the clays, carbonates and silicates is highly variable within platform sediments. These are intercalated over hundreds of metres, forming mineralogically and chemically heterogeneous metamorphic piles (Pêcher *et al.* 2002). During diagenesis and later metamorphism, the chemical elements migrated and were incorporated into new minerals. The initial chemical heterogeneity of the sediments is reflected by variations in the metamorphic rocks such as the marbles. Garnier *et al*. (2008) have shown that evaporites played a key role in the formation of ruby (and spinel at Hunza and Jegdalek) because molten salts mobilised locally derived Al and transition-metal elements present in the marbles (Giuliani *et al*. 2014, 2015). Different colours of spinel are due to the variable concentrations of Fe, V, Cr and Ti in the initial protolith and, thus, in the marble.

The Kuh-i-Lal spinel deposit is located in the Goran metamorphic series in the south-western Pamir Mountains. The high-grade metamorphic rocks (upper amphibolite to granulite facies) consist of thick metasedimentary units comprising biotite-sillimanite ± kyanite ± garnet gneiss and schist, migmatite, marble and calc-silicate rocks, along with subordinate granite, quartzite and amphibolite (Hubbard *et al*. 1999). The spinel deposit is hosted by Mg-rich enstatite-forsterite rocks (i.e. magnesian skarns). Spinel occurs as disseminations and aggregates in a forsterite-rich zone, which forms lenticular and concordant bodies ranging from 10 cm to 5 m thick and up to 30 m long. The magnesite marble hosts the assemblage sapphirine, gem spinel, amphibole, enstatite, forsterite, gem clinohumite, chondrodite, rutile, graphite, pyrrhotite and pyrite (Grew *et al*. 1994, 1998).

## MATERIALS AND METHODS

The samples characterised for this report include 115 unheated spinels from Kuh-i-Lal (101 windowed crystals, mostly of gem quality, and 14 faceted stones), three windowed samples from the Parawara mine, and one faceted stone from an unspecified location 'in the Afghan part of Badakhshan' (Figure 6). They were mostly pink to reddish pink and showed only minor colour variations between samples. The stones were purchased by one of the authors (DS) in the Namak Mandi gem market in Peshawar, Pakistan (2000 and 2001), and from Tajik, Afghan and Pakistani dealers in Bangkok (2014–2019). Most of the rough material was polished with one window (sometimes two or three windows) in order to document the internal features and perform chemical analyses.

Gemmological properties of 20 Tajik samples, as well as the three Parawara spinels and the 'Afghan-Badakhshan' stone, were collected at the Laboratory of Gem and Technological Materials (Tongji University, Shanghai, China). RI and SG values were measured with a refractometer and an electronic balance, respectively. Their fluorescence behaviour was observed under long- and short-wave UV radiation (365 and 254 nm) in a darkened room. Microscopic examination of all the samples was performed by author DS using a gemmological microscope from Schneider Gemmologie (Idar-Oberstein, Germany) equipped with a Zeiss Stemi DV4 optical system (40×–60× magnification). Photographic documentation of the inclusion features of selected samples was done using a Keyence VHX-6000 digital

**Figure 6:** The spinel samples used for this study are shown here. The rough pieces from Tajikistan range from 0.14 to 2.00 g and the faceted Tajik stones weigh 0.41–0.58 ct. The samples from the Parawara mine (black squares) are 0.31–0.76 g. The faceted spinel represented to be from the Afghan part of Badakhshan (black circle) weighs 1.38 ct. Photo by D. Seechompoo.

microscope (5×–200× magnification) at the Bellerophon Gem Lab (Bangkok, Thailand).

A confocal Raman spectrometer (Horiba Jobin Yvon LabRAM HR Evolution) was used at the Laboratory of Gem and Technological Materials to analyse mineral inclusions and the contents of cavities in about 25 selected spinel samples from Tajikistan. All spectra were measured using an excitation wavelength of 785 nm with the 50× objective of the microscope. The spectra were collected in the range of 100–2000 $cm^{-1}$ with a laser power of 50 mW. The maximum exposure time per scan was 15 s with a 10-scan accumulation. The confocal aperture was set at 100 µm with a slit width of 500 nm. The backscattered light was dispersed on a holographic grating (600 grooves/mm). Inclusions were identified by comparing the Raman spectra to those in the RUFF database (https://rruff.info).

Photoluminescence (PL) spectra were obtained in the 560–850 nm range on the same 24 spinel samples that were studied for their gemmological properties, using the same instrument and set-up as for the Raman spectra. Two scans with the 50× objective were performed, using an acquisition time of 5 s, a laser power of 50 mW and a confocal aperture of 50 µm.

Chemical analyses were obtained at the Laboratory of Gem and Technological Materials for all 115 Tajik spinels, as well as the three Parawara spinels and the 'Afghan-Badakhshan' stone, using an energy-dispersive X-ray fluorescence (EDXRF) unit manufactured by Skyray Instrument Inc. The spectra were acquired at room temperature and measured under vacuum. The acquisition time was 60 s, with an accelerating voltage of 10 kV and a beam current of 700 µA.

Twenty additional, relatively inclusion-free samples (not shown in Figure 6) from Kuh-i-Lal were analysed by laser ablation inductively coupled plasma mass spectrometry (LA-ICP-MS) at Wuhan Sample Solution Analytical Technology Co. (Wuhan, China), using an Agilent 7900 spectrometer with a GeoLasHD excimer laser-ablation system (193 nm with a frequency of 5 Hz and a pulse energy of 80 mJ). At least one measurement point (64 µm in diameter) was selected for each sample. The standards used were NIST glasses (SRM 610 and SRM 612) and USGS glasses (BCR-2G, BHVO-2G and BIR-1G). The experimental procedure and data processing (using ICPMSDataCal 10.8 software) followed the method of Liu *et al.* (2008), based on the normalisation of the sum of all metal oxides to 100 wt.%; the ablation yield

correction factor was used to correct the matrix-dependent absolute amount of material ablated during each run. Applying this correction and using the USGS glasses as multiple reference materials for external calibrations, elements in anhydrous minerals can be precisely analysed *in situ* by LA-ICP-MS without applying internal standardisation (Liu *et al.* 2008). Each analysis incorporated a background acquisition of approximately 30 s, followed by 40 s of data acquisition from the sample.

Ultraviolet-visible-near infrared (UV-Vis-NIR) absorption spectra of 30 windowed Tajik samples, the three Parawara spinels and the 'Afghan-Badakhshan' stone were obtained at the Laboratory of Gem and Technological Materials using a GEM-3000 spectrometer manufactured by Guangzhou Flag Electronic Technology Co. The spectra were acquired at room temperature in the range of 220–1000 nm with a resolution of 1 nm, integration time of 100 ms, average of 20 scans and smoothness of 2.

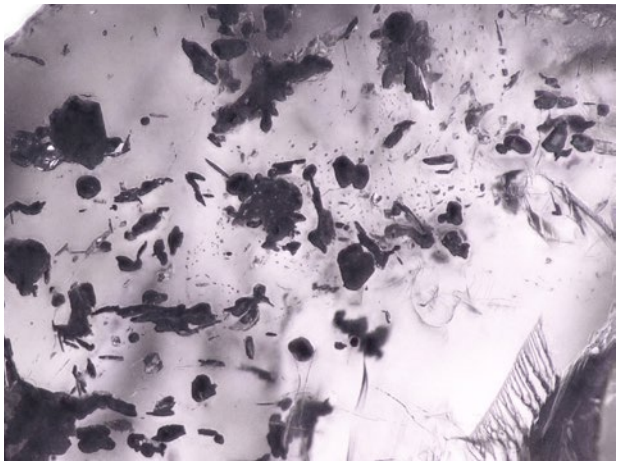

**Figure 7:** Graphite (which derives from the metamorphism of organic substances in the spinel host rock) is a frequent inclusion in Tajik spinel. It is present both as opaque black, mostly plate-like crystals (as shown here) and as a filling material in primary and (pseudo-)secondary cavities and fluid inclusions. Magnified 150×.

## RESULTS

### *Gemmological Properties*

The colours of the Kuh-i-Lal spinels varied from pink to purplish pink and, very rarely, orangey pink. The Parawara samples were pink to purple-pink and the 'Afghan-Badakhshan' stone was orangey pink. The standard gemmological properties of the Tajik spinels examined for this study, as well as those of Tajik spinels previously described, are given in Table I.

Detailed microscopic documentation of the internal features is described below for solid inclusions, cavities containing fluid and/or solid fillings, and partially healed fissures and fractures. The solid inclusions were identified by Raman spectroscopy and all photomicrographs were taken by author TR unless indicated otherwise.

**Solid Inclusions.** Isolated (single) solid inclusions were rather rare in our Tajik spinels, and a relatively small number of inclusion minerals were identified. Hereinafter, the inclusion minerals are arranged in order of most to least common. Graphite, spinels and carbonates were observed in about 10–15% of the documented samples; forsterite, apatite and zircon in about 5–10%; and mica, pyrite, clinohumite(?) and others in less than 5%.

Graphite was the most common inclusion mineral in the Tajik spinels. It was present both as isolated (mostly plate-like) crystals and as a component of the filling material in primary and (pseudo-)secondary cavities (see below). It formed opaque black grain-like crystals or irregular-rounded (more-or-less six-sided) platelets with a greyish metallic lustre (Figure 7). They were isolated

**Table I:** Gemmological properties of spinel from Kuh-i-Lal, Tajikistan.*

| Property | This study | Sturman (2009) | Malsy & Klemm (2010) | Chankhantha *et al.* (2020) |
|---|---|---|---|---|
| RI | 1.710–1.714 | 1.712–1.713 | 1.712–1.713 | 1.712–1.714 |
| SG | 3.55–3.58 | 3.59–3.62 | 3.58–3.59 | 3.58–3.60 |
| Long-wave UV | Moderate to strong red | Strong red | — * | Moderate to strong red |
| Short-wave UV | Inert to very weak | Weak red to weak-to-moderate orange | Yellow surface fluorescence | Inert or weak red |
| Polariscope | Isotropic; some samples show anomalous double refraction | — | — | Isotropic; no anomalous double refraction |

* — = not reported.

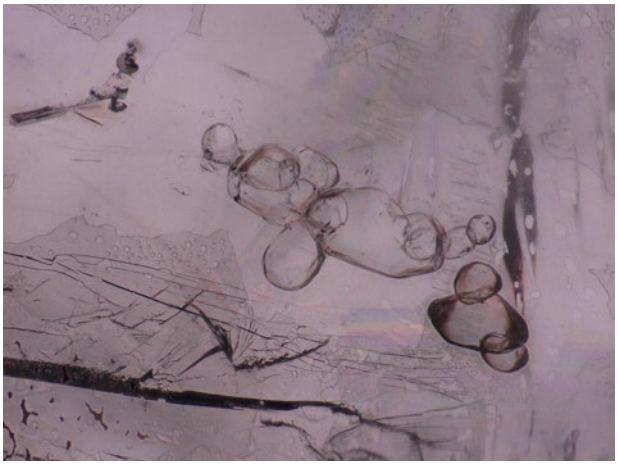

**Figure 8:** This aggregate in a Tajik spinel consists of slightly rounded, transparent colourless forsterite crystals of protogenetic origin. Magnified 150×.

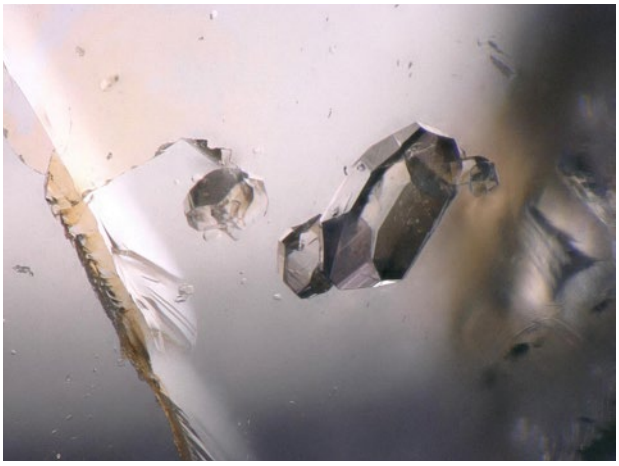

**Figure 9:** Well-developed, short-prismatic forsterite crystals such as these in a Tajik spinel are probably of syngenetic orign. Magnified 200×.

or arranged in clusters. Numerous graphite inclusions were also observed in the 'Afghan-Badakhshan' spinel.

Two members of the spinel group were present as well-developed octahedron-like crystals in a few samples. One of them was colourless to greyish, and the other was opaque black with sub-metallic lustre, and was identified as magnetite.

Carbonate inclusions (calcite, dolomite and magnesite) showed high relief in the host spinel. They typically formed transparent, colourless, euhedral-subhedral or (rarely) rhombohedron-like crystals. They were isolated or in cluster-like formations, sometimes together with other inclusion minerals. Carbonates also filled octahedron-like cavities in the spinels (see below).

Forsterite was seen as whitish translucent-to-opaque inclusions or less commonly as colourless transparent crystals. The first type were mostly subhedral to anhedral and showed distinct relief in the host spinel (Figure 8). The second type formed well-developed short-prismatic crystals (Figure 9).

Apatite occurred as transparent, colourless, often euhedral hexagonal-prismatic crystals of variable size. They were oriented in different directions and showed low relief in the host spinel (Figure 10). Raman spectra were inconclusive for identifying whether these inclusions were fluorapatite or hydroxylapatite.

Zircon generally formed euhedral, slightly elongated to long-prismatic crystals (Figure 11). Also common were tiny, transparent, colourless zircon crystals with the appearance of sugar grains.

Transparent mica inclusions (identified as biotite/phlogopite and, more rarely, as muscovite) were present in several of the Tajik spinels. These formed delicate, colourless or slightly yellowish, irregularly shaped or

**Figure 10:** Transparent colourless, well-formed, hexagonal-prismatic, doubly terminated apatite crystals of variable size are oriented in different directions and show low relief in the host Tajik spinel. Magnified 200×.

well-developed six-sided plates (Figure 12).

Pyrite occurred as irregularly rounded or euhedral crystals with many faces (Figure 13). It displayed a typical brass-like metallic lustre when observed with fibre-optic illumination.

Pale yellow, transparent, tablet-like crystals were tentatively identified as clinohumite (Figure 14).

Sulphur was identified in only one of our samples. Several euhedral, transparent, colourless, grain-like crystals with high relief were arranged in a cluster-like formation.

We were unable to identify the nature of an opaque black mineral rarely present on fissure planes (possibly as an epigenetic filler material) that displayed intense golden yellow metallic reflections.

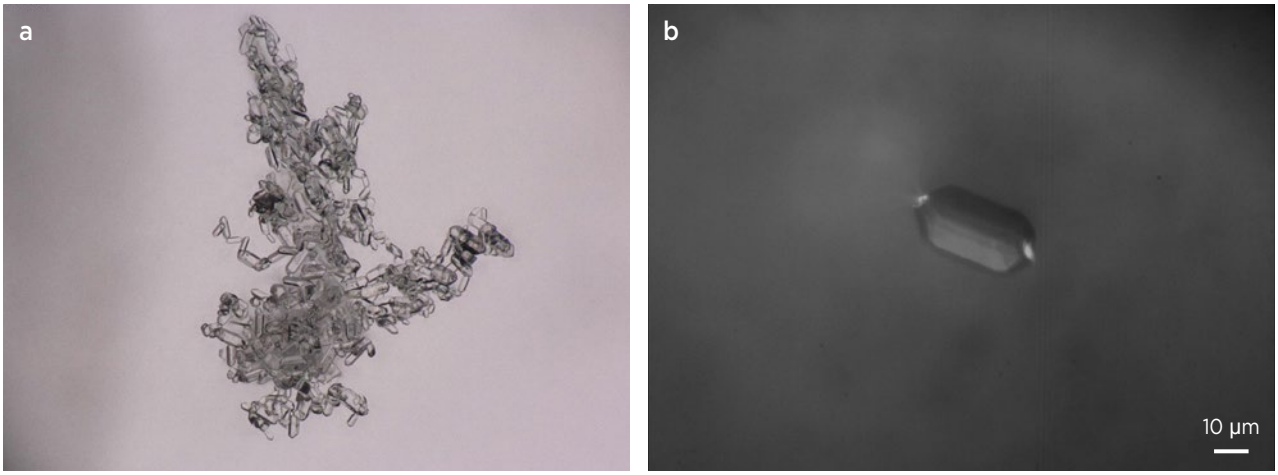


**Figure 11:** (**a**) This agglomeration (magnified 200×) in a Tajik spinel is composed of numerous transparent, colourless, short-prismatic zircon crystals oriented in various directions. The mineral was identified based on microscopic evidence. (**b**) The image of this isolated inclusion in a Tajik spinel was acquired during micro-Raman analysis, which identified it as zircon. Photomicrograph by Y. Liu.

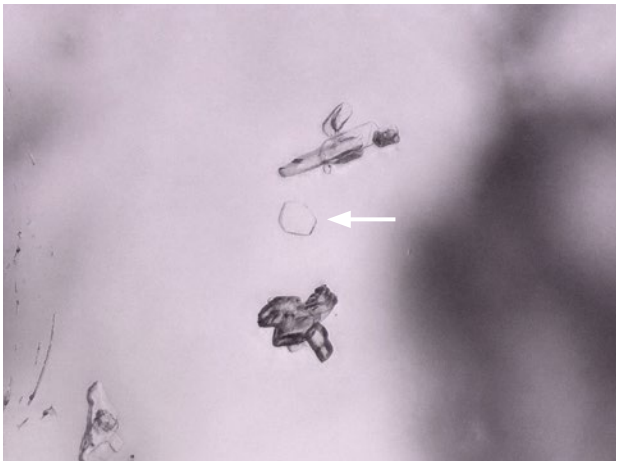

**Figure 12:** A transparent, colourless, six-sided mica platelet (see arrow) in a Tajik spinel is accompanied by a typical irregularly shaped cavity (lower left) and two groups of angular carbonate crystals that display high relief in the host spinel. Magnified 200×.

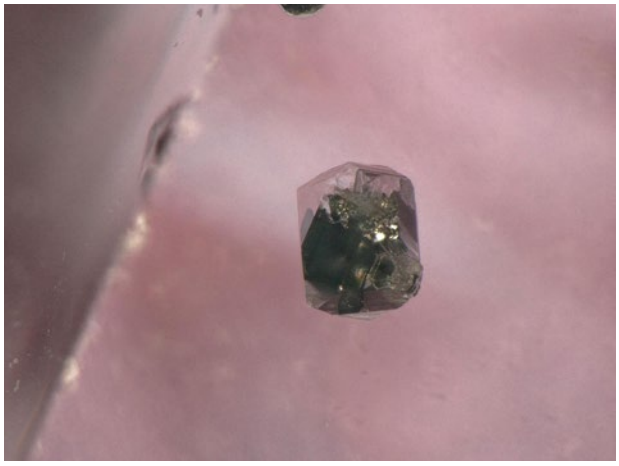

**Figure 13:** A well-developed pyrite crystal in a Tajik spinel displays many faces. When observed with fibre-optic illumination, such pyrite inclusions show a typical brassy metallic lustre. Magnified 200×.

**Cavities Containing Fluid or Solid Fillings.** In the Tajik spinels examined for this study, we frequently observed different types of these cavities, including primary and (pseudo-)secondary inclusions of variable size and shape and containing an array of filling materials. The primary cavities were mostly irregularly rounded and elongated to hose-like (Figure 15), or they displayed irregular angular forms (Figure 16). Octahedron-like (often distorted) primary cavities were less common.

Most of the cavities in our Tajik spinels contained only solid phases. These generally consisted of crystals of different mineral species (transparent colourless to greyish white crystals and opaque black graphite platelets of variable size). In addition to graphite, the following minerals were identified with Raman spectroscopy:

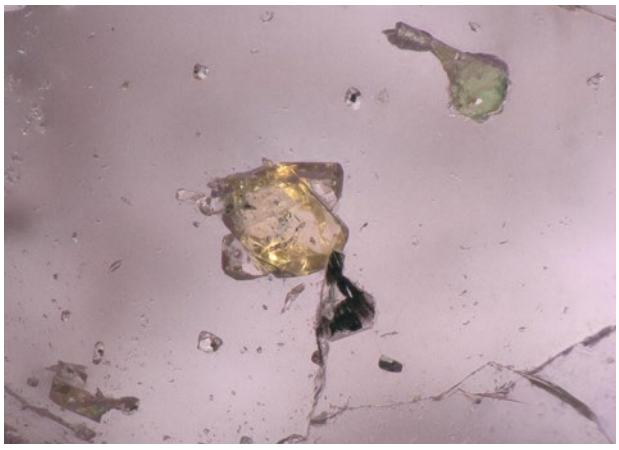

**Figure 14:** This pale yellow, transparent inclusion with intense yellow internal reflections shows well-developed, tablet-like forms. Tentatively identified as clinohumite, it is extremely rare in Tajik spinels. Magnified 200×.

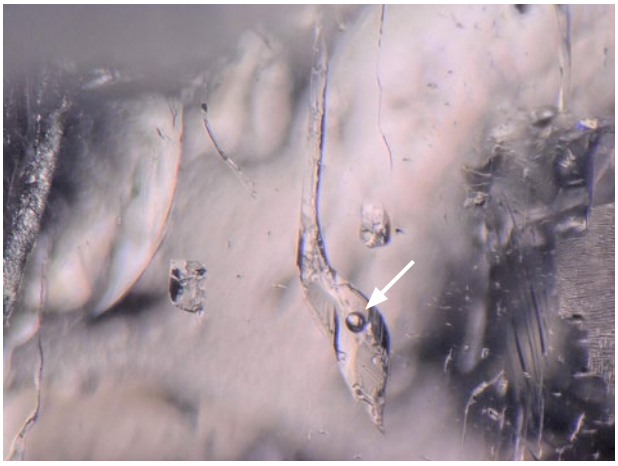

**Figure 15:** An irregular, elongated primary cavity contains a liquid and a gas bubble (see arrow). Such two-phase inclusions are rarely seen in Tajik spinels. Magnified 200×.

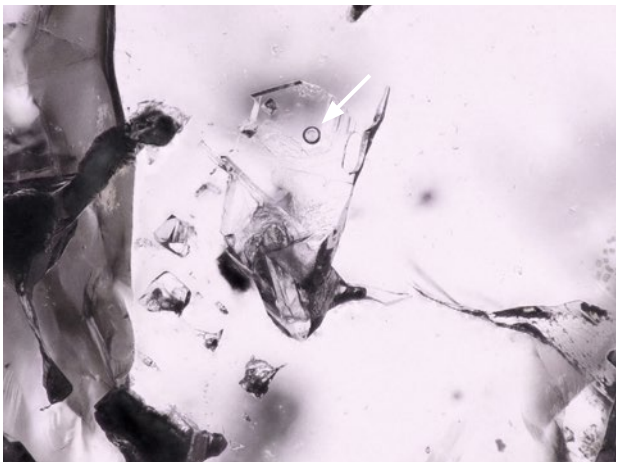

**Figure 16:** This irregularly shaped, angular, flattened primary cavity contains a multiphase filling consisting of several solid phases, a liquid and a small gas bubble (see arrow). Magnified 200×.

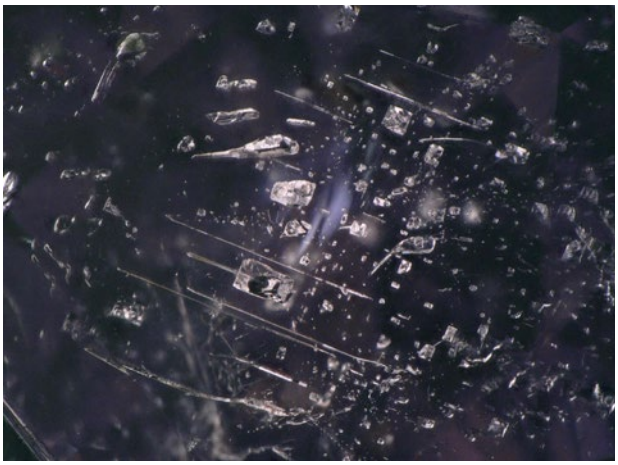

**Figure 17:** Elongated primary cavities and fine, reflective, tube- or needle-like inclusions such as these were seen only rarely in the Tajik spinels. Magnified 100×.

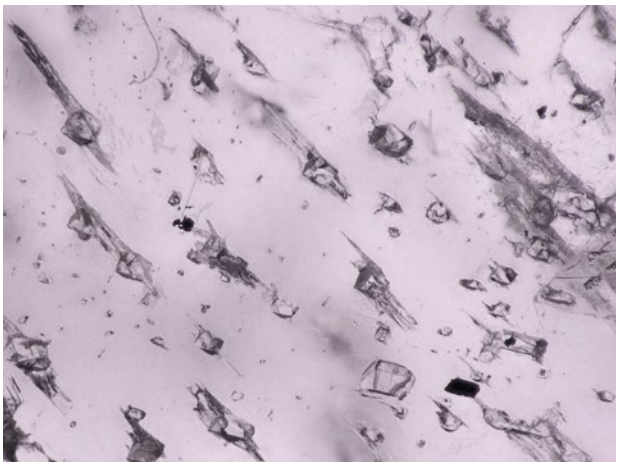

**Figure 18:** A partially healed fissure in this Tajik spinel consists of isolated, irregularly shaped cavities that are accompanied by delicate, planar tension fractures oriented more-or-less parallel to each other. Magnified 100×.

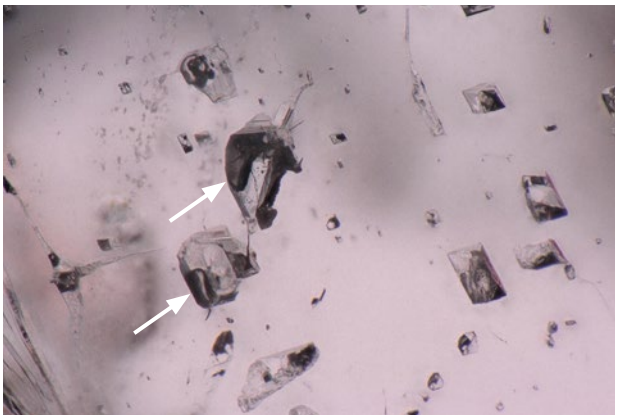

**Figure 19:** This fissure plane in a Tajik spinel hosts cavities consisting of both irregularly shaped and well-developed octahedron-like forms. Both cavity types contain crystals of various minerals. Black graphite (see arrows) is attached to some cavity surfaces. Magnified 150×.

various carbonates (calcite, dolomite and magnesite) and the silicates forsterite, zircon and micas (biotite/phlogopite and muscovite). Very scarce were cavities that contained two-phase liquid-and-gas fillings (usually with very small gas bubbles; again, see Figure 15) or multiphase cavities (Figure 16) containing solid, liquid and gas phases. Rarely seen were tube- or needle-like inclusions generally associated with primary cavities that were sometimes elongated (Figure 17).

**Partially Healed Fissures and Fractures.** Frequently present in the Tajik spinels were partially healed fissures with very poorly developed textures, usually composed of isolated constituents that displayed large variability in terms of size and shape (Figures 18 and 19). In addition, some fissure planes showed poorly developed healing

**Figure 20:** This fissure plane in a Tajik spinel displays poorly developed healing textures composed of isolated, irregular, elongated cavities oriented more-or-less parallel to each other. Magnified 150×.

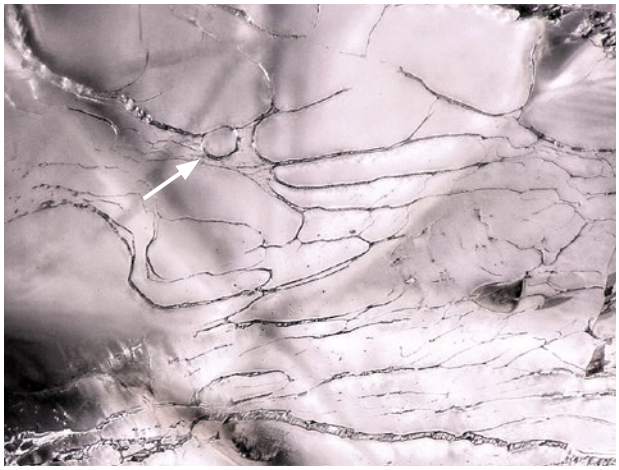

**Figure 21:** 'Classic' healing textures in the form of network- or fingerprint-like patterns are extremely rare in Tajik spinel. A flat gaseous inclusion (see arrow) occurs here in an irregularly shaped planar cavity, forming a two-phase liquid-and-gas inclusion. Magnified 200×.

textures composed of isolated, irregular, elongated cavities that were oriented more-or-less parallel to each other (Figure 20). Quite typical were partially healed fissure planes with irregularly shaped, planar cavities that had a frosted appearance resembling an icy crust. Moreover, our samples very rarely showed typical 'fingerprint' or network-like patterns.

Fillings in the (pseudo-)secondary fissure cavities consisted mainly of different mineral phases (colourless or greyish white crystals plus opaque black graphite platelets). Two-phase (liquid and gas) inclusions were very rare (Figure 21).

## Raman and PL Spectroscopy

The PL spectra (Figure 22) of the Tajik, Parawara and 'Afghan-Badakhshan' samples all showed a series of sharp peaks in the 640–760 nm range, with a strong zero-phonon line near 685 nm and vibronic sidebands of that line, plus other lines associated with $Cr^{3+}$ pairs (Saeseaw *et al.* 2009). The sharp PL spectral features indicate the samples are unheated.

## Chemical Composition

Table II shows the trace-element concentration ranges for Ti, V, Cr, Fe and Zn (in wt.% oxide) determined by EDXRF for the 119 samples in this study. This table also summarises the chemical data for Tajik spinels given by Malsy and Klemm (2010; by LA-ICP-MS) and Giuliani *et al.* (2017; by electron microprobe). LA-ICP-MS analyses of the additional 20 Tajik spinels from this study are given in Table III, together with the data from Malsy and Klemm (2010) and Chankhantha *et al.* (2020) for spinels from Tajikistan, Myanmar and Vietnam. The concentration ranges for the Tajik spinels determined by the two different analytical methods are in good accordance for the elements V, Cr and Fe. The ranges for Ti and Zn are broader for the EDXRF data (with higher concentrations). This is probably due to the larger number of samples analysed by EDXRF (119 vs 20 for LA-ICP-MS).

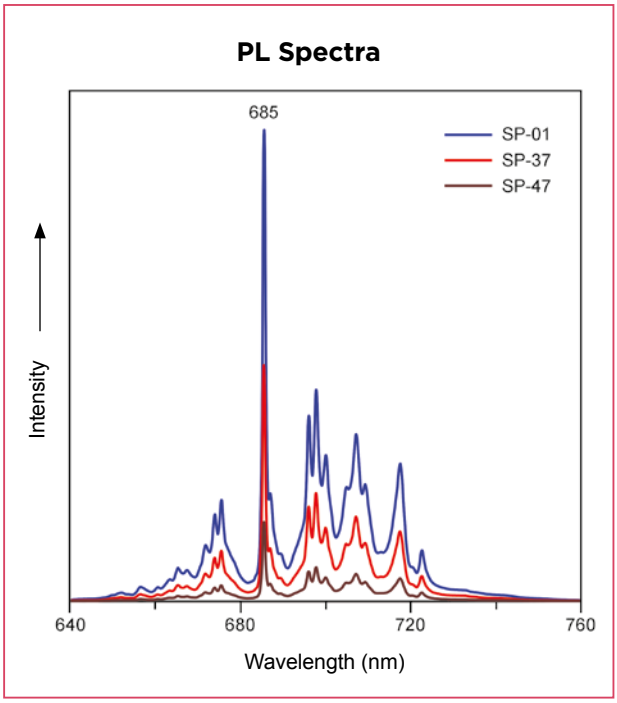


**Figure 22:** Representative PL spectra of three Tajik spinels show a typical peak sequence in the 640–760 nm range; the sharpness of the peaks indicates that the samples have not been heated.

**Table II:** Trace-element composition of spinel from Kuh-i-Lal, Tajikistan, and the two other localities analysed in this study.

| Oxide (wt.%) | Tajikistan | | | Parawara mine, Afghanistan | Afghan part of Badakhshan |
|---|---|---|---|---|---|
| | This study[a] | Malsy & Klemm (2010)[b] | Giuliani *et al.* (2017)[c] | This study[a] | This study[a] |
| $TiO_2$ | 0.01–0.03 | 0.01–0.02 | 0.01 | 0.01 | 0.03 |
| $V_2O_3$ | 0.02–0.08 | 0.03–0.07 | 0.15–0.25 | 0.03–0.05 | 0.09 |
| $Cr_2O_3$ | 0.03–0.13 | 0.04–0.13 | 0.08–0.12 | 0.05–0.07 | 0.06 |
| $Fe_2O_3$ | 0.15–0.66 | 0.13–0.52 | 0.22–1.02 | 0.30–0.42 | 0.97 |
| ZnO | 0.04–0.17 | 0.04–0.14 | 0.07 | 0.04–0.08 | 0.12 |

[a] Analyses by EDXRF. [b] Analyses by LA-ICP-MS. [c] Analyses by electron microprobe.

**Table III:** Chemical composition by LA-ICP-MS (in ppmw for elements and wt.% for oxides) for spinel from Tajikistan, Myanmar and Vietnam.

| Element/ oxide | Tajikistan | | | Myanmar | | Vietnam | |
|---|---|---|---|---|---|---|---|
| | This study | Malsy & Klemm (2010) | Chankhantha *et al.* (2020) | Malsy & Klemm (2010) | Chankhantha *et al.* (2020) | Malsy & Klemm (2010) | Chankhantha *et al.* (2020) |
| Ti<br>$TiO_2$ | 48–115<br>0.005–0.01 | 47–114<br>0.01–0.02 | 107–197<br>0.02–0.03 | 4.0–1570<br>0.001–0.26 | 441–1270<br>0.07–0.21 | 0.78–194<br>nd–0.03 | 24.8–157<br>0.004–0.03 |
| V<br>$V_2O_3$ | 189–366<br>0.03–0.06 | 155–382<br>0.03–0.07 | 261–432<br>0.05–0.08 | 22–5710<br>0.004–1.02 | 560–1050<br>0.10–0.19 | 22–1790<br>0.004–0.32 | 525–1600<br>0.09–0.29 |
| Cr<br>$C_2O_3$ | 255–820<br>0.04–0.12 | 245–870<br>0.04–0.13 | 280–475<br>0.04–0.07 | 6.8–17900<br>0.001–2.61 | 9130–15600<br>1.33–2.28 | 342–8690<br>0.05–1.27 | 772–3460<br>0.11–0.51 |
| Fe<br>$Fe_2O_3$ | 1940–3650<br>0.28–0.52 | 940–3655<br>0.13–0.52 | 2160–4250<br>0.31–0.61 | 14.0–8530<br>0.002–1.22 | 657–2010<br>0.09–0.29 | 1260–15600<br>0.18–2.23 | 4630–11600<br>0.66–1.66 |
| Zn<br>ZnO | 341–754<br>0.04–0.09 | 360–1155<br>0.04–0.14 | 589–755<br>0.07–0.09 | 321–2070<br>0.04–2.76 | 482–4320<br>0.06–0.54 | 80–7150<br>0.01–0.89 | 200–1460<br>0.02–0.18 |
| Li | 14–20 | 7.1–21 | — | 0.14–343 | — | 2.3–814 | — |
| Be | 4.9–12 | 5.9–13 | — | nd*–141 | — | 2.4–34 | — |
| Mn | 98–135 | 67–120 | — | 2.6–812 | — | 3.1–179 | — |
| Co | 0.62–1.6 | 0.40–1.5 | — | nd–14 | — | 0.28–15 | — |
| Ni | nd–2.08 | <0.33–2.0 | nd–3.65 | nd–78 | 6.22–40.6 | nd–245 | nd–42.1 |
| Cu | nd–1.09 | <0.15–1.4 | — | nd–1.2 | — | 0.13–5.0 | — |
| Ga | 179–298 | 136–275 | 159–316 | 1.3–401 | 61.0–226 | 21–355 | 81.4–238 |
| Zr | nd–0.22 | <0.013–0.04 | — | nd–0.43 | — | nd–0.086 | — |
| Sn | 1.6–3.4 | <0.084–0.71 | 42.1–53.6 | nd–26 | 24.9–38.9 | nd–0.49 | 46.6–58.5 |

*Abbreviation: nd = not detected

Binary correlation diagrams ($Fe_2O_3$ vs ZnO and $V_2O_3$ vs $Cr_2O_3$, as determined by EDXRF analysis) were plotted to show the distribution of the element population fields and to look for potential trends between the elements (Figure 23). The concentration ranges given by Malsy and Klemm (2010) and Chankhantha *et al.* (2020) are indicated by the arrows in the figures. Most of the Tajik samples fell in the concentration range of about 0.25–0.55 wt.% $Fe_2O_3$, 0.05–0.15 wt.% ZnO, 0.03–0.06 wt.% $V_2O_3$ and 0.05–0.10 wt.% $Cr_2O_3$.

## *UV-Vis-NIR Spectroscopy*

The UV-Vis-NIR absorption spectra of our Tajik samples (e.g. Figure 24) showed mixed Cr-Fe features with dominant $Cr^{3+}$ peaks at 410 and 540 nm. The $Fe^{2+}$ absorption at 387 nm is of variable intensity. A maximum at 544 nm (due to $Cr^{3+}$ + $Fe^{2+}$) was rarely observed. Bands associated with $Fe^{2+}$ at 372 nm and $V^{3+}$ (at 391 and 558 nm) were not observed. The spinel samples from Parawara and 'Afghan-Badakhshan' showed essentially the same UV-Vis-NIR spectral features.

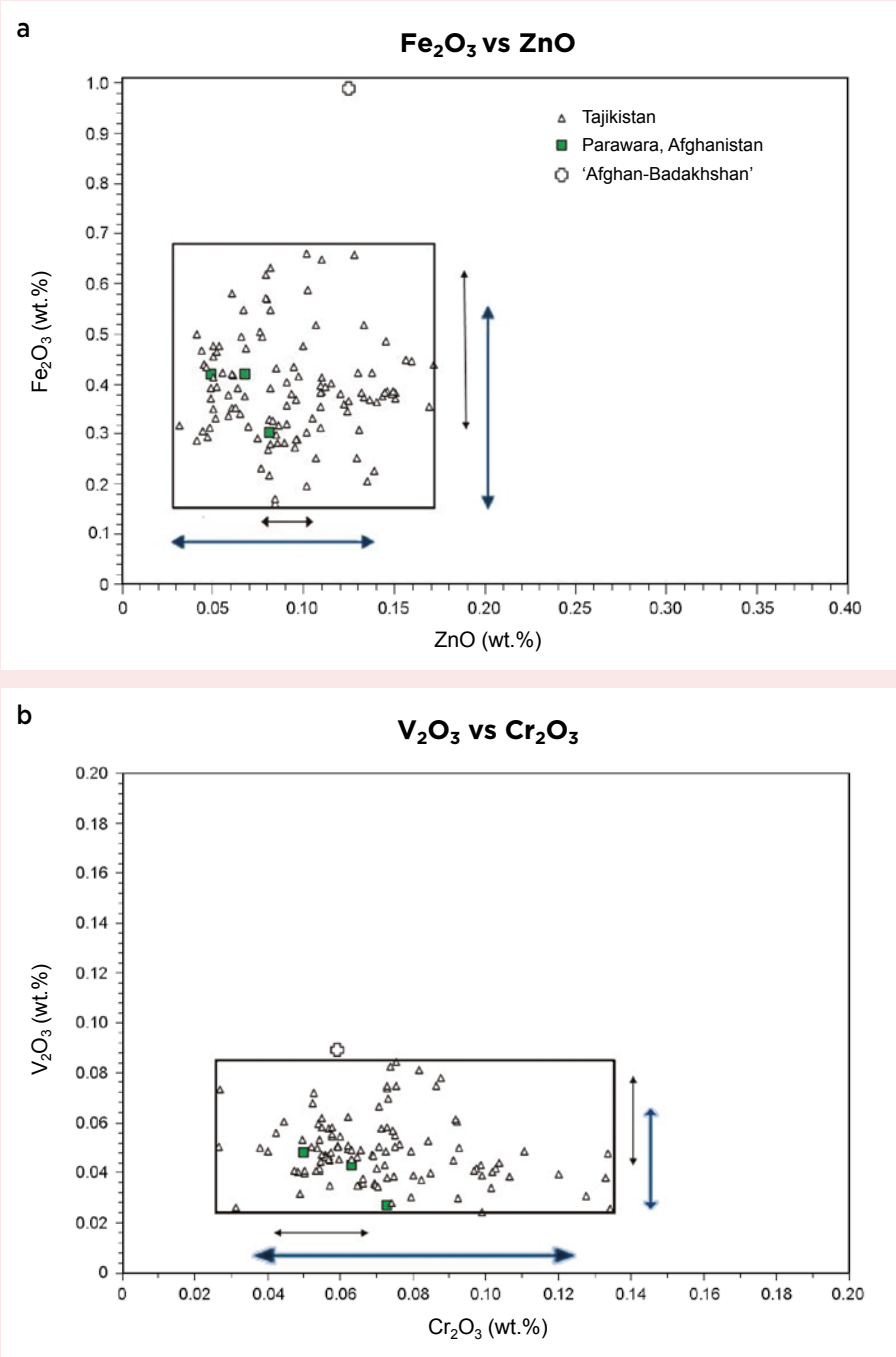


**Figure 23:** (**a**) $Fe_2O_3$ vs ZnO EDXRF data for the 115 Tajik spinels are plotted on this binary correlation diagram. The blue and black arrows indicate the ranges given by Malsy and Klemm (2010) and Chankhantha *et al.* (2020), respectively. The orangey pink 'Afghan-Badakhshan' spinel analysed in this study plots far outside the populated area. The three samples from the Parawara mine fall within the Kuh-i-Lal population field. (**b**) $V_2O_3$ vs $Cr_2O_3$ EDXRF data for the 115 Kuh-i-Lal spinels constrain a population field that is also encompassed by the concentration ranges given by Malsy and Klemm (2010; blue arrows) and Chankhantha *et al.* (2020; black arrows). The three samples from the Parawara mine fall within this field, but the Afghan-Badakhshan sample has a slightly higher V content than the Tajik samples.

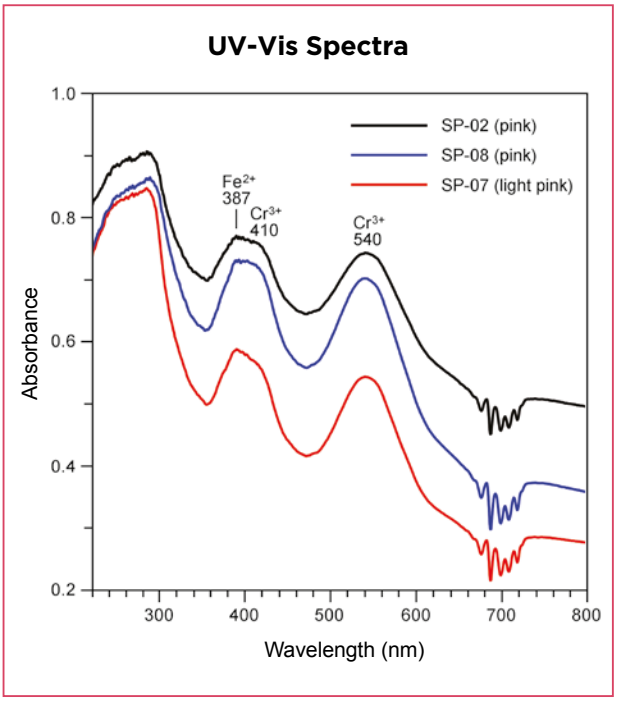


**Figure 24:** These representative UV-Vis absorption spectra of Tajik spinels show strong $Cr^{3+}$-related bands at 410 and 540 nm; the $Fe^{2+}$-related band at 387 nm was of variable intensity in the different samples. The features near 700 nm are due to luminescence of the Cr spin-forbidden bands that results from illuminating the sample with white light. The path length of the beam was 2–3 mm.

## DISCUSSION AND CONCLUSIONS

Spinels from the Kuh-i-Lal mining area in Tajikistan are most commonly pink to purplish pink and, very rarely, orangey pink. In general, their colour can be described as 'rose coloured'. Red Tajik spinels (such as the exceptional 16.33 ct octagonal-cut stone in Figure 2) are extremely rare.

The data for the samples examined for this study are in good accordance with published literature (cf. Sturman 2009; Malsy & Klemm 2010; Chankhantha *et al.* 2020). The optical, physical and chemical properties of Tajik spinels display relatively little variability compared to spinels from other localities, such as Myanmar and Vietnam. This is probably because the Tajik spinel mineralisation occurs within a rather uniform geological setting in a relatively small area of the Pyanj River Valley.

### *Internal Features*

The internal features of Tajik spinels have been described previously (Gübelin & Koivula 1986; Sturman 2009; Malsy & Klemm 2010; Chankhantha *et al.* 2020). Relatively few mineral inclusions have been identified: mica, carbonates and graphite (Gübelin & Koivula 1986); and zircon, phlogopite and graphite (Malsy & Klemm 2010). Graphite is derived from the metamorphism of organic substances in the host rock (Giuliani *et al.* 2018), and seems to have been widely available during the growth of the Tajik spinels. Other internal features include needle-like inclusions, negative crystals, light-scattering particles and partially healed fissures.

The assemblage of mineral inclusions identified in our Tajik spinels is consistent with their formation history (i.e. in a platform carbonate series that was metamorphosed to upper amphibolite facies; Garnier *et al.* 2008). The solid inclusions and the various fillings present in primary and (pseudo-)secondary cavities reflect the composition of impurities in the surrounding host rock.

Compared to spinels from Myanmar and Vietnam, which display a large variety of mineral inclusions, the internal world of Tajik spinel is less rich. The most notable inclusion mineral is the Mg-silicate forsterite ($Mg_2SiO_4$), but it was scarce in our samples. The presence of forsterite in primary and (pseudo-)secondary cavities and as isolated mineral inclusions is not surprising, since the Kuh-i-Lal spinel deposit is hosted by ultra-magnesian enstatite-forsterite rocks (magnesian skarns). The two types of forsterite inclusions documented in our samples probably represent two generations: protogenetic transparent colourless crystals with rounded edges (Figure 8), and syngenetic well-formed crystals (Figure 9). Forsterite inclusions have also been documented in spinels from Mogok, Tanzania and Sri Lanka (Phyo *et al.* 2019).

The most common and distinctive inclusions in spinels originating from various geographic locations and different geological-genetic environments are negative crystals—that is, generally octahedron-like cavities that reflect the shape of a spinel crystal (e.g. Gübelin & Koivula 2005; Malsy & Klemm 2010). The inclusion scenario in our Tajik spinels was dominated by primary and (pseudo)-secondary cavities that displayed large variations in size, shape and nature of the filling materials. Cavity fillings containing only mineral substances (most commonly carbonates) have been described in spinels from various localities (Gübelin & Koivula 1986, 2005; Malsy & Klemm 2010; Lomthong *et al.* 2019). The cavities in the Tajik spinels host graphite, micas, carbonates, zircon, forsterite and other solids. Those containing liquid-gas or multiphase fillings were extremely rare.

Most common in our Tajik spinels were partially healed fissures with (very) poorly developed, generally coarse textures that were composed of isolated constituents of variable size and shape. 'Classic' healing textures in the form of fingerprint or network-like patterns, sometimes with flat gaseous inclusions, were scarce.

## Comparison to Spinels from Afghanistan

Purple spinels from the Parawara mine in Afghanistan examined by one of the authors (DS) in Bangkok during the period 2017–2018 had very few (unidentified) solid inclusions in the form of colourless, transparent, irregularly shaped crystals that occurred singly or in small cluster-like formations. The faceted 1.38 ct stone reportedly from the Afghan part of Badakhshan examined in this study contained numerous opaque black (mostly plate-like) graphite crystals that were oriented in different directions.

Information about the internal features of Afghan spinels is very scarce in the literature. Boehm (2017) observed inclusions that resembled clusters and booklets of colourless mica in purple spinels from the Parawara mine. Belley and Palke (2021) reported that among the inclusions seen in an Afghan spinel from Badakhshan were fields of negative crystals (presumably hosting fluid inclusions), tiny black dust-like particles and colourless minerals. Some of the inclusions were identified by Raman spectroscopy as phlogopite, and an elongate inclusion was tentatively identified as an amphibole-group mineral.

## Chemical Composition

The chemical composition of the Tajik spinels in this study is consistent with data reported by Malsy and Klemm (2010) and Chankhantha *et al.* (2020; cf. Tables II and III). However, it differs to some extent from the data given by Giuliani *et al.* (2017), who obtained a relatively high Fe concentration (up to about 1 wt.% $Fe_2O_3$) that has not been reported elsewhere for Tajik spinel. The V contents measured by Giuliani *et al.* (2017) are also distinctly higher than the concentrations given elsewhere. The ranges obtained by Chankhantha *et al.* (2020) for Zn and Cr are narrower than those reported by Malsy and Klemm (2010) and obtained in this study (Figure 23).

The trace-element contents summarised in Table III show good matches except for Sn. Malsy and Klemm (2010) reported very low Sn contents (<0.084–0.71 ppmw), while Chankhantha *et al.* (2020) gave 42.1–53.6 ppmw Sn. The Tajik spinels analysed for this study had Sn contents of 1.6–3.4 ppmw, between those of the other two studies.

In general, the chemical composition of spinels from the Himalayan mountain range reflects the geological-geochemical signature in the marble units of the metamorphosed platform carbonate series that hosts the spinel mineralisation. The large variation in some minor and trace elements in the spinels—even in the same mining area (e.g. Cr for Mogok spinel)—indicates that the abundance of these elements was subject to distinct variations, even within small-scale domains.

According to Hubbard *et al.* (1999), the metamorphic rocks on the Afghan side of the Pyanj River consist largely of migmatitic, banded or augen biotite gneiss locally containing garnet and sillimanite. These rocks are similar to the Goran Series and Shakhdara Series above the Khorog meta-igneous suite in Tajikistan (Hubbard *et al.* 1999). The metamorphic rocks at Sar-e-Sang (including the Parawara spinel mine) include whiteschists and other ultra-magnesian rocks remarkably similar to those described at Kuh-i-Lal and other localities on the Tajikistan side of Badakhshan. The Sar-e-Sang rocks experienced a two-stage metamorphic evolution with pressure and temperature conditions virtually identical to those inferred for the Tajik side (Hubbard *et al.* 1999). This explains why the three spinels from the Parawara mine examined for this study plot within the chemical population fields occupied by the Kuh-i-Lal spinels in correlation diagrams (e.g. Figure 23).

## Geographic Origin Determination of Spinel

The current approach for the geographic origin determination of coloured stones is based on collecting a complete set of data for an unknown sample—physical-optical values, internal features (microscopic characteristics and identification of solid inclusions using Raman analysis), UV-Vis-NIR and infrared spectroscopy, and chemical fingerprinting—and comparing these properties to data obtained for reference samples of known locality that should be representative of the deposit's entire 'lifetime'. Most of these mineralogical-gemmological characteristics are of limited value for the origin determination of spinel due to considerable overlap among stones from various localities. Internal features might be helpful, but many spinels (especially those weighing <2 ct) lack any inclusions. In the case of the Tajik spinels, where forsterite is the most notable inclusion mineral, it must be emphasised that it is very rare. In addition, forsterite has been documented in spinels from other localities.

Considering the overlapping of internal and spectral features, chemical fingerprinting has emerged as a powerful tool for the geographic origin determination of spinels (and other coloured stones). Compared to their 'Himalayan cousins' from the Mogok Stone Tract in Myanmar and the Luc Yen–Yen Bai area in Vietnam, the Tajik spinels generally have the lowest concentration ranges for all five of the trace elements typically measured by EDXRF spectroscopy (Ti, V, Cr, Fe and Zn; see Table III). By using correlation diagrams involving these five elements, the separation of the Tajik spinels from their

Himalayan counterparts (and from spinels originating in Africa and Sri Lanka) is, in general, possible.

The use of trace-element profiles (plotted in various types of correlation diagrams) based on EDXRF and LA-ICP-MS data has become routine in the laboratories doing origin determination. Statistical trace-element data-processing techniques such as the 'selective plotting method' (Saeseaw *et al*. 2009; Palke *et al*. 2019), linear discriminant analysis (Chankhantha *et al*. 2020) and multi-element analysis using t-distributed stochastic neighbour embedding (Wang & Krzemnicki 2021) will be of increasing importance in the future. The authors hope that the chemical data provided in this article can contribute to these efforts with regard to spinel.

## REFERENCES


Ball, V. 1893. A description of two large spinel rubies, with Persian characters engraved upon them. *Proceedings of the Royal Irish Academy,* 3rd Series, **3**(1), 380–400 and Pl. 10.

Belley, P.M. & Palke A. 2021. Purple gem spinel from Vietnam and Afghanistan: Comparison of trace element chemistry, cause of color, and inclusions. *Gems & Gemology*, **57**(3), 228–238, https://doi.org/10.5741/gems.57.3.228.

Boehm, E. 2017. Gem Notes: Purple spinel from Badakhshan, Afghanistan. *Journal of Gemmology*, **35**(8), 696–697.

Chankhantha, C., Amphon, R., Rehman, H.U. & Shen, A.H. 2020. Characterisation of pink-to-red spinel from four important localities. *Journal of Gemmology*, **37**(4), 393–403, https://doi.org/10.15506/JoG.2020.37.4.393.

Garnier, V., Maluski, H., Giuliani, G., Ohnenstetter, D. & Schwarz, D. 2006. Ar-Ar and U-Pb ages of marble-hosted ruby deposits from Central and Southeast Asia. *Canadian Journal of Earth Sciences*, **43**(4), 509–532, https://doi.org/10.1139/e06-005.

Garnier, V., Giuliani, G., Ohnenstetter, D., Fallick, A.E., Dubessy, J., Banks, D., Vinh, H.Q., Lhomme, T. *et al*. 2008. Marble-hosted ruby deposits from Central and Southeast Asia: Towards a new genetic model. *Ore Geology Reviews*, **34**(1–2), 169–191, https://doi.org/10.1016/j.oregeorev.2008.03.003.

Giuliani, G., Ohnenstetter, D., Fallick, A.E., Groat, L.A. & Fagan, A. 2014. Chapter 2: The geology and genesis of gem corundum deposits. *In*: Groat, L.A. (ed) *Geology of Gem Deposits*, 2nd edn. Mineralogical Association of Canada Short Course Series Vol. 44, 29–112.

Giuliani, G., Dubessy, J., Banks, D.A., Lhomme, T. & Ohnenstetter, D. 2015. Fluid inclusions in ruby from Asian marble deposits: Genetic implications. *European Journal of Mineralogy*, **27**(3), 393–404, https://doi.org/10.1127/ejm/2015/0027-2442.

Giuliani, G., Fallick, A.E., Boyce, A.J., Pardieu, V. & Pham, V.L. 2017. Pink and red spinels in marble: Trace elements, oxygen isotopes, and sources. *Canadian Mineralogist*, **55**(4), 743–761, https://doi.org/10.3749/canmin.1700009.

Giuliani, G., Fallick, A.E., Boyce, A.J., Pardieu, V. & Pham, V.L. 2018. Origine géographique des spinelles chromifères et vanadifères associés aux marbres d'Asie et d'Afrique de l'Est. *Revue de Gemmologie A.F.G.*, No. 203, 17–25.

Grew, E.S., Pertsev, N.N., Yates, M.G., Christy, A.G., Marquez, N. & Chernosky, J.V. 1994. Sapphirine + forsterite and sapphirine + humite-group minerals in an ultra-magnesian lens from Kuhi-lal, SW Pamirs, Tajikistan: Are these assemblages forbidden? *Journal of Petrology*, **35**(5), 1275–1293, https://doi.org/10.1093/petrology/35.5.1275.

Grew, E.S., Pertsev, N.N., Vrána, S., Yates, M.G., Shearer, C.K. & Wiedenbeck, M. 1998. Kornerupine parageneses in whiteschists and other magnesian rocks: Is kornerupine + talc a high-pressure assemblage equivalent to tourmaline + orthoamphibole? *Contributions to Mineralogy and Petrology*, **131**(1), 22–38, https://doi.org/10.1007/s004100050376.

Gübelin, E.J. & Koivula, J.I. 1986. *Photoatlas of Inclusions in Gemstones*. ABC Edition, Zurich, Switzerland, 532 pp.

Gübelin, E.J. & Koivula, J.I. 2005. *Photoatlas of Inclusions in Gemstones*, Vol. 2. Opinio Publishers, Basel, Switzerland, 829 pp.

Harlow, G.E. & Bender, W. 2013. A study of ruby (corundum) compositions from the Mogok belt, Myanmar: Searching for chemical fingerprints. *American Mineralogist*, **98**(7), 1120–1132, https://doi.org/10.2138/am.2013.4388.

Hauzenberger, C.A., Hager, T., Baumgartner, L.P. & Hofmeister, W. 2001. High-grade metamorphism and stable isotope geochemistry of N-Vietnamese gem bearing rocks. *Proceedings of the Workshop on Gems and Minerals of Vietnam*, Hanoi, Vietnam, 124–138.

Hubbard, M.S., Grew, E.S., Hodges, K.V., Yates, M.G. & Pertsev, N.N. 1999. Neogene cooling and exhumation of upper-amphibolite-facies 'whiteschists' in the southwest Pamir Mountains, Tajikistan. *Tectonophysics*, **305**(1–3), 325–337, https://doi.org/10.1016/s0040-1951(99)00012-8.

Hughes, R.W. & Pardieu, V. 2006. Ruby & spinel from Tajikistan–Moon over the Pamirs. https://ruby-sapphire.com/articles/777-tajikistan-ruby-and-spinel, 1 September, accessed 21 February 2022.

Liu, Y., Hu, Z., Gao, S., Günther, D., Xu, J., Gao, C. & Chen, H. 2008. *In situ* analysis of major and trace elements of anhydrous minerals by LA-ICP-MS without applying an internal standard. *Chemical Geology*, **257**(1–2), 34–43, https://doi.org/10.1016/j.chemgeo.2008.08.004.

Lomthong, P., Schwarz, D., Zoysa, G., Yanyu, C. & Liu, Y. 2019. Spinels from Sri Lanka. *InColor*, No. 43, 40–52.

Malsy, A. & Klemm, L. 2010. Distinction of gem spinels from the Himalayan mountain belt. *Chimia*, **64**(10), 741–746, https://doi.org/10.2533/chimia.2010.741.

Ogden, J.M. 2020. The Black Prince's Ruby: Investigating the legend. *Journal of Gemmology*, **37**(4), 360–373, https://doi.org/10.15506/JoG.2020.37.4.360.

Okrusch, M., Bunch, T.E. & Bank, H. 1976. Paragenesis and petrogenesis of a corundum-bearing marble at Hunza (Kashmir). *Mineralium Deposita*, **11**(3), 278–297, https://doi.org/10.1007/bf00203079.

Palke, A.C., Saeseaw, S., Renfro, N.D., Sun, Z. & McClure, S.F. 2019. Geographic origin determination of blue sapphire. *Gems & Gemology*, **55**(4), 536–579, https://doi.org/10.5741/gems.55.4.536.

Pardieu, V. & Hughes, R.W. 2008. Spinel: Resurrection of a classic. *InColor*, No. 8, 10–18.

Pardieu, V. & Farkhodova, T. 2019. Spinel from Tajikistan: The gem that made famous the word "ruby". *InColor*, No. 43, 30–33.

Pêcher, A., Giuliani, G., Garnier, V., Maluski, H., Kausar, A.B., Malik, R.H. & Muntaz, H.R. 2002. Geology, geochemistry and Ar–Ar geochronology of the Nangimali ruby deposit, Nanga Parbat Himalaya (Azad Kashmir, Pakistan). *Journal of Asian Earth Sciences*, **21**(3), 265–282.

Phyo, M.M., Bieler, E., Franz, L., Balmer, W. & Krzemnicki, M.S. 2019. Spinel from Mogok, Myanmar—A detailed inclusion study by Raman microspectroscopy and scanning electron microscopy. *Journal of Gemmology*, **36**(5), 418–435, https://doi.org/10.15506/JoG.2019.36.5.418.

Rossovskiy, L.N., Kovalenko, S.I. & Ananjev, S.A. 1982. Conditions of ruby formation in marble. *Geologiya Rudnyh Mesorozhdeniy*, **24**(2), 57–66.

Saeseaw, S., Wang, W., Scarratt, K., Emmett, J.L. & Douthit, T.R. 2009. Distinguishing heated spinels from unheated natural spinels and from synthetic spinels: A short review of on-going research. Gemological Institute of America, 2 April, 13 pp., https://www.gia.edu/doc/Heated-spinel-Identification-at-April-02-2009.pdf.

Sturman, N. 2009. Lab Notes: Purplish pink spinel from Tajikistan—Before and after cutting. *Gems & Gemology*, **45**(1), 57–58.

Wang, H.A.O. & Krzemnicki, M.S. 2021. Multi-element analysis of minerals using laser ablation inductively coupled plasma time of flight mass spectrometry and geochemical data visualization using t-distributed stochastic neighbor embedding: Case study on emeralds. *Journal of Analytical Atomic Spectrometry*, **36**(3), 518–527, https://doi.org/10.1039/d0ja00484g.

## The Authors

**Dr Dietmar Schwarz**
Department of Jewelry, Zhejiang College of Tongji University, Jiaxing 314051, China; and Shanghai Gem and Material Technology Engineering Research Center, Tongji University, Shanghai 200092, China
and
Bellerophon Gem Lab, 26-28 Soi Mahesak 3, Bangkok 10500, Thailand
Email: drdietmarschwarz@hotmail.com

**Yicen Liu and Dr Zhengyu Zhou**
State Key Laboratory of Marine Geology and School of Ocean and Earth Science, Tongji University, Shanghai 200092, China; Laboratory of Gem and Technological Materials, Tongji University, Shanghai 200070, China
Email: liuyicen1998@126.com

**Pantaree Lomthong**
Consultant Gemmologist, Bangkok, Thailand

**Theodore Rozet**
Bellerophon Gem Lab, 26-28 Soi Mahesak 3, Bangkok 10500, Thailand

## Acknowledgements

We acknowledge Prof. Lijian Qi, Liang Chen and Wenxian Hua for their assistance with the sample analysis. This research was supported by special funding from the Shanghai Science and Technology Commission (15DZ2283200, 18DZ2281300) and the Gem Discipline Development Fund. The three anonymous reviewers are thanked for their valuable suggestions and comments. Many thanks to Pamir Gems Co. Ltd. (Bangkok) for providing photos.

Gem-A
INSTRUMENTS



OVER **100** PRODUCTS AVAILABLE

# Buy Gem-A Instruments online!


## View the full collection at:
## **shop.gem-a.com**

### GEM-A MEMBERS!

Login to the Gem-A Instruments website and gain instant access to discounted rates.

**Username** is your membership number.

**Password** is your surname with a capitalised first letter.

You must log in before adding products to your basket.

We recommend changing your password in the account settings.

**Figure 1:** This first-century BCE pair of Greek gold bracelets (each approximately 5.3 × 7.9 cm) is set with emerald, garnet, other gems and enamel, and is purportedly from the Olbia Treasure, found in Parutyne in what is today Ukraine. Given the jewellery's age, the emeralds are likely from Egypt. Acquired by Henry Walters, 1926; courtesy of The Walters Art Museum, Baltimore, Maryland, USA (inv. no. VO.59, 57.375 and 57.376).

# Cleopatra's Emerald Mines: The Marketing of a Myth

Jack M. Ogden

**ABSTRACT:** Mentions of emeralds and their history often refer to 'Cleopatra's emerald mines'. This appears on the internet, in gem books and gemmological education, and even in some of the 'dossiers' that gem laboratories provide to help market their clients' gems. This evocative linking of emeralds with the famous Egyptian queen—lover of Roman dictator Julius Caesar and wife of statesman Mark Antony, and made famous by Shakespeare and Elizabeth Taylor—is undoubtedly appealing, but where is the substantiation for this connection? The author's investigation suggests that Cleopatra had no special link with emeralds or the mines they came from. Her association with emerald's history probably originated from the shrewd marketing skills of the entrepreneurial nineteenth-century London jeweller Edwin Streeter.

*The Journal of Gemmology,* **38**(2), 2022, pp. 156–170, https://doi.org/10.15506/JoG.2022.38.2.156


In the first century CE, the Roman writer Pliny devoted an entire volume of his *Natural History* to gems (Book 37; Eichholz 1962), providing us with extraordinary insight into the variety of gem materials used in his time, as well as their properties and sources. He ranked emerald third in esteem among gems, after diamond and pearl, and stated that nothing was more intensely green and no colour had a more pleasing appearance (Eichholz 1962, p. 213). Admittedly, the Latin term he used—*smaragdus*—included some other green stones, but surviving jewellery demonstrates that emeralds were highly prized around his time. A spectacular example is a pair of bracelets from the Olbia Treasure (Figure 1), which date to a generation or two before Pliny. Various

localities for *smaragdus* were listed by Pliny, including Egypt, which is known as the primary source of emeralds in antiquity (Ogden 1990, pp. 82–88). In recent times, it has been commonplace to link the history of emeralds to Cleopatra, the famous first-century BCE queen of Egypt. This is an appealing association, but whence does it originate? This article looks back over the last century-and-a-half to help expose the background to this supposed connection with Cleopatra and how it seems to tie in with growing British commercial interest in the Egyptian emerald mines in the nineteenth and early twentieth centuries.

## EGYPT'S EMERALD MINES

Almost two centuries ago, the pioneering British Egyptologist John Gardner Wilkinson visited the historic emerald mines in the arid Wadi Sikait–Gebel Zabara region of the Eastern Desert of Egypt, between the Nile River and the Red Sea (Figure 2; for a map, see Jennings *et al.* 1993, p. 103). These were, he said, 'far less interesting than might be supposed' (Wilkinson 1835, p. 420). Today, however, no mention of these mines, whether in a gemmology textbook or popular account, fails to link them with Cleopatra, imbuing them with something of the exoticism and glamour of the Egyptian queen. What had changed?

Described by ancient Greek, Roman and Medieval Arab writers, these Egyptian deposits were the primary source of emeralds to the ancient and medieval worlds. The present author had the good fortune to visit two of these remote mining areas in 1989 as part of a small geological expedition. Emeralds were seen *in situ* as hexagonal prismatic crystals in a micaceous schist (Figure 3). Some of the ancient mine workings and habitations were still visible, and emeralds were found lying on the ground, albeit small and fractured (Figure 4). Many people have visited these remote mines over the years, and the geology of the deposits and the characteristics of the gems have been well studied and published, along with the archaeology of the mines and associated settlements (e.g. Shaw *et al.* 1999; Harrell 2004, 2006, in prep.; Sidebotham *et al.* 2008; Oller Guzmán *et al.* 2021). Harrell (2006, p. 5) noted:

> The beryl occurs in both the phlogopite schist and quartz/pegmatite veins and is restricted to within tens of centimetres of their contact. It is found as individual crystals or, more often, as small clusters of crystals. Crystals can be up to a few centimetres in length, but most are much shorter.

For the gemmological characteristics of the emeralds, see Jennings *et al.* (1993), and for recent trace-element analyses, see Gawad *et al.* (2022).

Archaeological evidence from the mines, ancient texts and surviving early jewellery shows that these deposits were not worked before about the time of Alexander

**Figure 2:** The emerald mining area in the Eastern Desert of Egypt lies in a rugged, inhospitable region. An observation station can be seen on the peak to the left. Photo © J. M. Ogden.

**Figure 3:** Emerald crystals are seen here in micaceous schist in the Wadi Sikait region, Egypt. The largest crystal is about 1 cm long. Photo © J. M. Ogden.

**Figure 4:** Emerald crystals are observed lying on the ground in the Wadi Sikait region. The largest crystal is about 1 cm across. Photo © J. M. Ogden.

the Great's invasion of Egypt in 332 BCE, and emeralds were not common in Greek jewellery until about the first century BCE. Later Greek examples are seen in necklaces and earrings, and less commonly in rings. However, one of the most spectacular examples is the pair of bracelets from the Olbia Treasure mentioned above (again, see Figure 1).

John Gardner Wilkinson indicated that the mines had been worked at least a thousand years before Alexander the Great (Wilkinson 1837, p. 231). This statement has long been discredited, and the various early Egyptian 'emeralds' that have been examined since his time have been identified as other gem materials (usually amazonite). We might be tempted to place more confidence in the identity of a bead found in an Egyptian burial site dating back more than 5,000 years because it was described as emerald by the Viennese mineralogist Prof. Cornelio Doelter (Junker 1919, p. 102). In theory, there is no reason why an emerald picked up from the desert floor could not make its way at that time to the markets in the Nile Valley, but in this case its description as a bead implies that it was drilled, something not possible during that period for such a relatively hard material.[1]

Egyptian emerald mining blossomed considerably after Egypt became a Roman province in 30 BCE, and the typically pale, included Egyptian emeralds became relatively common in Roman jewellery, usually retaining their hexagonal crystal form with just some superficial polishing and longitudinal drilling (e.g. Figure 5).[2] They are seen in Roman jewellery from throughout much of the Empire and are clearly recognisable in painted funerary portraits of the Roman period found in Egypt (Figures 6 and 7). The productivity of the mines was made possible by an almost unlimited supply of labourers. The Romans condemned criminals and prisoners of war to the Egyptian mines, a punishment viewed as equivalent to a death sentence. The reservoir of miners grew when the Roman persecution of Christians began. It is likely that many of these unfortunates were sent to work the Egyptian gold mines, although emeralds were likely referred to by the early Christian philosopher Clement of Alexandria when he mentioned 'gems dug up by those among us who are condemned to death' (Le Nourry 1857, col. 542).[3] And not just Christians were exiled to Egyptian mines. The Jewish historian Josephus indicated that after the capture of

[1] Emerald has a Mohs hardness of 7½–8 and thus requires emery to cut and polish it. There is no clear evidence for the use of emery in lapidary work until about 2000 BCE (see, e.g., Sax *et al.* 2000).

[2] Some authors have described surviving examples of Roman emeralds as rare, but this is not true. They are relatively abundant but tend to be found in jewellery from Roman Europe, Egypt and what is now Turkey, and not from Roman burial sites in Syria and down the Levantine coast. (The opposite is true of garnets.) One reason for their apparent scarcity is that they have often been described by other names, most commonly *plasma* in older works. Oxygen isotope studies of emeralds in Roman jewellery suggest that the Swat Valley of Pakistan and Habachtal in Austria possibly supplied some, in addition to Egypt (see Giuliani *et al.* 2000). Emeralds that were deeper green and had greater clarity (and typically with a different cutting style) began to appear in Late Roman jewellery and were perhaps from Pakistan, although there has been no detailed study of these to date.

[3] The Greek word translated here as 'gems' is *lithous* (λιθους). This can mean stones in general, not just gems, but from the context it certainly meant gems.

**Figure 5:** In this first- to second-century CE Roman emerald-and-gold necklace (33.5 cm long), all but one of the emeralds are simply drilled and superficially polished crystals. Courtesy of The Metropolitan Museum of Art, New York, New York, USA (inv. no. 21.29.2).

**Figure 6:** This mummy portrait of a woman wearing emerald jewellery is dated 100 CE, and attributed to the Isidora Master (Romano-Egyptian). It measures 48.0 × 36.0 × 12.8 cm and is painted in encaustic wax on linden wood with gilding. Courtesy of The J. Paul Getty Museum, Villa Collection, Malibu, California, USA (inv. no. 81.AP.42).

**Figure 7:** Detail of a first- to second-century CE painted funerary portrait from Egypt shows a gold chain and a necklace similar to that in Figure 5. Museum of Fine Arts, Boston, Massachusetts, USA (inv. no. 93.1451); photo © J. M. Ogden.

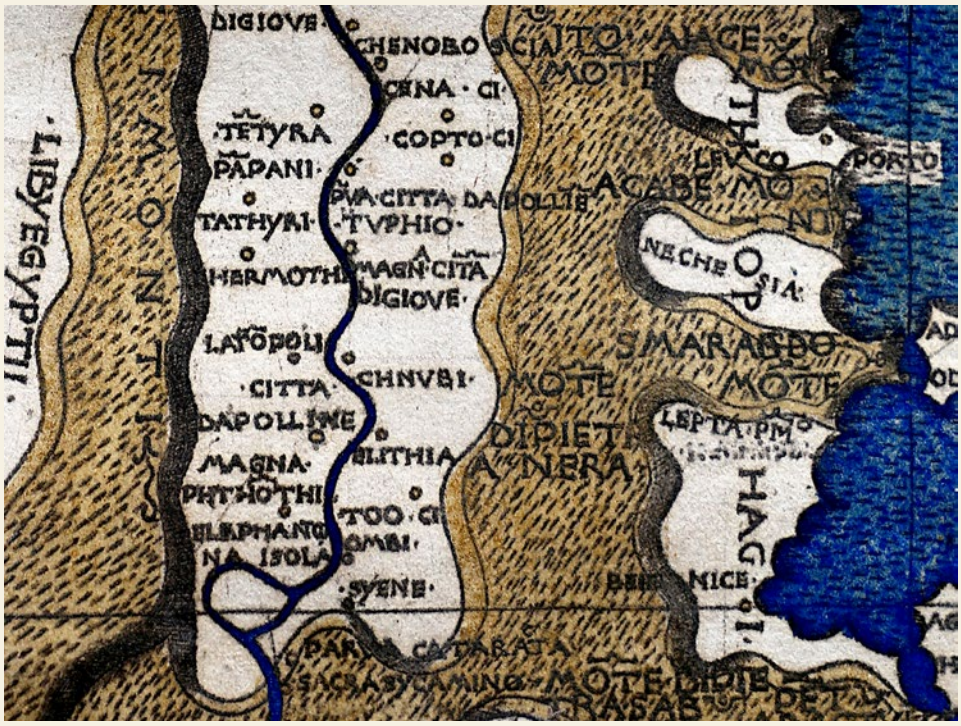


**Figure 8:** Detail of Francesco Berlinghieri's 1482 map of Egypt shows *Smaragdo Monte* (Emerald Mountain) at centre right. The word *Monte* has been abbreviated by truncating the 'n'. Courtesy of Wikimedia Commons.

Jerusalem in 70 CE many of those over 17 years old were sent to work there (Josephus 4.9.12).

The source of emeralds in Egypt had been noted by the Greek geographer Claudius Ptolemy in the second century CE (Nobbe 1843, p. 252), and maps showing his *Smaragdus Oros* (*Smaragdus Mons* in Latin, meaning Emerald Mountains) continued to be drafted based on his descriptions up to the eighteenth century. Figure 8 shows a detail of the Italian scholar Francesco Berlinghieri's 1482 map of Egypt; *Smaragdo Monte* is centre right. The Egyptian emerald mines were worked in medieval Islamic times and described in some detail by writers such as Ahmad Al-Tifashi, who died in 1253 (Huda 1998, p. 104). Ian Shaw and his colleagues mentioned that ceramic material found at the Gebel Zabara mining area dates to as late as the sixteenth century (Shaw *et al.* 1999, p. 206).

The first modern European to describe a visit to the area—having been 'told strange stories of the Mountain of Emeralds' (Bruce 1790, p. 204)—seems to have been the Scot James Bruce (1730–1794), who travelled in Egypt and Sudan between 1769 and 1773. He recorded that he visited the mines on 16 March 1769, but he does not seem to have been impressed, as he was 'little endowed with inclination to descend into any of them, where the air was probably bad' (Bruce 1790, p. 207). He picked up green fragments from the ground, but he considered them unlikely to be emerald and, in any case, inferior to the emeralds from South America (Bruce 1790, pp. 206–208). He noted, 'Having satisfied my curiosity as to these mountains…I returned to my boat, where I found all well, and an excellent dinner of fish prepared' (Bruce 1790, p. 209).[4] Judging by the timescale he gives, James Harrell (pers. comm. 2021) has suggested that he never reached the actual mines, but rather just water wells on the route to them.

Next came the French mineralogist and explorer Frédéric Cailliaud (1787–1869), a jeweller by training. He arrived in Egypt in 1815, keen to enlarge his collection of minerals. Muhammad Ali, the Ottoman viceroy and ruler of Egypt, sent him on a mission to investigate the gold and emerald mines in the Eastern Desert, which he hoped might prove to be of economic benefit to the country (Cailliaud 1822; Bednarski & Harer 2013). In 1816, after an arduous journey he arrived at the mines—possibly the first European to do so—and reported, 'As

[4] Bruce also visited the Isle of Zabargad in the Red Sea, the ancient source of peridot. He found some 'pieces of green pellucid chrystaline substance'. These were 'veiny, clouded, and not at all so hard as rock-crystal; a mineral production certainly, but a little harder than glass' (Bruce 1790, p. 206).

I was sitting on some pieces of rock, my eye suddenly glanced on a fragment of emerald, of a dark green. My surprise and joy made me forget all fatigue…' (Cailliaud 1822, p. 30). He described the mines and the occurrence of the emeralds. One mine went 80 feet (24.4 m) underground and was 'so considerable that 300 men might labour in it together' (Cailliaud 1822, p. 32). He returned to Cairo, informed Muhammad Ali of what he had found and was then charged with returning to the mines with labourers to work them. He did, with miners that were mainly Syrian, Greek and Albanian.[5] Cailliaud and his miners spent a month working there and, although they discovered a great many old tunnels, they did not achieve success in creating a new economic dawn for Egypt. It had been a hard trip. Cailliaud recounted that there was sometimes an almost total lack of water in the springs, and for six days 'the whole of our sustenance was a little biscuit dipped in water' (Cailliaud 1822, p. 40).

Over the next decade, various other European visitors to the mines included the Italian circus strongman-turned-Egyptologist Giovanni Belzoni, and also John Gardner Wilkinson, as mentioned above. Both provided maps. A detail of Belzoni's map is shown in Figure 9 (Belzoni 1820, pl. 38). Wilkinson's hand-drawn map, plus a few samples of emeralds from Gebel Zabara, are in the Natural History Museum, London. He noted that the mines had been opened by 'the present pasha, but have not produced emeralds of any value' (Wilkinson 1835, p. 420).

## CLEOPATRA

None of these early visitors to the mines made any mention of a connection to Queen Cleopatra, so where did this association come from? The Cleopatra portrayed to us by Shakespeare, and in the epic 1963 film with Elizabeth Taylor in the title role, as well as a host of other books, films, plays and artworks (e.g. Figure 10) was Cleopatra VII Philopator (r. 51–30 BCE). She was the final ruler of Egypt's Macedonian Ptolemaic dynasty, which was founded in the wake of Alexander the Great's conquest of the country in 330 BCE. Following Alexander's death in 323 BCE, his empire was split up and, after nearly two decades of warfare, one of his Greek generals, Ptolemy, established the Ptolemaic dynasty in Egypt. Nearly three centuries later, Cleopatra VII came to the throne. She set out to gain the help of Roman dictator Julius Caesar in the interminable fighting within the Ptolemaic family. In the words of the second-century-CE Roman historian Dio Cassius, she was 'a woman of surpassing beauty' who knew how to use it to

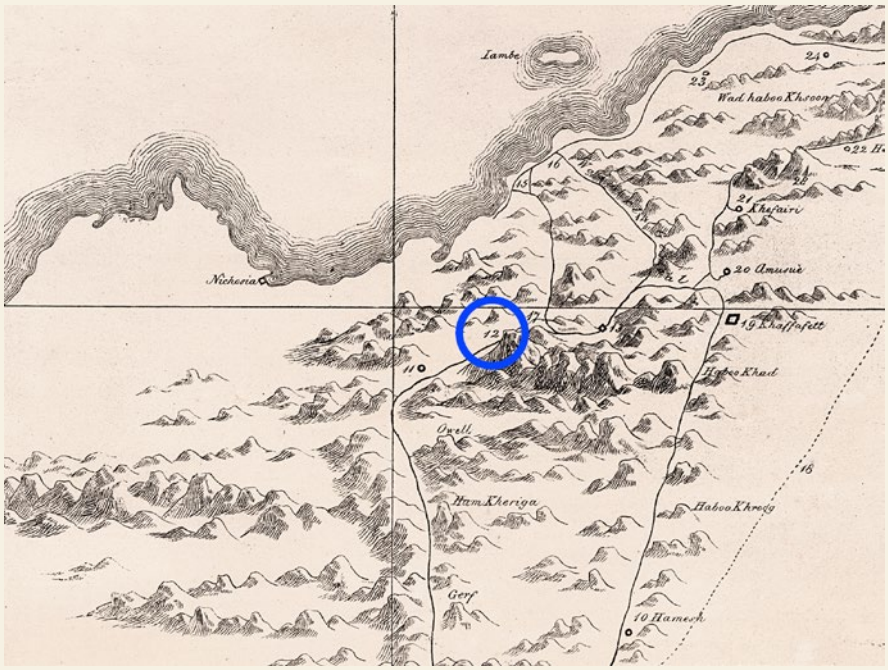


**Figure 9:** Detail of Giovanni Belzoni's 1820 'Map of Roads to the Mountains of the Emeralds and Berenice on the Red Sea' shows a point numbered 12 (circled here) and labelled in the map's key as 'Emerald Mountains'. From Belzoni (1820, pl. 38).

[5] In the 1890s, the explorer Ernest Ayscoghe Floyer saw the stone edifices built by these miners and commented that they were worse house builders than the Romans but better miners (Floyer 1893b, pp. 424-425).

**Figure 10:** Hans Markart's 'The Death of Cleopatra', painted 1875–1876, shows her adorned with emeralds. Museumslandschaft Hessen Kassel (inv. no. L 86); courtesy of Wikimedia Commons.

'subjugate everyone, even a love-sated man already past his prime', referring to Caesar, then in his 50s (Cary & Foster 1916, p. 169). In brief, Cleopatra then had an affair with Roman politician and general Mark Antony, and their joint war with Caesar's successor, the Roman Emperor Octavian, led to defeat, both their suicides, and Egypt becoming a Roman province in 30 BCE.

The politics and wars of the period were well discussed by Roman authors, who generally painted Cleopatra in a bad light although in reality she was a very capable ruler (for a recent study, see Roller 2010, in particular Appendix 5: Some Ancient Literary Descriptions of Cleopatra, pp. 168–172). There are only two surviving ancient mentions of Cleopatra in connection to emeralds. The Greek writer Plutarch, in his *Life of Antony* (Perrin 1920, p. 307), written in the late first century CE, described how Queen Cleopatra gathered together 'her treasure, her gold, silver, emeralds, pearls, ebony, ivory and cinnamon…'. She was threatening to burn it all. Note, though, that there was no particular focus on emeralds here. The Roman writer Marcus Annaeus Lucanus, usually known simply as Lucan, wrote a century after the events and described how, following Cleopatra's seduction of Caesar 'to purchase peace', she entertained him at an extravagant feast intended to impress. She was 'faint beneath the weight of gems and gold' she wore, and her palace was built of, and decorated with, an incredible array of luxurious products which, Lucan said, included agate, emerald, ebony, ivory, jasper, onyx, porphyry, tortoiseshell and other unspecified 'gems' (Duff 1928, p. 599). We cannot know how reliable his sources were or even if his 'emerald' is the same as ours, since he used the Latin term *smaragdus*. The stones he mentioned were not worn by the queen, but were inlaid in the doors of the entrance hall to the palace.[6]

The link between emeralds and Cleopatra appears to be a relatively modern construct that might have sprung from the increasing number of mentions of the Egyptian mines in the nineteenth century. For example, Cleopatra appears to be draped with emeralds in a nineteenth-century painting by Hans Makart (Figure 10). But the leap to claiming an ancient, special connection between emeralds and this glamorous queen seems to be associated with one Victorian jeweller.

## STREETER'S DREAM

Edwin Streeter was an eminent Bond Street (London) jeweller of the Victorian era (Figure 11). He was renowned for his pursuit of gems at their sources, including rubies in Burma, pearls in western Australia and sapphires in Montana, USA. He was even involved with a pearling concession in the Red Sea (Floyer 1893a, p. 141). Above all, he was a consummate salesman skilled in marketing his business and himself. One manifestation of this was his flexible approach to history, which he seems to have viewed more as a way to add romance to gems than to provide facts. For example, his confused testimony about the history of the Agra diamond presented during the famous 1895 court case involving the stone was ridiculed in the press (Ogden 2019). He also seems to have invented the story that the Nassak diamond had been looted from the temple of Shiva in Nassak, India—a report that has resonated to this day with recent demands that it be returned to the temple (Streeter 1882, p. 229; Ogden 2020, pp. 235–245)

Streeter's *Precious Stones and Gems, Their History and Distinguishing Characteristics* was first published in 1877. In this first edition, he briefly mentioned the emerald mines in Egypt, their ancient exploitation and their rediscovery by Frédéric Cailliaud. He noted several classical mentions of emeralds, but nothing in connection to Cleopatra. Two years later he published a second edition (Streeter 1879). Here, and in his third edition (Streeter 1882), the sections on the Egyptian emerald

[6] Indeed, not all gems were for personal ornamentation. Wonderful examples are provided by fragments of gilded bronze sheet with inlays of cabochon-cut amethyst, blue chalcedony, citrine, emerald, garnet, peridot and other gems that were excavated from the imperial residence at the *Horti Lamiani* in Rome (Cima & La Rocca 1986). These may have been architectural or furniture decorations.

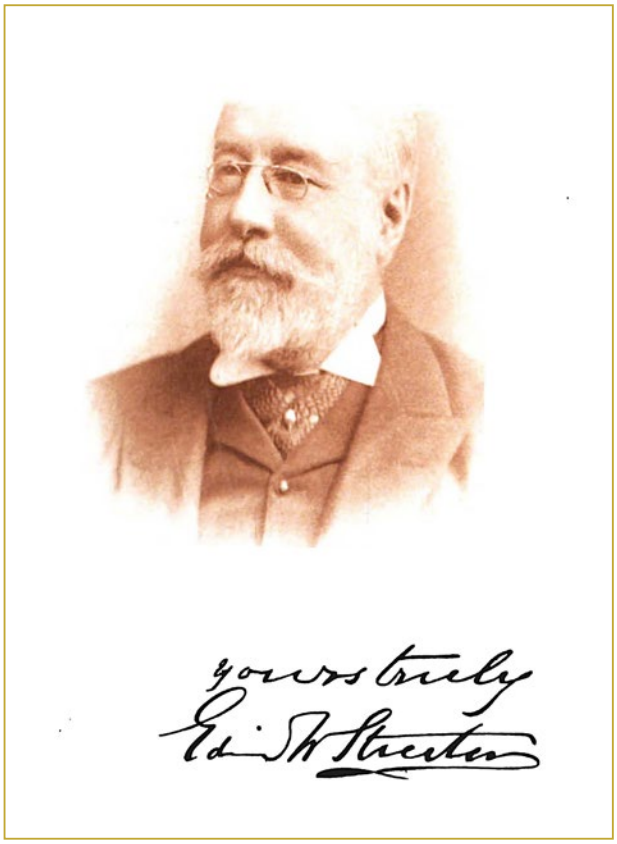


**Figure 11:** Edwin Streeter (from the frontispiece of the sixth edition of his *Precious Stones and Gems*, published in 1898) appears to have been responsible for the myth of Cleopatra's emeralds.

mines were significantly enlarged. He said a little more about Cailliaud finding emeralds there and then he made the rather strange comment: 'There is to this day as potent and operative a mesh of superstition guarding these ancient mines as in the days of Cleopatra I' (Streeter 1879, part 2, p. 24; Streeter 1882, part 2, p. 24). We might assume he meant the famous Cleopatra—Cleopatra VII, not her distant ancestor Cleopatra I—but clearly, he had started to associate Egyptian emeralds with Cleopatra. Indeed, around this time it seems he began to ponder the possibility of reopening the mines. In an interview Streeter gave to the *Daily Mail* newspaper in 1899 he explained: 'My first idea of getting emeralds from Eastern Egypt came to me from reading of Cleopatra…. I learned from a French gentleman [presumably Cailliaud's account] that the Zebara [Gebel Zabara] was unquestionably rich in the precious stone, and I at once took steps to secure a grant of land. For twenty years I have been trying to obtain the necessary right, but owing to a variety of causes, without success' (*Daily Mail*, 11 November 1899, p. 3). Twenty years before 1899 would bring us to 1879—and the date of that second edition of Streeter's book.

## FLOYER'S EXPEDITION

In his 1899 interview, Streeter said that Nubar Pasha (three-times prime minister of Egypt) had been favourable to his idea of re-establishing emerald mining and had even offered soldiers to guard the mines once they were reopened. At that time, Egypt was a British protectorate. In February 1891 Ernest Ayscoghe Floyer (Figure 12)—a British colonial official, explorer and since 1877 Inspector General of Egyptian Telegraphs—was sent by the Viceroy of Egypt (the khedive) on a scientific expedition to survey the mines in Egypt's Eastern Desert (Floyer 1892, 1893a,b). There was also an obvious military agenda. Floyer was accompanied by Major Ernest Frederick David of the 10th Sudanese infantry battalion and Major H. G. Dunning of the 2nd Camel Corps. Both were officers with distinguished military careers in Egypt and Sudan, and Dunning had been involved with military intelligence at least from 1889 (Floyer 1893a, p. 3).[7] This was a time of complex political and military interactions in the region involving Egypt, Sudan, Britain, Turkey and Italy. It was essential for Britain to identify easily passable routes across the Eastern Desert from the Red Sea to the Nile River, and to map the water wells that could supply troops moving along this corridor.

[7] For Dunning's involvement in military intelligence see, for example, Durham University Library archives, Wingate Papers SAD 155/4/123-124 and SAD 155/5/22-23 (March–April 1889).

**Figure 12:** Ernest Ayscoghe Floyer (detail from the frontispiece of his 1882 *Unexplored Balūchistan*) surveyed Egypt's emerald mines in the nineteenth century, first on behalf of Egypt and later for Edwin Streeter.

As he approached Wadi Sikait, Floyer described his first sighting of the emerald mines, which appeared 'like great rabbit burrows' (Floyer 1893b, p. 418). He was clearly entranced by the mines and their history, and he went into some detail about the latter in his 1893 account of the expedition (Floyer 1893a). Floyer was clearly aware of Streeter's interest, but the extent to which it prompted the expedition is unknown. A member of the expedition, Mohammed Bayoumi, descended deep into one mine and found 30 baskets of ore that had been abandoned by Cailliaud's miners 70 years earlier. All were brought to the surface, and one basket was sent to Streeter in London for 'scientific examination' (Floyer 1893a, pp. 108–109). Streeter also recorded that, 'One of these baskets, containing the ore, or talcose schist, from which the Emeralds were derived, is now in the author's possession, having been presented by Mr. Floyer, who had it sent direct from the Egyptian mines' (Streeter 1892, p. 226). Floyer (1893a, p. 108) recounted that tapping one piece of rock with a geological hammer detached several crystals of a brilliant green, which Streeter kindly mounted in a brooch. It appears that this brooch was intended for Floyer himself.

Following the expedition, Streeter quoted Floyer's report on his visit to the mines in which he said, 'Cleopatra gave, as presents to ambassadors, portraits of herself engraved on emeralds' (Streeter 1892, p. 223). In Floyer's account published the same year, he noted that the emerald mines 'supplied the Cleopatras [note the plural] with jewels' and 'one is mentioned as presented to Lathyrus, engraved with Cleopatra's portrait' (Floyer 1892, p. 828). The first statement clearly indicates where the emeralds were coming from. The second, repeated in Floyer's full report (Floyer 1893a, p. 99) and alluded to by Streeter (1892, p. 223), is untrue. Nevertheless, it has become one of the most persistent of the stories connecting Cleopatra with the gem. It is ubiquitous to this day, even in gemmological textbooks, but it seems to confuse two things. The mines were producing emeralds in the time of Cleopatra VII, and Plutarch indeed mentioned the presentation of an engraved emerald (Perrin 1914, pp. 477–479)—but not by her. According to him, in 86–85 BCE Lucullus, the commander of the Roman fleet, visited the Egyptian pharaoh Ptolemy IX, nicknamed Lathyrus, to request help. Ptolemy did not provide assistance, but he did present Lucullus with a costly emerald set in gold and engraved with his portrait.

The Greek word used by Plutarch was *smaragdos* (σμάραγδος, or *smaragdus* in Latin), from which came the word *emerald* (and most of the other terms used around the world for this gem). The earliest use of this Greek word was in the mid-fifth century BCE by the historian Herodotus, who reported seeing a pillar of *smaragdos* in the Temple of Heracles at Tyre, and noted that an engraved emerald was set in the gold ring owned by Polycrates, the tyrant of Samos, which he supposedly threw into the sea and that reappeared in a fish presented to him a few days later (Godley 1920, pp. 330–331; Godley 1921, pp. 54–55). The pillar is highly unlikely to have been emerald, and the gold ring is a bit earlier than we might expect to find an emerald, so perhaps it was green jasper or something similar. In the first century CE, the Roman writer Pliny (who actually considered Polycrates' ring to be sardonyx) praised the beauty of *smaragdus* with its colour that was 'delightful to the eye'. However, he also explained that the term represented 12 different varieties of stone, at most three of which were likely to have been emerald (Eichholz 1962, pp. 212–227).

In any case, Lathyrus *gave* a green gem, possibly an emerald, to an emissary, and he certainly didn't *receive* one from Cleopatra VII, who was born a decade after his death.

It is unknown whether Floyer was aware of Plutarch's mention of the gem given to Lucullus but mis-remembered it, or whether Streeter mis-prompted him. Streeter undoubtedly would have read of it in one of the editions of Charles William King's books on engraved gems (King 1866, p. 190 n.; King 1885, p. 138 n.). As noted above, Streeter did have a rather cavalier attitude towards history, and in the sixth edition of his book (1898) he mentioned emeralds 'found in Queen Cleopatra's mines in Upper Egypt' (Streeter 1898, p. 6).

## SETON KARR'S EXPEDITION

The entry for Ernest Ayscoghe Floyer in the *Dictionary of National Biography* says succinctly, 'As the result of Floyer's report these [emerald] mines were reopened' (Lee 1912, p. 37). It wasn't that straightforward. A more detailed study of the potential of the mines was essential, so in late 1897 Streeter asked Heywood Seton-Karr to explore them. Seton-Karr (1859–1938) was a British explorer, big-game hunter and amateur archaeologist who had served in the British Army in Egypt. The *Oxford Dictionary of National Biography* noted the following: 'In December 1897 he examined ancient emerald mines south-east of Edfu on behalf of Streeter & Co. Ltd, to whom the government had leased the mines. He found the Roman shafts largely filled with washed-in rubble and discovered a few fragments of emerald around the ore heaps' (Matthew & Harrison 2004, p. 884). In

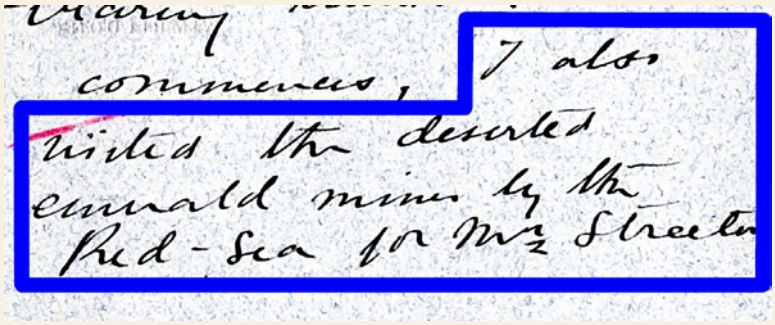

**Figure 13:** A 5 June 1898 letter from Heywood Seton-Karr to English archaeologist Augustus Pitt Rivers says, 'I also visited the deserted emerald mine by the Red Sea for Mr Streeter'. Courtesy of the Salisbury and South Wiltshire Museum (Letters L2103).

Streeter's sixth edition, he described how Seton-Karr brought back to him 'a quantity of rough Emerald, some of which has yielded stones of excellent quality' (Streeter 1898, p. 207). Further information on Seton-Karr's work at the emerald mines is unfortunately unavailable.[8]

In a 5 June 1898 letter from Seton-Karr to English archaeologist Augustus Pitt Rivers, to whom he supplied some of the prehistoric flint tools he found in Egypt, he said he 'was in Egypt the whole of last winter, and… visited the deserted emerald mine by the Red Sea for Mr Streeter' (Figure 13; Salisbury and South Wiltshire Museum, Letters L2103). Seton Karr recorded that his Egyptian miners had been 'splendid labourers', but he still thought it necessary to search them on the way back to Aswan on the Nile to see if they had appropriated any emeralds. He did not find any, but 'the day after I quitted Aswan, as I was informed by some tourists, emeralds were offered for sale in the bazaar' (Seton-Karr 1901).

Seton-Karr's expedition inspired Streeter that the mines would be 'well worth re-opening and working by our improved modern methods of mining…I have applied to the Egyptian Government for a concession, and at the time of writing am awaiting a reply to my application' (Streeter 1898, p. 207).

## THE CONCESSION

Streeter was highly optimistic about the future and planned to work the mines as a syndicate rather than form a company (*London Evening Standard*, 25 April 1900, p. 3). On 20 April 1899, Streeter & Co. was granted a five-year concession to search for emeralds in Egypt and three years to look for gold and other metals in the same area (*The Northern Whig*, 5 August 1904). The concession was bordered by the Red Sea on the east, the Abu Diab mountains on the north and the Hamrat Mukbud mountains on the south-west, features that were clearly marked on the various maps Floyer had published (Floyer 1892, 1893a,b; *Daily Mail*, 11 November 1899, p. 3). The concession encompassed both the Gebel Zabara and Wadi Sikait areas, and *The Daily Mail* reported that it covered 140 square miles (about 363 km$^2$); in reality it was nearer to 10,360 km$^2$. Streeter & Co were to give 10% of their profits to the Egyptian government (*Newcastle Daily Chronicle*, 19 May 1899, p. 4).

Later that same year, Streeter sent an expedition to the mines consisting of Donald A. MacAlister, A. A. Forster, a Dr Grote and, according to MacAlister, 'three Cornishmen'—experienced mining people (MacAlister 1900, p. 537). Streeter described the group as consisting of 'a manager, an engineer, a Cornish ganger, a smith, a carpenter, and an accomplished linguist' (*Westminster Gazette*, 11 November 1899, p. 8). The expedition set off with 130 camels and 'all necessary supplies for four months' (MacAlister 1900, p. 537). They originally intended to go by ship into the Red Sea, but it was decided that overland from the Nile would be preferable and cheaper. In his November 1899 interview with the *Daily Mail*, Streeter expressed his hope that he would visit the mines himself in February 1900, but the present author has found no evidence that he realised this ambition. Indeed, following Floyer's visit to the mines in 1891, Streeter had decided to go to Egypt to inspect the mines personally, but Floyer noted that this visit was delayed by the discovery of deposits in Australia that Streeter apparently said were easier to mine (Floyer 1893a, p. 109 and n.). Floyer did not mention the nature of these mines.

[8] An 1898 report by Seton-Karr titled 'Account of the examination of the emerald mines of Egypt for Streeter & Co. Ltd to whom the government have leased these mines' was in the library of the University of Liverpool, but when this author requested it during the preparation of this article, it was noted as missing. That seems to have been the only copy.

**Figure 14:** A photo from the 1899–1900 MacAlister expedition to the mines shows D. A. MacAlister, standing on A. A. Forster's shoulders, mining emeralds. Dr Grote stands to the left. Photo © Royal Geographical Society.

According to MacAlister (1900, p. 537), 'Messrs. Streeter & Co. equipped and dispatched an expedition with instructions to proceed to the so-called "Cleopatra's Emerald Mines," in the Wadil Sikait district (Northern Etbai)'. Photographs of MacAlister, Forster and Grote at the mines are preserved in the archives of the Royal Geographical Society. One of these shows MacAlister chipping away to free an emerald while standing on Forster's shoulders (Figure 14). The accompanying details of the photograph say 'Queen Cleopatra's Emerald Mines Expedition 1900'. In addition, MacAlister (1900) and Leopold Claremont (1913) published some other photographs from this expedition.

Employing such an evocative association with Cleopatra was a clever move by Streeter. It was the perfect time. Much of the later nineteenth-century archaeological excavation work in Greece and the Near East sought to link sites and finds to those named in the Bible or Classical myths—such as Heinrich Schliemann finding 'Priam's Treasure' at Troy in modern-day Turkey and 'Agamemnon's Mask' at Mycenae in Greece. During this time, there was also a flurry of mining enterprises across the British Empire. Both these factors tied in with the Victorian appetite for books on the discovery of lost cultures and treasures, often with blatant imperialist sub-texts. In 1885 the incredibly popular *King Solomon's Mines* was published by Sir H. Rider Haggard, often seen as the start of a genre that has persisted into modern times with films such as *Raiders of the Lost Ark* and *Tomb Raider*. Less well known today is Haggard's 1889 novel *Cleopatra*, equally popular in its day. An emerald pendant plays a major role when, attacked by a traitor, Cleopatra 'swift and supple as a tiger sprang to one side, so that he did but grasp her royal cloak, tearing it from its emerald clasp' (Haggard 1889, p. 290). This shows the book's obvious appeal to thrill-seeking Victorian readers, particularly those less familiar with Shakespeare's account of Cleopatra. Streeter must have seen the huge marketing opportunity in stressing the links between his Egyptian emerald venture and this alluring queen.

## THE END OF A DREAM

On 21 May 1902, the Egyptian Government granted Streeter an exclusive concession to mine for emeralds in Egypt for a term of 30 years, backdated to 1 January 1900, with the rights to subsequent prolongations of 15 years (*The Northern Whig*, 5 August 1904, p. 11). In January 1903, Streeter agreed to sell the concession to a Mr Oxley in return for £7,003 and a number of fully paid-up shares in the Egyptian Gold & Gem Syndicate Ltd, which was registered on 18 February 1903 (*The Northern Whig*, 5 August 1904, p. 11; *The Egyptian Gazette*, 17 July 1906 n.p.). Edwin Streeter was chairman of the syndicate, and the other directors were G. O. Haig, mining engineer Arthur C. Bicknell and Edwin's third son, Cecil Streeter (Streeter 1993, p. 150). The latter two are the signatories on the share certificate in Figure 15.[9] In the spring of 1903, the company hired a team of Cornish miners, who were to be paid £4 per week plus travel; they reached the emerald mines after a seven-week journey (*Cornishman*, 22 October 1903, p. 3). In early 1906, it was announced that a deep shaft had 'struck a gem-bearing formation underneath the old workings', and 'Emeralds of the finest quality, and more valuable than diamonds have already been found' (*Leeds Mercury*, 14 February 1906, p. 3). But although these results sounded favourable, Egyptian mining engineer Max Ismalun noted that the company did not do 'any appreciable work' at the mines, and they forfeited their mining rights when the Egyptian government issued new mining regulations in 1906 (Ismalun 1912, p. 190). Streeter's involvement by this time seems unclear. Streeter had received neither the money nor the shares Oxley had promised, and in the summer of 1906 he sued the Egyptian Gold & Gem Syndicate Ltd (*The Globe*, 9 July 1906, p. 11; *The Egyptian Gazette*, 17 July 1906, n.p.). Earlier that year the Egyptian Gold & Gem Syndicate Ltd appears to have been briefly struck off as a company (*Morning Post*, 8 May 1906, p. 3).

It became even more complicated. At the end of June 1905, another company had been set up—the Egyptian Gold and Emerald Company Ltd—with the object of acquiring the mining rights of the Sudan Finance Syndicate Ltd, and adopting an agreement with the Egyptian Gold & Gem Syndicate Ltd and Edwin Streeter, to carry on the business of mining and selling the gems. Streeter was to be one of the directors (*Westminster Gazette*, 7 July 1905, p. 11; *The Egyptian Gazette*, 12 July 1905, n.p.). However, the Egyptian Gold and Emerald Company Ltd


THE
No. of Certificate. 281
No. of Shares. 100
EGYPTIAN GOLD & GEM SYNDICATE, LIMITED.
Incorporated under the Companies Acts, 1862 to 1900.
Capital . . . £40,000.
Divided into 40,000 Ordinary Shares of £1 each.
This is to Certify that Miss Stewart M & Stewart S. of 29 Madison Road Tunsington London is the Registered Holder of One hundred Shares, numbered 13591 to 13690 inclusive, in the above-named Company, subject to the Memorandum and Articles of Association thereof, and that upon each of the said Shares the sum of Twenty Shillings has been paid up.
Given under the Common Seal of the said Company, this 4th day of September 1905.
Arthur C Bicknell
Cecil Streeter
Directors.
James Sullivan
Secretary.
ANY FURTHER PAYMENTS SINCE THE ISSUE OF THIS CERTIFICATE WILL BE FOUND CERTIFIED AT THE BACK HEREOF.
NO TRANSFER OF THE WHOLE OR ANY PART OF THE SHARES REPRESENTED BY THIS CERTIFICATE CAN BE RECOGNISED UNLESS IT BE DEPOSITED AT THE COMPANY'S OFFICE.

**Figure 15:** A certificate for 100 shares in The Egyptian Gold & Gem Syndicate Ltd is dated 4 September 1905 and signed by Arthur Bicknell and Cecil Streeter, directors. Photo courtesy of Historisches Wertpapierhaus AG.

[9] G. O. Haig also had other interests in the area. In 1901, he had been granted a gold-mining concession by the Egyptian Government for prospecting on the Sudan border (Anonymous 1905). He had also been a former director of the Nile Valley Company.

did not submit any of its statutory returns, and the project supposedly lapsed. But the company could not be struck off because it insisted it was carrying on business. It stayed in existence in title only, doing no business until 1917 when it was acquired by a Mr McMillan (*Truth*, 25 July 1917, p. 129). McMillan's various business enterprises were described as 'likely to deceive gullible investors' (*Truth*, 18 July 1917, p. 89), and not surprisingly the company was finally wound up in 1919 (Records of the Chancery Division, National Archives J 13/8170).

There was a flood of mining enterprises between 1880 and the outbreak of the First World War 'despite the high-risk nature of the business and the presence of unscrupulous company promoters who sought only pecuniary gain' (Mollan 2009, p. 229). Less than a month after the Egyptian Gold & Gem Syndicate Ltd was formed in 1903, it was said, with regard to new mining concessions in Egypt and Sudan in general, 'the road to the mines will be thickly bestrewn with the bones of the many ventures now being generated with such utter recklessness' (*Truth*, 12 March 1903, p. 686). Indeed, voluntary winding-up procedures for the Egyptian Gold & Gem Syndicate Ltd were started in September 1907 and dragged on until May 1912 (National Archives BT 34/1890/76429). The reasons for the delay were the outstanding claims against promoters and directors to the amount of £18,000. The Egyptian Gold & Gem Syndicate Ltd had put itself out of business, much as had Cleopatra 2,000 years earlier.

Streeter was perhaps not unscrupulous, but one might be justified in thinking him reckless. Patrick Streeter described his great-grandfather's short-lived venture to mine Montana sapphires, embarked on in 1891, as 'an unmitigated disaster' (Streeter 1998, p. 21). At the time of his death in 1923, someone who knew him well commented that 'He would make £1000 one minute and lose it the next….But for the casual manner in which he speculated, Mr Streeter would have died an immensely wealthy man….It never seemed to shock him if he incurred a heavy loss over a speculation' (*Belfast Telegraph*, 17 October 1923, p. 6). Another friend of Streeter's said, 'One of his last big ventures…was to send a party of investigators to Egypt to find emeralds. He said they were sure they were there in large quantities. So they were, but of very indifferent emerald' (*Belfast Telegraph*, 17 October 1923, p. 6).

## CONCLUSIONS

The frequently recounted stories that the Egyptian queen Cleopatra was particularly fond of emeralds and gave gems engraved with her own portrait to ambassadors have no real basis in recorded history. There are various instances associated with gems where romanticised fiction was presented as historical fact, and in this case the source can be traced to Edwin Streeter, the nineteenth-century London jeweller. He wrote several influential books on gems, but they sometimes dealt with history in an offhand manner. His Cleopatra association appears to have been based on optimistically selective readings and, perhaps, mis-readings of some classical authors' accounts. It is true that most, if not all, of the emeralds used during the three centuries ending with the death of Cleopatra originated from the mines of Egypt's Eastern Desert, but they were not common at that time. The mines were later known to the Romans, who exploited them on a larger scale, as *Mons Smaragdus*. There is less historical justification in describing the emerald mines of Egypt as 'Cleopatra's' than in referring to the Whitby jet occurrences in Britain as 'Queen Victoria's'.

Shakespeare's Domitius Enobarus said of Cleopatra, 'Age cannot wither her, nor custom stale' (*Anthony and Cleopatra*, Act II, Scene ii). The same can be said of Streeter's marketing acumen. He surely exaggerated the Cleopatra link with emeralds, more with marketing flare than observance of historical accuracy, making it arguably one of the most successful gem marketing campaigns ever. It had the 'celebrity endorsement' of one of the best-known, most glamourous women of all time, disguised as history. To this day, the Egyptian emerald mines are still often described as 'Cleopatra's mines', and even gemmological publications continue to cite the nebulous association between Cleopatra and emeralds as historical fact.

Perhaps future gemmologists will acknowledge that Cleopatra's love of emerald is just an appealing Victorian fabrication—and appreciate Edwin Streeter's consummate ability to 'romance the stone'.

## REFERENCES

Anonymous 1905. Egyptian Sudan Minerals, Limited. *The Mining Journal, Railway and Commercial Gazette*, **77**(3631), 25 March, 329.

Bednarski, A. & Harer Jr, W.B. 2013. The explorations of Frédéric Cailliaud. *Saudi Aramco World*, **64**(1), 36–43.

Belzoni, G.B. 1820. *Plates Illustrative of the Researches and Operations of G. Belzoni in Egypt and Nubia*. John Murray, London, 43 pp.

Bruce, J. 1790. *Travels to Discover the Source of the Nile, in the Years 1768, 1769, 1770, 1771, 1772, and 1773*. G. G. J. and J. Robinson, London, 670 pp., https://archive.org/details/travelstodiscove01bruc.

Cailliaud, F. 1822. *Travels in the Oasis of Thebes, and in the Deserts Situated East and West of the Thebaid: In the Years 1815, 16, 17, and 18*. R. Phillips & Co., London, 72 pp.

Cary, E. & Foster, H.B. (transl.) 1916. *Dio Cassius—Roman History*, Vol. 4, Books 41–45. Loeb Classical Library 66, Harvard University Press, Cambridge, Massachusetts, USA, 512 pp.

Cima, M. & La Rocca, E. (eds) 1986. *Le Tranquille Dimore Degli Dei: La Residenza Imperiale Degli Horti Lamiani*. Cataloghi Marsilio, Venice, Italy, 213 pp.

Claremont, L. 1913. Prehistoric emerald mines. *Knowledge*, **36**, April, 124–127.

Duff, J.D. (transl.) 1928. *Lucan—The Civil War*. Loeb Classical Library 220, Harvard University Press, Cambridge, Massachusetts, USA, 656 pp.

Eichholz, D.E. (transl.) 1962. *Pliny—Natural History*, Vol. 10, Books 36–37. Loeb Classical Library 419, Harvard University Press, Cambridge, Massachusetts, USA, 368 pp.

Floyer, E.A. 1882. *Unexplored Balūchistan: A Survey, with Observations Astronomical, Geographical, Botanical, etc., of a Route Through Mekran, Bashkurd, Persia, Kurdistan, and Turkey*. Griffith & Farran, London, 507 pp.

Floyer, E.A. 1892. Art. XV.—The mines of the northern Etbai or of northern Æthiopia. With a map, water-colour drawings and photographs by the scientific expedition to the northern Etbai. *Journal of the Royal Asiatic Society*, **24**(4), 811–833, https://doi.org/10.1017/s0035869x00022000.

Floyer, E.A. 1893a. *Étude sur le Nord-Etbai entre le Nil et la Mer Rouge*. Imprimerie Nationale, Cairo, Egypt, 192 pp.

Floyer, E.A. 1893b. Further routes in the Eastern Desert of Egypt. *Geographical Journal*, **1**(5), 408–431, https://doi.org/10.2307/1774067.

Gawad, A.E.A., Ene, A., Skublov, S.G., Gavrilchik, A.K., Ali, M.A., Ghoneim, M.M. & Nastavkin, A.V. 2022. Trace element geochemistry and genesis of beryl from Wadi Nugrus, south Eastern Desert, Egypt. *Minerals*, **12**(2), article 206 (22 pp.), https://doi.org/10.3390/min12020206.

Giuliani, G., Chaussidon, M., Schubnel, H.-J., Piat, D.H., Rollion-Bard, C., France-Lanord, C., Giard, D., de Narvaez, D. *et al*. 2000. Oxygen isotopes and emerald trade routes since antiquity. *Science*, **287**(5453), 631–633, https://doi.org/10.1126/science.287.5453.631.

Godley, A.D. (transl.) 1920. *Herodotus—The Persian Wars*, Vol. 1, Books 1–2. Loeb Classical Library 117, Harvard University Press, Cambridge, Massachusetts, USA, 528 pp.

Godley, A.D. (transl.) 1921. *Herodotus—The Persian Wars*, Vol. 2, Books 3–4. Loeb Classical Library 118, Harvard University Press, Cambridge, Massachusetts, USA, 448 pp.

Haggard, H.R. 1889. *Cleopatra: Being an Account of the Fall and Vengeance of Harmachis, the Royal Egyptian, as Set Forth by His Own Hand*. Longmans, Green, and Co., London, 336 pp.

Harrell, J.A. 2004. Archaeological geology of the world's first emerald mine. *Geoscience Canada*, **31**(2), 69–76.

Harrell, J.A. 2006. Archaeological geology of Wadi Sikait. *PalArch's Journal of Archaeology of Egypt/Egyptology*, **3**(1), article 626 (12 pp.).

Harrell, J.A. in prep. *Archaeology and Geology of Ancient Egyptian Stones*. University of Toledo Press, Toledo, Ohio, USA.

Huda, S.N.A. (transl.) 1998. *Arab Roots of Gemology – Ahmad ibn Yusuf Al Tifaschi's 'Best Thoughts on the Best of Stones'*. Scarecrow Press Inc., Lanham, Maryland, USA and London, 271 pp.

Ismalun, M. 1912. La situation minière d'Égypte. *L'Égypte Contemporaine*, **3**, 161–214.

Jennings, R.H., Kammerling, R.C., Kovaltchouk, A., Calderon, G.P., El Baz, M.K. & Koivula, J.I. 1993. Emeralds and green beryls of Upper Egypt. *Gems & Gemology*, **29**(2), 100–115, https://doi.org/10.5741/gems.29.2.100.

Junker, H. 1919. *Bericht über die Grabungen der Akademie der Wissenschaften in Wien auf den friedhöfen von El-Kubanieh-Nord, Winter 1910–1911*. Alfred Hölder, Vienna, Austria, x + 227 pp.

King, C.W. 1866. *The Handbook of Engraved Gems*. Bell & Daldy, London, 396 pp.

King, C.W. 1885. *Handbook of Engraved Gems*, 2nd edn. George Bell and Sons, London, 287 pp.

Le Nourry, D.N. 1857. *Clementis Alexandrini*. J.-P. Migne, Paris, France, 1,388 ff.

Lee, S. (ed) 1912. *Dictionary of National Biography*, 2nd supplement, Vol. 2. Smith, Elder & Co., London.

MacAlister, D.A. 1900. The emerald mines of northern Etbai. *Geographical Journal*, **16**(5), 537–549, https://doi.org/10.2307/1774868.

Matthew, H.C.G. & Harrison, B. (eds) 2004. *Oxford Dictionary of National Biography*, Vol. 30: Jenner–Keayne. Oxford University Press, Oxford, 998 pp. (see pp. 884–885), https://doi.org/10.1093/ref:odnb/61117.

Mollan, S.M. 2009. Business failure, capital investment and information: Mining companies in the Anglo-Egyptian Sudan, 1900–13. *Journal of Imperial and Commonwealth History*, **37**(2), 229–248, https://doi.org/10.1080/03086530903010368.

Nobbe, K.F.A. 1843. *Claudii Ptolemaei Geographia*, Vol. 1. Tauchnitz, Leipzig, Germany.

Ogden, J.M. 1990. *Gold jewellery in Ptolemaic, Roman and Byzantine Egypt*, Vol. 1: Text. PhD thesis, Durham University, Durham, 274 pp., http://etheses.dur.ac.uk/1457.

Ogden, J.M. 2019. The Agra diamond. *In*: Jaffer, A. (ed) *Beyond Extravagance: A Royal Collection of Gems and Jewels*, 2nd edn. Assouline, New York, New York, USA, 581–585.

Ogden, J.M. 2020. Two large diamonds from India. *In*: Balakrishnan, U.R. (ed) *Diamonds Across Time: Facets of Mankind*. World Diamond Museum, London, 219–245.

Oller Guzmán, J., Fernández Abella, D., Trevín Pita, V., Achon Casas, O. & García-Dils de la Vega, S. 2021. New evidence regarding emerald production in Roman Egypt at Wadi Sikait (Eastern Desert). *Journal of Near Eastern Studies*, **80**(1), 123–142, https://doi.org/10.1086/712784.

Perrin, B. (transl.) 1914. *Plutarch—Lives, Volume II: Themistocles and Camillus. Aristides and Cato Major. Cimon and Lucullus*. Loeb Classical Library 47, Harvard University Press, Cambridge, Massachusetts, USA, 630 pp.

Perrin, B. (transl.) 1920. *Plutarch—Lives, Volume IX: Demetrius and Antony. Pyrrhus and Gaius Marius*. Loeb Classical Library 101, Harvard University Press, Cambridge, Massachusetts, USA, 640 pp.

Roller, D.W. 2010. *Cleopatra: A Biography*. Oxford University Press, Oxford, 272 pp.

Sax, M., Meeks, N.D. & Collon, D. 2000. The early development of the lapidary engraving wheel in Mesopotamia. *Iraq*, **62**, 157–176, https://doi.org/10.2307/4200487.

Seton-Karr, H.W. 1901. The Egyptian emerald mines. *Geographical Journal*, **18**(1), https://doi.org/10.2307/1775774.

Shaw, I., Bunbury, J. & Jameson, R. 1999. Emerald mining in Roman and Byzantine Egypt. *Journal of Roman Archaeology*, **12**, 203–215, https://doi.org/10.1017/s1047759400017980.

Sidebotham, S.E., Hense, M. & Nouwens, H.M. 2008. *The Red Land: The Illustrated Archaeology of Egypt's Eastern Desert*. American University in Cairo Press, Cairo, Egypt, 424 pp.

Streeter, E.W. 1877. *Precious Stones and Gems, Their History and Distinguishing Characteristics*. Chapman & Hall, London, ix + 264 pp.

Streeter, E.W. 1879. *Precious Stones and Gems, Their History and Distinguishing Characteristics*, 2nd edn. Chapman & Hall, London, xiii + 141, 122 and 142 pp. (in three parts).

Streeter, E.W. 1882. *Precious Stones and Gems, Their History and Distinguishing Characteristics*, 3rd edn. George Bell & Sons, London, xiii + 141, 122 and 143 pp. (in three parts).

Streeter, E.W. 1892. *The Great Diamonds of the World: Their History and Romance*. George Bell & Sons, London, xxiii + 321 pp.

Streeter, E.W. 1898. *Precious Stones and Gems, Their History and Distinguishing Characteristics*, 6th edn. George Bell & Sons, London, xvi + 339 pp.

Streeter, P. 1993. *Streeter of Bond Street: A Biography of a Victorian Jeweller*. Matching Press, Harlow, 180 pp.

Streeter, P. 1998. Edwin Streeter: Further research. *Jewellery Studies*, **8**, 21–26.

Wilkinson, J.G. 1835. *Topography of Thebes, and General View of Egypt*. John Murray, London, 595 pp.

Wilkinson, J.G. 1837. *Manners and Customs of the Ancient Egyptians*, Vol. 1. John Murray, London, xxxiii + 406 pp.

## The Author

**Dr Jack M. Ogden FGA**
55 Florin Court, Charterhouse Square,
London EC1M 6EU
Email: jack@striptwist.com

## Acknowledgements

Thanks to Matthias Schmitt (HWPH Historisches Wertpapierhaus AG, Zorneding, Germany) for providing the image of the share certificate, to Lisbet Thoresen (Temecula, California, USA) for her useful comments about Egyptian emeralds and Cleopatra, and to Prof. James Harrell (University of Toledo, Ohio, USA) for his insights into James Bruce's itinerary.

# Over 110 years of experience in gemmology education

Our FGA and DGA Members are located around the world – join them by studying with Gem-A.

## STUDY IN ONE OF THREE WAYS

**At Gem-A HQ London**

**Worldwide at one of our ATCs**

**Online with practical lab classes in your area**

Find out more by contacting
**education@gem-a.com**

Gem-A
THE GEMMOLOGICAL ASSOCIATION OF GREAT BRITAIN

Gem-A, 21 Ely Place, London, EC1N 6TD, UK. T: +44 (0)20 7404 3334, W: www.gem-a.com. Registered charity no. 1109555.

# Hyalite Opal from Erongo, Namibia, Showing Green Daylight Fluorescence

Radek Hanus, Kamil Sobek, Kamila Johnová, Tomáš Trojek, Ján Štubňa, Tomáš Hanus and Kamila Jungmannová

**ABSTRACT:** Rare hyalite opal showing green daylight fluorescence was discovered in the Erongo region, Namibia, sometime prior to 2000. Raman spectroscopy confirms this hyalite to be opal-A, and the most interesting feature of the Raman spectra are bands associated with the hydroxyl-stretching regions in the mineral's structure. A doublet at 3602/3665 $cm^{-1}$ appears to be unique to opal from this locality and may be due to the vibration of water in an unusual structural-binding arrangement. Trace amounts of the uranyl molecule $(UO_2)^{2+}$ are responsible for the luminescence, which is unevenly distributed according to the opal's botryoidal structure. Measured radioactivity values are similar to those reported for other daylight-fluorescing opals (e.g. from Mexico), and are well below the global average terrestrial gamma dose rate.

*The Journal of Gemmology*, **38**(2), 2022, pp. 172–182, https://doi.org/10.15506/JoG.2022.38.2.172


While prospecting for gem material in central and northern Namibia in 2019 with the assistance of a local guide, authors RH and TH collected glassy opals from the Erongo Mountains showing extremely strong fluorescence that is readily visible even in daylight (i.e. indirect sunlight; Figure 1). Fluorescent hyalite was initially discovered in the Erongo region sometime before 2000 (Cooper 2000).

The Erongo Mountains form a prominent, semi-circular terrain 30 km in diameter located approximately 20 km north of Usakos in the Erongo region of central Namibia. Several different rock types occur in what is known as the Erongo Volcanic Complex (Cairncross 2001). This caldera-like volcano-plutonic structure consists of mafic lavas, felsic units and subvolcanic intrusive rocks (Pirajno 1990), and is the largest composite, bimodal complex in the Mesozoic Etendeka igneous province. Silicic magmatism took place in the largest igneous complexes of north-central Namibia (Damaraland region), including Erongo, Brandberg, Paresis and Messum. The silicic magmas have a hybrid origin, with varying contributions of crustal and mantle-derived melts. Age constraints suggest that crustal melting was caused by a short-lived thermal pulse related to the main Etendeka flood-basalt event (Wigand *et al*. 2004).

Hyalite is a relatively common constituent of miarolitic cavities hosted by granitic rocks of the Erongo Mountains. It forms spherical to tuberous botryoidal aggregates and was the last mineral phase that formed in the cavities. It occurs as local encrustations (typically 0.1–1.5 mm thick, according to the authors' observations) on crystals of schorl, quartz, fluorite, orthoclase, aquamarine, jeremejevite and other minerals present in the cavities (Cairncross 2001; Gentry *et al*. 2004; Cairncross & Bahmann 2006). The aesthetics of these mineral specimens are further enhanced by the distinct green fluorescence of some (but not all) of these opals in daylight. The hyalite is sometimes associated with uranium minerals, such as uranophane, metanovacekite and metazeunerite (Cairncross & Bahmann 2006).

Only small amounts of gem-quality hyalite have been produced so far from the Erongo Mountains. From the rough material obtained in 2019, 12 stones (0.21–1.34 ct) were faceted under the authors' supervision by gem cutter

**Figure 1:** These samples of hyalite from Namibia (up to 4 cm) exhibit daylight fluorescence, as shown here in indirect sunlight in Prague, Czech Republic. They formed some of the study samples for this report. Photo by R. Hanus.

Aleš Hladký. This article reports on the characteristics of fluorescent hyalite from the Erongo region in order to better understand the nature of its fluorescence.

## BACKGROUND

Opal ($SiO_2 \bullet nH_2O$) has been subdivided into three varieties—opal-A, opal-CT and opal-C—on the basis of its crystallinity as determined by X-ray diffraction (Jones & Segnit 1971). In this nomenclature, 'A' stands for amorphous, 'C' for cristobalite and 'T' for tridymite; the latter two minerals are polymorphs of $SiO_2$. Australian play-of-colour opal belongs to opal-A, so this is arguably the best-known variety. Opal-CT can be considered poorly crystallised cristobalite, with some degree of tridymite-like stacking (Guthrie *et al*. 1995). Recent studies suggest that opal-CT might be most common in terms of its number of occurrences. Opal-C is, at best, a rarity (Curtis *et al*. 2019). Opal-A was later subdivided into two groups (Langer & Flörke 1974). (1) Opal-AG has a gel-like structure that often consists of packed silica spheres generally 100–500 nm in diameter (Chojcan *et al*. 2013). As a result, they exhibit the play-of-colour seen, for example, in Australian opal. (2) Opal-AN has a glass-like structure forming a network. It is also known as *hyalite*, as it is transparent and has the visual attributes of a glass.

Hyalite is nominally colourless, but in some cases it is coloured by luminescence (Fritsch *et al*. 2015). Hyalite commonly shows green luminescence when exposed to UV radiation—with a stronger reaction to short-wave UV (254 nm)—as exhibited by material from various localities, including Mexico (Fritsch *et al*. 2014), Hungary, Argentina (Saruwatari *et al*. 2015), Japan (Takahashi *et al*. 2007; Ogawa *et al*. 2008; Saruwatari *et al*. 2015) and Namibia (Haughton *et al*. 1939). The green luminescence is caused by uranyl molecules present as an impurity in the opal (Fritsch *et al*. 2015; Pan *et al*. 2021). A small number of such hyalites also luminesce to daylight excitation because they absorb some visible light (in the violet range) and, thus, appear slightly yellow. Best known is the transparent green-yellow hyalite from

Zacatecas, Mexico (Fritsch *et al.* 2014, 2015; Megaw *et al.* 2018), but other occurrences are known, such as San Luis Potosí (also in Mexico; Butini *et al.* 2020) and Madagascar (Fritsch *et al.* 2015).

All varieties of opal contain variable amounts of water, usually 4–8% (Langer & Flörke 1974), both as molecular water and as silanol (SiOH) groups (Graetsch 1994). They also contain some impurities and trace elements. The most common impurity in their structure is Al, substituting for Si. Many other elements have been detected, including Ca, K, Mg, Fe, Na, U and rare-earth elements. The average total concentration of trace elements is about 1 wt.% (McOrist *et al.* 1994; McOrist & Smallwood 1995, 1997; Brown *et al.* 2004; Gaillou *et al.* 2008; Pewkliang *et al.* 2008).

Daylight fluorescence showing vivid, intense green colour has also been observed in some other gem materials (e.g. Fritsch *et al.* 2015). For example, some rare natural yellow diamonds fluoresce green in daylight due to the H3 centre, so they appear predominantly green in certain types of lighting (Moses 1997; Shigley & Breeding 2015). Some amber from the Dominican Republic and Indonesia is famous for a blue or green colour due to luminescence of organic compounds reacting to parts of visible light and, possibly, UV (Liu *et al.* 2014).

Daylight fluorescence can also be observed in synthetic materials. Some synthetic spinels exhibit bright green luminescence attributed to emission by $Mn^{2+}$ cations in their structure (Kane & Fritsch 1991; Sehgal & Girma 2016). The manufactured material most similar to the hyalite discussed in this article is known as 'Uralite', a silicate glass doped with traces of uranium. When translucent, it is known as 'Vaseline' glass (Fritsch *et al.* 2015).

## MATERIALS AND METHODS

For this study, we examined 1,300 g of rough hyalite collected by authors RH and TH (e.g. Figures 1 and 2), as well as the 12 faceted stones that were cut from this material (e.g. Figure 3). In addition, one sample of rough hyalite was processed into a thin section for microscopic examination.

Gemmological properties were obtained at author RH's laboratory in Prague, Czech Republic. RIs were measured on the faceted samples with a GIA Duplex II refractometer, and SG values were determined hydrostatically on the same stones. Rough and cut samples were examined with an Optika Optigem-2 polarising microscope (model B-510POL-I) at 50× magnification, in an immersion cell filled with distilled water (RI = 1.333). Fluorescence and phosphorescence were observed in the rough and cut samples using 5 W long- and short-wave UV lamps (365 and 254 nm, respectively) and a 405 nm LED source. Fluorescence zoning was observed using a gemmological immersion microscope (magnification 20–120×) with distilled water. (Most oils cannot be used as the immersion liquid because their fluorescence would obscure observation.)

Inclusions and other internal features present in 10 rough samples were studied at the electron microscopy laboratory of Charles University in Prague with a Tescan Vega scanning electron microscope (SEM) equipped with an Oxford Instruments X-Max 50 energy-dispersive spectroscopy (EDS) system. We used an accelerating voltage of 15 kV and beam current of 1.50 nA, and the following natural and synthetic reference materials were employed as analytical standards: jadeite (Na[*K*α]), sanidine (K[*K*α]), $Al_2O_3$ (Al[*K*α]), periclase (Mg[*K*α]),

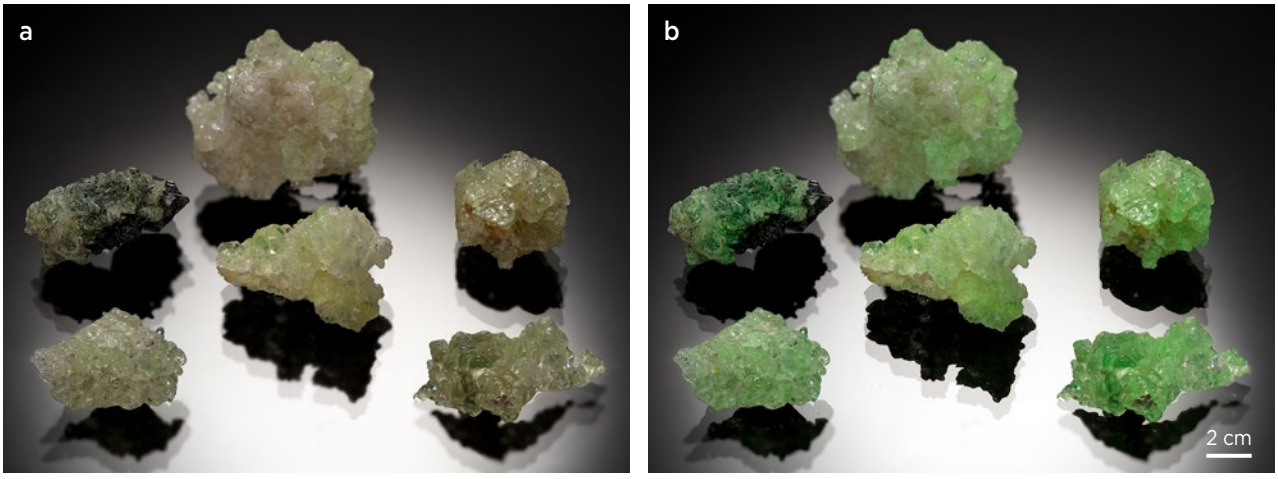


**Figure 2:** Namibian hyalite forms as botryoidal overgrowths. These specimens are illuminated (**a**) in fluorescent lighting and (**b**) with additional long-wave UV radiation to show their strong green luminescence. Photos by R. Hanus.

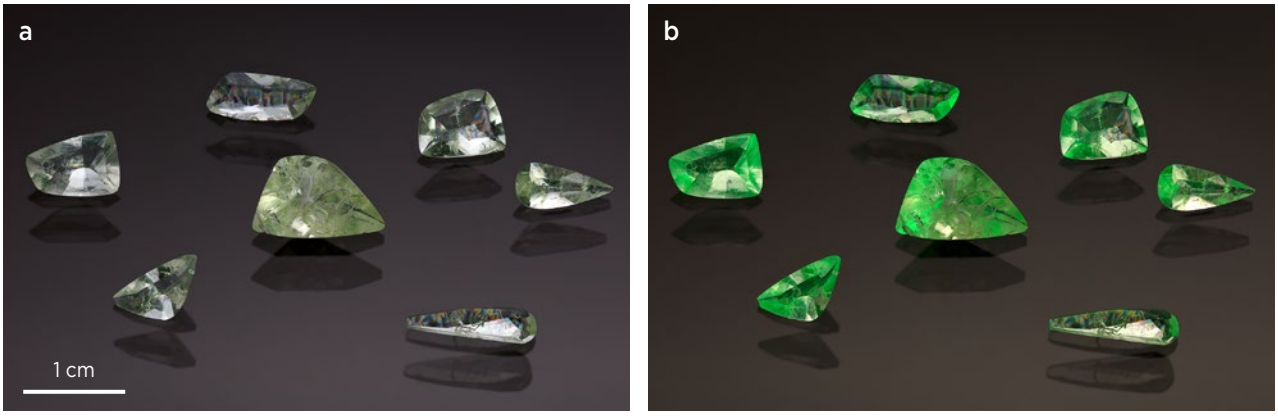


**Figure 3:** Seven of the faceted hyalites (0.21–1.34 ct) from Namibia examined for this study are shown here (**a**) in fluorescent lighting and (**b**) with additional long-wave UV radiation causing vivid green fluorescence. Photos by Pavel Škácha.

quartz (Si[*K*α]), diopside (Ca[*K*α]), rutile (Ti[*K*α]), hematite (Fe[*K*α]), Cr-Mn spinel (Cr[*K*α] and Mn[*K*α]) and cubic zirconia (Zr[*K*α]).

Raman spectra of all rough and cut samples were obtained at room temperature at the Department of Geological Sciences, Masaryk University, Czech Republic, with a Horiba Jobin Yvon LabRAM HR Evolution Raman spectrometer system equipped with a Peltier-cooled CCD detector and coupled to an Olympus BX41 microscope. Photoluminescence (PL) and Raman spectra were calibrated using the Rayleigh line. Spectra were obtained with a 532 nm Nd:YAG laser, 633 nm He-Ne laser and a 473 nm frequency-doubled diode laser in the 100–3800 $cm^{-1}$ range. We used a diffraction grating with 1,800 grooves/mm, an entrance slit of 100 µm, a confocal hole of 300 µm and a 50× long-working-distance objective. Acquisition time was set to 80 s and four accumulations to improve signal-to-noise ratio with the green and red lasers. PL spectra were obtained for 2 s with two accumulations. Data were processed with SeaSolve PeakFit 4.1.12 software and LabSpec 6 software.

Additional PL spectra of about 20 of the rough samples and all of the faceted stones were obtained in author RH's laboratory with a GL Gem Spectrometer NIR PL405, which is a dual-purpose unit for PL and visible-near infrared (Vis-NIR) spectroscopy (300–1000 nm). The spectra were obtained using 405 nm laser excitation with a power of 50 mW.

For identification of crystalline and amorphous phases, approximately 10 rough samples were analysed by powder X-ray diffraction (XRD) at the University of Chemistry and Technology, Department of Solid State Chemistry, Prague. The instrumentation consisted of a Bruker D2 Phaser diffractometer operated at room temperature with para-focusing Bragg-Brentano geometry and Co(*K*α) radiation. Phase composition was determined with Stanford University's X'Pert HighScore software in conjunction with the International Center for Diffraction Data PDF-4+ database.

Radioactivity of natural radionuclides was measured at the Department of Dosimetry and Application of Ionizing Radiation, Faculty of Nuclear Sciences and Physical Engineering, Czech Technical University in Prague, using semiconductor gamma spectrometry with a 30% high-purity germanium detector. Approximately 140 pieces of rough opal (150 g total weight) without any mineral inclusions visible at 10× magnification were chosen for measurement. The emission of each sample was measured for 17 hours, which was determined to be sufficient for high-precision measurement. Because the amount of material was insufficient for standard measurement in a 0.5 l Marinelli beaker, the sample needed to be analysed in Petri-dish geometry with a diameter of 11.5 cm (Marinelli & Hill 1948). Such geometry is not available in our laboratory, so we determined the efficiency of detection using Monte Carlo simulation (Goorley *et al.* 2012). This method brought relatively high uncertainty into the results as compared to certified determination using the activity etalon. This process of determining radionuclide content was performed according to standard methods used in our laboratory and approved by the State Office for Nuclear Safety, Czech Republic. General principles of gamma spectrometry and radionuclide content evaluation can be found in Gilmore and Hemingway (1995).

## RESULTS AND DISCUSSION

### *Standard Gemmological Properties*

The faceted stones were colourless and transparent without any impurities visible to the unaided eye. The RI ranged from 1.449 to 1.452, with the most frequent

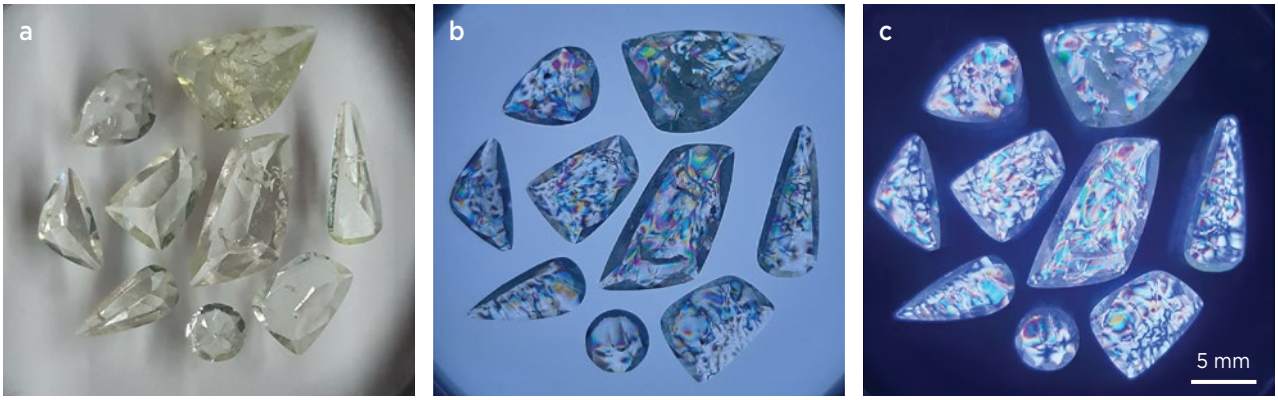


**Figure 4:** These faceted Namibian hyalites (**a**, 0.21–1.34 ct) are shown between partially crossed polarisers (**b**) and between fully crossed polarisers (**c**). Cross-polarised light reveals inhomogeneous interference colours that are probably due to localised strain. Photos by R. Hanus.

being 1.451. By comparison, the RI range of hyalite from Zacatecas, Mexico, is 1.460–1.461 (Megaw *et al.* 2018). In general, the RI values of hyalite vary slightly, ranging from about 1.44 to 1.46, depending on water content (Graetsch 1994). The SG values were between 2.06 and 2.11 (most commonly 2.08). By comparison, the SG of hyalite from Zacatecas is 2.13 (Megaw *et al.* 2018).

In cross-polarised light, the faceted stones and thin section showed interference colours (Figure 4) that varied within individual samples (botryoidal hyalite aggregates) and depended on the thickness of the hyalite. The interference colour patterns correlated to the distribution of cracks and conchoidal zonal patterns, and were less noticeable near the thinner edges of the samples. The interference colours corresponded to areas of strain, and varied according to the direction of the strain, typically from grey first-order colours (with a dark extinction cross pattern) to blue and yellow second-order colours (see Figures 4 and 5). The same appearance was reported by Fritsch *et al.* (2015) for hyalite from Zacatecas, Mexico. Moreover, Rogers (1928, p. 75) mentioned hyalite's colloform structure and its 'double refraction due to strain set up in hardening of the gel'. The strain evident in the Namibian hyalite is most likely due to irregular hardening of the gel from which it formed (cf. Rogers 1928; Graetsch 1994).

The green fluorescence of the Namibian hyalite showed the same high intensity with different excitation wavelengths (254, 365 and 405 nm). This fluorescence is caused by trace amounts of uranyl molecules $(UO_2)^{2+}$ (see PL spectroscopy section below)—the same as for opals from Mexico (Fritsch *et al.* 2015; Megaw *et al.* 2018). The uniform fluorescence intensity with different excitation wavelengths could be due to extreme activity of the uranyl ions. No phosphorescence was observed in the studied samples.

Internal layering corresponding to the botryoidal structure appeared in most of the hyalite samples. The layers showed variable strength of green luminescence. The distribution of the green luminescence within the individual faceted stones was quite inhomogeneous (Figure 6). This inhomogeneity was visible using a microscope with both 365 and 405 nm excitation, as well as with a loupe in natural daylight. Most of the strong green UV-luminescing areas corresponded to areas of convergence of the botryoidal structure and along associated fractures (Figure 7). By contrast, the central areas of the botryoidal spheres showed less luminescence.

Solid mineral inclusions were noted in 10 rough samples, and the results of SEM-EDS analysis indicated that they consisted mostly of Fe- and Mn-(hydr)oxides, sometimes with traces of Ba-bearing limonite. The limonite filled tiny sub-microscopic cavities between individual spherical domains of the botryoidal regions.

Tiny needles or crystals of black tourmaline and, in one case, 'staffelite', were observed filling a cavity. 'Staffelite' is an epigenetic white opaque carbonate-fluorapatite

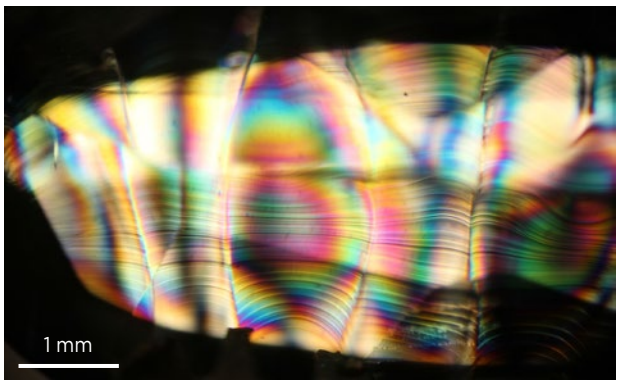


**Figure 5:** Layered growth structures and various interference colours are seen in this thin section (0.03–0.04 mm thickness) of Namibian hyalite immersed in distilled water and observed between crossed polarisers. Photomicrograph by R. Hanus.

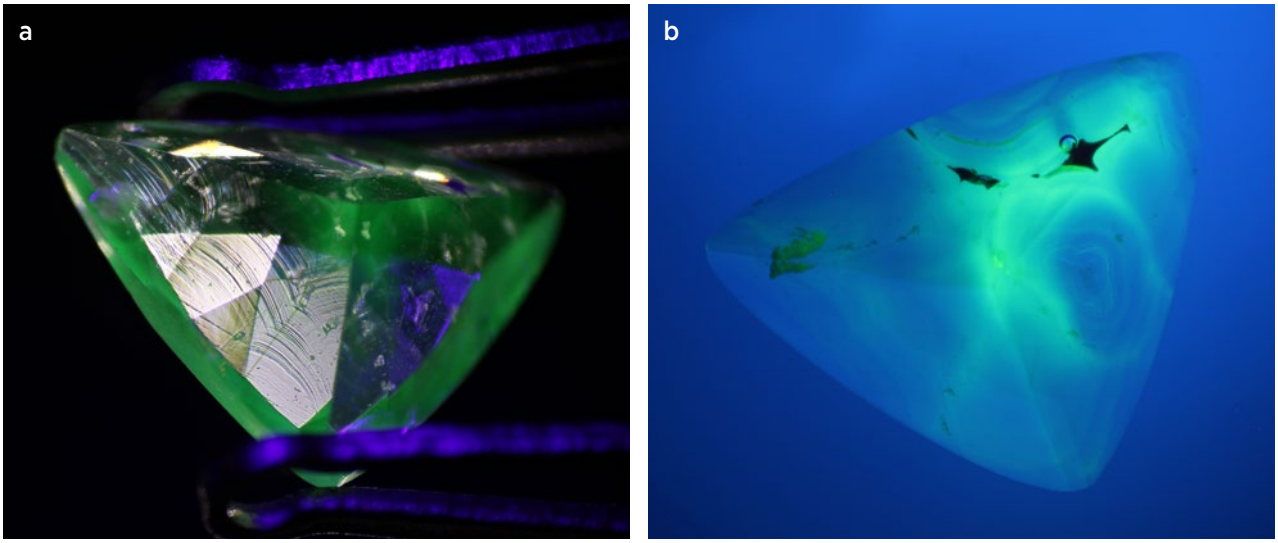


**Figure 6:** (**a**) The botryoidal structure and fluorescence of this 0.28 ct Namibian hyalite are revealed with some incident reflected light and long-wave UV radiation. (**b**) Areas of green fluorescence appear to relate to the opal's botryoidal structure, as shown here immersed in distilled water during exposure to long-wave UV radiation. Photomicrographs by R. Hanus.

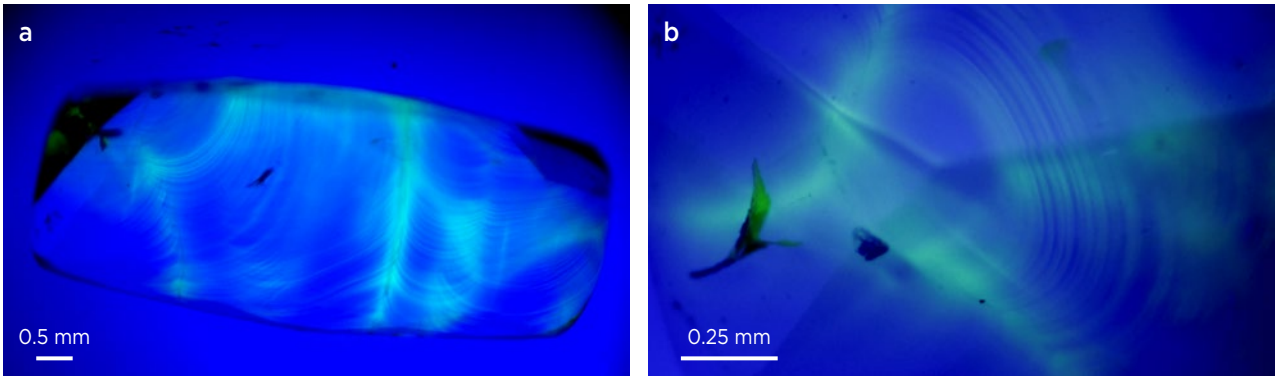


**Figure 7:** (**a**) The fluorescent zones only partially correspond to the growth structure of the hyalite, concentrating more along the convergence of botryoidal banding and associated fractures in this sample. (**b**) Fluorescent zones do not always correspond to the layered botryoidal structure, as seen in this sample in immersion during exposure to long-wave UV radiation. Photomicrographs by R. Hanus.

that can be easily confused with chalcedony due to its very similar appearance from this locality. In addition, 'staffelite' is commonly intimately intergrown with chalcedony. Other mineral inclusions consisted of irregular colourless anisotropic masses (not identified) surrounded by strain halos (Figure 8a), and dark brown-to-black inclusions in the form of thin films (Figure 8b).

## *Raman Spectroscopy*

Raman spectroscopy with the 532 and 633 nm lasers showed broad silica spectral features in the 100–600 $cm^{-1}$ range, with several weak bands between 700 and 1200 $cm^{-1}$ belonging to amorphous opal (Figure 9). According to Ivanov *et al.* (2011), the major band at about 460 $cm^{-1}$ belongs to the opal-A structure. Also present in the spectra of all samples was a peak at around 790 $cm^{-1}$ due to symmetric Si–O–Si stretching vibrations, and another peak at about 975 $cm^{-1}$ assigned to Si-OH bonds in silanol groups (McMillan 1984: Saruwatari *et al.* 2015; Sodo *et al.* 2016). An additional peak was sometimes seen at around 1550 $cm^{-1}$, but it was completely absent from the 633 nm-excited spectrum (again, see Figure 9).

Compared to other fluorescent opals, the distinctive broad band at around 460 $cm^{-1}$ was significantly stronger than the feature at approximately 435 $cm^{-1}$ recorded for samples from Mexico (Fritsch *et al.* 2015; Butini *et al.* 2020). This shift could be caused by radiation damage similar to that reported for zircon (Nasdala *et al.* 2019). Conversely, the intensity of the peak at about 1550 $cm^{-1}$ was much lower than observed for the hyalite from Mexico (cf. Fritsch *et al.* 2015). Variations in the 1550 $cm^{-1}$ peak may be related to the presence of some impurity.

A doublet with maxima at 3602 and 3665 $cm^{-1}$ was

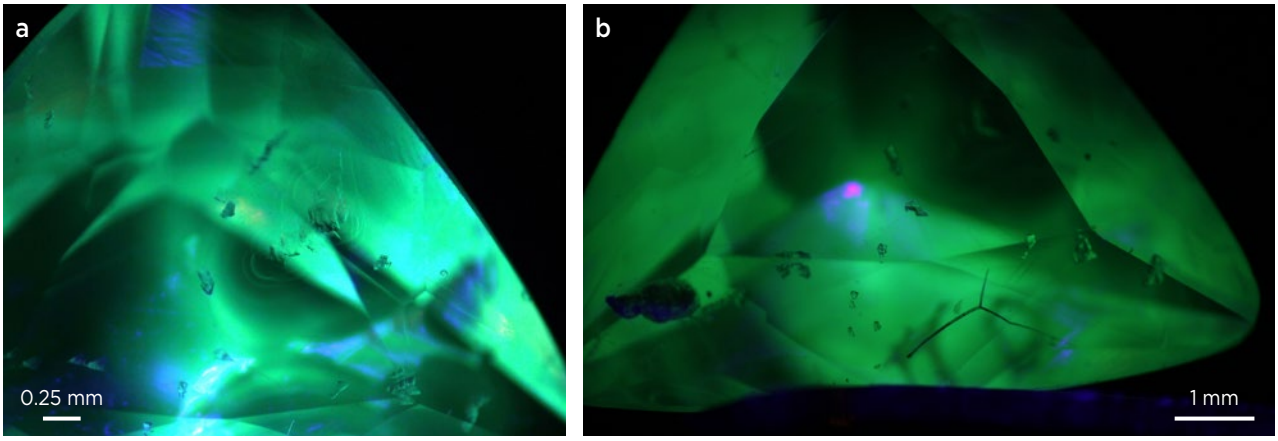


**Figure 8:** (**a**) Strain halos are associated with unidentified solid anisotropic crystalline inclusions in some of the hyalite samples. (**b**) A thin film of limonite forms a 'Mercedes-Benz pattern' in this hyalite, which also contains numerous unidentified anisotropic crystalline inclusions. Both photos were taken with darkfield illumination during exposure to long-wave UV radiation. Photomicrographs by R. Hanus.

present in the Raman spectra of all tested samples, but does not correlate with commonly measured water bands in the structure of opal. This feature is not due to photoluminescence, because the doublet was essentially the same when excited by the two lasers of different wavelengths (see Figure 9). Thus, we infer that this doublet is a vibration of water in some non-typical structural-binding arrangement, or it could be related to the O-H stretching modes and isolated silanol groups that have been measured in opal at 3410 and 3650 $cm^{-1}$ by infrared spectroscopy (Eckert *et al.* 2015). Another explanation might be features in the hydroxyl-stretching region of some other mineral present in the form of micro-inclusions, such as hydroxylclinohumite, hydroxylapatite or, most likely, kaolinite minerals (Johnston *et al.* 1998; Lin *et al.* 2000; Pasteris *et al.* 2012).

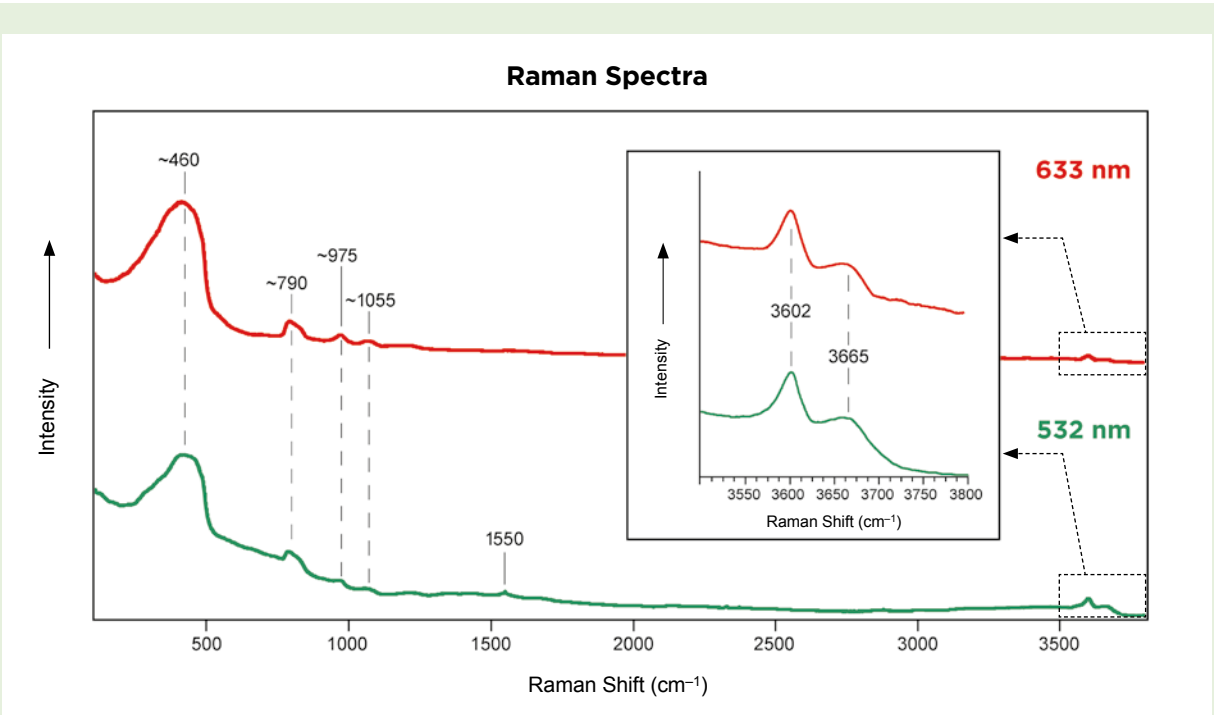


**Figure 9:** Raman spectra of a representative Namibian hyalite are similar for 532 and 633 nm laser excitation. With the former wavelength, however, a small peak is visible at around 1550 $cm^{-1}$ (previously recorded in opal from Zacatecas, Mexico). The inset showing the 3500–3800 $cm^{-1}$ region reveals a doublet at 3602 and 3665 $cm^{-1}$ associated with water or hydroxyl stretching.

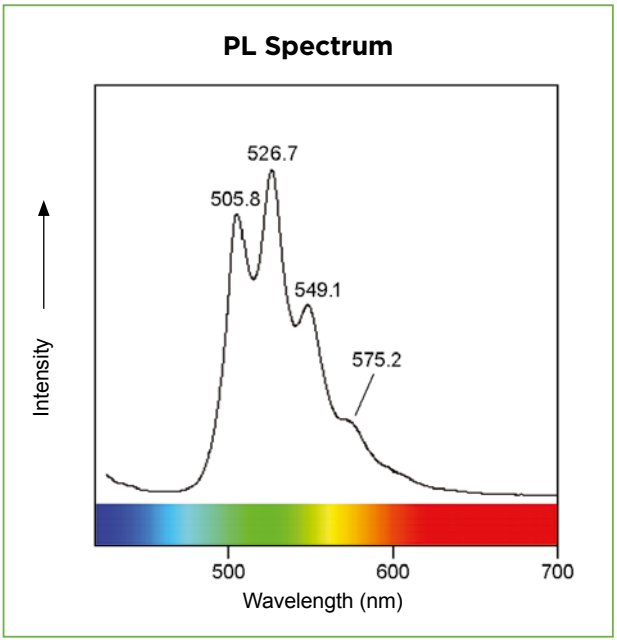


**Figure 10:** PL spectroscopy of the Namibian hyalite with 405 nm excitation displays four maxima typical of the $(UO_2)^{2+}$ ion. A remnant of an artefact at 410 nm, caused by the excitation radiation, is also visible.

## PL Spectroscopy

The opals' PL spectra showed typical uranyl emission features (Faulques *et al.* 2015), with a wide region of emission from about 470 nm to almost 650 nm. The PL spectra of all samples displayed a series of peaks (Figure 10) at around 506, 527, 549, 575 and, sometimes, 604 nm. No features were present in the adjacent near-IR region. The greatest intensity was at 526.7 nm, in the green region, as expected from the colour of the opals' emission. The maximum emission is similar to that in the spectra of hyalite from Zacatecas and San Luis Potosí in Mexico (Fritsch *et al.* 2015; Butini *et al.* 2020). The peaks between 500 and 580 nm have been attributed to the uranyl cation $(UO_2)^{2+}$ (Gaillou *et al.* 2011; Fritsch *et al.* 2015; Butini *et al.* 2020). This characteristic sequence of uranyl electronic transitions agrees with previous studies that detected similar luminescence in minerals containing uranyl cations in various sites in their structures (Driscoll *et al.* 2014; Faulques *et al.* 2015).

Excitation with the 473 nm laser showed only strong luminescence peaks in the 490–580 nm region (Figure 11) due to the uranyl emission features described above.

## XRD Analysis

The powder XRD analyses were aimed at assessing whether the hyalite is only opal-AN or if there are any features typical of opal-CT. From the obtained XRD patterns it was evident that the structure was completely amorphous, with a characteristic broad band belonging most likely to opal-AN structure. The presence of chalcedony, 'staffelite' and tourmaline in the hyalite were also verified by the XRD analyses.

## Radioactivity

We detected relatively high activity of radionuclides of the uranium-actinium decay chain (parent nuclide $^{235}U$) and uranium-radium decay chain (parent nuclide $^{238}U$). While each of these series has a different nuclide decay ratio, the individual radionuclides are in a state of permanent radioactive balance, so their relative activity is the same (taking into account measurement precision). The time needed to reach equilibrium for both of these uranium decay chains is approximately one million years.

In the hyalite samples, the activity of each measured radionuclide in the uranium-actinium decay chain was around 1000 Bq/kg*, and for the uranium-radium decay chain the activity of each radionuclide was around

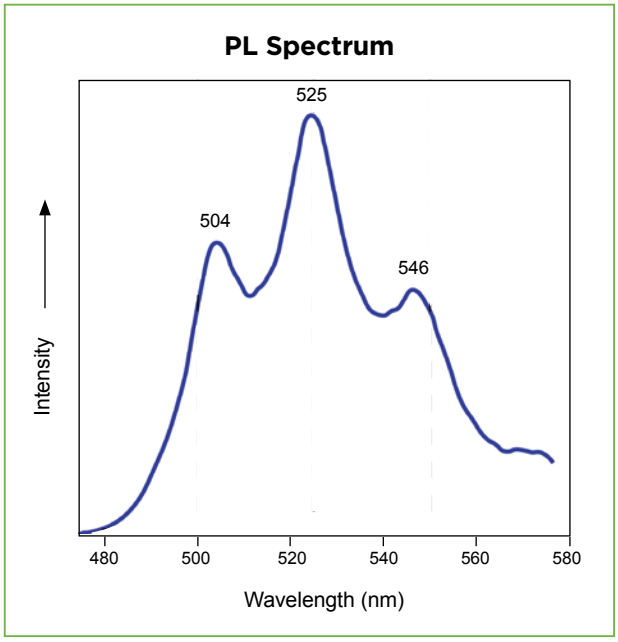


**Figure 11:** Luminescence peaks due to uranyl emission features are seen in the Namibian hyalite with 473 nm excitation.

* Units of measure used to express radioactivity vary depending on whether they represent the radiation emitted by a source, the physical dose of radiation received by a subject, or the biological effect of the dose received. *Bequerel* (Bq; usually expressed as Bq/kg) is a measure of the radiation **emitted** by a radioactive substance. *Gray* (Gy; usually expressed as Gy/h or, in this case, nGy/h) is a measure of a dose of radiation **received** or absorbed by a subject. *Sievert* (Sy; usually Sy/h) expresses the biological **effect** of a dose of radiation, and the relationship of effect (Sy) to dose (Gy) depends on the nature of a specific radionuclide decay chain and other factors.

**Table I:** Activities of radionuclides in hyalite from Erongo, Namibia.

| Decay Chain | Radionuclide | Mass activity (Bq/kg) |
|---|---|---|
| Uranium-Actinium | $^{235}$U | 960 ± 150 |
| | $^{227}$Th | 980 ± 150 |
| | $^{223}$Ra | 1040 ± 150 |
| Uranium-Radium | $^{234}$Pa[a] | 19,100 ± 3000 |
| | $^{226}$Ra | 23,500 ± 3500 |
| | $^{214}$Bi[b] | 21,600 ± 3200 |
| | $^{214}$Pb[b] | 23,600 ± 3500 |

[a] Metastable radionuclide.

[b] Standard hermetic procedure was not followed to measure the activity of these radionuclides, so these measurements are approximate.

22,000 Bq/kg (Table I). (For comparison, the activity of the natural potassium isotope in a banana is about 31,000 Bq/kg, so a banana is more radioactive than this hyalite.) The activity of radionuclides in the $^{232}$Th decay chain and $^{40}$K decay chain was extremely low, so these values can be neglected.

Overall, the activity of natural radionuclides ($^{235}$U, $^{238}$U and their decay products) in our hyalite samples from Erongo was significantly greater than that of common rocks. For example, the activity of $^{238}$U in typical granite is around 50 Bq/kg, while the average activity in the earth's crust is estimated at 35 Bq/kg; by comparison, uranium ore has an activity of 10–1000 kBq/kg. Compared to the global average terrestrial gamma dose rate (1 m above ground) of about 55 nGy/h* (UNSCEAR 1988), the contribution from a hyalite gem seems insignificant.

To estimate the health risks associated with wearing a small gem (as used in jewellery) near the human body (IAEA 2003), we assumed a 5 ct stone located 10 cm from the body centre (such as worn in a necklace). With an estimated gamma dose rate (from the $^{238}$U and $^{235}$U decay chains) of 0.08 nGy/h* ($8.0 \times 10^{-5}$ µSv/h*), this is well below the average ambient radiation level mentioned above.

## CONCLUSIONS

Daylight-fluorescent hyalite from the Erongo Mountains of Namibia is a highly attractive collector's stone. Although faceted gems have so far rarely weighed more than 1 ct, the possibility of finding larger pieces may just be a matter of time and further prospecting.

Raman spectra of this opal were best measured using a green laser (532 nm). Features related to silicon tetrahedra vibrations, such as the band at about 460 cm$^{-1}$, which differs from the 435 cm$^{-1}$ band observed for hyalite from Mexico, might have shifted due to differences in the degree of crystallinity and impurities. The Raman spectrum of the Namibian hyalite also might be 'contaminated' by photoluminescence features associated with the uranyl cation responsible for the strong fluorescence.

The unusually intense green fluorescence to daylight is caused by uranium in the form of the uranyl cation $(UO_2)^{2+}$. The fluorescence was not homogeneous when viewed with a microscope, and appears to originate from zones or layers of the opal enriched in uranyl. Due to the uranium content, small amounts of radioactivity were detected in this opal (around 22,000 Bq/kg), which poses an insignificant risk to human health.

## REFERENCES


Brown, L.D., Ray, A.S. & Thomas, P.S. 2004. Elemental analysis of Australian amorphous banded opals by laser-ablation ICP-MS. *Neues Jahrbuch für Mineralogie, Monatshefte*, **2004**(9), 411–424, https://doi.org/10.1127/0028-3649/2004/2004-0411.

Butini, F., Cattaneo, G.L., Precisvalle, N., Sodo, A. & Zorzi, F. 2020. Characterization of the fluorescent hyalite of San Luis Potosí, Mexico. *Italian Gemological Review*, No. 10, 65–74.

Cairncross, B. 2001. Aquamarine from Erongo Mtn., Namibia. *Mineralogical Record*, **32**(1), 63–64.

Cairncross, B. & Bahmann, U. 2006. Famous mineral localities: The Erongo Mountains, Namibia. *Mineralogical Record*, **37**(5), 361–470.

Chojcan, J., Sachanbiński, M., Idczak, R. & Konieczny, R. 2013. Positron annihilation in precious and common opals. *Nukleonika*, **58**(1), 225–228.

Cooper, M.P. 2000. Ste-Marie-aux-Mines show 1999. *Mineralogical Record*, **31**(1), 97–100.

Curtis, N.J., Gascooke, J.R., Johnston, M.R. & Pring, A. 2019. A review of the classification of opal with reference to recent new localities. *Minerals*, **9**(5), article 299 (21 pp.), https://doi.org/10.3390/min9050299.

Driscoll, R.J.P., Wolverson, D., Mitchels, J.M., Skelton, J.M., Parker, S.C., Molinari, M., Khan, I., Geeson, D. *et al*. 2014. A Raman spectroscopic study of uranyl minerals from Cornwall, UK. *RSC Advances*, **4**(103), 59137–59149, https://doi.org/10.1039/c4ra09361e.

Eckert, J., Gourdon, O., Jacob, D.E., Meral, C., Monteiro, P.J.M., Vogel, S.C., Wirth, R. & Wenk, H.-R. 2015. Ordering of water in opals with different microstructures. *European Journal of Mineralogy*, **27**(2), 203–213, https://doi.org/10.1127/ejm/2015/0027-2428.

Faulques, E., Kalashnyk, N., Massuyeau, F. & Perry, D.L. 2015. Spectroscopic markers for uranium(VI) phosphates: A vibronic study. *RSC Advances*, **5**(87), 71219–71227, https://doi.org/10.1039/c5ra13558c.

Fritsch, E., Spano-Franco, T. & Megaw, P. 2014. Gem Notes: Green daylight-fluorescent hyalite opal from Mexico. *Journal of Gemmology*, **34**(4), 294–296.

Fritsch, E., Megaw, P.K.M., Spano, T.L., Chauviré, B., Rondeau, B., Gray, M., Hainschwang, T. & Renfro, N. 2015. Green-luminescing hyalite opal from Zacatecas, Mexico. *Journal of Gemmology*, **34**(6), 490–508, https://doi.org/10.15506/JoG.2015.34.6.490.

Gaillou, E., Delaunay, A., Rondeau, B., Bouhnik-le-Coz, M., Fritsch, E., Cornen, G. & Monnier, C. 2008. The geochemistry of gem opals as evidence of their origin. *Ore Geology Reviews*, **34**(1–2), 113–126, https://doi.org/10.1016/j.oregeorev.2007.07.004.

Gaillou, E., Fritsch, E. & Massuyeau, F. 2011. Luminescence of gem opals: A review of intrinsic and extrinsic emission. *Australian Gemmologist*, **24**(8), 200–201.

Gentry, R.M., Wise, M.A., & Pierro, R.C. 2004. Pocket paragenesis of the Erongo pegmatites, Namibia. *Rocks & Minerals*, **79**, 187.

Gilmore, G. & Hemingway, J.D. 1995. *Practical Gamma-Ray Spectrometry*. John Wiley and Sons, Chichester, 314 pp.

Goorley, T., James, M., Booth, T., Brown, F., Bull, J., Cox, L.J., Durkee, J., Elson, J. *et al*. 2012. Initial MCNP6 release overview. *Nuclear Technology*, **180**(3), 298–315, https://doi.org/10.13182/nt11-135.

Graetsch, H. 1994. Structural characteristics of opaline and microcrystalline silica minerals. *In*: Heaney, P.J., Prewitt, C.T. & Gibbs, G.V. (eds) *Silica*. Mineralogical Society of America, Washington DC, USA, 209–232, https://doi.org/10.1515/9781501509698-011.

Guthrie, G.D., Bish, D.L. & Reynolds, R.C. 1995. Modeling the X-ray diffraction pattern of opal-CT. *American Mineralogist*, **80**(7–8), 869–872, https://doi.org/10.2138/am-1995-7-823.

Haughton, S.H., Frommurze, H.F., Gevers, T.W., Schwellnus, C.M. & Rossouw, P.J. 1939. *The Geology and Mineral Deposits of the Omaruru Area, South West Africa*. Union of South Africa, Department of Mines, Geological Survey, Pretoria, South Africa, 160 pp.

IAEA 2003. *Guidelines for Radioelement Mapping Using Gamma Ray Spectrometry Data*. IAEA-TECDOC-1363, International Atomic Energy Agency, Vienna, Austria, 184 pp., https://www-pub.iaea.org/MTCD/Publications/PDF/te_1363_web.pdf.

Ivanov, V.G., Reyes, B.A., Fritsch, E. & Faulques, E. 2011. Vibrational states in opals revisited. *Journal of Physical Chemistry C*, **115**(24), 11968–11975, https://doi.org/10.1021/jp2027115.

Johnston, C.T., Helsen, J., Schoonheydt, R.A., Bish, D.L. & Agnew, S.F. 1998. Single-crystal Raman spectroscopy study of dickite. *American Mineralogist*, **83**(1–2), 75–84, https://doi.org/10.2138/am-1998-1-208.

Jones, J.B. & Segnit, E.R. 1971. The nature of opal I. Nomenclature and constituent phases. *Journal of the Geological Society of Australia*, **18**(1), 57–68, https://doi.org/10.1080/00167617108728743.

Kane, R.E. & Fritsch, E. 1991. Gem Trade Lab Notes: Spinel with unusual green fluorescence. *Gems & Gemology*, **27**(2), 112–113.

Langer, K. & Flörke, O.W. 1974. Near-infrared absorption spectra (4000–9000 $cm^{-1}$) of opals and the role of "water" in the $SiO_2 \cdot nH_2O$ minerals. *Forschritte der Mineralogie*, **52**, 17–51.

Lin, C.C., Liu, L.G., Mernagh, T.P. & Irifune, T. 2000. Raman spectroscopic study of hydroxyl-clinohumite at various pressures and temperatures. *Physics and Chemistry of Minerals*, **27**(5), 320–331, https://doi.org/10.1007/s002690050261.

Liu, Y., Shi, G. & Wang, S. 2014. Color phenomena of blue amber. *Gems & Gemology*, **50**(2), 134–140, https://doi.org/10.5741/gems.50.2.134.

Marinelli, L.D. & Hill, R.F. 1948. Studies on dosage in cancer therapy. *In*: *Brookhaven Conference Report: Symposium on Radioiodine*, BNL-C-5, Brookhaven National Laboratory, Upton, New York, USA, 28–30 July, 98–105.

McMillan, P. 1984. Structural studies of silicate glasses and melts—Applications and limitations of Raman spectroscopy. *American Mineralogist*, **69**(7–8), 622–644.

McOrist, G.D. & Smallwood, A. 1995. Trace elements in coloured opals using neutron activation analysis. *Journal of Radioanalytical and Nuclear Chemistry*, **198**(2), 499–510, https://doi.org/10.1007/bf02036566.

McOrist, G.D. & Smallwood, A. 1997. Trace elements in precious and common opals using neutron activation analysis. *Journal of Radioanalytical and Nuclear Chemistry*, **223**(1–2), 9–15, https://doi.org/10.1007/bf02223356.

McOrist, G.D., Smallwood, A. & Fardy, J.J. 1994. Trace elements in Australian opals using neutron activation analysis. *Journal of Radioanalytical and Nuclear Chemistry*, **185**(2), 293–303, https://doi.org/10.1007/bf02041302.

Megaw, P.K.M., Fritsch, E., Spano, T.L. & Gray, M. 2018. Geology and mineralogy of Electric Opal™: Green daylight-luminescing hyalite opal from Zacatecas, Mexico. *Rocks & Minerals*, **93**(5), 404–413, https://doi.org/10.1080/00357529.2018.1477007.

Moses, T. 1997. Gem Trade Lab Notes: Diamond—Two noteworthy stones from the Americas. *Gems & Gemology*, **33**(1), 54–55.

Nasdala, L., Akhmadaliev, S., Chanmuang N, C., Zowalla, A., Csato, C. & Rüb, M. 2019. $^{4}$He irradiation of zircon, $ZrSiO_4$, using a micro-patterned, Si-based energy filter. *Nuclear Instruments and Methods in Physics Research Section B: Beam Interactions with Materials and Atoms*, **443**, 38–42, https://doi.org/10.1016/j.nimb.2019.01.046.

Ogawa, H., Makino, K., Ishibashi, T. & Nakano, S. 2008. Fluorescence of hyalite in pegmatite from Naegi granite, Nakatugawa. *Annual Meeting of Japan Association of Mineralogical Sciences*, presentation R4-10, https://doi.org/10.14824/jakoka.2008.0.108.0.

Pan, Y., Li, D., Feng, R., Wiens, E., Chen, N., Chernikov, R., Götze, J. & Lin, J. 2021. Uranyl binding mechanism in microcrystalline silicas: A potential missing link for uranium mineralization by direct uranyl co-precipitation and environmental implications. *Geochimica et Cosmochimica Acta*, **292**, 518–531, https://doi.org/10.1016/j.gca.2020.10.017.

Pasteris, J.D., Yoder, C.H., Sternlieb, M.P. & Liu, S. 2012. Effect of carbonate incorporation on the hydroxyl content of hydroxylapatite. *Mineralogical Magazine*, **76**(7), 2741–2759, https://doi.org/10.1180/minmag.2012.076.7.08.

Pewkliang, B., Pring, A. & Brugger, J. 2008. The formation of precious opal: Clues from the opalization of bone. *Canadian Mineralogist*, **46**(1), 139–149, https://doi.org/10.3749/canmin.46.1.139.

Pirajno, F. 1990. Geology, geochemistry and mineralisation of the Erongo volcanic complex, Namibia. *South African Journal of Geology*, **93**(3), 485–504.

Rogers, A.F. 1928. Natural history of the silica minerals. *American Mineralogist*, **13**(3), 73–92.

Saruwatari, K., Katsurada, Y., Odake, S. & Abduriyim, A. 2015. Lab Notes: Uranium contents of hyalite. *Gems & Gemology*, **51**(4), 431–432.

Sehgal, A. & Girma, D. 2016. Lab Notes: Unusual yellowish green spinel. *Gems & Gemology*, **52**(2), 194–195.

Shigley, J.E. & Breeding, C.M. 2015. Visible absorption spectra of colored diamonds. *Gems & Gemology*, **51**(1), 41–43 (with chart), https://doi.org/10.5741/gems.51.1.41.

Sodo, A., Casanova Municchia, A., Barucca, S., Bellatreccia, F., Della Ventura, G., Butini, F. & Ricci, M.A. 2016. Raman, FT-IR and XRD investigation of natural opals. *Journal of Raman Spectroscopy*, **47(**12), 1444–1451, https://doi.org/10.1002/jrs.4972.

Takahashi, Y., Akabane, H., Imai, H., Kometani, M., Muroi, K., Kuniga, M. & Yamamoto, S. 2007. On the occurrence of opal at the Shin-yu hot spring, Tateyama. *Tateyama Caldera Research*, **8**, 1–4.

UNSCEAR 1988. *Sources, Effects and Risks of Ionizing Radiation*. United Nations Scientific Committee on the Effects of Atomic Radiation, United Nations, New York, New York, USA, 645 pp., https://doi.org/10.18356/81528a73-en.

Wigand, M., Schmitt, A.K., Trumbull, R.B., Villa, I.M. & Emmermann, R. 2004. Short-lived magmatic activity in an anorogenic subvolcanic complex: $^{40}$Ar/$^{39}$Ar and ion microprobe U–Pb zircon dating of the Erongo, Damaraland, Namibia. *Journal of Volcanology and Geothermal Research*, **130**(3–4), 285–305, https://doi.org/10.1016/s0377-0273(03)00310-x.

## The Authors

**Dr Radek Hanus[1], Kamil Sobek[2], Dr Kamila Johnová[3], Prof. Tomáš Trojek[3], Dr Ján Štubňa[4], Tomáš Hanus[1,5] and Kamila Jungmannová[1,6]**

[1] Gemological Laboratory, Prague, Czech Republic. Email: hanusrdk@gmail.com
[2] Dept. of Geological Sciences, Masaryk University, Faculty of Science, Brno, Czech Republic. Email: sobekk@mail.muni.cz
[3] Czech Technical University in Prague, Faculty of Nuclear Sciences and Physical Engineering, Prague, Czech Republic
[4] Gemmological Laboratory, Constantine the Philosopher University in Nitra, Slovakia
[5] Gymnázium Hostivice, Hostivice, Czech Republic
[6] Koněprusy Caves, Koněprusy, Czech Republic

## Acknowledgements

We thank Assoc. Prof. Jan Cempírek (Masaryk University) for help with clarifying the unusual optical properties of the opals in cross-polarised light. Also, one of the anonymous reviewers is thanked for assistance with presenting the information in the Background section. This work was supported by the European Regional Development Fund project 'Centre for Advanced Applied Sciences' (No. CZ.02.1.01/0.0/0.0/16_019/0000778), KEGA 026UKF-4/2021 – Identification of the Gemmological Materials, KEGA CZ.02.1.01/0.0/0.0/16_019/0000778 and the Internal Grant Agency of Masaryk University (No. CZ.02.2.69/0.0/0.0/19_073/0016943).

**Figure 1:** These deep blue gahnites from Jemaa, Nigeria, form part of the material examined for this study. The oval stone on the right weighs 1.34 ct. Photo by T. Stephan.

# On the Colour Mechanism of Blue Gahnite from Nigeria

Tom Stephan, Ulrich Henn and Stefan Müller

**ABSTRACT:** Gem-quality blue gahnite from Jemaa in central Nigeria has gemmological properties (RI and SG) and a chemical composition indicating relatively pure gahnite (90.7–91.3%). The blue colour is caused by a region of transmission between a system of dominant $Fe^{2+}$- and $Co^{2+}$-related absorption bands centred in the orange-to-green spectral range and an absorption edge in the UV region. The UV edge is strongly temperature dependent and, upon heating of the gahnite to 1000°C and 1400°C, shifts towards the visible range, resulting in blue-green and green colouration, respectively. The green colour component is related to $Fe^{3+}$, whereas the blue hue of the unheated gahnite is due predominantly to $Co^{2+}$.

*The Journal of Gemmology*, **38**(2), 2022, pp. 183–193, https://doi.org/10.15506/JoG.2022.38.2.183


Among the minerals of the spinel supergroup, the zinc member gahnite (ideally $ZnAl_2O_4$) is found only sporadically in gem quality. Transparent green specimens from Brazil were described by Bank (1975). Green-to-blue material from Nigeria was characterised in detail by Jackson (1982). The latter locality, in the Jemaa region of central Nigeria, is associated with granitic pegmatites (Jacobson & Webb 1946). In recent years, some parcels of rough deep blue gahnite from Nigeria (e.g. Figure 1) entered the gem trade, and short notes were published in the gemmological literature (Boehm & Laurs 2018; Hain & Sun 2019).

Jackson (1982) attributed the blue colour of Nigerian gahnite to $Fe^{2+}$, and mentioned an interesting colour modification from blue to blue-green and dark 'olive' green when the material is heated to temperatures of 1000°C and 1400°C, respectively. Subsequent detailed research on the causes of green-to-blue colouration in Nigerian gahnite (Fregola *et al.* 2014) proved the blue material to be coloured by a combination of absorption features associated with $Fe^{2+}$, $Fe^{3+}$ and $Co^{2+}$. The role of $Co^{2+}$ as a chromophore in Nigerian gahnite, in addition to $Fe^{2+}$, was also mentioned briefly by Hain and Sun (2019).

Generally, higher Fe contents in gahnite produce a stronger UV absorption edge extending into the visible spectral range that causes a green colour, while specimens with lower Fe that also contain Co show green-blue to blue colouration (Taran *et al.* 2005; Fregola *et al.* 2014). The aim of this study is to further investigate this interdependency of Fe and Co, mainly to show how strongly $Co^{2+}$ influences the colour of blue Nigerian gahnite, as well as to document and interpret the annealing effect described by Jackson (1982).

## CRYSTAL CHEMISTRY

Minerals with the spinel structure are found in a wide range of geological environments—both on Earth and in extraterrestrial contexts—making them important for scientific research. The structure and crystal chemistry of spinel-group minerals have been the focus of many studies, starting with initial publications in 1915 and continuing to the present (for a thorough review, see Bowles *et al.* 2011).

The spinel structure is generally characterised by close-packed oxygen atoms with metal atoms in tetrahedral and octahedral sites. To date, the spinel supergroup consists of 56 minerals with the general chemical formula $AB_2X_4$ (Bosi *et al.* 2019). The occupancy of the X position differentiates the oxyspinel (oxygen), thiospinel (sulphur) and selenospinel (selenium) groups. Gem-quality spinel minerals belong to the oxyspinel group, with the general chemical formula $A^{2+}B_2^{3+}O_4$, where A and B represent divalent or trivalent metal ions ($M^{2+}$ or $M^{3+}$, respectively). The spinel subgroup contains several species with $Al^{3+}$ as the dominant B cation, the most common being:

- Spinel ($MgAl_2O_4$)
- Hercynite ($FeAl_2O_4$)
- Gahnite ($ZnAl_2O_4$)
- Galaxite ($MnAl_2O_4$)

These end members form complete solid solutions. Gem-quality spinels are usually Mg rich (i.e. the mineral spinel, or 'common' spinel; $MgAl_2O_4$). Mixed crystals of spinel and gahnite, the so-called gahnospinels, have less significance as gems, and relatively pure gahnite is rare in gem quality.

The colour range of gem spinel varies from red and purple to blue, green-blue and bluish green. The chromophores $Cr^{3+}$, $V^{3+}$, $Fe^{2+}$, $Fe^{3+}$ and $Co^{2+}$, as well as $Mn^{3+}$, are responsible for this wide range of colours (Schmetzer *et al.* 1989).

## MATERIALS AND METHODS

The study samples consisted of 81 crystals and crystal fragments (3–6 mm in size), and six faceted stones (0.22–1.34 ct), from Jemaa, Nigeria (e.g. Figure 1). The majority of the samples were loaned or donated by Gemstore24 and Arnoldi International, and some were from the collection of the German Gemmological Association. All of them were transparent, and most were deep blue in colour, although a few showed a slightly greenish hue. Some of the crystals were euhedral octahedra, but most showed a flattened or distorted octahedral shape. The waterworn appearance of their edges indicates they were mined from a secondary occurrence.

For comparison, several additional samples were investigated for their chemical composition (especially Co contents) and optical absorption spectra. These included four faceted (0.41–1.53 ct) and three rough (with parallel-polished windows) Fe ± Co-bearing blue spinels from other localities (Sri Lanka, Vietnam and an unspecified location), and a flux-grown Co-bearing synthetic spinel (Figure 2).

All six faceted Nigerian samples were tested by standard gemmological methods at the German Gemmological Association. RI was measured with a digital refractometer (Presidium Refractive Index Meter II) and SG was determined hydrostatically. The rough material was identified, and the identity of the cut stones was confirmed, by Raman spectroscopy using a Magilabs GemmoRaman instrument. Internal features were studied with a gemmological microscope, and inclusions were identified with Raman micro-spectroscopy using a Renishaw inVia unit with 514 and 785 nm laser excitation.

The chemical composition of the six faceted Nigerian gahnites, and all the comparison samples, was analysed at the Institute of Geosciences (Johannes Gutenberg University Mainz, Germany) with a JEOL JXA-8200 electron probe micro-analyser (EPMA) equipped with five wavelength-dispersive spectrometers. Analytical

**Figure 2:** This 0.47 ct flux-grown synthetic spinel is coloured by cobalt. Photo by T. Stephan.

conditions were 20 kV accelerating voltage, 20 nA beam current and a beam diameter of 5 µm. The counting time was generally 30 s (or 40 s for Fe and Mn). For analysis, *K*α-lines were used for each element, and special care was taken with overlapping peaks such as Fe(*K*α) and Co(*K*α). Standards consisted of well-characterised natural and synthetic oxide and silicate minerals. The matrix correction was done using a customised spinel program developed by the Petrology Working Group of the Institute of Geosciences. End-member composition was calculated with EMG software (End-Members Generator; Ferracutti *et al.* 2015).

Optical absorption spectra of all faceted and ten rough Nigerian gahnites, as well as the comparison samples, were collected at the DSEF German Gem Lab with a PerkinElmer Lambda 950S ultraviolet-visible-near infrared (UV-Vis-NIR) spectrometer, in the 200–2500 nm range with a resolution of 1 nm. The rough samples were analysed through parallel-polished windows. Deuterium and tungsten halogen lamps were used as light sources. The major detector change took place at 810 nm; longer wavelengths were recorded with an InGaAs detector, and shorter wavelengths with a photomultiplier tube (PMT detector). In the 200–810 nm range the slot width was fixed to 4 nm, and for 810–2500 nm it was variable (2–4 mm). The device was equipped with an integration sphere to collect scattered light. For spectral fitting, MagicPlot non-linear curve-fitting software was used. The L*a*b* colour coordinates were calculated between 380 and 780 nm (using the CIE standard illuminant D65 and a 2° standard observer) with LabCognition Panorama 4.0 software.

Heat-treatment experiments were performed at the German Gemmological Association on two rough Nigerian gahnites with parallel-polished windows, using a Nabertherm LHT 02/18 electric furnace. The samples were placed in ceramic ($Al_2O_3$) crucibles and heated in air. First they were heated for one hour at 1000°C and then for one hour at 1400°C (with a one-hour ramp-up time to the final temperature). After each heating interval they were taken directly out of the furnace and allowed to cool to ambient conditions.

## RESULTS

### *Gemmological Properties*

The RI of the Nigerian gahnites ranged between 1.791 and 1.798, and their SG varied from 4.34 to 4.66. These properties fall within the general ranges reported for gem-quality gahnite (Bank 1975, 1983; Jackson 1982; Boehm & Laurs 2018; Hain & Sun 2019), and are relatively close to the values described for pure gahnite (Winchell & Winchell 1967): RI = 1.805 and SG = 4.62.

Most of the samples contained crystalline and liquid inclusions. The solid inclusions consisted of transparent, corroded crystal clusters (identified as quartz); euhedral hexagonal prisms (beryl); rounded, colourless to slightly yellow crystals (zircon), often surrounded by tension halos; black tabular inclusions (tentatively identified as columbite), also often surrounded by tension halos; flat, tabular, hexagonal crystals (mica); and reddish brown, often rounded inclusions (sphalerite). In addition, negative crystals and two-phase partially healed fractures were observed.

### *Chemical Composition*

The analysed samples had a composition relatively close to end-member gahnite, with approximately 91% $ZnAl_2O_4$ (see Table I). Most of the remainder consisted of the hercynite component ($FeAl_2O_4$), while galaxite ($MnAl_2O_4$) and spinel ($MgAl_2O_4$) components were present in amounts less than 1%. The analyses correspond well to data previously reported for Nigerian gahnite (D'Ippolito *et al.* 2013).

Low contents of Co were detected, ranging between 0.02 and 0.03 wt.% CoO. Such traces of Co have been previously reported in blue 'cobalt spinel' and gahnite (Shigley & Stockton 1984; Chauviré *et al.* 2015; D'Ippolito *et al.* 2015; Schollenbruch *et al.* 2021). Our measurements revealed comparable Co concentrations to some cobalt spinels from Sri Lanka (0.02–0.04 wt.% CoO), while a reference sample from Vietnam showed a distinctly higher concentration (0.07 wt.% CoO).

**Table I:** Chemical composition by EPMA of six blue gahnites from Nigeria.

| Sample | 1 | 2 | 3 | 4 | 5 | 6 |
|---|---|---|---|---|---|---|
| **Oxides (wt.%)** | | | | | | |
| $Al_2O_3$ | 56.47 | 57.08 | 56.99 | 57.31 | 57.30 | 57.55 |
| FeO[a] | 3.18 | 2.97 | 2.97 | 3.05 | 2.90 | 2.93 |
| CoO | 0.02 | 0.02 | 0.02 | 0.02 | 0.03 | 0.02 |
| MnO | 0.09 | 0.08 | 0.07 | 0.09 | 0.08 | 0.08 |
| MgO | 0.20 | 0.18 | 0.19 | 0.20 | 0.18 | 0.20 |
| ZnO | 39.97 | 39.59 | 39.64 | 39.23 | 39.41 | 39.14 |
| **Total** | 99.92 | 99.92 | 99.89 | 99.90 | 99.91 | 99.92 |
| **Cations per 4 oxygens** | | | | | | |
| Al | 2.010 | 2.023 | 2.022 | 2.028 | 2.028 | 2.032 |
| $Fe^{2+}$ | 0.080 | 0.075 | 0.075 | 0.077 | 0.073 | 0.074 |
| Co | <0.001 | <0.001 | <0.001 | <0.001 | <0.001 | <0.001 |
| Mn | 0.002 | 0.002 | 0.002 | 0.002 | 0.002 | 0.002 |
| Mg | 0.009 | 0.008 | 0.009 | 0.009 | 0.008 | 0.009 |
| Zn | 0.892 | 0.879 | 0.881 | 0.870 | 0.874 | 0.866 |
| **Total[b]** | 0.984 | 0.965 | 0.968 | 0.959 | 0.958 | 0.951 |
| **End members (%)** | | | | | | |
| Gahnite ($ZnAl_2O_4$) | 90.70 | 91.20 | 91.19 | 90.84 | 91.31 | 91.10 |
| Hercynite ($FeAl_2O_4$) | 8.18 | 7.75 | 7.74 | 8.01 | 7.61 | 7.75 |
| Galaxite ($MnAl_2O_4$) | 0.22 | 0.21 | 0.20 | 0.23 | 0.23 | 0.21 |
| Spinel ($MgAl_2O_4$) | 0.90 | 0.84 | 0.87 | 0.92 | 0.85 | 0.94 |

[a] All iron reported as FeO. [b] Includes all elements except Al.

## *Optical Absorption Spectra*

The UV-Vis-NIR absorption spectra of our Nigerian blue gahnite samples showed three dominant absorption-band systems (Figure 3). The strongest was located in the NIR range, the second towards the UV and the third in the visible range. Interpretation and assignment of the absorption bands was carried out in comparison to reference data from the literature (Schmetzer *et al.* 1989; Taran *et al.* 2005, 2009; D'Ippolito *et al.* 2013, 2015; Fregola *et al.* 2014; Palke & Sun 2018). The most important absorption bands, and their attributions, are listed in Table II.

The dominant absorption band system in the NIR range below 8300 $cm^{-1}$ (above 1200 nm) is attributed to spin-allowed *d-d* transitions of tetrahedrally coordinated $Fe^{2+}$. The Co-bearing samples showed some smaller bands between 9000 and 6500 $cm^{-1}$ (1100–1550 nm); as shown in Figure 3, these were prominent in some spectra (d and e) and weak in others (a and c). These bands were absent from samples coloured mainly by iron (Figure 3b).

A strong band system towards the UV region is explained by oxygen-metal charge-transfer (OMCT) processes, mainly $O^{2-} \rightarrow Fe^{3+}$ and $O^{2-} \rightarrow Fe^{2+}$. These OMCT bands form both a consistent increase in absorption towards the UV and an absorption edge at around 30,000 $cm^{-1}$ (330 nm).

Between these two strong band systems, a series of weaker bands in the visible region is caused by a combination of mostly spin-forbidden, but also spin-allowed, transitions mainly of the chromophores $Fe^{2+}$, $Co^{2+}$ and (minor) $Fe^{3+}$. In combination, their overlapping absorption bands create a transmission window in the blue region. To distinguish the individual bands, however, is difficult.

## *Spectral Fitting and Colour Mechanism*

To demonstrate the influence of $Co^{2+}$ on gahnite colouration, the absorption spectra were mathematically deconvoluted by spectral fitting. For spectral fitting, the absorption spectra were plotted on a wavenumber ($cm^{-1}$) scale. The wavenumber values are proportional to the photon energy of the light, which facilitates comparison of diagnostic features such as HWHM (half width at half maximum) across the entire spectrum. For colour calculation, the fitted spectra were recalculated to a wavelength (nm) scale.

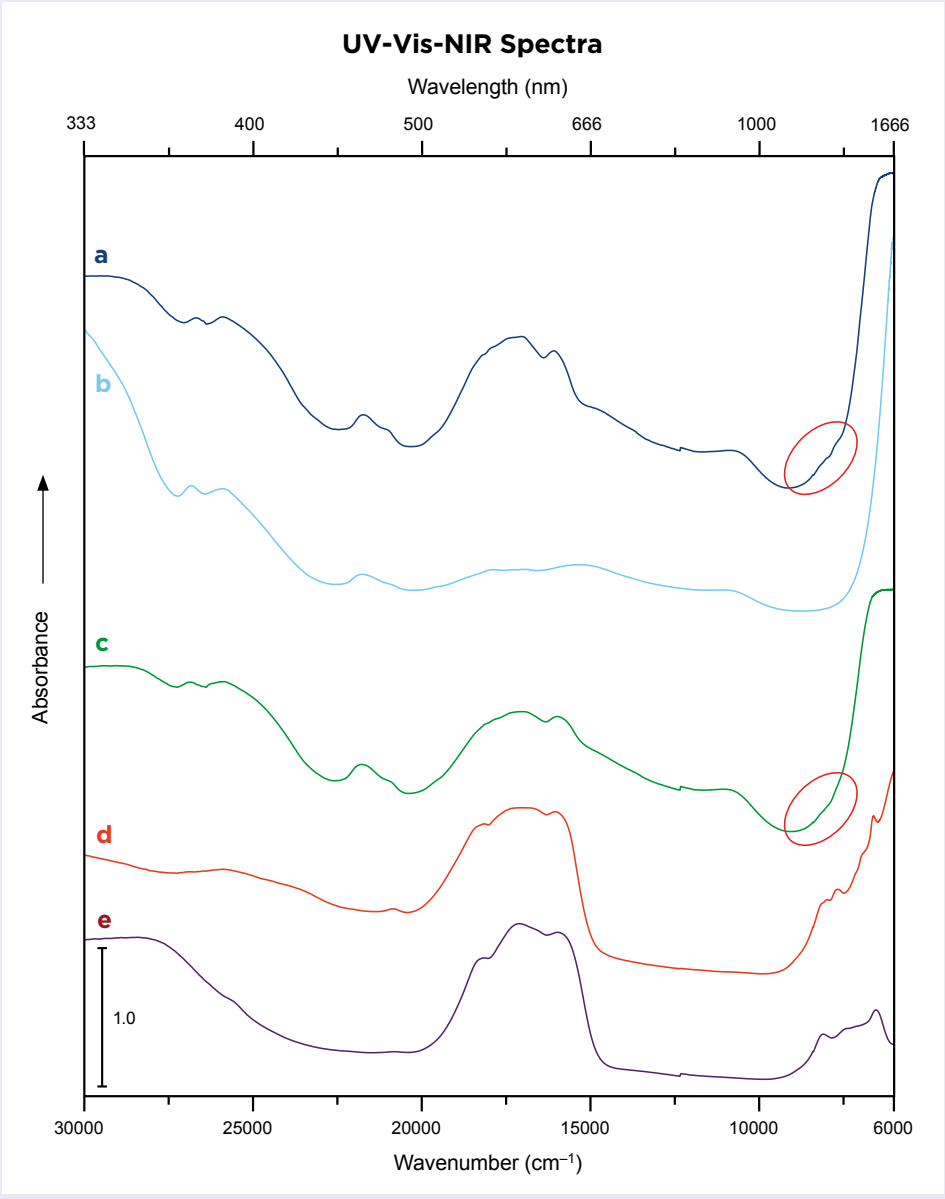


**Figure 3:** Representative UV-Vis-NIR absorption spectra are shown for: (**a**) blue Co- and Fe-bearing Nigerian gahnite, (**b**) Fe-bearing blue spinel, (**c**) Fe- and Co-bearing blue spinel from Sri Lanka, (**d**) blue spinel from Vietnam coloured predominantly by Co and minor amounts of Fe, and (**e**) blue flux-grown synthetic spinel coloured only by Co. Note the strong $Co^{2+}$ bands visible in some spectra (d and e) between 1100 and 1550 nm (9000 and 6500 $cm^{-1}$), which are also visible as weaker bands in other spectra (a and c), as indicated by the red ellipses. See Table II for a full list of band positions and attributions; the tiny feature at 810 nm seen in some of the spectra is an artefact due to a detector change. The spectra are shifted vertically for clarity.

**Development of the $Co^{2+}$ Model.** To develop the $Co^{2+}$ model, we used the blue flux-grown synthetic spinel coloured by $Co^{2+}$ (Figure 2), without a significant influence of Fe in the visible-range absorption spectrum. Chemical analysis of this sample identified it as almost pure spinel, with 72.43 wt.% $Al_2O_3$ and 26.96 wt.% MgO, as well as 0.11 wt.% FeO and 0.05 wt.% CoO. Both Zn and Mn were below detection limit.

After modelling the background (Figure 4a), the residual spectrum was fitted with 12 Gaussian curves (Figure 4b). In the visible range, three bands from 18,314 to 15,816 $cm^{-1}$ (546–632 nm) are described in the literature for $Co^{2+}$ (see Table II). Due to their asymmetry, however, for each of these three bands we used two Gaussian curves to describe them with the MagicPlot software (which only allows symmetrical Gaussian curves). The bands in the NIR region are strongly present in the absorption spectrum of the synthetic spinel (Figure 3e) and are seen as shoulders in the absorption spectra of the natural Co-bearing gahnites and spinels (Figure 3a, c, d). These NIR bands were also fitted using a total of six Gaussian curves, and Table III shows the band positions, HWHMs, amplitudes and areas calculated for these curves.

To develop the $Co^{2+}$ model, the band positions and HWHMs were fixed, and then all 12 Gaussian curves were joined together by setting the area of the curve for the '$Co^{2+}$_1' band in Table III to a factor of 1, and expressing the area of the other 11 bands as multiples of that factor. When using this model, the described parameters (band positions and HWHMs) must be fixed, and then the

**Table II:** Maxima of the major absorption bands in the UV-Vis-NIR spectra of blue gahnite from Nigeria (calculated by spectral fitting) compared to literature data.[a]

| Wavenumber ($cm^{-1}$)[b] | Fitted position ($cm^{-1}$) | Fitted position (nm) | Assignment |
|---|---|---|---|
| 26850–26640 | 26674 | 375 | $^{IV}Fe^{2+}$ |
| 25730–15989 | 25899 | 386 | $^{IV}Fe^{2+}$ |
| 24870–24675 | 24937 | 401 | $^{VI}Fe^{3+}$ |
| 21826–21656 | 21667 | 462 | $^{VI}Fe^{3+}$ |
| 21120–20833 | 20982 | 477 | $^{IV}Fe^{2+}$ |
| *18314–17943* | 18389 and 18236 ($Co^{2+}$)<br>17875 ($Fe^{2+}$) | 544 and 548 ($Co^{2+}$)<br>559 ($Fe^{2+}$) | $^{IV}Co^{2+}$<br>$^{IV}Fe^{2+}$ |
| *17059–16932* | 17375 and 16554 ($Co^{2+}$)<br>16740 and 16017 ($Fe^{2+}$) | 576 and 603 ($Co^{2+}$)<br>597 and 624 ($Fe^{2+}$) | $^{IV}Co^{2+}$<br>$^{IV}Fe^{2+}$ |
| *15911–15816* | 15872 and 15434 | 630 and 647 | $^{IV}Co^{2+}$ |
| 14945–14814 | 14559 | 687 | $^{VI}Fe^{2+}$–$^{VI}Fe^{3+}$-IVCT<br>$^{IV}Fe^{2+}$–$^{VI}Fe^{3+}$-ECP |
| 12778–12604 | 12863 | 777 | $^{VI}Fe^{2+}$<br>$^{IV}Fe^{2+}$–$^{VI}Fe^{3+}$-ECP |
| 10939–10629 | 10690 | 935 | $^{VI}Fe^{2+}$ |
| *8200*[c] | — | 1220[c] | Presumably $^{IV}Co^{2+}$ |
| *8000*[c] | — | 1250[c] | Presumably $^{IV}Co^{2+}$ |
| *7750*[c] | — | 1290[c] | Presumably $^{IV}Co^{2+}$ |

[a] Abbreviations: ECP = exchange-coupled pair, $^{IV}$ = tetrahedral coordination, IVCT = intervalence charge transfer, $^{VI}$ = octahedral coordination. Unless stated otherwise, wavenumber values are from D'Ippolito *et al.* (2015).

[b] Bands related to $Co^{2+}$ are shown in italics.

[c] These three bands have been documented by the authors only in Co-bearing spinel and gahnite, but they have not been mentioned in the literature (probably because they are on the flank of the strong $Fe^{2+}$-related system in the near-infrared region). The wavenumber and wavelength positions given here are the maxima of the corresponding bands visually observed in absorption spectra. See Table III for the fitted positions ($Co^{2+}$_6 to $Co^{2+}$_12).

software can just vary the amplitudes of the curves—and since their areas are joined, the ratios between them always remain the same. This deconvolution method has the advantage that one can focus on peaks which do not strongly overlap those of other chromophores.[1]

**Applying the $Co^{2+}$ Model to Nigerian Gahnite.** The influence of $Co^{2+}$ on the colouration of Nigerian gahnite was determined in three steps:

1. The background of the spectra of the Nigerian gahnite samples (e.g. Figure 5a) was modelled (see Figure 5b). The background system is a combination of the OMCT bands, the spin-allowed transition of $Fe^{2+}$ and minor reflections at the surface of the samples.

2. The $Co^{2+}$ model obtained from the synthetic spinel above was used to calculate the influence of $Co^{2+}$ on the colour of the Nigerian gahnite (Figure 5c). The

[1] The best fit can be achieved when using a model for each chromophore, developed with samples coloured solely by that chromophore. The flux-grown synthetic spinel used to develop the $Co^{2+}$ model is structurally different from gahnite, so slightly different band positions, HWHMs and symmetry would be expected when preparing such a model using gahnite coloured solely by $Co^{2+}$ (which, to the authors' knowledge, does not exist in either natural or synthetic form). Work is in progress to prepare models for $Fe^{2+}$ and $Fe^{3+}$ in spinel.

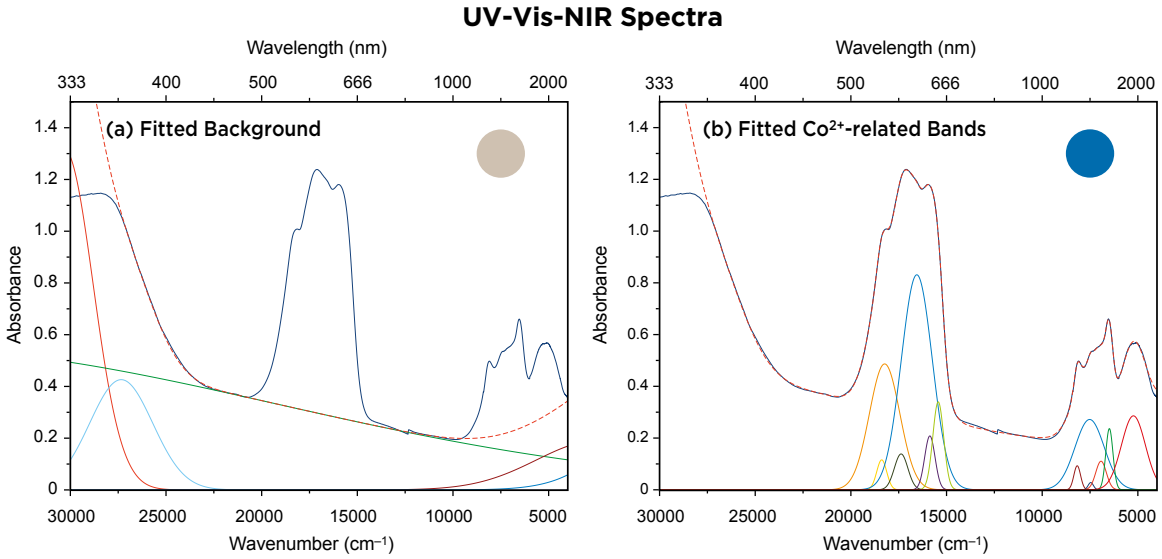


**Figure 4:** The absorption spectrum of a blue flux-grown synthetic spinel coloured only by Co was deconvoluted mathematically by spectral fitting, showing (**a**) the background band system and (**b**) the fitted $Co^{2+}$-related bands. These latter bands were used to prepare a model in order to calculate the influence of $Co^{2+}$ on the colour of Nigerian gahnite. The colour circles depict the corresponding colour calculated from the fitted spectrum (dashed red line), and the deconvoluted spectral curves are shown at the bottom on the x-axis.

intensity of this band system was evaluated using the Co bands between 9000 and 6500 $cm^{-1}$ (1100–1550 nm), since these bands are not strongly overlapped by Fe bands.

3. The residual component was spectrally fitted to demonstrate the influence of the Fe-related bands (see Figure 5d and Table IV). This is a combination of spin-allowed and spin-forbidden transitions, mainly of

**Table III:** Parameters used to develop the model for demonstrating the influence of $Co^{2+}$ on the colour of Nigerian gahnite.*

| Band | Position ($cm^{-1}$) | HWHM ($cm^{-1}$) | Amplitude | Area | Factor |
|---|---|---|---|---|---|
| $Co^{2+}$_1 | 18388.79 | 306.84 | 0.12 | 75.58 | 1.00 |
| $Co^{2+}$_2 | 18235.54 | 936.02 | 0.49 | 969.54 | 12.83 |
| $Co^{2+}$_3 | 17375.02 | 414.89 | 0.14 | 122.36 | 1.62 |
| $Co^{2+}$_4 | 16553.93 | 953.13 | 0.83 | 1686.35 | 22.31 |
| $Co^{2+}$_5 | 15872.28 | 318.79 | 0.21 | 141.30 | 1.87 |
| $Co^{2+}$_6 | 15434.31 | 333.73 | 0.34 | 241.54 | 3.20 |
| $Co^{2+}$_7 | 8169.78 | 206.81 | 0.09 | 40.87 | 0.54 |
| $Co^{2+}$_8 | 7520.48 | 899.86 | 0.27 | 520.81 | 6.89 |
| $Co^{2+}$_9 | 7461.57 | 162.21 | 0.03 | 9.68 | 0.13 |
| $Co^{2+}$_10 | 6924.62 | 325.18 | 0.11 | 76.50 | 1.01 |
| $Co^{2+}$_11 | 6489.05 | 220.21 | 0.24 | 110.93 | 1.47 |
| $Co^{2+}$_12 | 5231.87 | 735.51 | 0.29 | 447.62 | 5.92 |

* Each value is rounded to two decimals. Position and HWHM values must be fixed to use the model.

$Fe^{2+}$ and minor $Fe^{3+}$. Both, but especially $Fe^{3+}$, have a strong influence on the OMCT bands. This influence was included in the 'background system' in step 1.

Based on the results obtained with the deconvolution method described above, both Fe and Co have a strong influence on the colour of the blue Nigerian gahnite. The colour circles calculated from the spectral fitting (see Figure 5), however, demonstrate that the background system and the Fe-related bands mainly influence tone, whereas the blue hue is predominantly produced by $Co^{2+}$, despite its low concentration (only 0.02–0.03 wt.% CoO).

## HEAT TREATMENT

Generally, gahnites with a higher Fe content show green colouration due to the stronger OMCT band system towards the UV region (Taran *et al.* 2005), while those containing lower Fe content and additionally with $Co^{2+}$ show blue-green to blue colours (Fregola *et al.* 2014). This, however, is not consistent with the description given by Jackson (1982), who mentioned a colour modification from blue to green by heat treatment, since heating does not change Fe content.

To investigate this further, heat treatment experiments were performed on two of the rough Nigerian

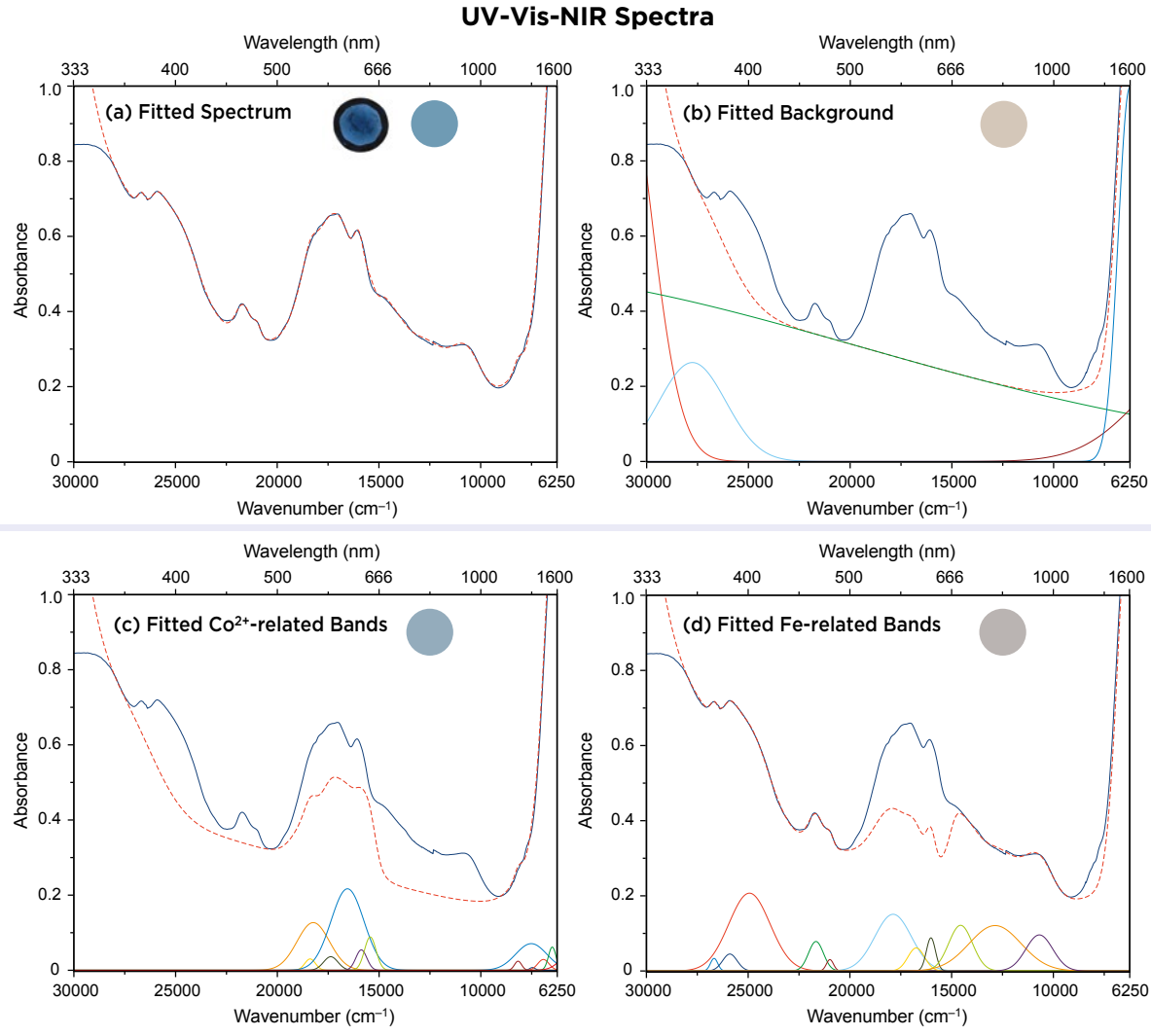


**Figure 5:** The absorption spectrum of a blue Nigerian gahnite was deconvoluted by spectral fitting. Shown here are (**a**) the fitted spectrum, (**b**) the background band system, (**c**) the influence of the Co bands and (**d**) the calculated residual influence of Fe; the deconvoluted spectral curves are shown on the x-axis (b–d). For each part (a–d), the colour circle shows the corresponding colour calculated from the fitted spectrum (dashed red line). Since these colours are typically calculated from transmission spectra, the photo of the blue gahnite sample (see spectrum a) is also taken with transmitted light (photo by T. Stephan of a 6-mm-diameter stone). Despite its low concentration, Co has the strongest influence on colour.

**Table IV:** Parameters obtained in this study for the Fe-related bands in blue gahnite from Nigeria.*

| Band | Position ($cm^{-1}$) | HWHM ($cm^{-1}$) | Amplitude | Area |
|---|---|---|---|---|
| $Fe^{2+}$_1 | 26673.56 | 211.04 | 0.03 | 15.02 |
| $Fe^{2+}$_2 | 25898.92 | 421.14 | 0.05 | 40.40 |
| $Fe^{3+}$_1 | 24937.46 | 1191.89 | 0.21 | 525.42 |
| $Fe^{3+}$_2 | 21667.03 | 430.37 | 0.08 | 71.86 |
| $Fe^{2+}$_3 | 20981.55 | 205.54 | 0.03 | 13.24 |
| $Fe^{2+}$_4 | 17875.05 | 1057.03 | 0.15 | 339.62 |
| $Fe^{2+}$_5 | 16740.08 | 480.93 | 0.06 | 62.80 |
| $Fe^{2+}$_6 | 16016.78 | 263.72 | 0.09 | 49.50 |
| $Fe^{2+}/Fe^{3+}$-IVCT_1 | 14559.16 | 688.24 | 0.12 | 178.12 |
| $Fe^{2+}/Fe^{3+}$-IVCT_2 | 12863.19 | 1498.85 | 0.12 | 385.67 |
| $Fe^{2+}$_7 | 10689.95 | 781.55 | 0.10 | 159.66 |

* These have not been fitted with respective models for the influence of iron on gahnite colouration, but are the mathematical best description of the residual spectral component after applying the $Co^{2+}$ model.

gahnite samples. After heating at 1000°C they became darker greyish blue with a slightly greenish hue, and after heating at 1400°C they became dark bluish green. The corresponding absorption spectra are shown in Figure 6.

D'Ippolito *et al.* (2013) mentioned that the colour of gahnite is highly sensitive to variations in the oxidation state of Fe. In the spectra shown in Figure 6, with increasing temperature there is a strong increase in the intensity of the band at 21,667 $cm^{-1}$ (462 nm) assigned to spin-forbidden $Fe^{3+}$ transitions. The shoulder at 24,937 $cm^{-1}$ (401 nm), also assigned to $Fe^{3+}$, increased in intensity as well, but is hidden by the more intense absorption edge after heat treatment. Most important is the stronger overall absorption in the blue-to-violet range, which shifts the transmission window towards the green spectral region. For heating of corundum, this is mainly explained by the formation of defect centres (trapped holes involving $Mg^{2+}$ and $Fe^{3+}$; e.g. Emmett & Douthit 1993, 2017). The increasing intensities of the spin-forbidden $Fe^{3+}$ transitions, however, indicate that $Fe^{2+}$ is partly oxidised to $Fe^{3+}$. Based on this, we infer that the greater absorption in the blue-to-violet range is due to a stronger $O^{2-} \rightarrow Fe^{3+}$ charge transfer. Additional experiments are needed to prove whether the colour modification is reversible in a reducing atmosphere.

To the authors' knowledge, the heat treatment of blue Nigerian gahnite in oxidising conditions is not of commercial interest to the gem market, since the colours produced are not of an attractive hue and/or are generally over dark.

## CONCLUSION

The availability of blue Co- and Fe-bearing gahnites from Nigeria is an interesting addition to the trade and for gem collectors. Their deep blue colour is due to a combination of $Co^{2+}$ and $Fe^{2+}$, as well as minor $Fe^{3+}$. The optical absorption spectrum is mainly dominated by the $Fe^{2+}$ band system, but—despite its low concentration—$Co^{2+}$ is mainly responsible for the blue colour.

Heating to 1000°C and 1400°C in oxidising conditions produces darker greyish-greenish blue to dark bluish green colours, caused mainly by more intense $O^{2-} \rightarrow Fe^{3+}$ charge-transfer bands, due to the oxidation of $Fe^{2+}$ to $Fe^{3+}$. Consequently, the green colour does not depend on the Fe content, as previously described, but on the amount of $Fe^{3+}$, as reported by D'Ippolito *et al.* (2013).

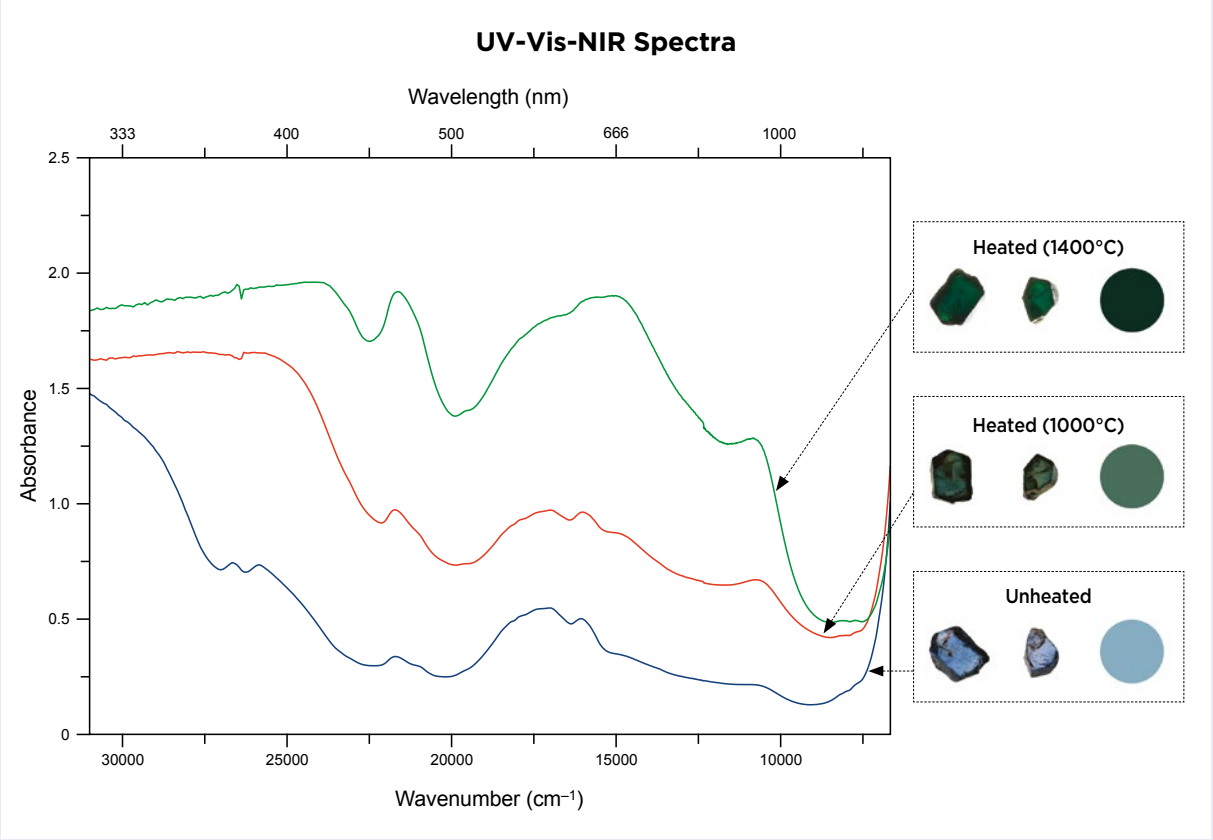


**Figure 6:** These absorption spectra show the effects of heating blue Nigerian gahnite. The spectra are from the smaller sample pictured (approximately 3 mm thick), while the images of the larger sample provide another example of the colour modification due to heating. The colour circles show the corresponding colour calculated from each spectrum. Note the shift of the absorption edge towards longer wavelengths with heating. The drop in absorbance below about 400 nm for the heated samples is an instrumental artefact. Photos by T. Stephan; samples are 5.3 and 4.9 mm long.

## REFERENCES


Bank, H. 1975. Durchsichtiger grüner Gahnit aus Brasilien. *Zeitschrift der Deutschen Gemmologischen Gesellschaft*, **24**, 90–91.

Bank, H. 1983. Über Gahnospinelle und Gahnite. *Zeitschrift der Deutschen Gemmologischen Gesellschaft*, **32**(2–3), 141–142.

Boehm, E. & Laurs, B.M. 2018. Gem Notes: Blue gahnite from Nigeria. *Journal of Gemmology*, **36**(2), 96–97.

Bosi, F., Biagioni, C. & Pasero, M. 2019. Nomenclature and classification of the spinel supergroup. *European Journal of Mineralogy*, **31**(1), 183–192, https://doi.org/10.1127/ejm/2019/0031-2788.

Bowles, J.F.W., Howie, R.A., Vaughan, D.J. & Zussman, J. 2011. *Rock-Forming Minerals. Volume 5A. Non-Silicates: Oxides, Hydroxides and Sulphides*, 2nd edn. The Geological Society, London, xii + 920 pp. (see pp. 329–356).

Chauviré, B., Rondeau, B., Fritsch, E., Ressigeac, P. & Devidal, J.-L. 2015. Blue spinel from the Luc Yen district of Vietnam. *Gems & Gemology*, **51**(1), 2–17, https://doi.org/10.5741/gems.51.1.2.

D'Ippolito, V., Andreozzi, G.B., Bosi, F., Hålenius, U., Mantovani, L., Bersani, D. & Fregola, R.A. 2013. Crystallographic and spectroscopic characterization of a natural Zn-rich spinel approaching the endmember gahnite ($ZnAl_2O_4$) composition. *Mineralogical Magazine*, **77**(7), 2941–2953, https://doi.org/10.1180/minmag.2013.077.7.05.

D'Ippolito, V., Andreozzi, G.B., Hålenius, U., Skogby, H., Hametner, K. & Günther, D. 2015. Color mechanisms in spinel: Cobalt and iron interplay for the blue color. *Physics and Chemistry of Minerals*, **42**(6), 431–439, https://doi.org/10.1007/s00269-015-0734-0.

Emmett, J.L. & Douthit, T.R. 1993. Heat treating the sapphires of Rock Creek, Montana. *Gems & Gemology*, **29**(4), 250–272, https://doi.org/10.5741/gems.29.4.250.

Emmett, J.L. & Douthit, T.R. 2017. Treatments. *In*: Hughes, R., Manorotkul, W. & Hughes, E.B. (eds) *Ruby & Sapphire: A Gemologist's Guide*. RWH Publishing/Lotus Publishing, Bangkok, Thailand, 197–247.

Ferracutti, G.R., Gargiulo, M.F., Ganuza, M.L., Bjerg, E.A. & Castro, S.M. 2015. Determination of the spinel group end-members based on electron microprobe analyses. *Mineralogy and Petrology*, **109**(2), 153–160, https://doi.org/10.1007/s00710-014-0363-1.

Fregola, R.A., Skogby, H., Bosi, F., D'Ippolito, V., Andreozzi, G.B. & Hålenius, U. 2014. Optical absorption spectroscopy study of the causes for color variations in natural Fe-bearing gahnite: Insights from iron valency and site distribution data. *American Mineralogist*, **99**(11–12), 2187–2195, https://doi.org/10.2138/am-2014-4962.

Hain, M. & Sun, Z. 2019. Gem News International: Blue gahnite from Nigeria. *Gems & Gemology*, **55**(3), 434–436.

Jackson, B. 1982. Gem quality gahnite from Nigeria. *Journal of Gemmology*, **18**(4), 265–276, https://doi.org/10.15506/JoG.1982.18.4.265.

Jacobson, R.R.E. & Webb, J.S. 1946. *The Pegmatites of Central Nigeria*. Geological Survey of Nigeria Bulletin No. 17, Colchester, 61 pp.

Palke, A.C. & Sun, Z. 2018. What is cobalt spinel? Unraveling the causes of color in blue spinels. *Gems & Gemology*, **54**(3), 262.

Schmetzer, K., Haxel, C. & Amthauer, G. 1989. Colour of natural spinels, gahnospinels and gahnites. *Neues Jahrbuch für Mineralogie, Abhandlungen*, **160**(2), 159–180.

Schollenbruch, K., Blauwet, D., Malsy, A.-K. & Bosshard, V. 2021. Cobalt-blue spinel from northern Pakistan. *Journal of Gemmology*, **37**(7), 726–737, https://doi.org/10.15506/JoG.2021.37.7.726.

Shigley, J.E. & Stockton, C.M. 1984. 'Cobalt-blue' gem spinels. *Gems & Gemology*, **20**(1), 34–41, https://doi.org/10.5741/gems.20.1.34.

Taran, M.N., Koch-Müller, M. & Langer, K. 2005. Electronic absorption spectroscopy of natural ($Fe^{2+}$, $Fe^{3+}$)-bearing spinels of spinel s.s.-hercynite and gahnite-hercynite solid solutions at different temperatures and high-pressures. *Physics and Chemistry of Minerals*, **32**(3), 175–188, https://doi.org/10.1007/s00269-005-0461-z.

Taran, M.N., Koch-Muller, M. & Feenstra, A. 2009. Optical spectroscopic study of tetrahedrally coordinated $Co^{2+}$ in natural spinel and staurolite at different temperatures and pressures. *American Mineralogist*, **94**(11–12), 1647–1652, https://doi.org/10.2138/am.2009.3247.

Winchell, A.N. & Winchell, H. 1967. *Elements of Optical Mineralogy: An Introduction to Microscopic Petrography*, 4th edn. John Wiley & Sons, New York, New York, USA, 551 pp.

## The Authors

**Dr Tom Stephan and Dr Ulrich Henn FGA**
German Gemmological Association, Prof.-Schlossmacher-Str. 1, D-55743 Idar-Oberstein, Germany. E-mail: t.stephan@dgemg.com

**Stefan Müller**
German Foundation for Gemstone Research – DSEF German Gem Lab, Prof.-Schlossmacher-Str. 1, D-55743 Idar-Oberstein, Germany

## Acknowledgements

Sample material was kindly loaned and partly donated by the companies Gemstore24 (Herrsching am Ammersee, Germany) and Arnoldi International (Idar-Oberstein, Germany). The chemical analyses were carried out by Dr Stephan Buhre of the Petrology Working Group at the Institute of Geosciences, Johannes Gutenberg University Mainz, Germany. We further thank the anonymous reviewers for many helpful comments.

# Gem-A Notices

## MESSAGE FROM GEM-A CEO ALAN HART

We continue to live in challenging times, but adjusting to the world in the time of COVID, rising costs and current global events has taught us that it is important to stay resilient and adaptable in the face of change. 'Good' might be good enough for some, but most of us want more than that. We strive to be better than good, and we want to do greatness! I, like all Gem-A Members, have been passionate about the mission and vision of Gem-A being a world-class provider of Gem-A education and Membership services. To that end, Gem-A staff have been working hard to provide the best learning experience to our global students. In order to do this, we have shifted gears to return to face-to-face teaching where possible, enhance our Online and Distance Learning (ODL) programmes through the introduction of tutor-led videos, and continue to support our Accredited Teaching Centres worldwide.

I am proud to confirm that we have successfully launched *GemIntro*, an entry-level, online-only course that educates those starting or progressing their careers, while also satisfying the curiosity of gem enthusiasts. The course was created to offer an introduction to gemstones, incorporating 11 lessons, more than 50 videos and 30 hours of self-guided study (see next page for further information). I believe *GemIntro* has the power to increase confidence, expand knowledge and foster a whole new appreciation for gemstones among those who are new to the study.

Looking further ahead, we will return to an in-person, traditional Gem-A conference this autumn, held as a one-day event on 6 November. Registrations for the conference will open soon and I encourage you to save the date. I personally look forward to offering a warm welcome to many of our Members and associates whom we have not had the opportunity to see for some time.

I would like to extend my sincerest thanks once again for your ongoing support. I hope you enjoy this issue of *The Journal*, and I look forward to seeing many of you again in the near future.

## UKRAINE MESSAGE

It is with great sadness that we watch the events unfolding in Ukraine. Our hearts go out to those affected by the war in Ukraine. We stand for peace, and we join organisations worldwide in calling for an end to this senseless war and ongoing suffering of individuals and families. Our global Membership, students, staff and partners stand united in these uncertain times as we continue to provide world-class gemmology education and Membership services to support the gem and jewellery trade. Naturally, we understand there can be a sense of helplessness seeing this tragedy unfold and a wish to aid those who are suffering. Gem-A feels that internationally respected charities such as the Red Cross are well placed to act, and have the expertise and experience to deliver much-needed aid. Accordingly, trustees and staff have already made personal donations to the British Red Cross Humanitarian Appeal (BRCHA) in excess of £1,000. The UK tax system allows BRCHA to claim an additional 25% on top of this donation. This reclaim can only be made on personal donations, not on corporate or pooled donations. We encourage Gem-A Members to donate to BRCHA or similar charities and, if possible, use the Gift Aid facility.


## *GEMINTRO* NOW AVAILABLE FOR REGISTRATIONS

*GemIntro* is the first entry-level course offered by Gem-A which is available entirely online. Candidates can go at their own pace and discover the basics of gemmology from home. Participants will work towards an accredited Ofqual Level 2 qualification, accompanied by a formal Gem-A certificate. This interactive and informative course is designed for those who are already working in the gem and jewellery trade, and want to develop their knowledge further, as well as for gem enthusiasts who are curious about delving deeper into gemmology. Those wishing to explore the many career opportunities associated with the study and application of gemmology may also find the course effective. Registrations are now being accepted, and students will have access to course materials for six months from the registration date. *GemIntro* is priced at £220, and no previous qualifications or experience are required. More information can be found at https://gemintro.gem-a.com. To discuss becoming a *GemIntro* reseller or for bulk licensing packages, email education@gem-a.com.

## MEMBERSHIP EVENTS

For our Members, we have lined up some fantastic in-person sessions and discussions for 2022. Justin Prim successfully delivered a workshop on 'The Science of Gemcutting' at our London headquarters on Friday 1 April. This popular in-person course covered advanced optics, software design and design aesthetics, along with an extensive exploration of colour and how the cutter can manipulate and master it through cut design. Justin also demonstrated the use of CAD software Gem Cut Studio to modify the design of a pre-existing stone to prepare it for an optimal recut.

A Gem Central event took place on Thursday 19 May at our London headquarters featuring Rui Galopim de Carvalho, who focused on CITES (Convention on International Trade of Endangered Species of Flora and Fauna) regarding biogenic gems. On Wednesday 29 June, Gem-A will host another Gem Central event delivered by former Gem-A tutor Beth West, who will talk about her experiences, in collaboration with Diamonds for Peace, in training local diamond miners in the western region of Liberia. Gem-A was one of the sponsors of this initiative to provide basic toolkits to diamond mining communities.


Gem-A will be making recorded segments of many in-person events available to our Members this year so that, even if you cannot make it to London, you can still benefit from the knowledge conveyed by our esteemed speakers.

## OBITUARIES

### Dr Charles Edward Samuel (Charley) Arps

1 October 1935–19 March 2022

Charles Arps was a versatile geologist with a wide range of interests. In 1970 he joined what was then the National Museum of Geology and Mineralogy (Rijksmuseum van Geologie en Mineralogie) in Leiden, the Netherlands, as a research assistant specialising in rock and mineral associations, mineral paragenesis and gemmology. Immediately upon his appointment, his long collaboration with Dr Pieter C. Zwaan began in the museum-based Netherlands Gem Laboratory. They were given a wide range of assignments by companies and individuals, and a major and impactful case took place in 1987—when Gerrit-Jan Heijn (part of a leading entrepreneurial family in the Netherlands) was kidnapped. Because diamonds and gems were part of the ransom demanded, Charley and Pieter worked closely with the police, the judiciary and diamond companies.

Charley's fondness for geological fieldwork and for imparting his knowledge to the widest possible audience

led to various museum exhibitions on geology, especially on volcanoes and meteorites. As for gem research, he wrote books about pearls and diamonds and was co-author of the book *Elementary Gemmology* (1996). In gemmological journals he wrote about gems from Sri Lanka, opal from Indonesia and emerald from Africa. He was also an associate editor of *The Journal* for many years, working primarily with editor Roger Harding and production editor Mary Burland.

The National Museum of Geology and Mineralogy merged in 1984 with the National Museum of Natural History, which became known as 'Naturalis' when the new building opened in 1998. Charley was closely involved with this development and was active for a long time in the management of the museum. In addition to his aforementioned work on exhibitions, he tirelessly stressed the significance of the Netherlands Gem Laboratory, geological research and good management of the geological collections in the broadest sense.

For many years, Charley was an active member of the International Mineralogical Association's (IMA) Commission of New Minerals and Mineral Names. In 1997, together with Dr Bernard Leake and many other mineralogists, he co-wrote the IMA subcommittee report 'Nomenclature of amphiboles', a standard work on the naming rules for amphiboles, which was only revised in 2012.

Within the framework of the Netherlands Gem Laboratory, Charley was a delegate of the International Gemmological Conference for a long time. He was also involved in discussions with The World Jewellery Confederation (CIBJO).

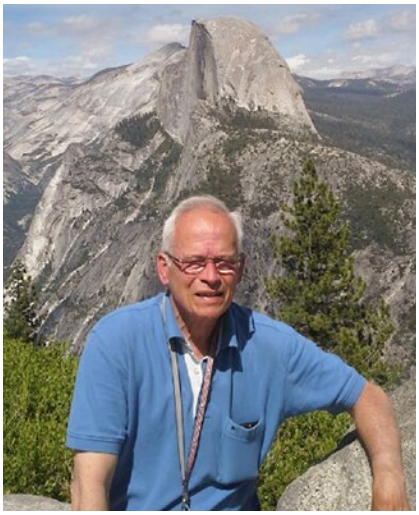

Dr Charles Arps visiting Yosemite National Park, California, USA.

With his charm and humour, Charley was very pleasant to work with. He was a living memory of the collections for his colleagues in the museum, and he was always accessible, responding quickly as a source of information. He was also very pleasant company for his many colleagues, nationally and internationally, and he had many good friends. Wherever he was, a geological map of the area in question was always brought out, and he gave a detailed explanation of the geology or insight into the special local wines or cuisine.

We hold beautiful memories of a unique colleague.

**Dr J. C. (Hanco) Zwaan FGA**
Netherlands Gem Laboratory and
Naturalis Biodiversity Center
Leiden, The Netherlands

## Dr Jan Kanis

1927–2021

Jan Kanis was born on 8 December 1927 in Kampen, the Netherlands. After the Second World War, between 1947 and 1956, he completed his geological studies at Leiden University with a dissertation focused on the Asturias region of Spain. Titled *Geology of the eastern zone of the Sierra del Brezo (Palencia-Spain)*, it was sponsored by Instituto de Investigaciones Geológicas 'Lucas Mallada' in Madrid. Together with Dr Robert Wagner, a prominent paleo-botanist and specialist in carboniferous stratigraphy, he was one of the initial dozen geologists from Leiden who did geological fieldwork in Asturias and Cantabria, Spain.

After obtaining his PhD, Jan gained vast experience in mining during a three-year contract in Tanzania with the New African Mica Company (a branch of Otto Gerdau Company, based in New York, USA). He became a local managing director and opened a new branch in Rhodesia (now Zimbabwe). The company mined and exported mica, beryl and U-bearing minerals such as uraninite.

In 1959, Jan established himself as a consulting geologist in Rhodesia. He was also an active partner in opening up graphite deposits in Rhodesia and formed the Rho-German Graphite Company, together with Graphitwerk Kropfmühl AG, Munich. From 1967 to 1970 he was also a partner in the development of the Gwaai River copper mine, later sold to Messina Transvaal Co. of South Africa. Together with seven partners and the Munich-based firm Agrob as consultants, he established Cerama Industries (Pvt) Ltd, a ceramic tile factory that

used local raw materials in Rhodesia. This enterprise lasted until about 1972–1973. He then established and owned 50% of Natural Dimension Stones (Pvt) Ltd, a company that quarried 'black granite' for export to Japan. However, quarrying stopped in 1975 due to the closure of Beira harbour in Mozambique, at a time when there was no other export route due to sanctions. Meanwhile, Jan also exploited four aquamarine and tourmaline deposits, operated a gem-cutting workshop with 20 employees, and dealt internationally in rough and cut gemstones. Dr John Saul recalls that the first cut stone he ever purchased was from Jan, an approximately 20 ct red tourmaline (J. Saul, pers. comm. 2022).

In 1976, Jan moved to South Africa because of the economic and political problems in Zimbabwe. He relocated his gem-cutting workshop to Johannesburg and continued dealing in gems. Later, in 1985, he sold all his business interests in South Africa and returned to Europe, settling in Veitsrodt, near Idar-Oberstein, Germany. During this time, in 1985–1987, he became a director and founding member of the International Colored Gemstone Association (ICA).

Jan then concentrated on his geological consulting activities, in particular the evaluation and exploitation of gem occurrences. It was during this time that he became one of the pioneers in field gemmology. He became internationally known as a specialist in the exploration and mining of beryl and emerald occurrences, as well as gem-bearing pegmatites in general. For the United Nations Development Programme he completed a gem exploration mission in Orissa, India, between 1991 and 1995. The goal was to assess how to empower local people to improve their livelihoods by identifying potential mining sites for the commercial production of various stones, including ruby, garnet, chrysoberyl and beryl (*Nahe Zeitung*, No. 226, 28 September 1994).

Jan was a consultant for the Sandawana emerald mines in Zimbabwe (1994–1999) and also advised the Netherlands Management Corporation Programme on gem projects in Namibia and Tanzania. In addition, he worked as a consultant for a private company in Brazil involved with mining tourmaline and aquamarine, and was connected with the new Piteiras emerald mine of Seahawk Minerals Ltd, near the Belmont emerald mine in the Nova Era region in Minas Gerais. In 2005 and 2008 Jan conducted two studies for the Zambian government, on the establishment of a gemstone exchange (commissioned by the European Union) and on setting up a new gemmological institute (commissioned by the World Bank). Around 2008–2014 he did consulting work for the MVV emerald mine near Caiçara do Rio do Vento in Rio Grande do Norte, Brazil.

Throughout this time, Jan was also involved with other consulting projects in Zambia (emeralds), Kenya (rubies), Malawi (sapphires), Nigeria (sapphires), Democratic Republic of the Congo (emeralds) and China (rubies).

During his career, Jan authored and co-authored many articles published in *The Journal of Gemmology* and *Gems & Gemology*. Some of the topics included hessonite occurrences in Orissa (1994), emerald and green beryl from central Nigeria (1996), sapphires from the Andranondambo region in Madagascar (1996), emeralds from the Machingwe (1991) and Sandawana (1997) mines in Zimbabwe, sapphires from Antsiranana in northern Madagascar (2000) and emeralds from the Fazenda Bonfim region in Rio Grande do Norte (2012). He contributed to the book series *Gemmologia Europa* (edited by Dr Margherita Superchi and published by CISGEM, Milan, Italy) on gems from Mozambique, Zambia, Zimbabwe and southern Africa (1988), on the tourmaline group (1990) and on emeralds from Africa (1999). In *Lapis* magazine he published on the exploration methods used to find the new emerald deposit at Piteiras, and in *extraLapis* he authored an article on golden beryl from the Baboon Hill mine (Zimbabwe) and also contributed to a volume titled *Emeralds of the World*.

In addition to ICA, Jan was a member of the Gemmological Association of Great Britain and the German Gemmological Society, an honorary member of the Gemmological Association of All Japan, and an executive committee member and honorary member (since 1968) of the International Gemmological Conference, originally founded by Prof. Dr Edward Gübelin.

Jan's fluency in Dutch, Afrikaans, English, German and Spanish, along with a good working knowledge of Portuguese and French, helped him a great deal in his career, and was consistent with his cosmopolitan nature and life.

Dr Jan Kanis, at 82 years old, after a long day at an emerald occurrence in the Fazenda Bonfim region, Rio Grande do Norte, Brazil. Photo by J. C. Zwaan, 2009.

In 2014, after a long career in gems and gem mining, Jan moved from Germany to Portugal. He told me with great pleasure that, from that time on, he was no longer a geologist, but turned into a farmer. With his wife Luisa, he took care of the land on their inherited farm.

Jan had just turned 94 years old when he passed away on 25 December 2021. The opening of his thesis included this quote from Pär Lagerkvest's *Dvärgen*: 'The man for whom a rock is something valuable, will be surrounded by riches wherever he goes'. This provides a nice summation of Jan's life, as does the following quote taken from the notice of his passing away: 'The spirit of things resides in those who contemplate them'. Jan was a true professional and a good friend to many in the gem community.

**Dr J. C. (Hanco) Zwaan FGA**
Netherlands Gem Laboratory and
Naturalis Biodiversity Center
Leiden, The Netherlands

## Dr Rolf Tatje
1956–2022

Dr Rolf Tatje was a well-known German gem and mineral collector and gemmological reviewer. He passed away on 15 February 2022.

Rolf was born in 1956 in Oldenburg, Germany. In 1976, he began his studies of the English and French languages at the University of Bochum and the University of Duisburg, and he graduated as a linguist with a Master of Arts degree in 1982. From 1983 until 2000, he worked as an assistant professor at universities in Duisburg, Wuppertal and Bielefeld in Germany, as well as in Nimes, France. In July 1994, Rolf received his PhD *magna cum laude* at the University of Duisburg. His dissertation was titled *The technical terminological language of mineralogy: An analysis of French and German scientific literature*.

Since 2000, Rolf worked as a freelance translator. As a qualified lover of language, in addition to his excellent command of English and French, he had good knowledge of Italian, Spanish and Dutch, along with basic knowledge of Japanese.

Already as a boy, he searched for gems and minerals when visiting mining areas. He started collecting them and became a 'gem addict'. Besides assembling gem species from every mineral group, his passion was collecting coloured diamonds of natural origin. Mostly they were very small—about 0.04–0.12 ct—so that he could afford them, but they included some stunning stones. His collection spanned a palette of pinks/reds, greens and blues.

Throughout his life, Rolf didn't achieve much luxury because he spent most of his earnings on gems and books. He loved gemmological literature, and over a period of many years he was an enthusiastic book reviewer for *The Journal of Gemmology* and *Gems & Gemology*. He also wrote abstracts of various articles from the literature for the latter journal. In addition, he served as a guest reviewer of several articles published in *The Journal* that covered historical topics (especially diamonds).

For more than 20 years, Rolf was also a valuable contributor, researcher, advisor and translator for my own books on asterism.

Rolf's life was filled with passion for gems, minerals and books. The gemmological and gem collectors' world will miss him greatly. I miss Rolf as an important member of my book team, a fine communicator, an intellectual adviser and especially a good friend. Sometimes, after heavy discussions on gemmology, literature or life, Rolf would say, in a heavy northern German slang, '*So moak wee daat*' ('So, we are going to do it this way'). *Sic erat scriptum*.

**Martin P. Steinbach**
Steinbach – Gems with a Star
Idar-Oberstein, Germany

## ERRATUM

In Noel Deeks' obituary in the Notices section of *The Journal* (Vol. 38, No. 1, 2022, pp. 95–96), an editing error indicated that James Walker was an industrial machinery manufacturing company. James Walker should have been indicated as one of UK's leading high-street jewellers.

# Learning Opportunities

## CONFERENCES AND SEMINARS

**Prospectors & Developers Association of Canada (PDAC 2022) Conference**
28–29 June 2022
Online
https://www.pdac.ca
*Session of interest*: A Big Challenge in Diamond Mine Development: Diamond Price Estimation

**Goldschmidt2022**
10–15 July 2022
Honolulu, Hawaii, USA, and online
https://2022.goldschmidt.info
*Session of interest*: Gems and Gem Minerals as Precious Indicators of Diverse Earth Processes

**23rd General Meeting of the International Mineralogical Association (IMA 2022)**
18–22 July 2022
Lyon, France
https://www.ima2022.fr
*Sessions of interest*: (1) Haüy 200 Years On: What News in Gem Research? (2) Mineralogy and Gemology in Cultural Heritage; (3) New Insights into Diamond Mineralogy, Geochemistry and Petrology; (4) Gemstones from the Deep: A Celebration of the Career of George E. Harlow

**Hong Kong International Jewellery Show**
29 July–2 August 2022
Hong Kong
https://www.hktdc.com/event/hkjewellery/en/intelligence-hub
*Note*: Includes a seminar programme

**6th Mediterranean Gemmological & Jewellery Conference**
12–14 August 2022
Thessaloniki, Greece
https://gemconference.com
*Note*: Will include post-conference gem, mineral and mine tours to North Macedonia, Kosovo and Serbia.

**NAJA 58th Annual Mid-Year Education Conference**
13–14 August 2022
Online
https://najaappraisers.com/event/58th-annual-mid-year-education-conference-virtual

**Amberif Fall 2022 International Fair of Amber & Jewellery**
1–3 September 2022
Gdańsk, Poland
https://amberif.pl/en/o-targach/programme
*Note*: Includes a seminar programme

**23rd Federation for European Education in Gemmology (FEEG) Symposium**
3 September 2022
Paris, France
http://www.feeg-education.com/symposium

**32nd International Conference on Diamond and Carbon Materials**
4–8 September 2022
Lisbon, Portugal
https://www.elsevier.com/events/conferences/international-conference-on-diamond-and-carbon-materials

**Maine Pegmatite Workshop**
7–12 September 2022
Bethel, Maine, USA
http://www.maine-pegmatite-workshop.com

**19th Rendez-Vous Gemmologiques de Paris**
8 September 2022
Paris, France
https://www.afgems-paris.com/rdv-gemmologique

**JVA Registered Valuer Conference**
9–11 September 2022
Loughborough, Leicestershire
https://thejva.org/jewellery-watch-valuer-conference

**Vicenzaoro**
9–13 September 2022
Vicenza, Italy

https://www.vicenzaoro.com/en
*Note*: Includes a seminar programme

**85th Annual American Society of Appraisers (ASA) International Conference**
10–12 September 2022
Tampa, Florida, USA, and online
https://www.appraisers.org/asa-international-conference

**Jewellery & Gem World Hong Kong**
16–19 September 2022
Hong Kong
https://jgw.exhibitions.jewellerynet.com/specialevent
*Note*: Includes a seminar programme

**Geological Society of America Annual Meeting (GSA Connects 2022)**
9–12 October 2022
Denver, Colorado, USA, and online
https://community.geosociety.org/gsa2022/home
*Session of interest*: Gemological Research in the 21st Century—Gem Minerals and Localities

**Canadian Gemmological Association (CGA) Conference**
21–23 October 2022
Vancouver, British Columbia, Canada
https://canadiangemmological.com

**Gem-A Conference**
6 November 2022
London
https://gem-a.com/event/conference-2022

**Inhorgenta Munich**
24–27 February 2023
Munich, Germany
https://www.inhorgenta.com/en
*Note*: Includes a seminar programme

**37th International Gemmological Conference (IGC 2023)**
22–26 May 2023
Tokyo, Japan
https://www.igc-gemmology.org/igc-2023
*Note*: Includes pre- and post-conference field trips to jadeite deposits and a pearl farm.

## OTHER EDUCATIONAL OPPORTUNITIES

**Gem-A Workshops and Courses**
Gem-A, London and online
https://gem-a.com/education
https://gemintro.gem-a.com

**Gemstone Safari to Tanzania**
Dig for sapphires and garnets in the Umba Valley and then visit various deposits for ruby-in-zoisite, emerald, iolite, chrysoprase, scapolite, etc., with optional three-day gem-cutting class.

6–23 July 2022 and 11–28 January 2023
https://www.free-form.ch/tanzania/gemstonesafari.html

**Gem Legacy Adventures**
Rough gem buying, mine excursions and a visit to a gem faceting school in northern Tanzania and southern Kenya.

21–30 July 2022
https://gemlegacyadventures.com

1–7 August 2022
https://gem-a.com/east-africa-field-trip-2022

**Lectures with The Society of Jewellery Historians**
Society of Antiquaries of London, Burlington House
www.societyofjewelleryhistorians.ac.uk/current_lectures

- Karl Schmetzer—The Late 14th-Century Royal Crown of Blanche of Lancaster
  28 June 2022
- Maria Filomena Guerra—Fresh Scientific Insights in Ancient Egyptian Gold Technology
  27 September 2022
- Usha Balakrishnan—The Jewellery of the Nizam of Hyderabad
  22 November 2022
- Natasha Awais-Dean—Jewels Captured in Perpetuity: The Jewellery Book of Anne of Bavaria
  24 January 2023
- Vivian Watson—History of Hatton Garden
  28 March 2023
- Patrick Davison—Contemporary Maker Talking About His Own Work
  27 June 2023

# New Media

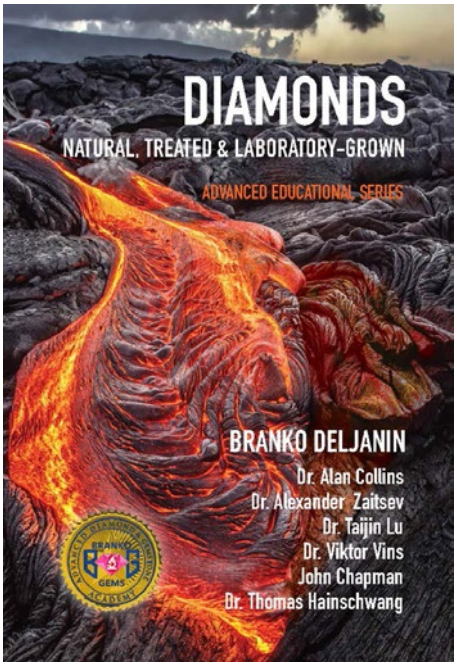


## Diamonds: Natural, Treated and Laboratory-Grown

**By Branko Deljanin with Alan Collins, Alexander Zaitsev, Taijin Lu, Viktor Vins, John Chapman and Thomas Hainschwang, 2021. Gemmological Research Industries Inc., Vancouver, British Columbia, Canada, www.brankogems.com/shop/books/diamonds-natural-treated-and-lab-grown, 193 pages, illus., ISBN 978-1777369224 hardcover or 978-1777369231 softcover. USD119.95 hardcover or USD79.95 softcover.**

This book is divided into three main parts. Section I covers the key spectroscopic features of natural, synthetic and treated diamonds. Section II includes the production of lab-grown diamonds in China and the colour treatments of natural and synthetic diamonds. Section III describes instrumentation for the testing and identification of diamonds.

Section I of the book—perhaps my favourite—consists of two parts, written by Drs Alan Collins and Alexander Zaitsev, who are two of the most prominent researchers on the characterisation and detection of defects and optical centres in diamond. Dr Collins' contribution, on defects in natural, synthetic and treated diamonds, is a delight to read. The language is clear, with easy-to-follow explanations of the main impurities and their complexes, and the ways to detect them using optical spectroscopic techniques. He breaks up the text into digestible, concise summaries of some of the most prominent defects in natural and synthetic diamonds. He also touches on the origins of colour in diamond and discusses how HPHT annealing plays a vital role in the conversion of nitrogen aggregates and optical centres that affect colouration.

Dr Zaitsev then provides a brief but very informative overview of optical spectroscopy techniques before delving deeper into the plethora of optical centres found in natural and synthetic diamonds. The effects of irradiation on colour treatments of diamond are introduced here, along with the identification of the prominent GR1 optical centre as a strong indicator of this type of treatment, as well as a multitude of others. This might be a little heavy going for the less technical gemmologist, but it sheds much light on the richness and complexity of this subject.

Section II also contains two very useful parts. The first, by Dr Taijin Lu of the National Gemstone Testing Centre in China, lists the current major Chinese producers of synthetic diamonds (mostly by HPHT methods). (A similar overview is given by the same author in the 3rd edition of another book co-authored by Branko Deljanin: *Laboratory-grown Diamonds*.) The capacity and scope of China's industrial and gem-quality synthetic diamond production, as reported here, is phenomenal and has seen a large amount of investment over the past decade. An interesting topic touched upon briefly is the threat of 'hybrid diamonds', in which a layer of CVD synthetic diamond is grown on a natural substrate, potentially evading detection.

In the second part of Section II, Dr Viktor Vins of Velman Ltd (Novosibirsk, Russia) reveals how different colour treatments can be applied to diamond using combinations of irradiation and annealing at various temperatures. He goes into just the right amount of detail, describing the principal defects involved (e.g. H3 and H4) and how they are transformed from existing defects in the starting material. Some impressive results of these treatments are shown. In particular, he demonstrates how natural brown diamonds are first transformed to green-yellow stones and then, through his pioneering multistep process, into 'Imperial Red' diamonds.

Section III provides a detailed review of the instrumentation available for the gemmological testing and identification of diamond. It is subdivided into three topics: comparison of portable instruments, principles of gem instruments, and the testing of untreated and treated natural and synthetic diamonds by spectroscopy and fluorescence imaging.

The first of these, 'Comparison of Portable Instruments

for Screening and ID of Natural and Laboratory Grown Diamonds' by Branko Deljanin, highlights the ongoing issue of undisclosed synthetic diamonds in parcels of loose stones and mounted in jewellery. The author discusses the three types of instruments available: screening, screening-and-detection, and referral-and-detection. This provides the reader with a good overview of available equipment, plus the costs, benefits, limitations and referral rates, along with an easy-to-understand explanation of their principles of operation. The author encourages potential buyers of diamond-screening or verification instruments to research what is available and then to select a device—or combination of instruments—that best suits their specific requirements.

The second part of Section III, 'Principles of Gem Instruments for Diamond Origin ID' by John Chapman, discusses equipment that aids a gemmologist beyond the capabilities of the naked eye. It highlights some of the measurement types that underpin the key instruments used to detect whether a diamond is natural or synthetic. The author discusses the principles of UV transmission, UV fluorescence, fluorescence spectroscopy, and UV-Vis-NIR and infrared spectroscopy. He also provides a valuable overview of the equipment, costs, analysis and training required for each technique.

The third part of Section III is 'Testing Untreated and Treated Natural Diamonds as well as Synthetic Diamonds by Spectroscopy and Fluorescence Imaging' by Dr Thomas Hainschwang. The author showcases luminescence images of, and the spectroscopic distinctions between, both HPHT and CVD synthetic diamonds and their natural counterparts. Also provided is a comprehensive overview of the spectroscopic properties of naturally coloured and treated-colour diamonds. Colour ranges that are covered are violet to red, mixed colours and black.

The book finishes with an appendix providing test results from the Canadian Gemmological Laboratory for 30 natural and synthetic diamonds and 7 imitations, followed by a glossary of terms and abbreviations used in the book.

This book is an excellent reference for those who are new to the field or those with limited experience in gemmology with regards to spectroscopy of the important defects and colour centres in diamond and, particularly, the generation of colour by treatments. One minor criticism is that some of the material is repeated from other books by the same author.

**Dr Peter M. P. Lanigan and**
**Dr Colin D. McGuinness**
De Beers Ignite
Maidenhead, Berkshire


## Gems, Colours & Wild Stories: 175 Years of Constantin Wild

**Ed. by Constantin Wild and Nina Hald, 2021. Constantin Wild GmbH & Co. KG, Idar-Oberstein, Germany, and Arnoldsche Art Publishers, Stuttgart, Germany, https://arnoldsche.com/produkt/gems-colours-wild-stories, 304 pages, illus., ISBN 978-3897906266. EUR124.00 hardcover with slipcase.**

This is a rather special book for gem enthusiasts and collectors. It is evident that this book is going to be different based on the very colourful slipcase and the fact that 'Wild Stories' is in the title. Constantin Wild is the great-grandson of the company's founder, and he is a true asset to the gem industry. I know him personally, and I have been familiar with the company since before he was born. (With the help of my parents, in 1960 I sent small tourmalines I had collected in the Pala District's mine dumps to the company to facet.)

This book lives up to Constantin's reputation as a colourful and extraordinary gem purveyor. With the help of editor and renowned jewellery expert Nina Hald, he has produced a lavish work filled with exquisite photos of rare and beautiful gemstones. The book was published to mark the company's 175th anniversary, and it covers its long and interesting history over the course of five generations. Several guest authors provide pages or chapters covering Constantin's amazing story.

One of my favourite chapters is 'The Making of Colour' (26 pages), which includes the quotes 'No cutting – no

colour' (Nina Hald) and 'It is always an exciting challenge to transform a natural crystal into a perfect gem' (Constantin Wild). Here we read pages covering sections on 'Facets of a Lapidary', 'Digging Deep – Standing Proud', 'Determining the Cut', 'The Process, Bringing Out the Facets', 'Of Round Shapes, Soft Shimmer', 'Pleochroism – the Case of Several Colours', 'The Agate Cutters' and 'Art Works'. You can get a feel for the lapidary content just from these subtitles.

Another favourite chapter is 'Superlative Jewelry' (by Nina Hald, 50 pages), which is dedicated to famous jewellery designers—Bulgari, Paloma Picasso, David Webb, Mikimoto, Temple St Clair, Cindy Chow and many more—with the jewels they designed, set with gems supplied by the Wild company.

One of the last chapters profiles well-known historic and modern collectors and collections. Several are covered, including the 'Somewhere in the Rainbow Collection' that began in 2008 and contains more than 1,500 gems and jewellery creations curated by Shelly Sergent. It also includes the collection of Michael Scott, whose goal is to acquire pieces showcasing quality and beauty in order to tell the emotional story of the impact of gem colours. He has displayed his peerless collection in several showings, including the Shanghai Museum in 2005, Royal Ontario Museum in 2008–2009 and twice at the Bowers Museum in Santa Ana, California, USA.

The final chapter is a discreet, thoughtful look at the company itself. Historic and modern photos depict the lovely Wild offices, including the 'Wild chamber of power' and the strongroom housing the heart of the company: the gems on display.

Constantin Wild says in the book, 'I have the most wonderful profession in the world', and he concludes with the simple 'Thank you for sharing my love'.

This volume is well worth its asking price, and its large size makes it suitable as a 'coffee table' book. I recommend that anyone who enjoys gems or jewellery add it to their library.

**Bill Larson FGA**
Pala International
Fallbrook, California, USA

# Other Book Titles

## CULTURAL HERITAGE

**African Ivories in the Atlantic World, 1400–1900/ Marfins Africanos no Mundo Atlântico, 1400–1900**
Ed. by José da Silva Horta, Carlos Almeida and Peter Mark, 2021. Centro de História da Universidade de Lisboa, Lisbon, Portugal, 705 pages, ISBN 978-9898068361, http://hdl.handle.net/10451/50982 (in English and Portuguese). Free PDF.

**Collectio Mineralium: The Catalog of Holy Roman Emperor Leopold II's Mineralogical Collection**
Ed. by Annarita Franza, Johannes Mattes and Giovanni Pratesi, 2022. Cataloghi e Collezioni Series, Firenze University Press, Florence, Italy, 170 pages (print) or 282 pages (PDF), ISBN 978-8855184939, e-ISBN 978-8855184946 (PDF) or e-ISBN 978-8855184953 (online), https://doi.org/10.36253/978-88-5518-494-6. EUR24.90 softcover or free PDF/web view.

**Dante. Le Gemme nella Divina Commedia: Considerazioni Gemmologiche/Gems in the Divine Comedy: Gemmological Considerations**
By Enrico Butini and Flavio Butini, 2021. L'Erma di Bretschneider, Rome, Italy, 80 pages, ISBN 978-8891322074 or e-ISBN 978-8891322098 (in Italian and English). EUR65.00 hardcover or EUR52.00 PDF.

**The Gems of Dante's Divine Comedy**
By Ann C. Pizzorusso, 2021. Da Vinci Press, New York, New York, USA, 61 pages, ISBN 978-1940613062. USD8.55 softcover.

**Handbook of Cultural Heritage Analysis**
Ed. by Sebastiano D'Amico and Valentina Venuti, 2022. Springer Nature Switzerland AG, Cham, Switzerland, xxxvi + 2,256 pages, ISBN 978-3030600150 or e-ISBN 978-3030600167, https://doi.org/10.1007/978-3-030-60016-7. EUR980.99 hardcover or EUR962.99 eBook.

**Jewels, Jewelry, and Other Shiny Things in the Buddhist Imaginary**
Ed. by Vanessa R. Sasson, 2021. University of Hawaii

Press, Honolulu, Hawaii, USA, 368 pages, e-ISBN 978-0824889524, https://doi.org/10.1515/9780824889524. USD148.00 PDF.

## DIAMOND

**The Slave Province, Canada – Geological Evolution of an Archean Diamondiferous Craton**
By H. Helmstaedt, S.J. Pehrsson and M.P. Stubley, 2021. Special Paper 51, Geological Association of Canada, St John's, Newfoundland, Canada, 216 pages, ISBN 978-1897095898. CDN75.00 softcover.

## GEM LOCALITIES

**The Gems of Hiddenite, North Carolina: Mining History, Geology and Mineralogy**
By Mark I. Jacobson and Wade E. Speer, 2021. McFarland & Company Ltd, Jefferson, North Carolina, USA, 227 pages, ISBN 978-1476684697. USD39.95 softcover.

**Mineralogy of Arizona, 4th edn.**
By Raymond W. Grant, Ronald B. Gibbs, Harvey W. Jong, Jan C. Rasmussen and Stanley B. Keith, 2022. University of Arizona Press, Tucson, Arizona, USA, 744 pages, ISBN 978-0816543588 (hardcover), ISBN 978-0816543571 (softcover) or e-ISBN 978-0816545223. USD75.00 hardcover or USD49.95 softcover or eBook.

## GENERAL REFERENCE

**Dictionnaire des Joailliers, Bijoutiers et Orfèvres en France, de 1850 à nos Jours [Dictionary of Jewellers and Goldsmiths in France, from 1850 to the Present]**
By Remi Verlet, 2022. L'École des Arts Joailliers, Paris, France, 2,400 pages (dictionary) and 1,056 pages (index), no ISBN (in French). EUR650.00 two-volume boxed set.

**Fleischer's Glossary of Mineral Species, 13th edn.**
By Malcolm E. Back, 2022. Education Publication Vol. 1, Mineralogical Association of Canada, Québec, Canada, 448 pages, ISBN 978-0921294641. CDN45.00 (in Canada) or USD45.00 (outside Canada) softcover.

**Mineral Identification Manual: Clues from Their Geological Provenance**
By George W. Robinson, Jeffrey R. Chiarenzelli and Susan Robinson, 2022. Education Publication Vol. 2, Mineralogical Association of Canada, Québec, Canada, 208 pages, ISBN 978-0921294658. CDN55.00 (in Canada) or USD55.00 (outside Canada) softcover.

**Natural History Museum Book of Gemstones: A Concise Reference Guide**
By Robin Hansen, 2022. Natural History Museum, London, 240 pages, ISBN 978-0565092245. GBP14.99 softcover; republished as *Gemstones: A Concise Reference Guide* by Princeton University Press, Princeton, New Jersey, USA, ISBN 978-0691214481, USD19.95 softcover; and CSIRO Publishing, Clayton, Victoria, Australia, ISBN 978-1486315246, AUD34.99 softcover. (Available from the Gem-A Shop at https://shop.gem-a.com/product/gemstones-by-robin-hansen for GBP14.99.)

**Rockhounding for Beginners: Your Comprehensive Guide to Finding and Collecting Precious Minerals, Gems, Geodes, & More**
By Lars W. Johnson with Stephen M. Voynick, 2021. Adams Media, Stoughton, Massachusetts, USA, 240 pages, ISBN 978-1507215272. USD17.99 softcover.

## JEWELLERY HISTORY

**The Ideal Past: Revival Jewels**
By Beatriz Chadour-Sampson and Sandra Hindman, 2022. Les Enluminures, Paris, France, 120 pages, no ISBN. USD18.00 softcover.

**The Modern Guide to Antique Jewellery**
By Beth Bernstein, 2022. ACC Art Books, Woodbridge, Suffolk, 192 pages, ISBN 978-1788841580. GBP25.00 hardcover.

## JEWELLERY AND *OBJETS D'ART*

**Adorned by Nature: Adornment, Exchange & Myth in the South Seas**
By Wolfgang Grulke, 2022. At One Communications, Dorset, 400 pages, ISBN 978-1916039445. GBP40.00 softcover.

**Babetto: The Entity of Being/L'Entità dell'Essere/ Die Einheit des Seins**
By Fred Jahn, Friedhelm Mennekes, Andrea Nante and Thereza Pedrosa, 2022. Arnoldsche Art Publishers, Stuttgart, Germany, 328 pages, ISBN 978-3897906631 (in English, German and Italian). EUR48.00 hardcover.

**Cameos and Intaglios: The Art of Engraved Stones/ Camées et Intailles: L'art des Pierres Gravées**
By Philippe Malgouyres, 2022. Editions Gallimard and L'École des Arts Joailliers, Paris, France, 76 pages, ISBN 978-2072943270 (English) or ISBN 978-2072943263 (French). EUR14.50 softcover.

**Cartier and Islamic Art: In Search of Modernity**
By Heather Ecker, Judith Henon-Reynaud, Évelyne Possémé, Sarah Schleuning, Agustín Arteaga, Pierre-Alexis Dumas, Olivier Fabet *et al.*, 2022. Thames & Hudson, New York, New York, USA, 320 pages, ISBN 978-0500024799. USD70.00 hardcover.

**Dreher Masterworks at the Houston Museum of Natural Science**
Ed. by Joel Bartsch and Gloria Staebler, 2022. Lithographie Ltd, Arvada, Colorado, USA, 368 pages, ISBN 978-1734131093. USD101.25 hardcover.

**North by Northwest: The Jewelry of Laurie Hall**
By Susan Cummins and Damian Skinner, 2022. Arnoldsche Art Publishers, Stuttgart, Germany, 128 pages, ISBN 978-3897906471. EUR28.00 hardcover.

**Tiaras of Dreams, Dreaming of Tiaras**
By Michèle Gazier and Kristjana S. Williams, 2022. Rizzoli, New York, New York, USA, 10 pages, ISBN 978-0847871599. USD35.00 hardcover 'pop-up' book.

**Traditional French Jewelry**
By Michael C. W. Fieggen, 2021. Self-published, 300 pages, ISBN 978-2957637614. EUR75.00 softcover.

**Vintage Jewellery: Collecting and Wearing Vintage Classics**
By Caroline Cox, 2022. Wellbeck Publishing Group, London, 256 pages, ISBN 978-1802791112. GBP20.00 hardcover.

**A World of Invention: Rings from the Goldsmiths' Company Collection 1961–2022**
By Frances Parton and Dora Thornton, 2022. The Goldsmiths' Company, London, 120 pages, ISBN 978-0907814405. GBP20.00 softcover.

## MISCELLANEOUS

**Advanced Jewellery CAD Modelling in Rhino**
By Jack Meyer, 2022. The Crowood Press, Marlborough, Wiltshire, 240 pages, ISBN 978-0719840418. GBP20.00 softcover.

**A Collection of My Best Gemstone Faceting Designs, Vol. 4**
By Andrew Ian Brown, 2022. Self-published, 152 pages, ISBN 979-8405730745. AUD49.00 softcover.

**Lithomania: Design Lab #11**
Ed. by Claudia Banz and Ute Eitzenhöfer, 2022. ACC Art Books, Woodbridge, Suffolk, 272 pages, ISBN 978-3897906600 (in English and German). GBP32.00 softcover.

**Rock & Gems: Un Viaggio Tra Musica e Pietre Preziose [A Journey Between Music and Precious Stones]**
By Annalaura Sita, 2021. Arcana Editore, Rome, Italy, 176 pages, ISBN 978-8892770232 (in Italian). EUR16.00 softcover.

**Thames Mudlarking: Searching for London's Lost Treasures**
By Jason Sandy and Nick Stevens, 2021. Shire Publications, London, 96 pages, ISBN 978-1784424329. GBP9.99 softcover.

## ORGANIC/BIOGENIC GEMS

**Consuming Ivory: Mercantile Legacies of East Africa and New England**
By Alexandra Celia Kelly, 2021. University of Washington Press, Seattle, Washington, USA, 278 pages, ISBN 978-0295748771 (hardcover) or ISBN 978-0295748818 (softcover). USD99.00 hardcover or USD30.00 softcover.

## SOCIAL STUDIES

**Flight of the Diamond Smugglers: A Tale of Pigeons, Obsession, and Greed Along Coastal South Africa**
By Matthew Gavin Frank, 2022. Liveright, New York, New York, USA, 224 pages, ISBN 978-1631496028 (hardcover) or ISBN 978-1324091554 (softcover). USD25.95 hardcover or USD16.95 softcover.

**Refracted Economies: Diamond Mining and Social Reproduction in the North**
By Rebecca Jane Hall, 2022. University of Toronto Press, Toronto, Ontario, Canada, 286 pages, ISBN 978-1487540838 (hardcover), ISBN 978-1487540845 (softcover), e-ISBN 978-1487540869 (eBook) or e-ISBN 978-1487540852 (PDF). CAD85.00 hardcover or CAD34.95 softcover, eBook or PDF.

# Literature of Interest

## COLOURED STONES

**An analysis of geochemical features of crystallization of emeralds as an approach to determine the deposit of them.** M.P. Popov, V.I. Solomonov, A.V. Spirina, M.A. Ivanov, V.V. Kuptsova and A.G. Nikolaev, *News of the Ural State Mining University*, **2**(62), 2021, 16–21, https://doi.org/10.21440/2307-2091-2021-2-16-21.*

**Characterization of natural silicate garnets by means of non-destructive testing methods.** I. Balčiūnaitė, I. Ignatjev, D. Kaminskas, G. Niaura and E. Norkus, *Chemija*, **32**(3–4), 2021, 107–126, https://doi.org/10.6001/chemija.v32i3-4.4549.*

**Color measurement of yellow sapphire by UV-Vis reflectance spectroscopy.** N. Tipkanon, N. Monarumit, T. Lhuaamporn and W. Wongkokua, *Journal of Physics: Conference Series*, **2145**, 2021, article 012062 (4 pp.), https://doi.org/10.1088/1742-6596/2145/1/012062.*

**Comparative study on gemological characteristics of rhodonite jade in Brazil and Xinjiang of China.** Q. Tan, T. Lei, L. He, L. Ruan and Q. Ruan, *Superhard Material Engineering*, **33**(5), 2021, 52–57 (in Chinese with English abstract).

**Comparison of chemical composition and spectroscopy of purple-brownish red garnet from Zambia, Tanzania and Australia.** Y. Zhong, M. Qu and A.H. Shen, *Spectroscopy and Spectral Analysis*, **42**(1), 2022, 184–190, https://tinyurl.com/hbfwpmwe (in Chinese with English abstract).*

**Copper isotopic variation of turquoise in low-temperature growth process and its significance for origin traceability.** T. Lei, Z. Wang and Y. Li, *Earth Science*, **47**(4), 2022, 1371–1382, https://doi.org/10.3799/dqkx.2021.138 (in Chinese with English abstract).*

**Gem topaz from the Schneckenstein Crag, Saxony, Germany: Mineralogical characterization and luminescence.** M. Zeug, L. Nasdala, C. Chanmuang N. and C. Hauzenberger, *Gems & Gemology*, **58**(1), 2022, 2–17, https://doi.org/10.5741/gems.58.1.2.*

**Gem-quality blue sapphires ($Al_2O_3$-corundum variety) from the Milas-Yatağan region, Muğla, Turkey.** M. Hatipoğlu and E. Çoban, *Academia Letters*, 2021, article 4085 (5 pp.), https://doi.org/10.20935/al4085.*

**Gemmological characteristic of colorless petalite.** L. Yu and R. Liao, *Superhard Material Engineering*, **33**(4), 2021, 51–58 (in Chinese with English abstract).

**Gemmological and mineralogical characteristics of nephrite from Longxi, Sichuang Province.** W. Wang, Z. Liao, Z. Zhou, J. Shang, P. Li, D. Cui, L. Li and Q. Chen, *Journal of Gems & Gemmology*, **24**(1), 2022, 20–27, https://tinyurl.com/4ymb2cba (in Chinese with English abstract).*

**Helium, neon and argon in alkaline basalt-related corundum megacrysts: Implications for their origin and forming process.** W. Guo, H. He, L. Qiao, Z. Liu, F. Su, J. Li, G. Shi and R. Zhu, *Geochimica et Cosmochimica Acta*, **322**, 2022, 71–93, https://doi.org/10.1016/j.gca.2022.01.016.

**Inclusion and spectral characteristics of sapphire from Ilakaka, Madagascar.** B. Liang and M. Chen, *Journal of Gems & Gemmology*, **24**(1), 2022, 28–38, https://tinyurl.com/mry7z7sm (in Chinese with English abstract).*

**Iron oxide inclusions and exsolution textures of rainbow lattice sunstone.** S. Jin, Z. Sun and A.C. Palke, *European Journal of Mineralogy*, **34**(2), 2022, 183–200, https://doi.org/10.5194/ejm-34-183-2022.*

**Laboratory identification characteristic of purple jadeite.** S. Li, H. Zhou and Z. Lin, *Journal of Gems & Gemmology*, **24**(1), 2022, 48–57, https://tinyurl.com/2p882jb7 (in Chinese with English abstract).*

**$Mn^{3+}$ and the pink color of gem-quality euclase from northeast Brazil.** L. Gilles-Guéry, L. Galosy, J. Schnellrath, B. Baptiste and G. Calas, *American Mineralogist*, **107**(3), 489–494, 2021, https://doi.org/10.2138/am-2021-7838.

**Nephrite of Bazhenovskoye chrysotile–asbestos deposit, Middle Urals: Localization, mineral**

**composition and color.** E.V. Kislov, Y.V. Erokhin, M.P. Popov and A.G. Nikolayev, *Minerals*, **11**(11), 2021, article 1227 (14 pp.), https://doi.org/10.3390/min11111227.*

**New giant gem corundum boulder from Sri Lanka.** T. Leelawathanasuk, S. Promwongnan, P. Wathanakul, V. Pisutha-Arnond, W. Atichat and G. Zoysa, *Gemmology Today*, March 2022, 50–53, https://tinyurl.com/24dmt6yc.*

**New and unusual cat's eyes and asteriated gems.** M.P. Steinbach, L. Kiefert and J. Fiedler, *Journal of Gems & Gemmology*, **24**(1), 2022, 1–11, https://tinyurl.com/bdem322m.*

**Padparadscha sapphire & the ownership of words.** R. Hughes, *Gemmology Today*, March 2022, 40–49, https://tinyurl.com/3b6j3f6d.*

**Provenance determination of turquoise in the southern Yigediwo site of Jinta County, Gansu Province.** D. Zhang, Y. Li and G. Xi, *Journal of Mineralogy and Petrology*, **42**(1), 2022, 1–7 (in Chinese with English abstract).

**Raman spectrum characteristic of associated minerals of turquoise from Mongolia.** J. Liu, M. Yang and L. Liu, *Journal of Gems & Gemmology*, **24**(1), 2022, 12–19, https://tinyurl.com/2p9fyp5s (in Chinese with English abstract).*

**Raman studies on zoisite and tanzanite for gemmological applications.** A. Coccato, D. Bersani, M.C. Caggiani, P. Mazzoleni and G. Barone, *Journal of Raman Spectroscopy*, **53**(3), 2022, 550–562, https://doi.org/10.1002/jrs.6203.

**Research on parameters optimization of digital imaging system in red–yellow jadeite color measurement.** Z. Liu, Y. Guo, Y. Shang and B. Yuan, *Scientific Reports*, **12**(1), 2022, article 3617 (13 pp.), https://doi.org/10.1038/s41598-022-07715-1.*

**Study on the correlation between trace elements and colorimetric parameters of natural blue sapphire.** D. Zhou, T. Lu and J. Zhang, *Color Research & Application*, **47**(3), 2021, 691–696, https://doi.org/10.1002/col.22755.

**Study on spectral characteristics and color formation cause of pink nephrite from Xinjiang.** J. Tang and H. Wang, *Superhard Material Engineering*, **33**(4), 2021, 59–65 (in Chinese with English abstract).

**Validation with Raman spectroscopy of lapis lazuli provenance study.** M. Saleh, *Il Nuovo Cimento C*, **44**(1), 2021, article 24 (10 pp.), https://doi.org/10.1393/ncc/i2021-21024-7.*

## CULTURAL HERITAGE

**An archaeometric investigation of gems and glass beads decorating the double-arm reliquary cross from Liège, Belgium.** Y. Bruni, F. Hatert, M. Demaude, N. Delmelle, P. George and J. Maquet, *Heritage*, **4**(4), 2021, 4542–4557, https://doi.org/10.3390/heritage4040250.*

**Colours of gemmy phosphates from the Gavà Neolithic mines (Catalonia, Spain): Origin and archaeological significance.** Y. Díaz-Acha, M. Campeny, L. Casas, R. Di Febo, J. Ibañez-Insa, T. Jawhari, J. Bosch, F. Borrell *et al.*, *Minerals*, **12**(3), 2022, article 368 (27 pp.), https://doi.org/10.3390/min12030368.*

**Les gemmes de deux pièces maîtresses méconnues de la collection Adèle de Rothschild au Château d'Écouen 2) Le Taj [The gems of two little-known masterpieces from the Adèle de Rothschild collection at the Château d'Écouen 2) The Taj].** G. Panczer, G. Choumil, J. Rohou and G. Riondet, *Revue de Gemmologie A.F.G.*, No. 215, 2022, 7–11 (in French).

**The history of mineralogy and gemology in Iran.** M. Yazdi, *Earth Sciences History*, **40**(2), 2021, 566–580, https://doi.org/10.17704/1944-6187-40.2.566.

**A holistic provenance and microwear study of pre-colonial jade objects from the Virgin Islands: Unravelling mobility networks in the wider Caribbean.** A.C.S. Knaf, C.G. Falci, Habiba, C.J. Toftgaard, J.M. Koornneef, A. van Gijn, U. Brandes, C.L. Hofman *et al.*, *Journal of Archaeological Science: Reports*, **41**, 2022, article 103223 (18 pp.), https://doi.org/10.1016/j.jasrep.2021.103223.*

**New attribution of the Adoration of the Shepards medallion.** J. Grqzawska, *Bursztynisko (The Amber Magazine)*, No. 46, 2022, 60–64, https://tinyurl.com/37xzenhc (in English and Polish).*

**Spectroscopic study of the coloured gems in a 19th century pendant from Einsiedeln Abbey.** S. Karampelas and M. Wörle, *Journal of Raman Spectroscopy*, **53**(3), 2022, 563–569, https://doi.org/10.1002/jrs.6194.

## DIAMONDS

**Color genesis of brown diamond from the Mengyin kimberlite, China.** G. Wu, X. Yu, F. Liu, H. Li, Z. Long and H. Wang, *Crystals*, **12**(4), 2022, article 449 (22 pp.), https://doi.org/10.3390/cryst12040449.*

**Diamond Reflections. Deep-focus earthquakes: The heartbeat of a diamond factory?** E.M. Smith, Ed., *Gems & Gemology*, **58**(1), 2022, 72–79, https://tinyurl.com/4j33py28.*

**Inclusions in diamonds probe Earth's chemistry through deep time.** M. Alvaro, R.J. Angel and F. Nestola, *Communications Chemistry*, **5**(1), 2022, article 10 (3 pp.), https://doi.org/10.1038/s42004-022-00627-1.*

**Large diamonds: Why now?** P. Sandberg, *Gems&Jewellery*, **31**(1), 2022, 30–33.

**Morphology of diamond crystals and mechanism of their growth.** V.M. Kvasnytsya, *Journal of Superhard Materials*, **43**(2), 2021, 75–84, https://doi.org/10.3103/s1063457621020076.

**Morphology and FTIR characteristics of the alluvial diamond from the Yangtze craton, China.** C. Cao, J. Yang, F. Zeng, F. Liu, S. Yang and Y. Wang, *Crystals*, **12**(4), 2022, article 539 (14 pp.), https://doi.org/10.3390/cryst12040539.*

**Regeneration growth as one of the principal stages of diamond crystallogenesis.** I.V. Klepikov, E.A. Vasilev and A.V. Antonov, *Minerals*, **12**(3), 2022, article 327 (16 pp.), https://doi.org/10.3390/min12030327.*

**Spectroscopy of diamonds from the M.V. Lomonosov deposit.** E.A. Vasilev, G.Y. Kriulina and V.K. Garanin, *Geology of Ore Deposits*, **63**(7), 2022, 668–674, https://doi.org/10.1134/s1075701521070096.

## FAIR TRADE

**Analysing sustainable concerns in diamond supply chain: A fuzzy ISM-MICMAC and DEMATEL approach.** S. Shanker and A. Barve, *International Journal of Sustainable Engineering*, **14**(5), 2021, 1269–1285, https://doi.org/10.1080/19397038.2020.1862351.*

**Diamond mining in northern Angola results in environmental disaster in southern Congo (DRC).** P. Minieri, *Rivista Italiana de Gemmologia/Italian Gemological Review*, No. 14, 2022, 20–24.

**Estimating the regional development in gems [*sic*] mining areas in Brazil.** L.d.A.M. Brandão, I.d.A. Nääs and P.L.d.O. Costa Neto, *European Journal of Sustainable Development Research*, **5**(4), 2021, article em0172 (8 pp.), https://doi.org/10.21601/ejosdr/11284.*

**Gem and jewellery solutions and innovations.** O. Quiniquini, *JNA*, No. 433, 2022, 46–49, https://tinyurl.com/4a5rhb5h (in English and Chinese).*

**Letting it shine: Governance for equitable coloured gemstone supply chains.** Coloured Gemstones Working Group, *Gemmology Today*, March 2022, 54–58, https://tinyurl.com/4epsj4k3.*

**Supporting sustainable development goal 5 gender equality and entrepreneurship in the tanzanite mine-to-market.** J.A. Denoncourt, *Sustainability*, **14**(7), 2022, article 4192 (19 pp.), https://doi.org/10.3390/su14074192.*

**Sustainability into luxury gemstone industry.** F. Vincent, C.-M. Ivan and S.R. Patil, *2021 Global Fashion Marketing Conference at Seoul/2021 Korean Scholars of Marketing Science International Conference*, 5–7 November 2021, 237–238, https://doi.org/10.15444/gfmc2021.04.02.03.*

**Vibrant jewellery prospects in the NFT [non-fungible token] world.** B. Sto. Domingo, *JNA*, No. 433, 2022, 10–15, https://tinyurl.com/3ykkmmn5 (in English and Chinese).*

## GEM LOCALITIES

**Artisanal opal mining and associated environmental and socio-economic issues in opal mine sites of Wollo Province, Ethiopia.** W. Getaneh and M. Shikur, *GeoJournal*, 2021 (published online 15 May), 17 pp., https://doi.org/10.1007/s10708-021-10440-3.

**Capelinha: Titanite and epidote deposits of the Capelinha region, Minas Gerais, Brazil.** A. Bartorelli, C. Cornejo, M.L.d.S.C. Chaves, C.H. Dias and A.W. Romano, *Mineralogical Record*, **53**(3), 2022, 315–363.

**The Ekati and Diavik diamond mines.** C.J. Stefano and J.H. Betts, *Mineralogical Record*, **53**(2), 2022, 243–259.

**Formation of sediment-hosted opal-AG at Lightning Ridge (New South Wales, Australia): Refining the deep weathering model.** J. Herrmann and R. Maas,

*Journal of Geology*, **130**(2), 2022, 77–110, https://doi.org/10.1086/718833.

**History of emerald mining in the Habachtal deposit of Austria, part II.** K. Schmetzer, *Gems & Gemology*, **58**(1), 2022, 18–46, https://doi.org/10.5741/gems.58.1.18.*

**Honey and diamonds [mining in Liberia].** B. West, *Gems&Jewellery*, **31**(1), 2022, 24–27.

**L'Île d'Elbe, un rêve accessible pour les amateurs de belles gemmes et de minéraux [The island of Elba, an accessible dream for lovers of beautiful gems and minerals].** F. Bernard-Perrottey, *Revue de Gemmologie A.F.G.*, No. 215, 2022, 4–6 (in French).

**Mineralogy and geochemistry of nephrite from Wolay deposited [*sic*], Kunar, east Afghanistan.** S.S. Obiadi, M.A. Amini and F. Fazli, *Journal of Mechanical, Civil and Industrial Engineering*, **3**(1), 2022, 56–65, https://doi.org/10.32996/jmcie.2022.3.1.6.*

**Naryn-Gol Creek sapphire placer deposit, Buryatia, Russia.** E.V. Kislov, A.V. Aseeva, V.V. Vanteev, A.Y. Sinyov and O.A. Eliseeva, *Minerals*, **12**(5), 2022, article 509 (16 pp.), https://doi.org/10.3390/min12050509.*

**The origin of gem spodumene in the Hamadan pegmatite, Alvand plutonic complex, western Iran.** R. Sheikhi Gheshlaghi, M. Ghorbani, A.A. Sepahi, R. Deevsalar, K. Nakashima and R. Shinjo, *Canadian Mineralogist*, **60**(2), 2022, 249–266, https://doi.org/10.3749/canmin.2000087.

**Origin of the subduction-related Tieli nephrite deposit in northeast China: Constraints from halogens, trace elements, and Sr isotopes in apatite group minerals.** H. Xu and F. Bai, *Ore Geology Reviews*, **142**, 2022, article 104702 (18 pp.), https://doi.org/10.1016/j.oregeorev.2022.104702.*

**Pressure-temperature-fluid constraints for the formation of the Halo-Shakiso emerald deposit, southern Ethiopia: Fluid inclusion and stable isotope studies.** C.-A. Nicol, D. Marshall, H.C. Einfalt and D. Thorkelson, *Canadian Mineralogist*, **60**(1), 2022, 29–48, https://doi.org/10.3749/canmin.2000069.

**The rebirth of Yogo: Sapphire production at Montana's historic mine.** O. Gonzalez, *Gems&Jewellery*, **31**(1), 2022, 18–21.

## INSTRUMENTATION AND TECHNOLOGY

**Automatic gemstone classification using computer vision.** B. Chow and C. Reyes-Aldasoro, *Minerals*, **12**(1), 2021, article 60 (21 pp.), https://doi.org/10.3390/min12010060.*

**Color filters: Useful tools that gemologists should use but often don't.** C. Evans, *GemGuide*, **41**(2), 2022, 16–17.

**Raman photoluminescence – An efficient way to distinguish natural diamonds and lab grown diamonds.** G.A. Kumar, N. Prabavathy and L. Biswal, *IOP Conference Series: Materials Science and Engineering*, **1225**, 2022, article 012023 (12 pp.), https://doi.org/10.1088/1757-899x/1225/1/012023.*

**Rapid gemstone screening and identification using fluorescence spectroscopy.** T.H. Tsai and U.F.S. D'Haenens-Johansson, *Applied Optics*, **60**(12), 2021, article 3412 (10 pp.), https://doi.org/10.1364/ao.419885.*

**Use of three portable instruments for fast screening and ID of natural and laboratory-grown diamonds.** B. Deljanin, *Rivista Italiana de Gemmologia/Italian Gemological Review*, No. 14, 2022, 35–45.

## JEWELLERY HISTORY

**Copie, répliques et reproductions du collier de la Reine [Copy, replicas and reproductions of the Queen's necklace].** C. Joannis, *Revue de Gemmologie A.F.G.*, No. 215, 2022, 12–13 (in French).

**Louis XIV's blue gems: Exceptional rediscoveries at the French National Museum of Natural History.** F. Farges, in R. Pellens, Ed., *Natural History Collections in the Science of the 21st Century*, ISTE Ltd and John Wiley & Sons Inc., London and Hoboken, New Jersey, USA, 2021, 27–36, https://doi.org/10.1002/9781119882237.ch3.

## LAPIDARY TOPICS

**The cut or the stone? [large faceted carbonado diamond].** B. West, *Gems&Jewellery*, **31**(1), 2022, 40–41.

**History and utility of gemstone reflection pattern generation analysis.** M. Cowing, *Gemmology Today*, March 2022, 62–67, https://tinyurl.com/bdf57786.*

## MISCELLANEOUS

**2022: Bold, bright colours everywhere.** N. Ahline, *Gems&Jewellery*, **31**(1), 2022, 37–39.

**The challenge of the cabochon [to gem identification].** N. Zolotukhina, *Gemmology Today*, March 2022, 68–74, https://tinyurl.com/muk7ekcf.*

**Dialectics of association and dissociation: Spaces of valuation, trade, and retail in the gemstone and jewelry sector.** L. Thomsen and M. Hess, *Economic Geography*, **98**(1), 2021, article 1989302 (19 pp.), https://doi.org/10.1080/00130095.2021.1989302.*

**Gemstones.** D.W. Olson, in *Mineral Commodity Summaries 2022*, U.S. Geological Survey, Reston, Virginia, USA, 2022, 68–69, https://pubs.usgs.gov/periodicals/mcs2022/mcs2022-gemstones.pdf.*

## NEWS PRESS

**The crown jewels you have never seen.** M. Lazazzera, *New York Times*, 24 March 2022, https://www.nytimes.com/2022/03/24/fashion/italy-crown-jewels-rome.html.*

**Luxury brands make waves in jewellery world with bespoke diamond cuts.** M. Lazazzera, *Financial Times*, 10 April 2022, https://www.ft.com/content/4d73cf3b-97a1-432d-866d-9cb7032756df.*

**Why the renewed interest in crystals? The pandemic.** A. Cheney, *New York Times*, 26 January 2022, https://www.nytimes.com/2022/01/26/fashion/jewelry-crystals-jacquie-aiche-beverly-hills-california.html.*

## ORGANIC/BIOGENIC GEMS

**Amber in Texas.** V. Friedman, *Bursztynisko (The Amber Magazine)*, No. 46, 2022, 86–88, https://tinyurl.com/37xzenhc (in English and Polish).*

**Conservation of amber: Selected topics.** K. Kwiatkowska, *Bursztynisko (The Amber Magazine)*, No. 46, 2022, 48–52, https://tinyurl.com/37xzenhc (in English and Polish).*

**Coral-ID: A forensically validated genetic test to identify precious coral material and its application to objects seized from illegal traffic.** B. Lendvay, L.E. Cartier, F. Costantini, N. Iwasaki, M.V. Everett, M.S. Krzemnicki, A. Kratzer and N.V. Morf, *Forensic Science International: Genetics*, **58**, 2022, article 102663 (11 pp.), https://doi.org/10.1016/j.fsigen.2022.102663.*

**Distinguish mammoth and elephant ivory with stable water isotopes.** S. Ziegler, *Academia Letters*, 2021, article 4314 (8 pp.), https://doi.org/10.20935/al4314.*

**The fossil resins of Europe.** M. Kazubski, *Bursztynisko (The Amber Magazine)*, No. 46, 2022, 89–92, https://tinyurl.com/37xzenhc (in English and Polish).*

**Photoluminescence in Indonesian fossil resins.** Y. Li, Z. Zhang, X. Wu and A.H. Shen, *Spectroscopy and Spectral Analysis*, **42**(3), 2022, 814–820, https://tinyurl.com/3r764z5m (in Chinese with English abstract).*

**Reconstruction of amber ornaments.** E. Popkiewicz, *Bursztynisko (The Amber Magazine)*, No. 46, 2022, 74–76, https://tinyurl.com/37xzenhc (in English and Polish).*

**Survey history and exploration status of amber resources in the Lublin region.** R. Kramarska, *Bursztynisko (The Amber Magazine)*, No. 46, 2022, 93–98, https://tinyurl.com/37xzenhc (in English and Polish).*

## PEARLS

**Luster measurement of pearl by UV-Vis reflectance spectroscopy.** C. Salyacheewin, N. Monarumit and W. Wongkokua, *Journal of Physics: Conference Series*, **2145**, 2022, article 012063 (4 pp.), https://doi.org/10.1088/1742-6596/2145/1/012063.*

**Measuring shape parameters of pearls in batches using machine vision: A case study.** X. Liu, S. Jin, Z. Yang, G. Królczyk and Z. Li, *Micromachines*, **13**(4), 2022, article 546 (14 pp.), https://doi.org/10.3390/mi13040546.*

**The presence of irregular layers on the nacre of the high- and low-quality *Pinctada fucata martensii* pearls.** G. Muhammad, T. Fujimura, A. Sahidin and A. Komaru, *Aquaculture, Aquarium, Conservation & Legislation – International Journal of the Bioflux Society*, **15**(1), 2022, 510–519, http://www.bioflux.com.ro/docs/2022.510-519.pdf.*

**Renaissance et perles baroques [Renaissance and baroque pearls].** A. Quédillac, *Revue de Gemmologie A.F.G.*, No. 215, 2022, 14–15 (in French).

**The value of pearls: A historical review and current trends.** A Sato and L.E. Cartier, *GemGuide*, **41**(3), 2022, 4–10.

**X-ray micro-tomography as a method to distinguish and characterize natural and cultivated pearls.** L. Vigorelli, E. Croce, D. Angelici, R. Navone, S. Grassini, L. Guidorzi, A. Re and A. Lo Giudice, *Condensed Matter*, **6**(4), 2021, article 51 (25 pp.), https://doi.org/10.3390/condmat6040051.*

## SIMULANTS

**Characterization of coated colorless synthetic moissanite.** H. Choi, Y. Kim, H. Jang and J. Seok, *Journal of the Korean Crystal Growth and Crystal Technology*, **32**(1), 2022, 7–11, https://doi.org/10.6111/JKCGCT.2022.32.1.007 (in Korean with English abstract).*

**Frabozmenná sklenená imitácia alexandritu/ Colour-change glass as a [*sic*] alexandrite imitation.** J. Štubňa, *Gemologický Spravodajca (Gemmological Newsletter)*, **11**(2), 2021, 5–12, https://www.gu.fpv.ukf.sk/images/GS/2021_2_gs.pdf (in Slovak with English abstract).*

**Identification of a new alkyd resin of gem imitation.** L. Yu, *Superhard Material Engineering*, **33**(5), 2021, 58–63 (in Chinese with English abstract).

**Our friends the inclusions. The detective at the party of inclusions. Twelfth episode [imitation/synthetic opal, turquoise and lapis lazuli].** L. Costantini and C. Russo, *Rivista Italiana de Gemmologia/Italian Gemological Review*, No. 14, 2022, 7–11.

## SYNTHETICS

**A brief description of identification methods of HPHT and CVD lab-grown diamonds and the latest market analysis.** J.C.C. Yuan and L. Qi, *Journal of Gems & Gemmology*, **23**(6), 2021, 40–50, https://tinyurl.com/3jpa7sfc (in Chinese with English abstract).*

**The composition of the fluid phase in inclusions in synthetic HPHT diamonds grown in system Fe–Ni–Ti–C.** V. Sonin, A. Tomilenko, E. Zhimulev, T. Bul'bak, A. Chepurov, Y. Babich, A. Logvinova, T. Timina *et al.*, *Scientific Reports*, **12**(1), 2022, article 1246 (9 pp.), https://doi.org/10.1038/s41598-022-05153-7.*

**Effect of temperature control gradient and time on the quality of synthetic jadeite.** C. Zhang, M. Chen and Y. Zou, *Journal of Gems & Gemmology*, **24**(1), 2022, 58–67, https://tinyurl.com/yckhsa85 (in Chinese with English abstract).*

**The future star in gems? Can lab-grown diamonds add value to luxury brands?** P. Mihailovich, C. Taylor and A. Brunschweiger, *Journal of Gems & Gemmology*, **23**(6), 2021, 58–73, https://tinyurl.com/jhymnxbd.*

**Historical notes on the Biron synthetic pink beryl and its early popularity.** C. Cumo, *Rivista Italiana de Gemmologia/Italian Gemological Review*, No. 14, 2022, 27–29.

**The influence of light path length on the color of synthetic ruby.** B. Yuan, Y. Guo and Z. Liu, *Scientific Reports*, **12**(1), 2022, article 5943 (15 pp.), https://doi.org/10.1038/s41598-022-08811-y.*

**Laboratory-grown diamond: A gemological laboratory perspective.** S. Eaton-Magana, T. Ardon and C.M. Breeding, *Journal of Gems & Gemmology*, **23**(6), 2021, 23–59, https://tinyurl.com/5n82deet.*

**Laboratory-grown diamond: The importance of developing value system through brand building.** L. Guo and W. Xie, *Journal of Gems & Gemmology*, **23**(6), 2021, 84–89, https://tinyurl.com/4xbhm8tk (in Chinese with English abstract).*

**A multi-methodological investigation of natural and synthetic red beryl gemstones.** G.D. Gatta, I. Adamo, A. Zullino, V. Gagliardi, R. Lorenzi, N. Rotiroti, L. Faldi and L. Prosperi, *Minerals*, **12**(4), 2022, article 439 (16 pp.), https://doi.org/10.3390/min12040439.*

**Present and future of laboratory-grown diamond and natural diamond detection methods.** A.H. Shen, *Journal of Gems & Gemmology*, **23**(6), 2021, 1–11, https://tinyurl.com/2fkazc6z (in Chinese with English abstract).*

**Progress in synthesis and analysis of lab-grown diamond.** J. Li, J. Hu, P. Su, J. Lu, J. Zang and Y. Wang, *Journal of Gems & Gemmology*, **23**(6), 2021, 12–24, https://tinyurl.com/yc3yhdvr (in Chinese with English abstract).*

**Spectral characteristic of natural and HPHT-grown type Ib diamonds.** Z. Song, S. Tang, W. Zhu, B. Gao, Y. Li and T. Lu, *Journal of Gems & Gemmology*, **23**(6), 2021, 51–57, https://tinyurl.com/cp8ve499 (in Chinese with English abstract).*

**Study on the microstructure and spectra of regrown quartz crystals from Chinese jewelry market.** D. Zhou, T. Lu, H. Dai, J. Lv, S. Chen, Z. Song and J. Zhang, *Crystals*, **11**(9), 2021, article 1145 (7 pp.), https://doi.org/10.3390/cryst11091145.*

**Synthesis of jadeite: Review and perspective.** L. Ouyang, F. He and Y. Xing, *Journal of Synthetic Crystals*, **51**(3), 2022, 559–570, https://tinyurl.com/yc4bu93d (in Chinese with English abstract).*

## TREATMENTS

**Effects of spectral characteristics of high temperature high pressure annealed brown CVD diamonds.** X. Liu, M. Chen, G. Wu, S. Lu and Y. Bai, *Spectroscopy and Spectral Analysis*, **42**(1), 2022, 258–264, https://tinyurl.com/2p8vvfth (in Chinese with English abstract).*

**A review of binderless polycrystalline diamonds: Focus on the high-pressure–high-temperature sintering process.** J. Guignard, M. Prakasam and A. Largeteau, *Materials*, **15**(6), 2022, article 2198 (36 pp.), https://doi.org/10.3390/ma15062198.*

**Specifics of high-temperature annealing of brown CVD single crystal diamonds at graphite-stable and diamond-stable conditions.** V. Vins, A. Yelisseyev, S. Terentyev and S. Nosukhin, *Diamond and Related Materials*, **118**, 2021, article 108511 (9 pp.), https://doi.org/10.1016/j.diamond.2021.108511.

**Spectroscopic characteristics and identification methods of color-treated purplish red diamonds.** S. Ye, M. Chen, G. Wu and S. He, *Spectroscopy and Spectral Analysis*, **42**(1), 2022, 191–196, https://tinyurl.com/yna9tpuz (in Chinese with English abstract).*

**Study on colour and identification characteristics of natural and dyed fire opal in the market.** B. Zhao, Z. Hu, D. Han, Y. Pan, M. Zhu and C. Chen, *Journal of Gems & Gemmology*, **24**(1), 2022, 39–47, https://tinyurl.com/2md8zcj8 (in Chinese with English abstract).*

**Study on the gemmological characteristics of filled morganite.** Y. Wu, Q. Chen, A. Zhao, X. Li and P. Bao, *Spectroscopy and Spectral Analysis*, **42**(2), 2022, 575–581, https://tinyurl.com/2p8wt3ue (in Chinese with English abstract).*

**Study of the mechanism of color change of prehnite after heat treatment.** Q. Wang, Q. Guo, N. Li, L. Cui and L. Liao, *RSC Advances*, **12**(5), 2022, 3044–3054, https://doi.org/10.1039/d2ra00318j.*

## COMPILATIONS

***G&G* Micro-World.** Blue apatite in smoky quartz • Apatite before and after fissure filling with oil • Acicular troughs associated with green radiation stains on a rough diamond • Spessartine in aquamarine • Hematite in diamond • Hyalite containing fluorite and other internal features • 'Herringbone' in peridot • Extraterrestrial-like inclusion in ruby • Maze-like 'fingerprint' in spinel • Multiphase inclusion in topaz • Spinel with högbomite-filled dislocations • YAG with flux-filled fractures • Growth hillocks on aquamarine. *Gems & Gemology*, **58**(1), 2022, 62–71, https://tinyurl.com/2zabzy7x.*

**Gem News International.** Tucson 2022 report • Inclusions in agate from Sichuan, China • Cavity filling in emerald • Yellowish green enstatite • Star topaz from Vietnam • Davemaoite inclusion in diamond • Near-colourless type IIb diamond • Dyed barite-calcite composite imitating turquoise • Amber beads filled with epoxy resin • Irradiated amber. *Gems & Gemology*, **58**(1), 2022, *Gems & Gemology*, **58**(1), 2022, 80–136, https://tinyurl.com/2p8svjz7.*

**Lab Notes.** HPHT-processed type Ia diamond • Yellow-to-green diamonds colored by Ni impurities • Nailhead spicule in a Russian emerald • Dyed green fluorite rough • Repaired fracture in grandidierite • 16.41 ct CVD synthetic diamond • Unusual laser drill holes in an HPHT-grown synthetic diamond • Hydrothermal synthetic ruby. *Gems & Gemology*, **58**(1), 2022, 48–58, https://tinyurl.com/bdfww544.*

**Article freely available for download or reading online, as of press time*


# REGISTER NOW!

# GemINTRO

***GemIntro*** is a Level 2, online, entry-level course which will introduce you to the fascinating world of gemmology and the enormous variety of beautiful gems available. You can discover the basics of gemmology at your own pace - perfect for anyone looking to start or grow their career in the gems and jewellery trade, or for those completely new to gemmology and with an interest in gems.

## Register now at **gem-a.com/gemintro**

Gem-A
THE GEMMOLOGICAL ASSOCIATION OF GREAT BRITAIN

Gem-A, 21 Ely Place, London, EC1N 6TD, UK. T: +44 (0)20 7404 3334, W: www.gem-a.com. Registered charity no. 1109555.